N°d'ordre NNT : 2020LYSET009

THÈSE DE DOCTORAT DE L'UNIVERSITÉ DE LYON
opérée au sein de
l'École Nationale des Travaux Publics de l'État

École Doctorale N° 162
Mécanique, Energétique, Génie Civil et Acoustique (MEGA)

Spécialité / discipline de doctorat : Génie Civil

Soutenue publiquement le 29/06/2020, par :

Reuber Arrais Freire

Utilisation de géogrilles en fibre de verre pour le renforcement des couches d'enrobé bitumineux

APPENDICES

Devant le jury composé de :

DJERAN MAIGRE, Irini	Prof., INSA de Lyon	Présidente
CHAZALLON, Cyrille	Prof., INSA de Strasbourg	Rapporteur
CANESTRARI, Francesco	Prof., Università Politecnica delle Marche	Rapporteur
RIOT, Mathilde	Expert, Afitexinov	Examinatrice
POUGET, Simon	Dr., EIFFAGE Infrastructures	Examinateur
DI BENEDETTO, Hervé	Prof., Université de Lyon/ENTPE	Directeur de thèse
SAUZÉAT, Cédric	Prof., Université de Lyon/ENTPE	Co-Directeur de thèse
LESUEUR, Didier	Dr., Afitexinov	Invité
VAN ROMPU, Julien	Dr., EIFFAGE Infrastructures	Invité

N°d'ordre NNT : 2020LYSET009

DOCTORAL THESIS OF THE UNIVERSITY OF LYON
prepared at
École Nationale des Travaux Publics de l'État

Doctoral School N° 162
Mécanique, Energétique, Génie Civil et Acoustique (MEGA)

Specialty: **Civil Engineering**

Publicly defended the 29th of June 2020 by:

Reuber Arrais Freire

Use of fiberglass geogrids to the reinforcement of bituminous mixtures layers

ANNEXES

---

before the committee composed of:

DJERAN MAIGRE, Irini	Prof., INSA de Lyon	President
CHAZALLON, Cyrille	Prof., INSA de Strasbourg	Reviewer
CANESTRARI, Francesco	Prof., Università Politecnica delle Marche	Reviewer
RIOT, Mathilde	Expert, Afitexinov	Examiner
POUGET, Simon	Dr., EIFFAGE Infrastructures	Examiner
DI BENEDETTO, Hervé	Prof., Université de Lyon/ENTPE	Advisor
SAUZÉAT, Cédric	Prof., Université de Lyon/ENTPE	Co-advisor
LESUEUR, Didier	Dr., Afitexinov	Invited
VAN ROMPU, Julien	Dr., EIFFAGE Infrastructures	Invited

TABLE OF CONTENTS

APPENDIX A1 – COMPLEX MODULUS TEST RESULT: BITUMINOUS MIXTURES

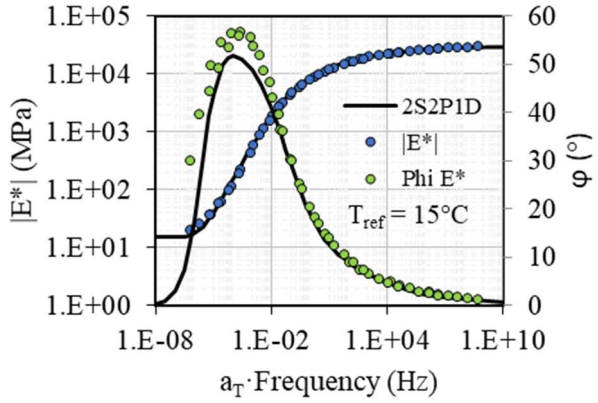

(a)

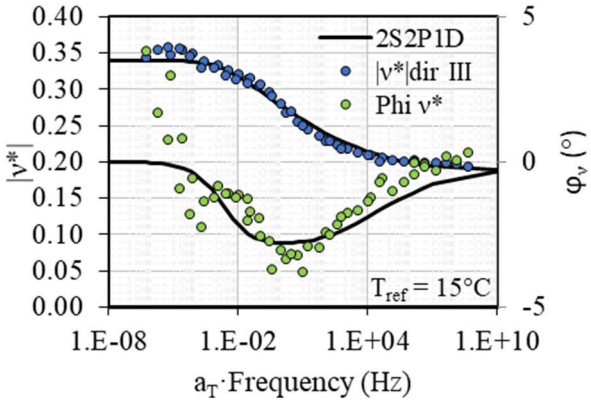

(b)

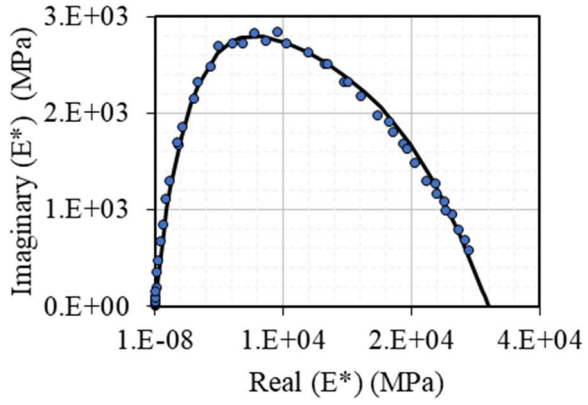

(c)

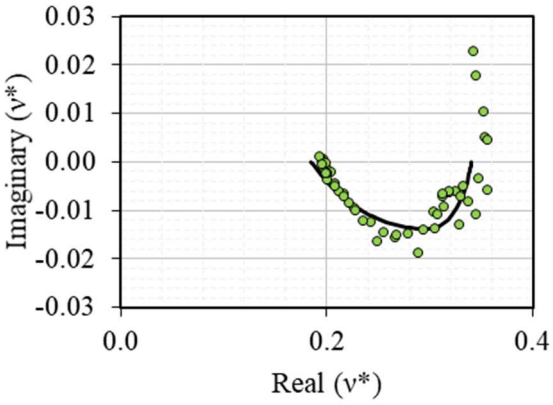

(d)

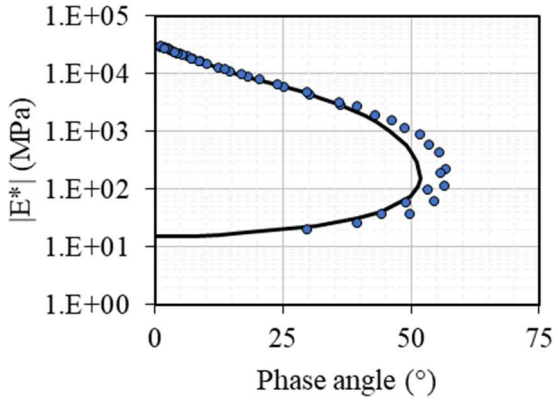

(e)

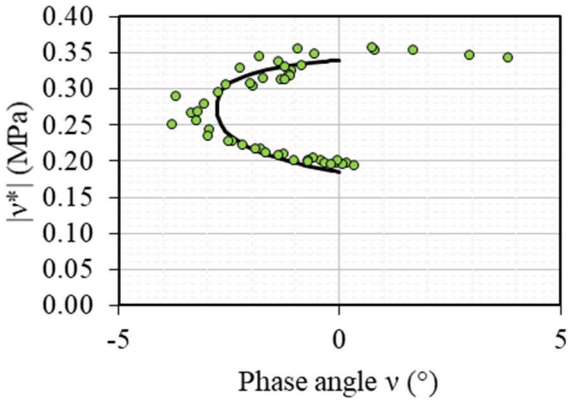

(f)

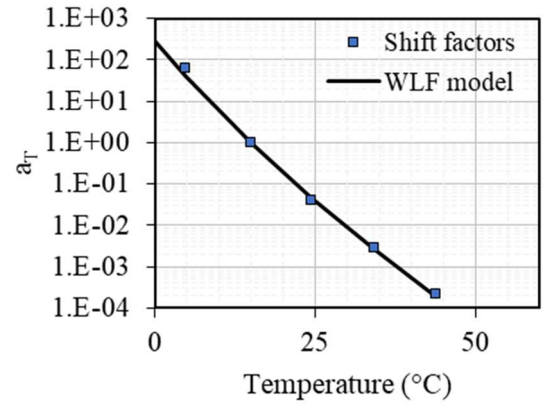

(g)

Figure A1-1. Complex modulus test results and 2S2P1D simulations for A1-V2: (a) Master curves of $|E^*|$ and φ_E, (b) Master curves of $|\nu^*|$ and φ_ν, (c) Cole-Cole of E^*, (d) Cole-Cole of ν^*, (e) Black space of E^*, (e) Black space of ν^*, (f) shift factors with WLF model

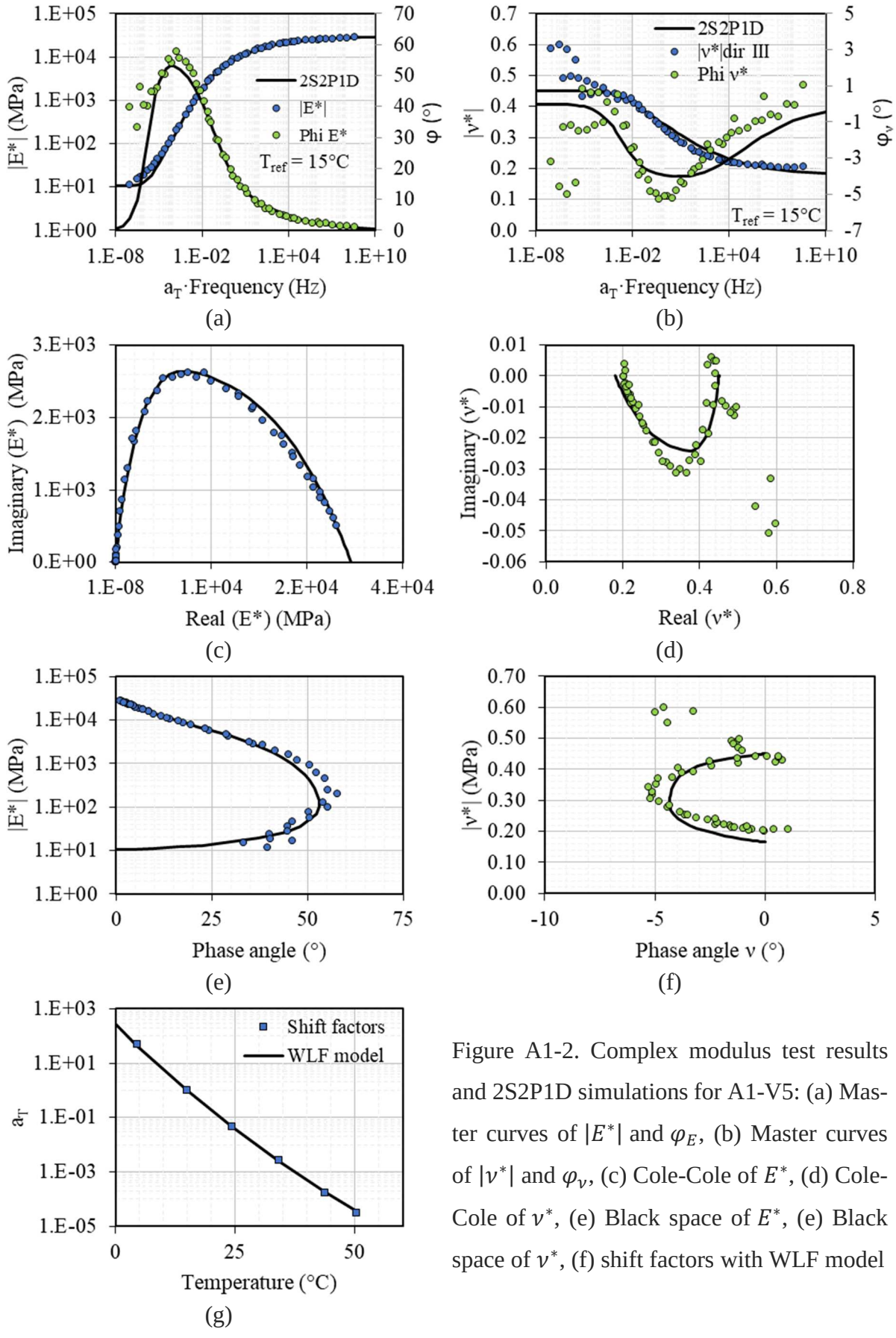

Figure A1-2. Complex modulus test results and 2S2P1D simulations for A1-V5: (a) Master curves of $|E^*|$ and φ_E, (b) Master curves of $|\nu^*|$ and φ_ν, (c) Cole-Cole of E^*, (d) Cole-Cole of ν^*, (e) Black space of E^*, (e) Black space of ν^*, (f) shift factors with WLF model

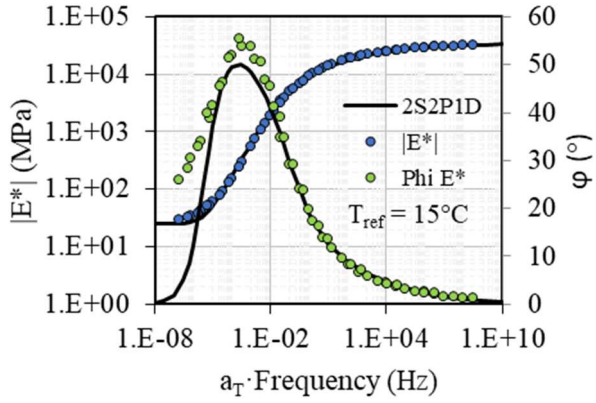

(a)

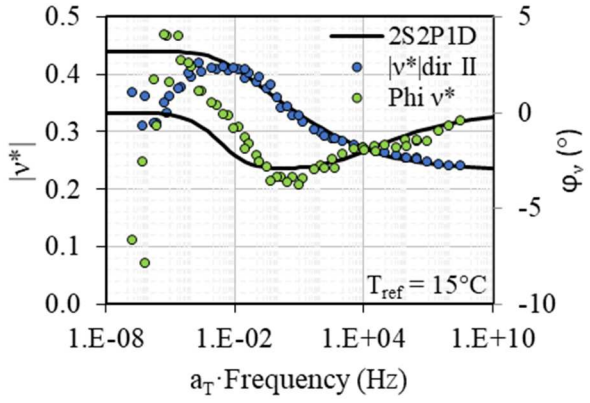

(b)

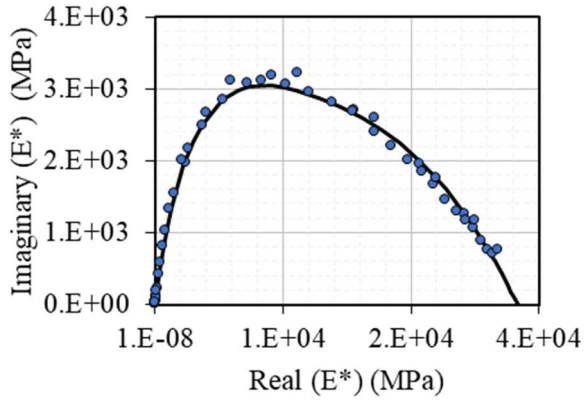

(c)

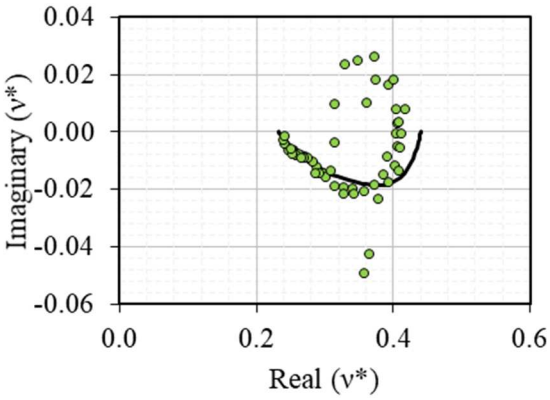

(d)

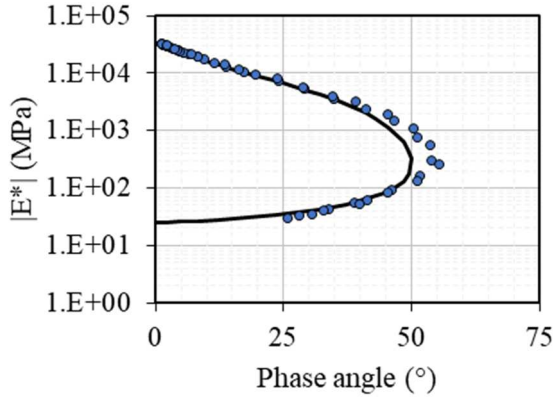

(e)

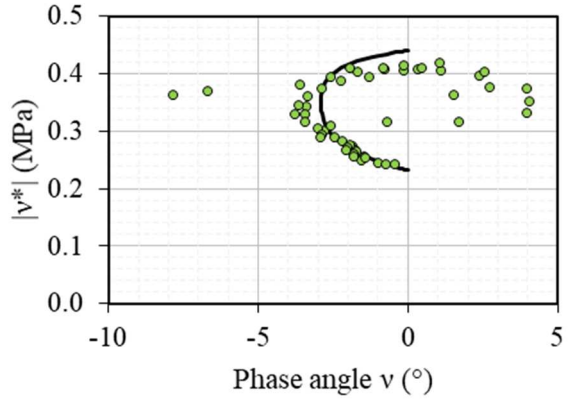

(f)

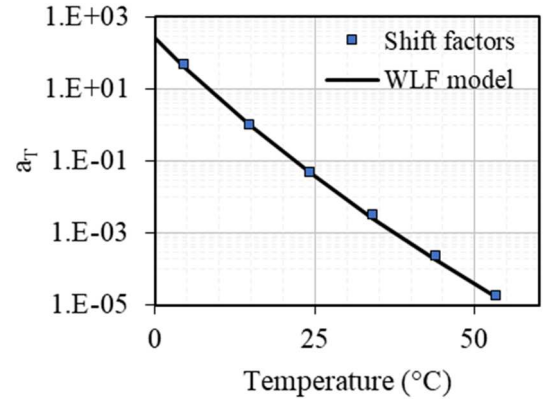

(g)

Figure A1-3. Complex modulus test results and 2S2P1D simulations for A1-H3: (a) Master curves of $|E^*|$ and φ_E, (b) Master curves of $|\nu^*|$ and φ_ν, (c) Cole-Cole of E^*, (d) Cole-Cole of ν^*, (e) Black space of E^*, (e) Black space of ν^*, (f) shift factors with WLF model

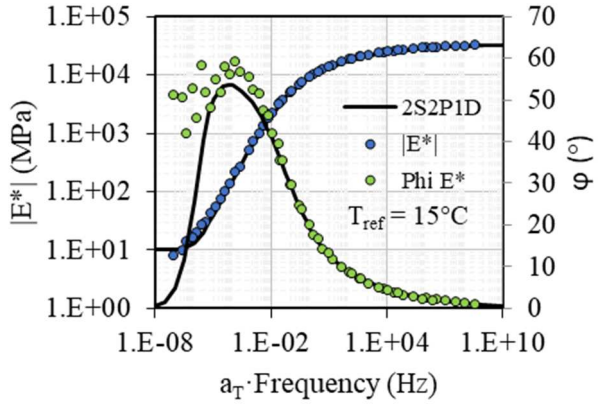

(a)

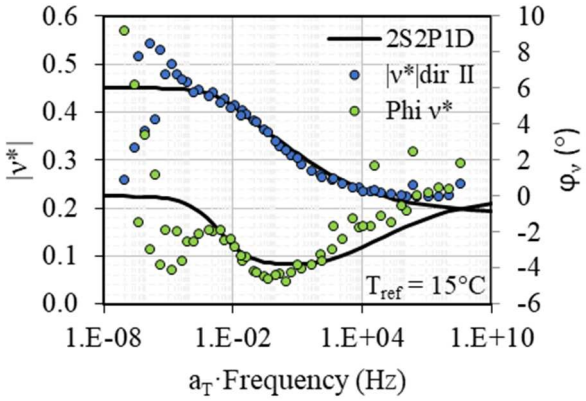

(b)

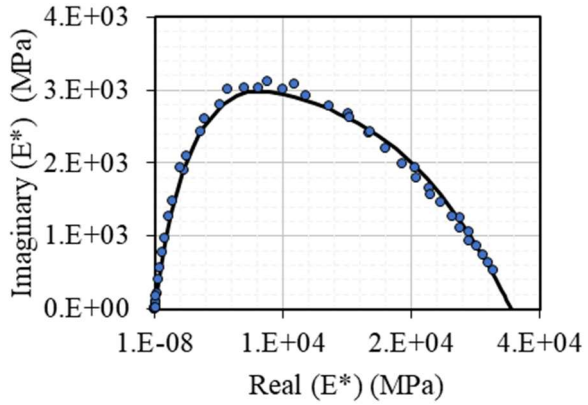

(c)

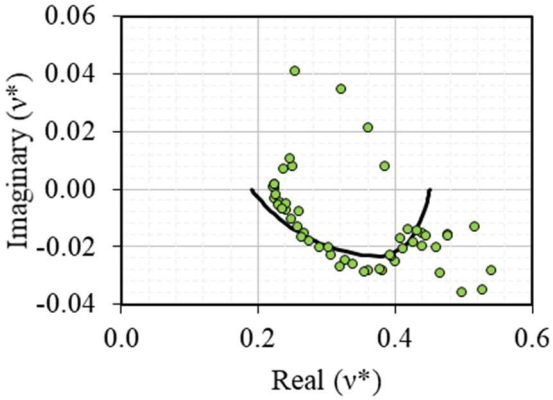

(d)

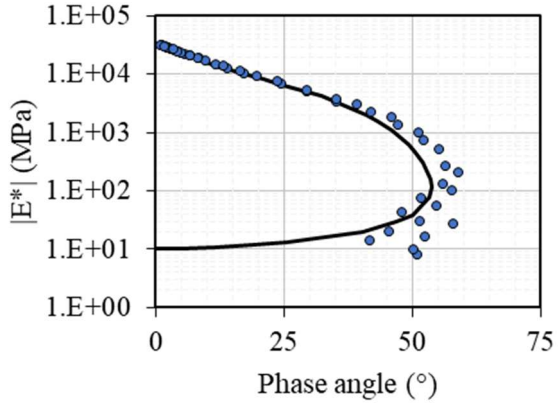

(e)

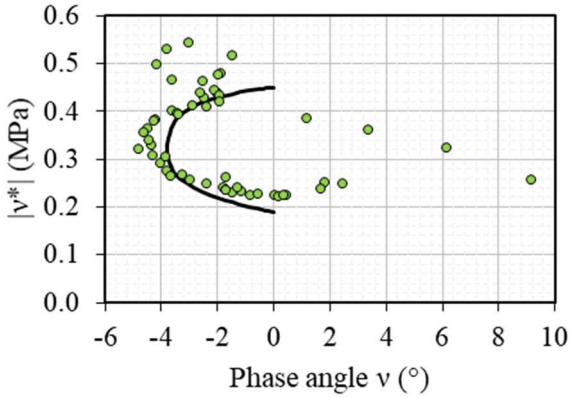

(f)

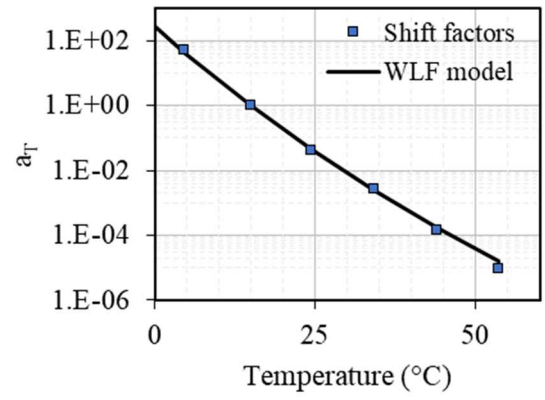

(g)

Figure A1-4. Complex modulus test results and 2S2P1D simulations for A1-H4: (a) Master curves of $|E^*|$ and φ_E, (b) Master curves of $|\nu^*|$ and φ_ν, (c) Cole-Cole of E^*, (d) Cole-Cole of ν^*, (e) Black space of E^*, (e) Black space of ν^*, (f) shift factors with WLF model

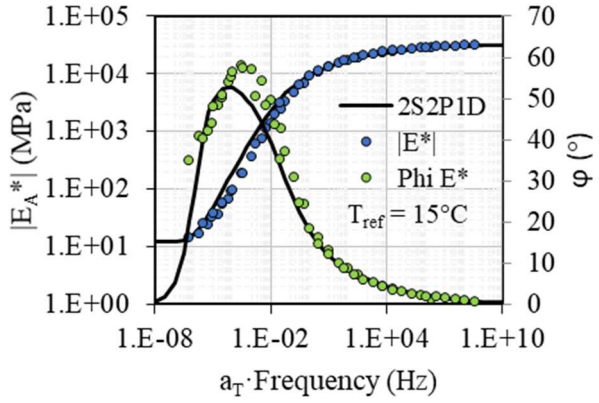

(a)

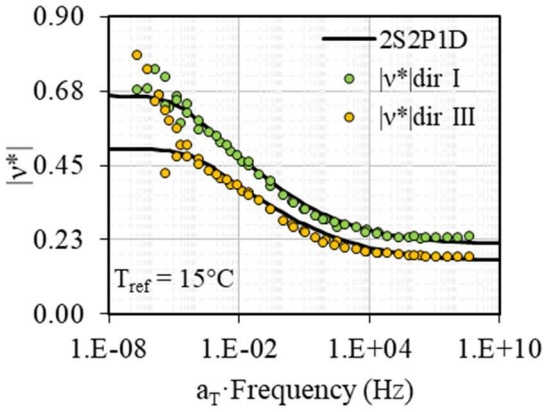

(b)

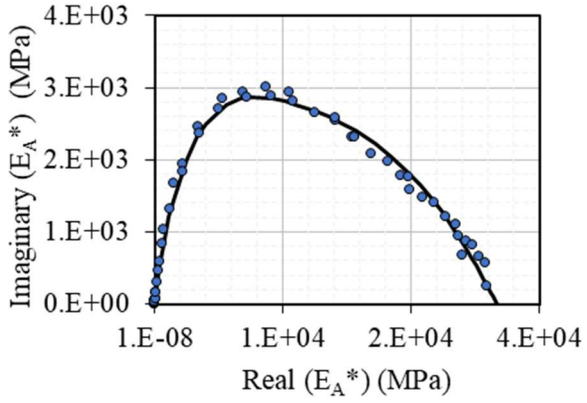

(c)

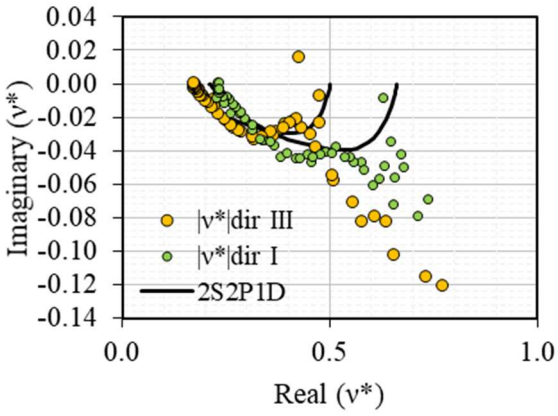

(d)

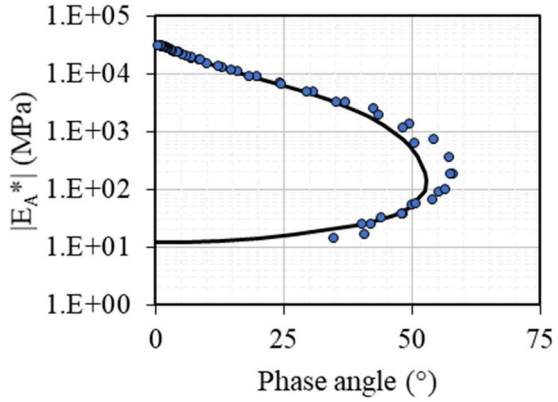

(e)

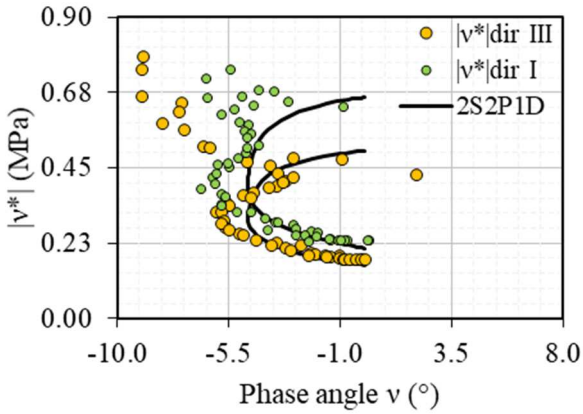

(f)

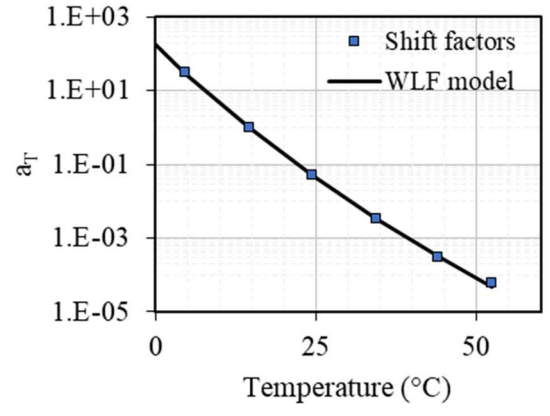

(g)

Figure A1-5. Complex modulus test results and 2S2P1D simulations for B2-V1 (bituminous mixture): (a) Master curves of $|E^*|$ and φ_E, (b) Master curves of $|\nu^*|$, (c) Cole-Cole of E^*, (d) Cole-Cole of ν^*, (e) Black space of E^*, (e) Black space of ν^*, (f) shift factors with WLF model

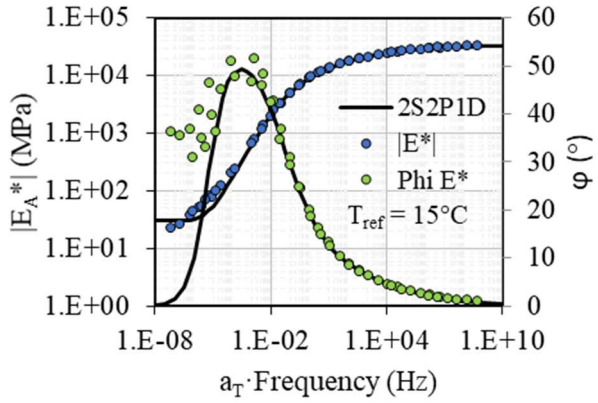

(a)

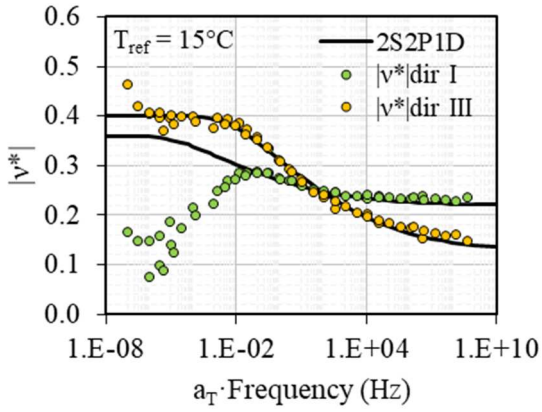

(b)

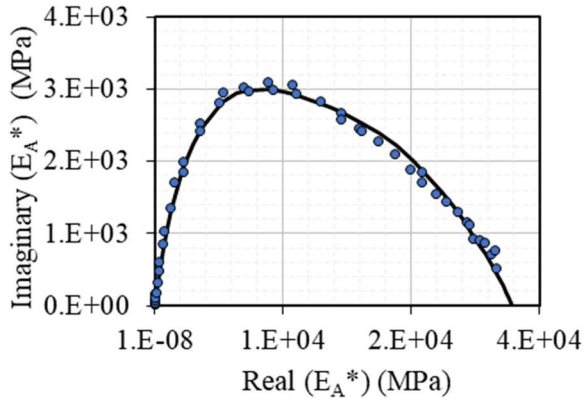

(c)

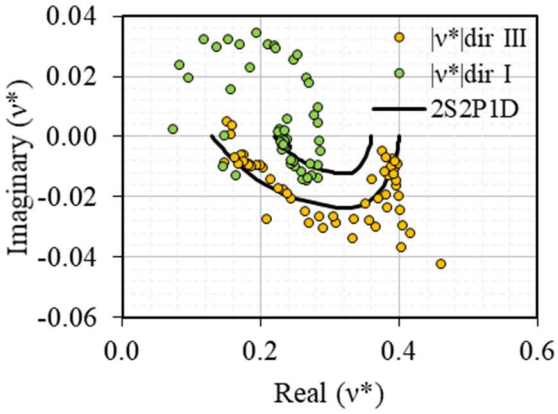

(d)

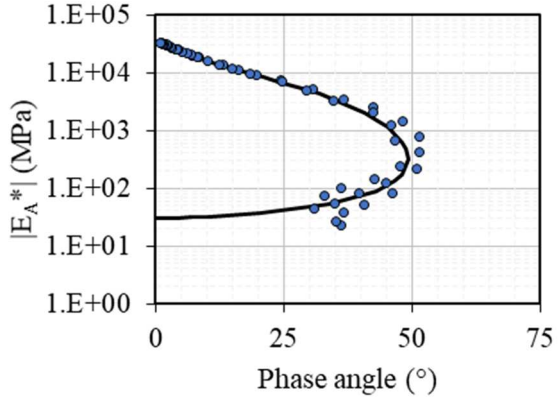

(e)

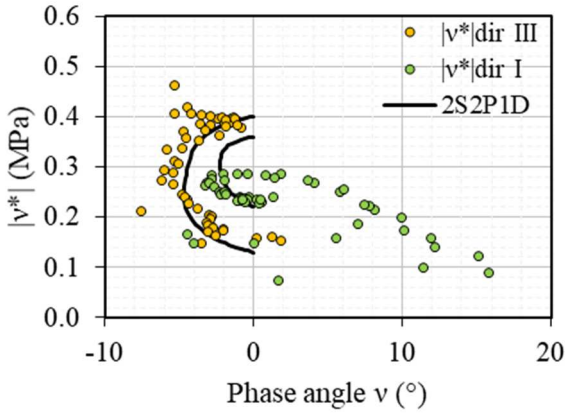

(f)

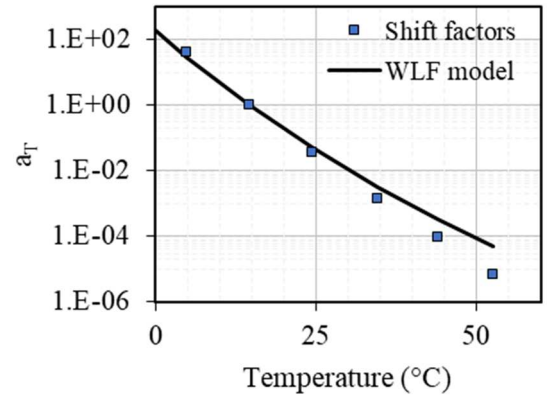

(g)

Figure A1-6. Complex modulus test results and 2S2P1D simulations for B2-V2 (bituminous mixture): (a) Master curves of $|E^*|$ and φ_E, (b) Master curves of $|\nu^*|$, (c) Cole-Cole of E^*, (d) Cole-Cole of ν^*, (e) Black space of E^*, (e) Black space of ν^*, (f) shift factors with WLF model

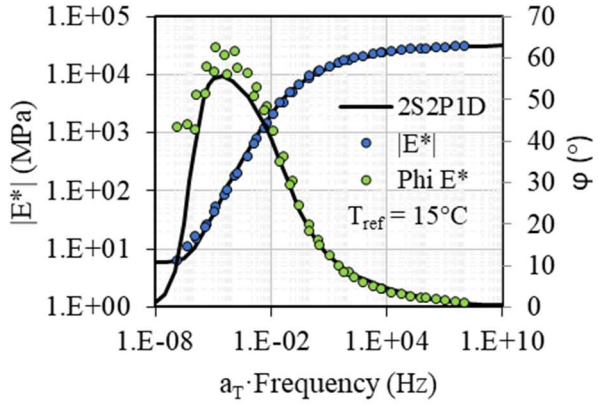

(a)

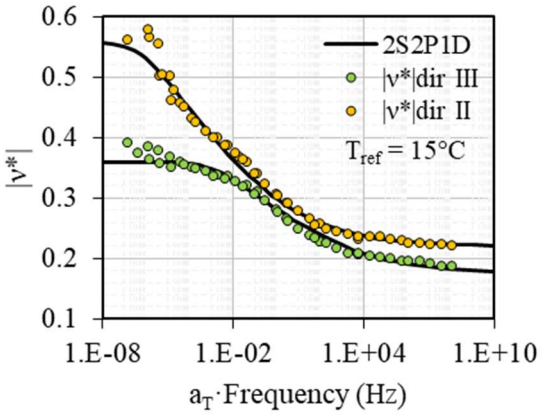

(b)

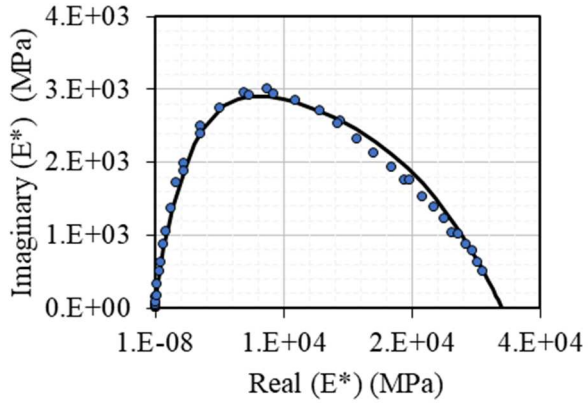

(c)

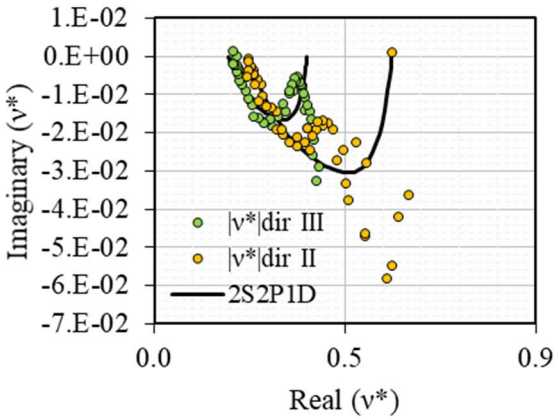

(d)

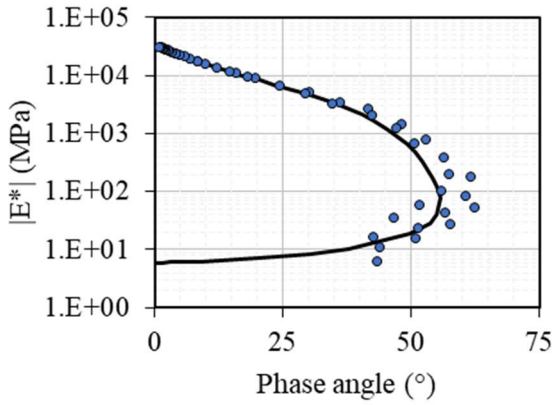

(e)

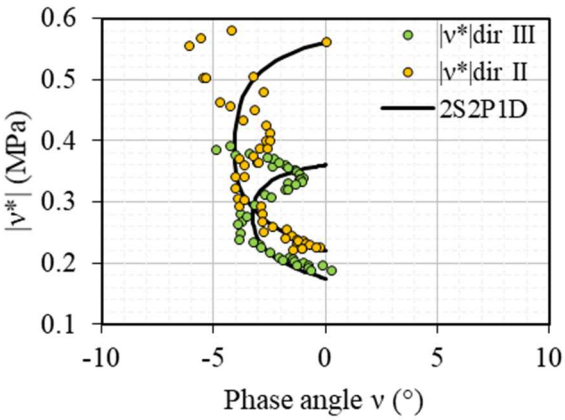

(f)

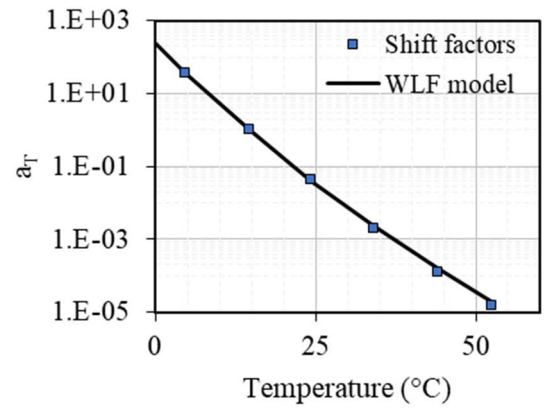

(g)

Figure A1-7. Complex modulus test results and 2S2P1D simulations for B1-H1: (a) Master curves of $|E^*|$ and φ_E, (b) Master curves of $|\nu^*|$, (c) Cole-Cole of E^*, (d) Cole-Cole of ν^*, (e) Black space of E^*, (e) Black space of ν^*, (f) shift factors with WLF model

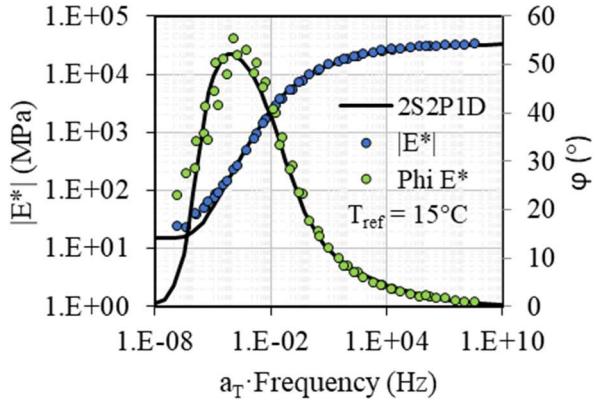

(a)

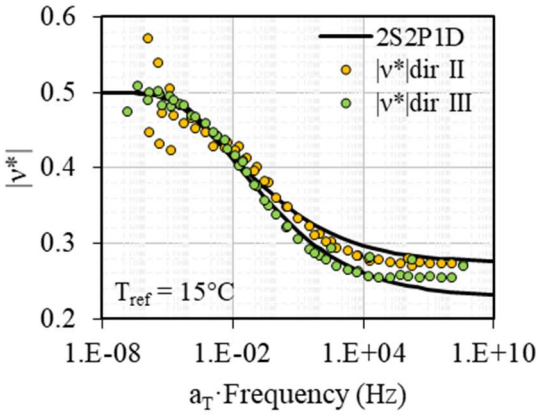

(b)

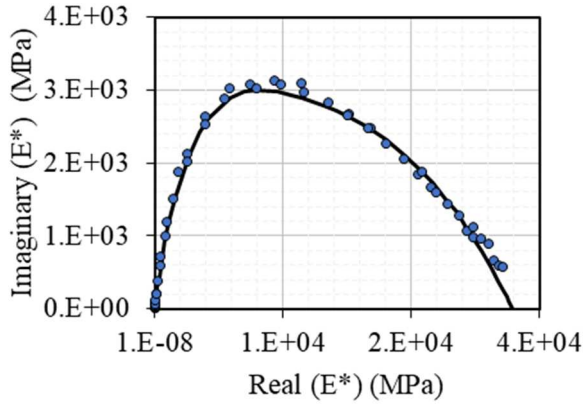

(c)

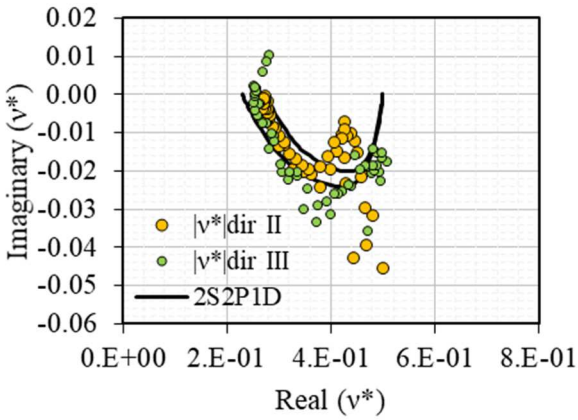

(d)

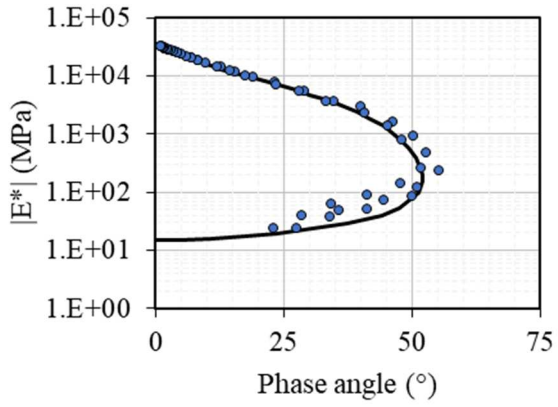

(e)

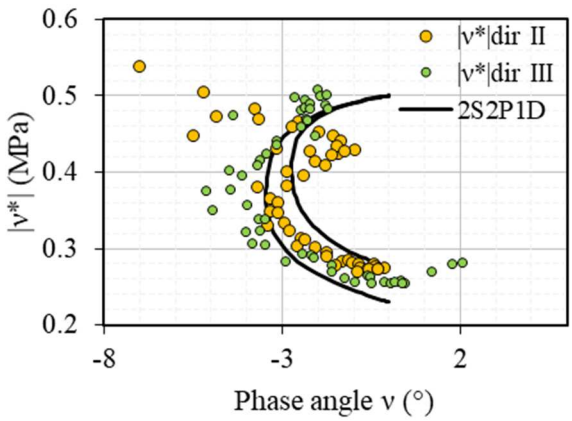

(f)

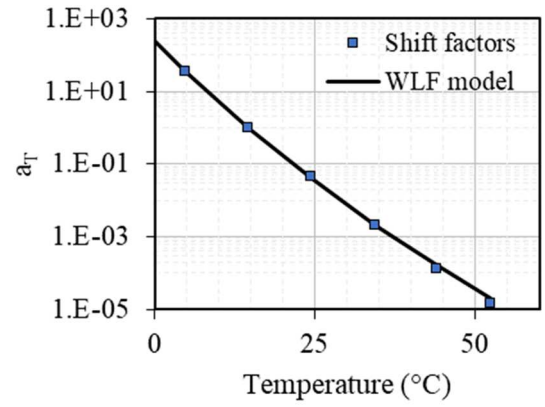

(g)

Figure A1-8. Complex modulus test results and 2S2P1D simulations for B1-H2: (a) Master curves of $|E^*|$ and φ_E, (b) Master curves of $|\nu^*|$, (c) Cole-Cole of E^*, (d) Cole-Cole of ν^*, (e) Black space of E^*, (e) Black space of ν^*, (f) shift factors with WLF model

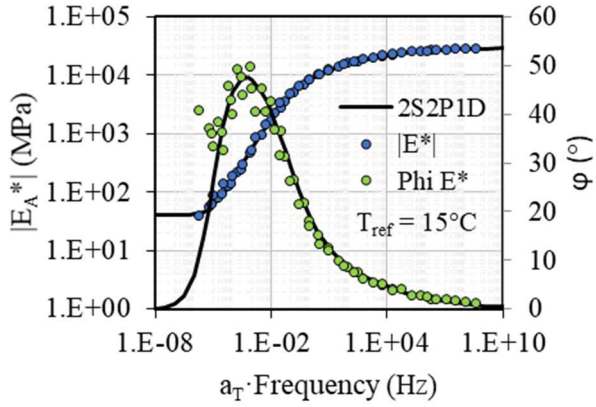

(a)

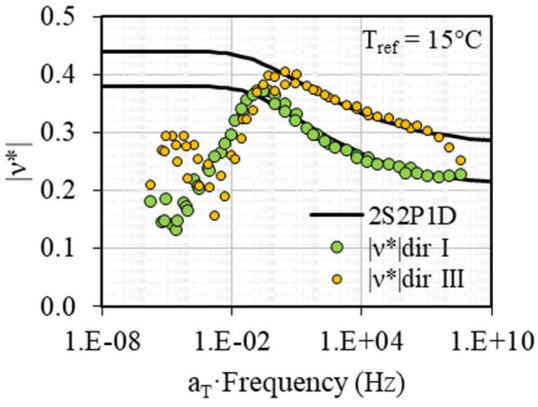

(b)

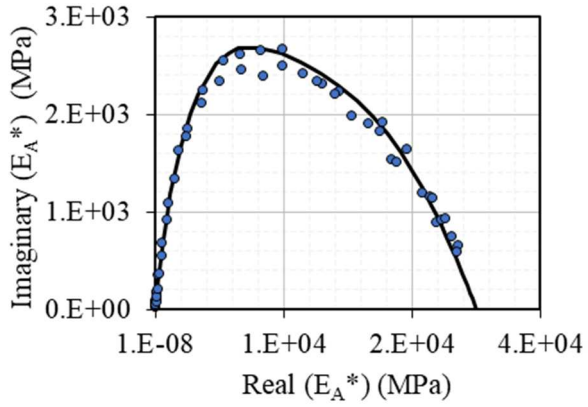

(c)

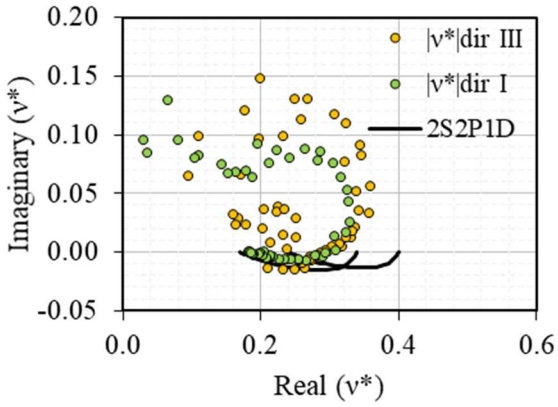

(d)

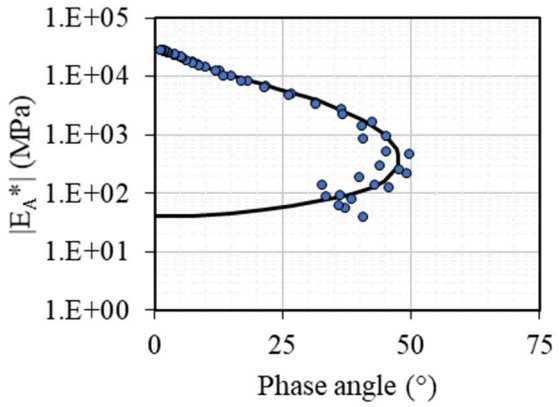

(e)

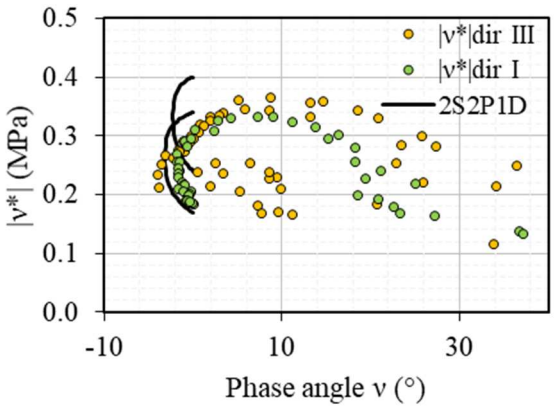

(f)

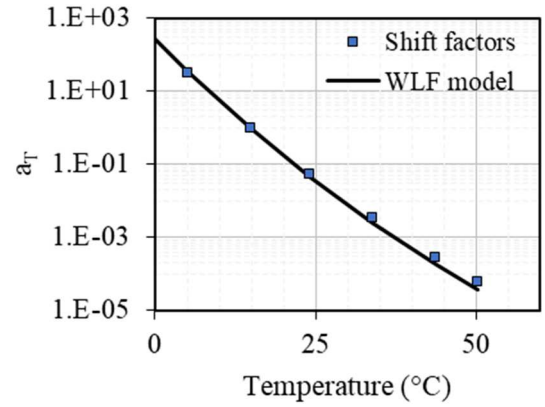

(g)

Figure A1-9. Complex modulus test results and 2S2P1D simulations for CE-V10 (bituminous mixture): (a) Master curves of $|E^*|$ and φ_E, (b) Master curves of $|\nu^*|$, (c) Cole-Cole of E^*, (d) Cole-Cole of ν^*, (e) Black space of E^*, (e) Black space of ν^*, (f) shift factors with WLF model

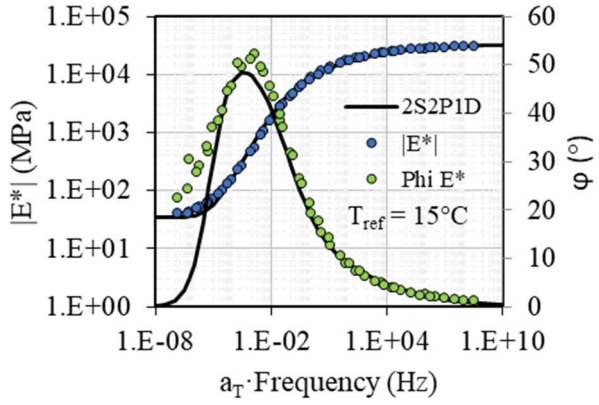

(a)

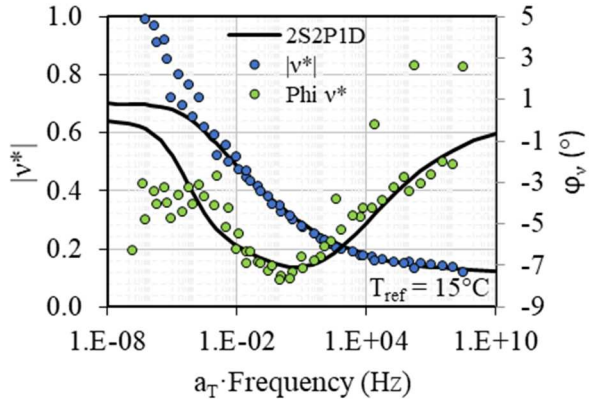

(b)

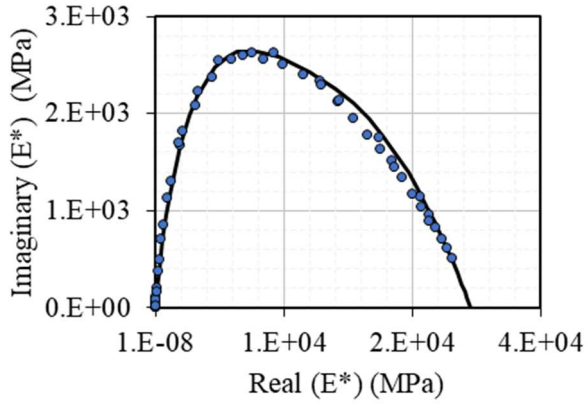

(c)

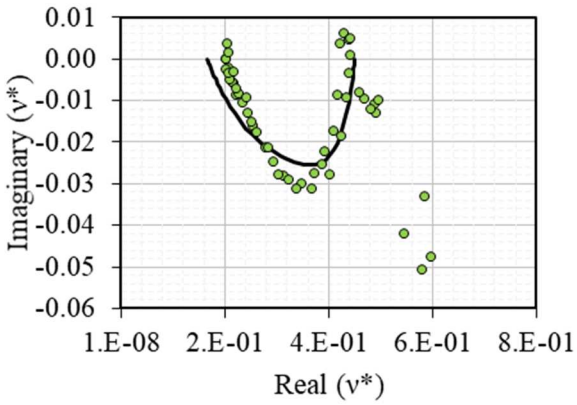

(d)

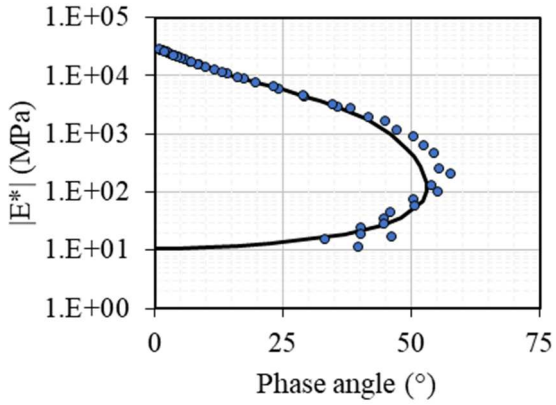

(e)

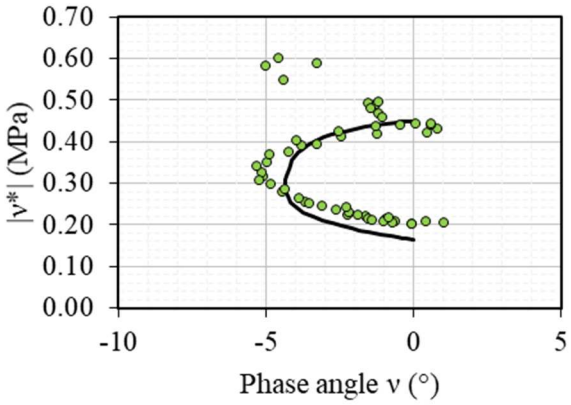

(f)

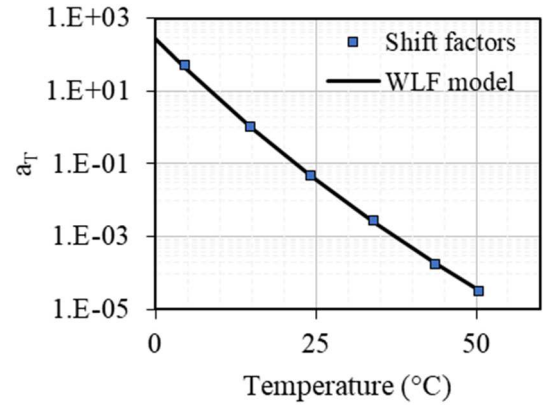

(g)

Figure A1-10. Complex modulus test results and 2S2P1D simulations for CE-H4: (a) Master curves of $|E^*|$ and φ_E, (b) Master curves of $|\nu^*|$ and φ_ν, (c) Cole-Cole of E^*, (d) Cole-Cole of ν^*, (e) Black space of E^*, (e) Black space of ν^*, (f) shift factors with WLF model

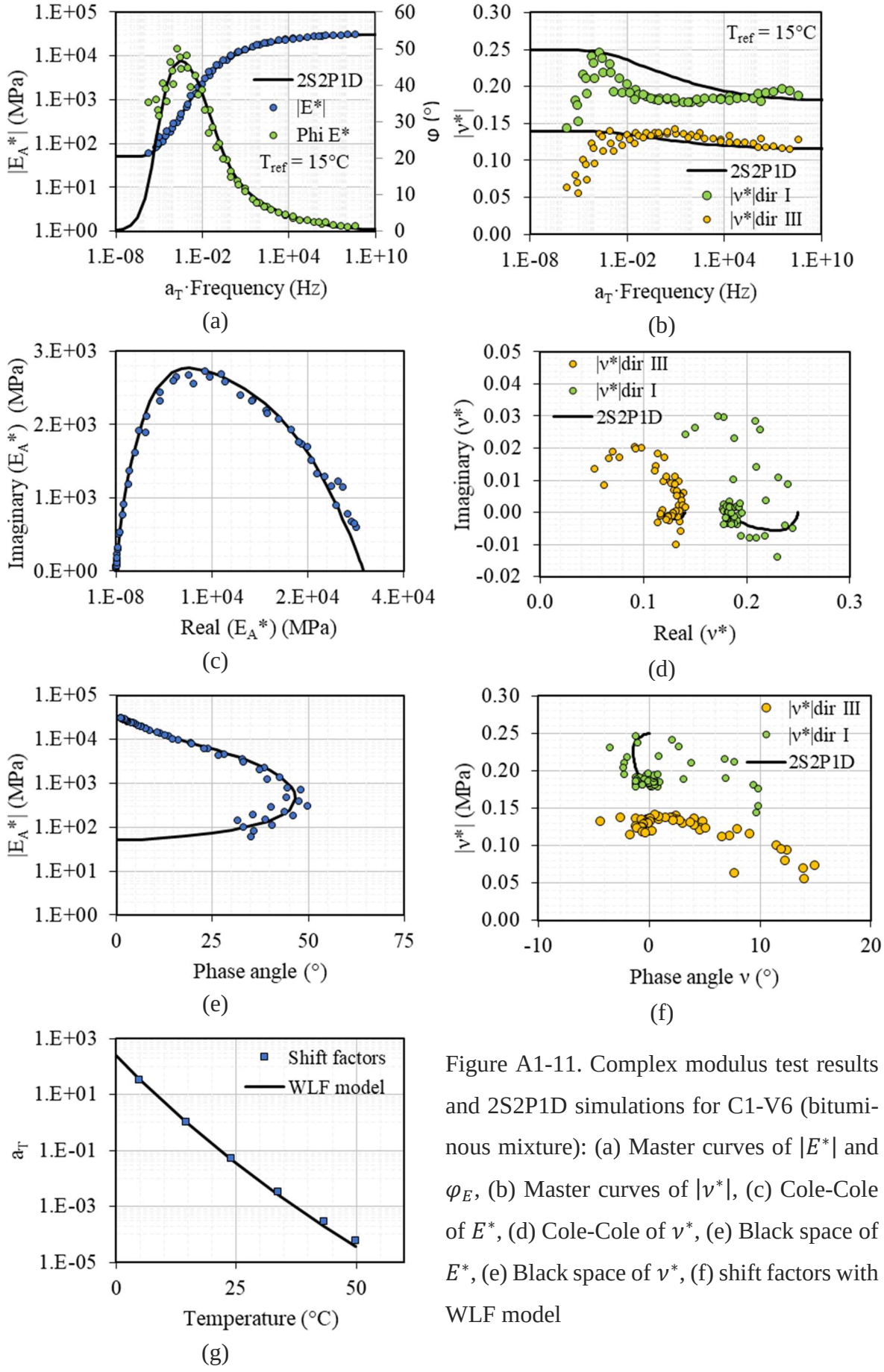

Figure A1-11. Complex modulus test results and 2S2P1D simulations for C1-V6 (bituminous mixture): (a) Master curves of $|E^*|$ and φ_E, (b) Master curves of $|\nu^*|$, (c) Cole-Cole of E^*, (d) Cole-Cole of ν^*, (e) Black space of E^*, (e) Black space of ν^*, (f) shift factors with WLF model

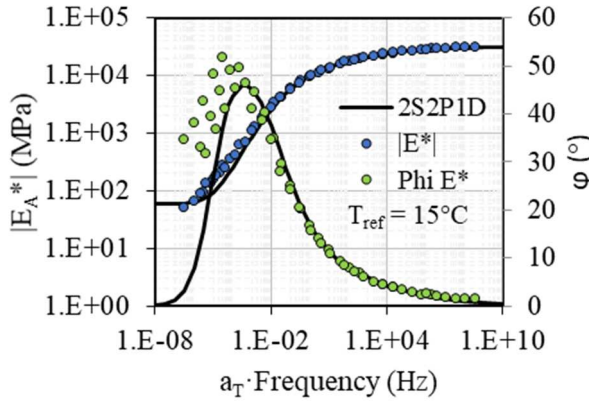

(a)

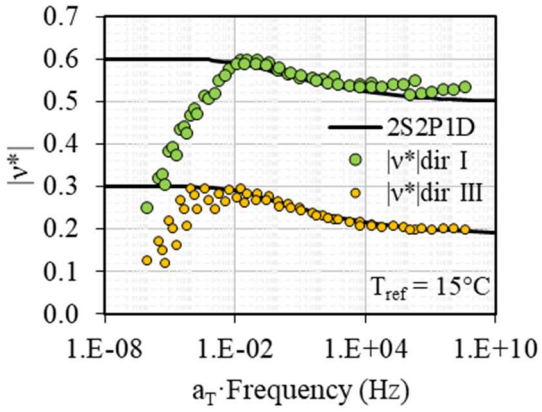

(b)

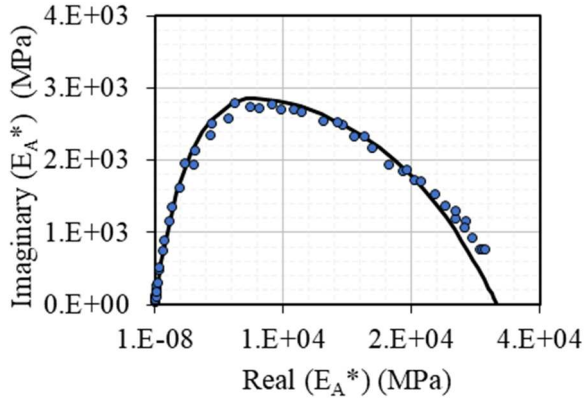

(c)

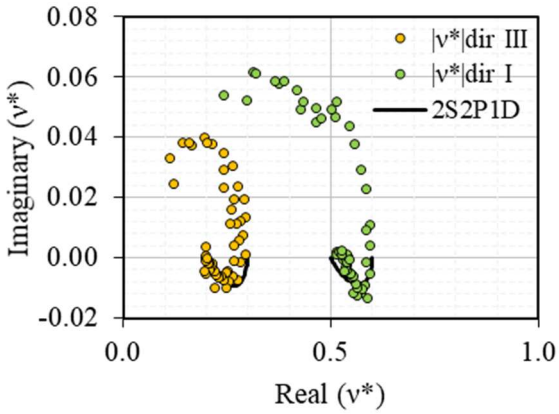

(d)

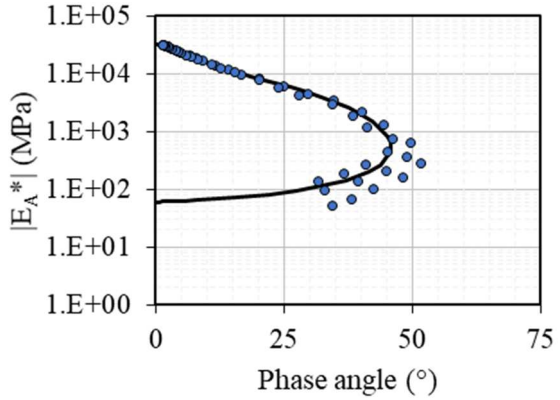

(e)

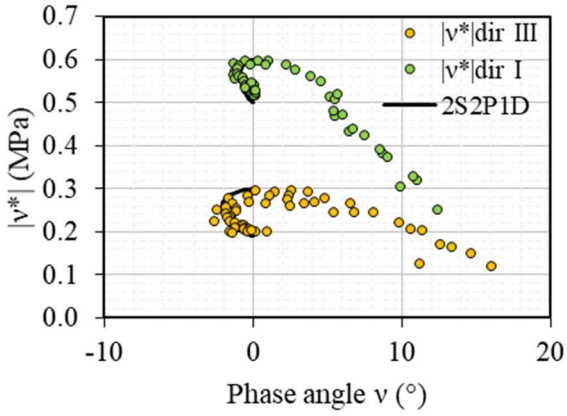

(f)

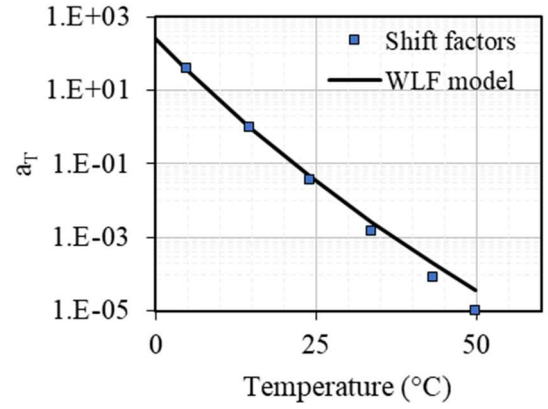

(g)

Figure A1-12. Complex modulus test results and 2S2P1D simulations for C2-V1 (bituminous mixture): (a) Master curves of $|E^*|$ and φ_E, (b) Master curves of $|\nu^*|$, (c) Cole-Cole of E^*, (d) Cole-Cole of ν^*, (e) Black space of E^*, (e) Black space of ν^*, (f) shift factors with WLF model

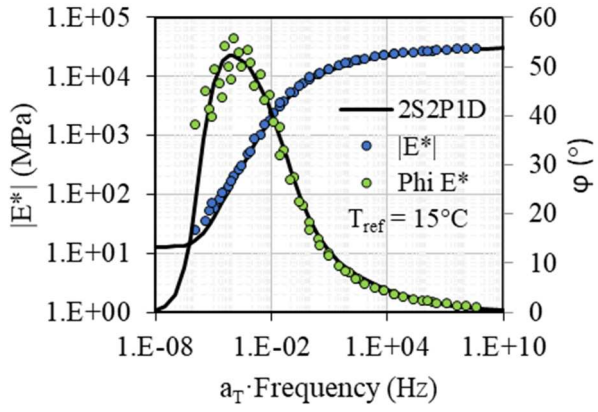

(a)

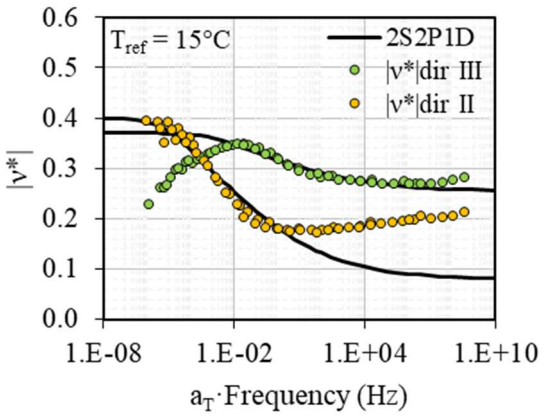

(b)

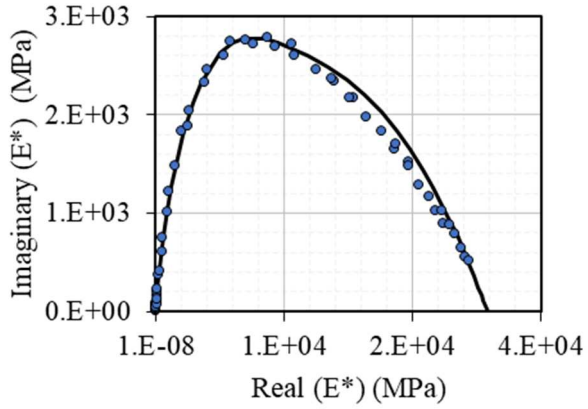

(c)

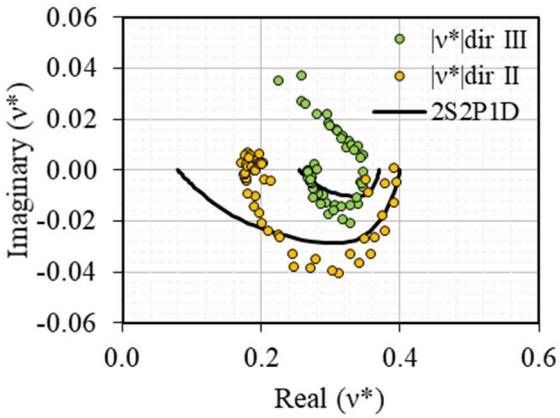

(d)

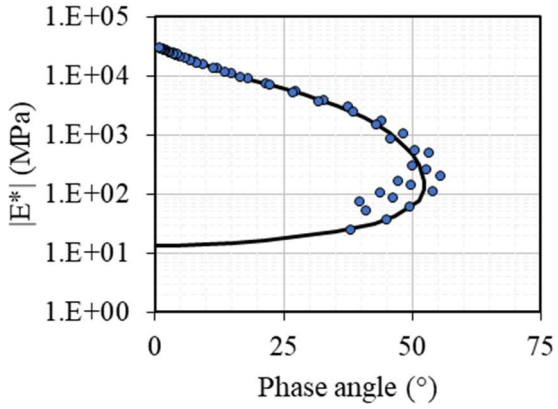

(e)

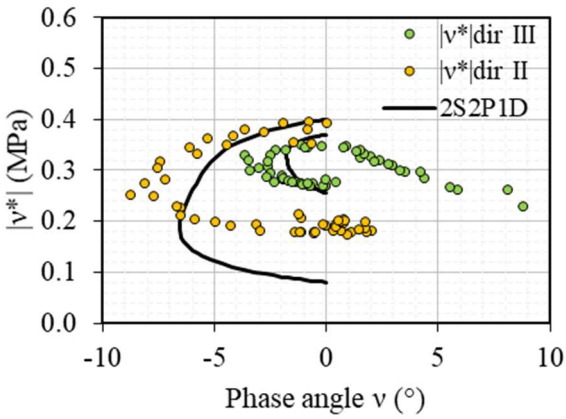

(f)

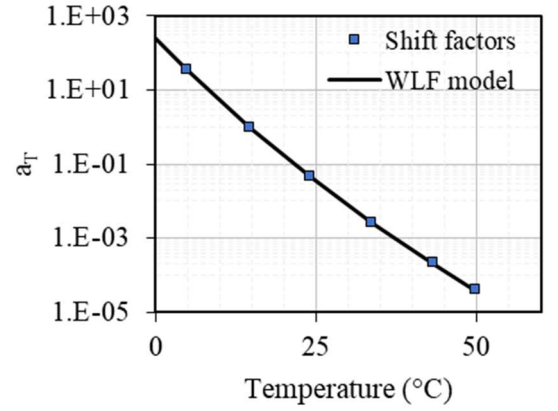

(g)

Figure A1-13. Complex modulus test results and 2S2P1D simulations for C2-H1: (a) Master curves of $|E^*|$ and φ_E, (b) Master curves of $|\nu^*|$, (c) Cole-Cole of E^*, (d) Cole-Cole of ν^*, (e) Black space of E^*, (e) Black space of ν^*, (f) shift factors with WLF model

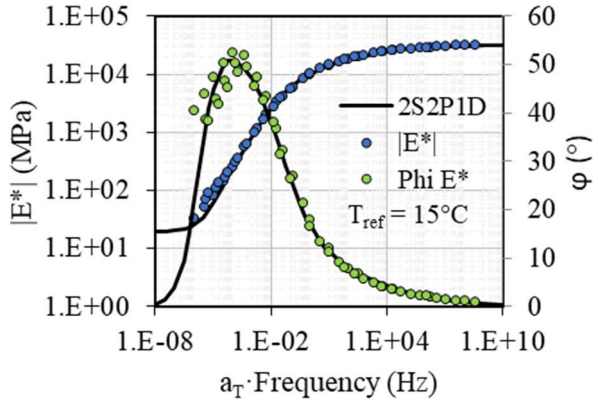

(a)

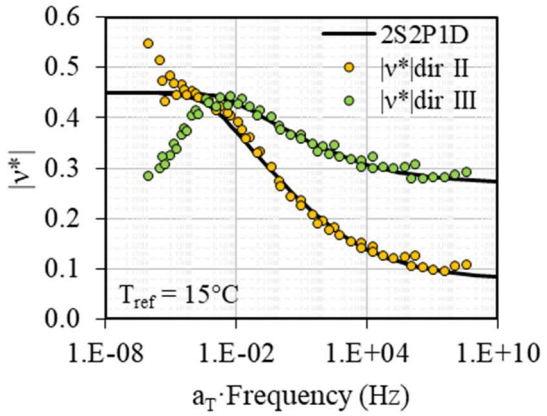

(b)

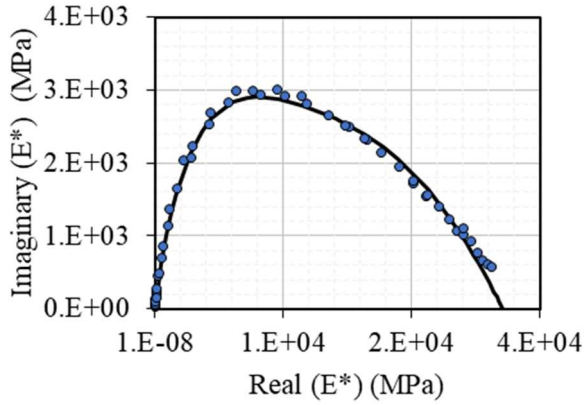

(c)

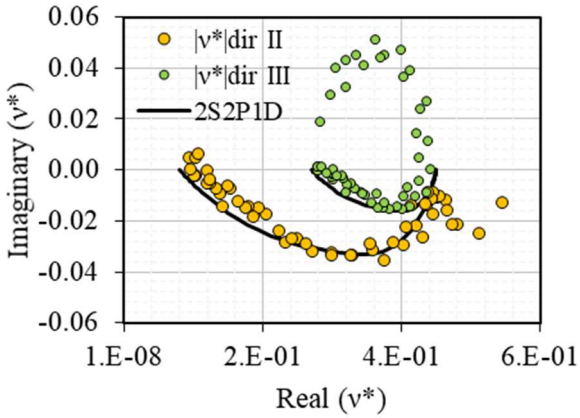

(d)

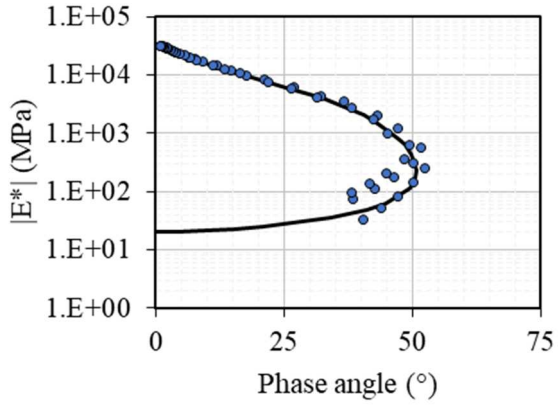

(e)

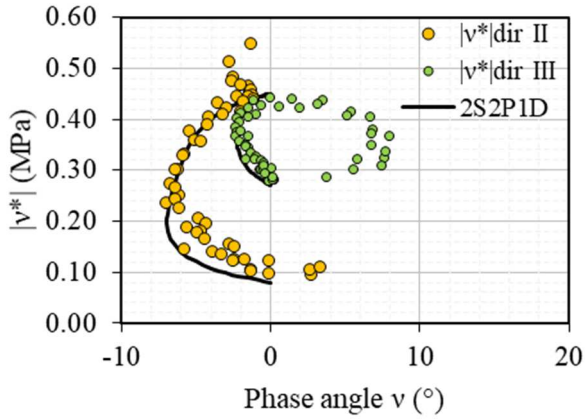

(f)

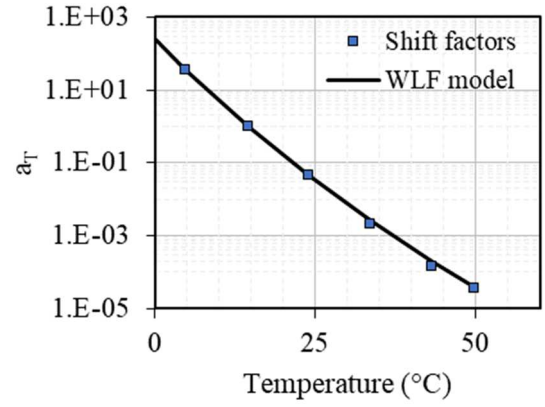

(g)

Figure A1-14. Complex modulus test results and 2S2P1D simulations for C2-H3: (a) Master curves of $|E^*|$ and φ_E, (b) Master curves of $|\nu^*|$, (c) Cole-Cole of E^*, (d) Cole-Cole of ν^*, (e) Black space of E^*, (e) Black space of ν^*, (f) shift factors with WLF model

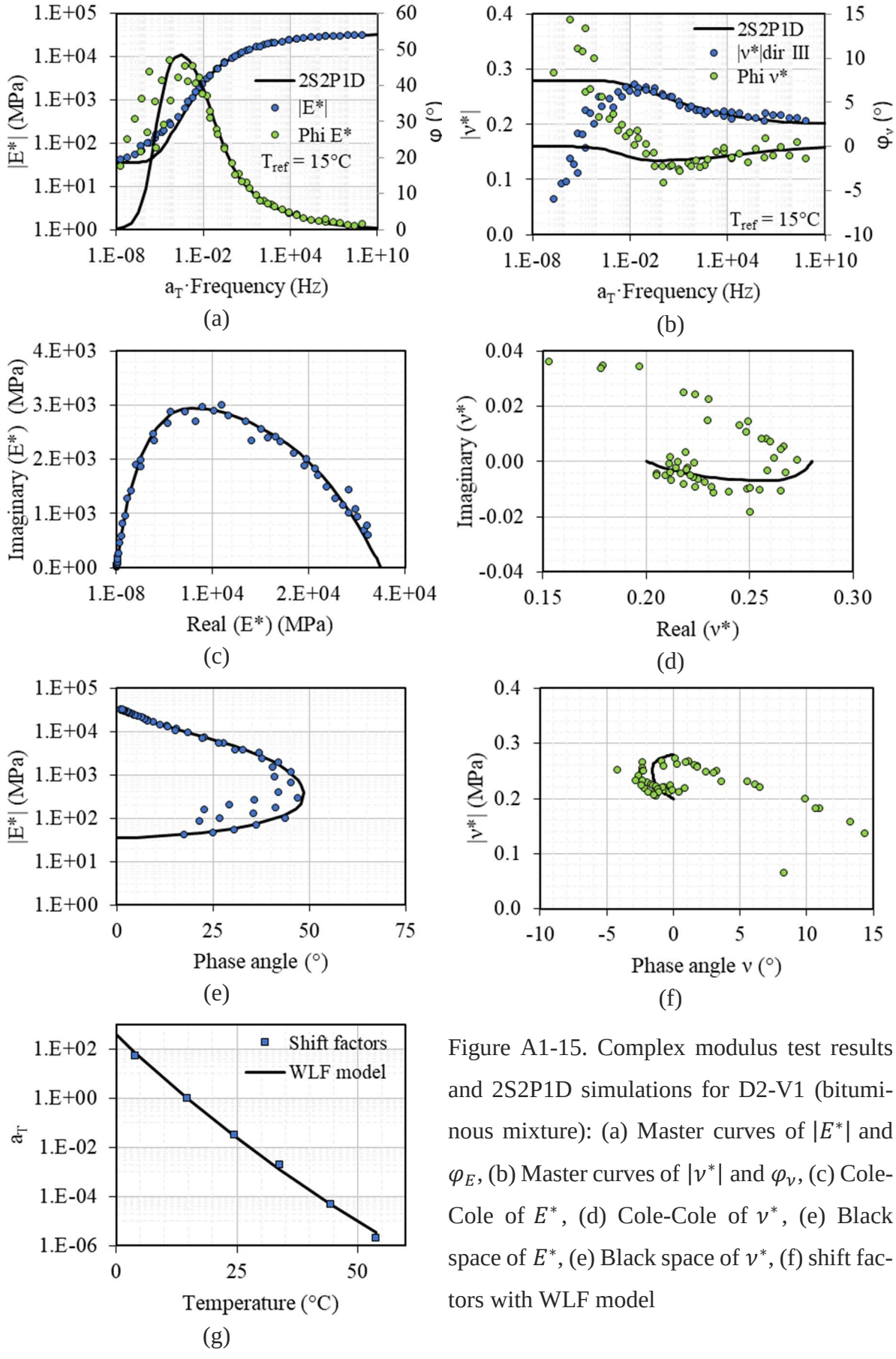

Figure A1-15. Complex modulus test results and 2S2P1D simulations for D2-V1 (bituminous mixture): (a) Master curves of $|E^*|$ and φ_E, (b) Master curves of $|\nu^*|$ and φ_ν, (c) Cole-Cole of E^*, (d) Cole-Cole of ν^*, (e) Black space of E^*, (e) Black space of ν^*, (f) shift factors with WLF model

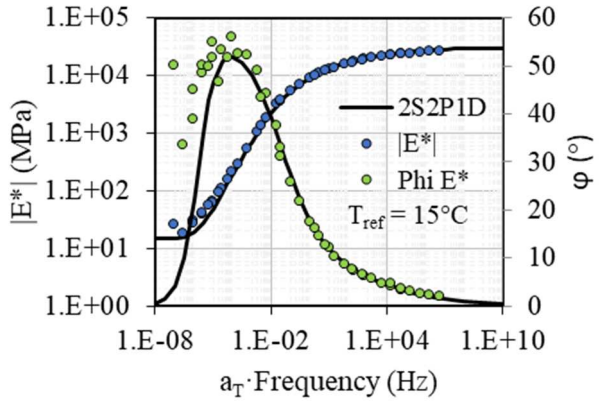

(a)

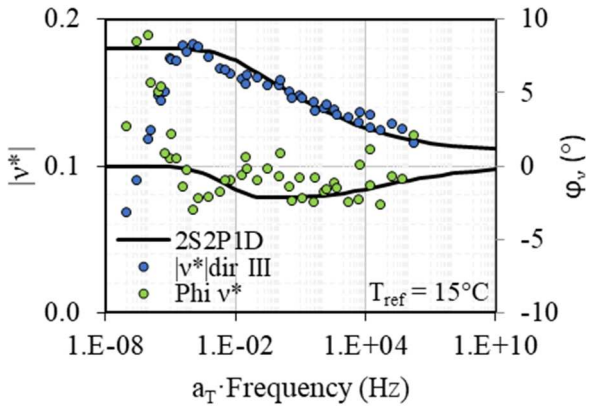

(b)

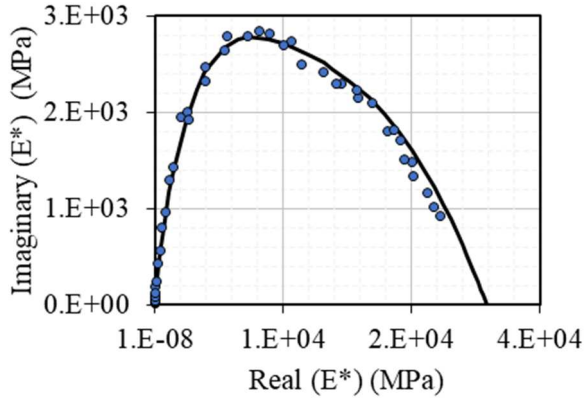

(c)

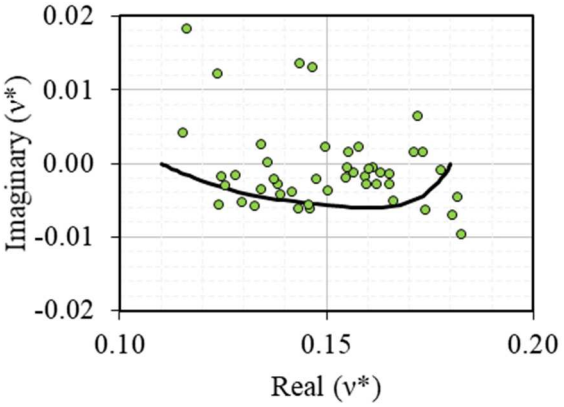

(d)

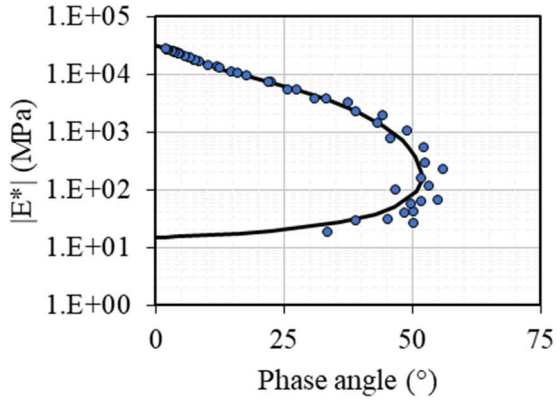

(e)

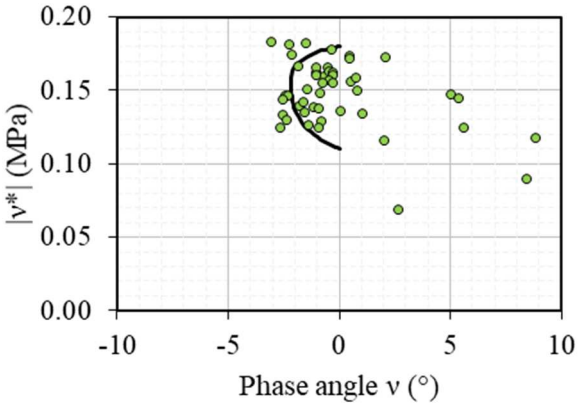

(f)

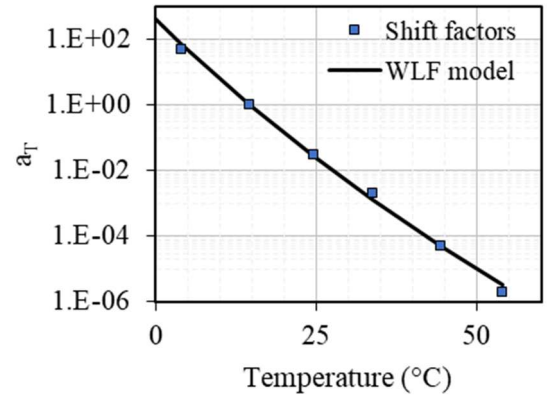

(g)

Figure A1-16. Complex modulus test results and 2S2P1D simulations for D2-V3 (bituminous mixture): (a) Master curves of $|E^*|$ and φ_E, (b) Master curves of $|\nu^*|$ and φ_ν, (c) Cole-Cole of E^*, (d) Cole-Cole of ν^*, (e) Black space of E^*, (e) Black space of ν^*, (f) shift factors with WLF model

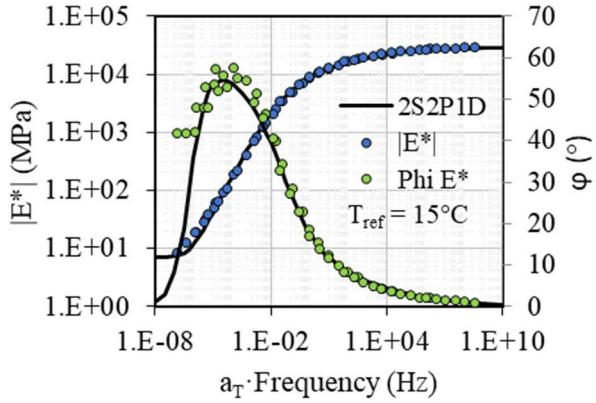

(a)

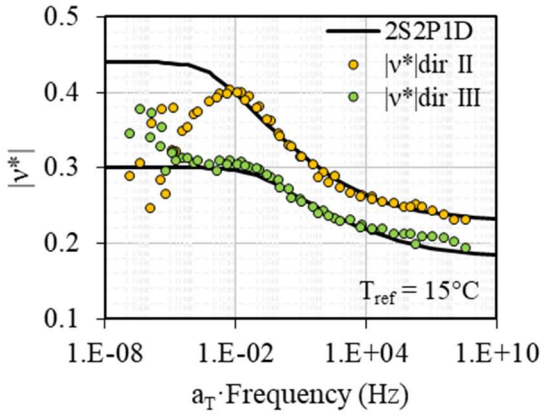

(b)

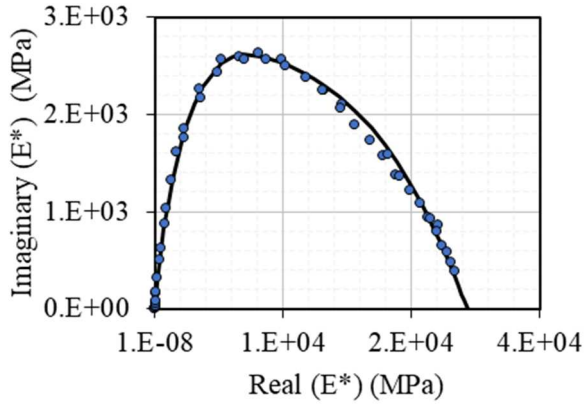

(c)

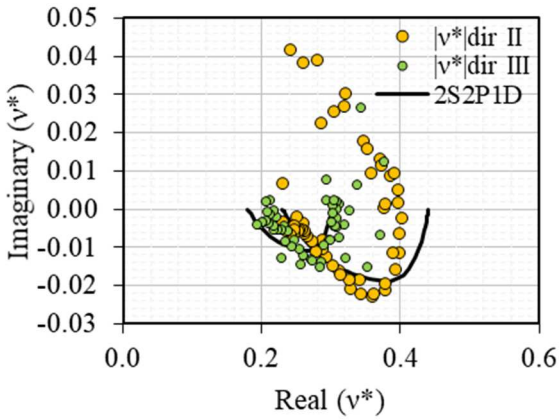

(d)

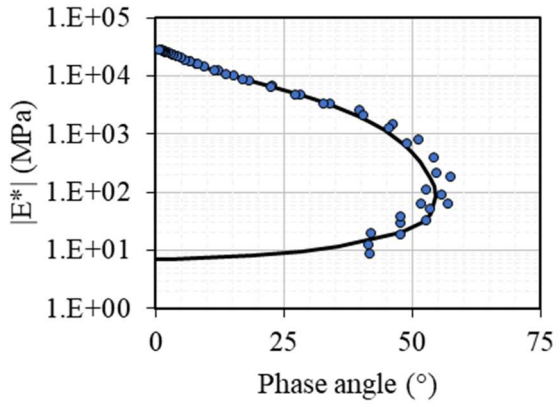

(e)

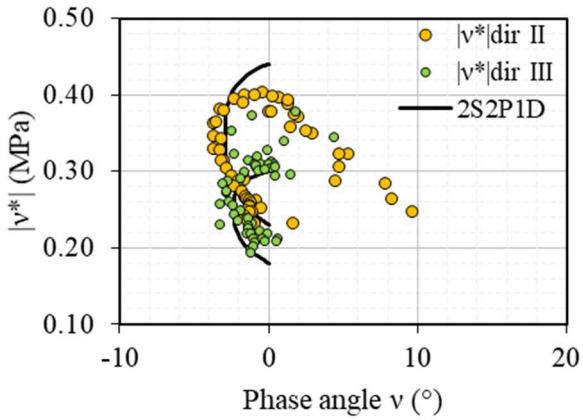

(f)

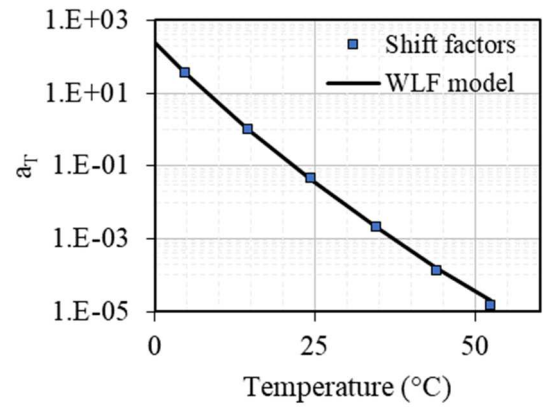

(g)

Figure A1-17. Complex modulus test results and 2S2P1D simulations for D1-H1: (a) Master curves of $|E^*|$ and φ_E, (b) Master curves of $|\nu^*|$, (c) Cole-Cole of E^*, (d) Cole-Cole of ν^*, (e) Black space of E^*, (e) Black space of ν^*, (f) shift factors with WLF model

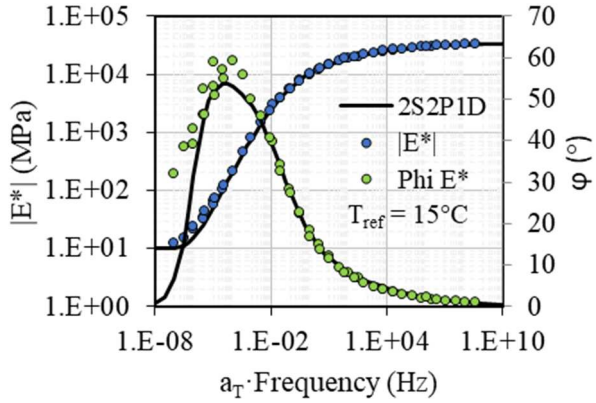

(a)

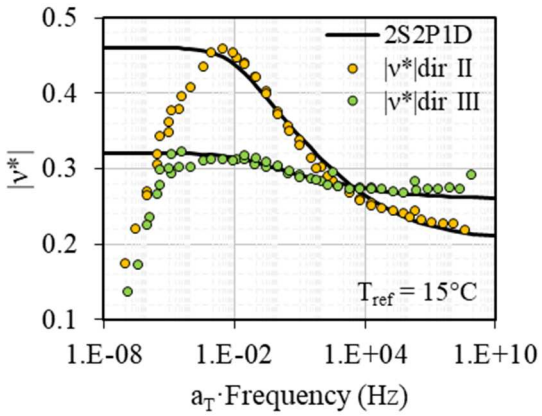

(b)

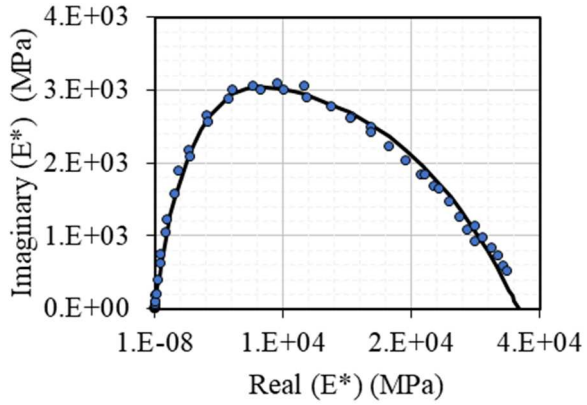

(c)

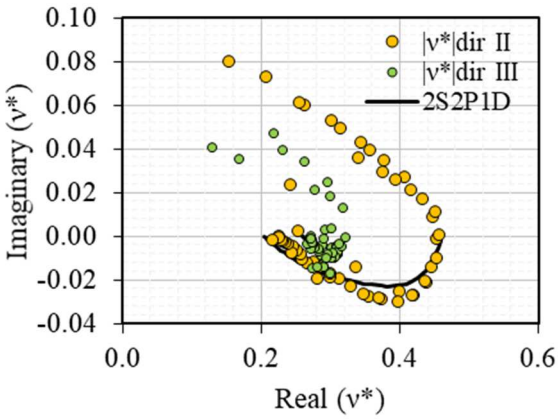

(d)

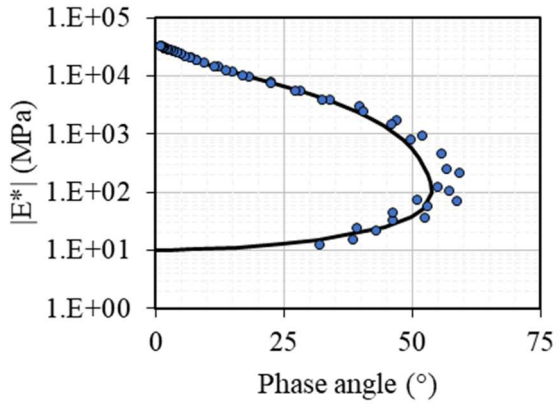

(e)

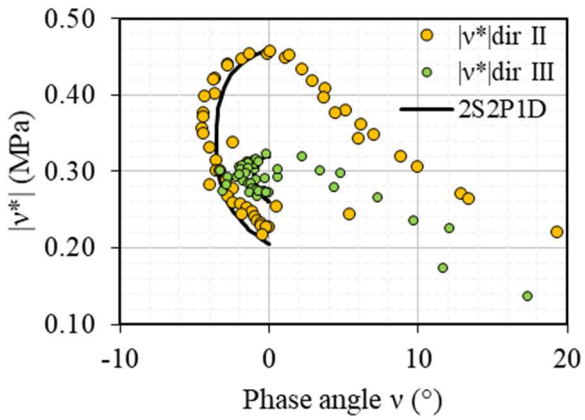

(f)

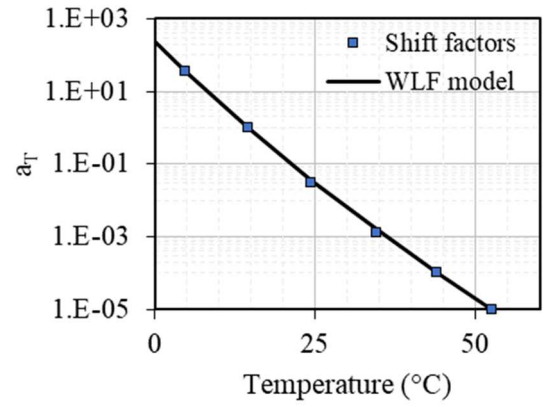

(g)

Figure A1-18. Complex modulus test results and 2S2P1D simulations for D1-H3: (a) Master curves of $|E^*|$ and φ_E, (b) Master curves of $|\nu^*|$, (c) Cole-Cole of E^*, (d) Cole-Cole of ν^*, (e) Black space of E^*, (e) Black space of ν^*, (f) shift factors with WLF model

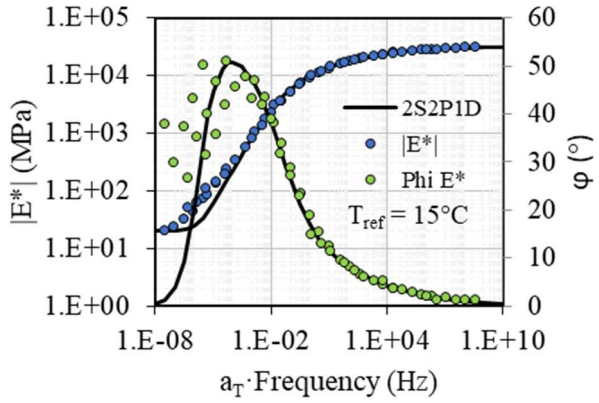

(a)

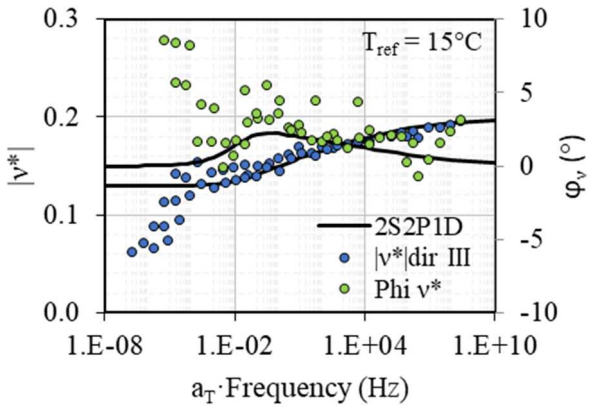

(b)

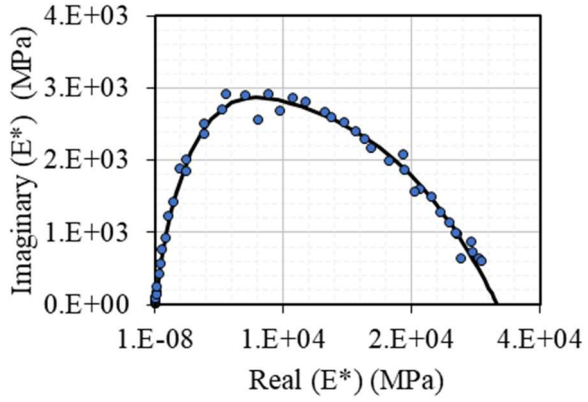

(c)

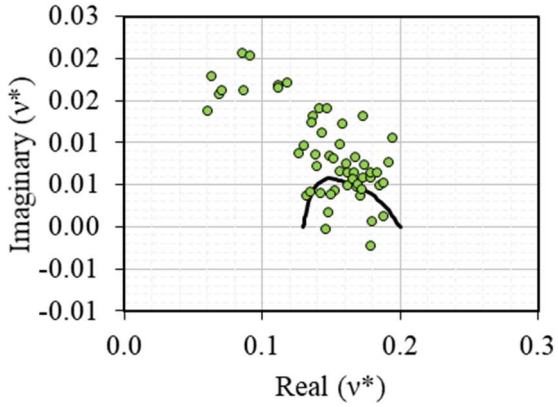

(d)

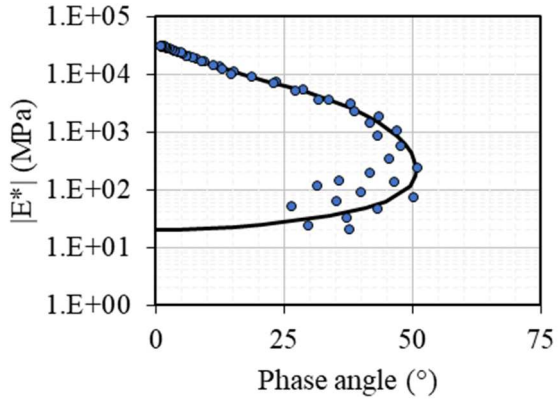

(e)

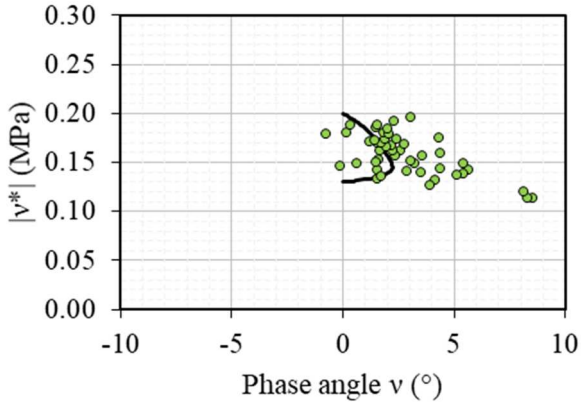

(f)

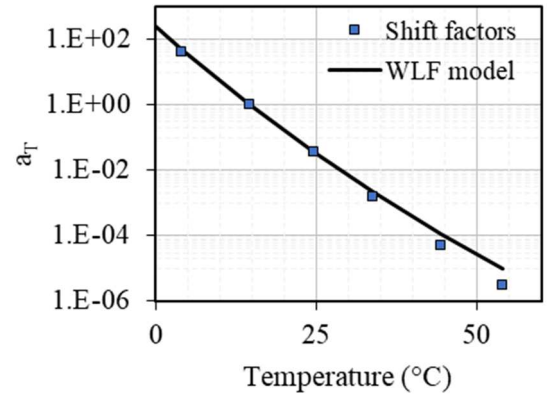

(g)

Figure A1-19. Complex modulus test results and 2S2P1D simulations for E2-V4 (bituminous mixture): (a) Master curves of $|E^*|$ and φ_E, (b) Master curves of $|\nu^*|$ and φ_ν, (c) Cole-Cole of E^*, (d) Cole-Cole of ν^*, (e) Black space of E^*, (e) Black space of ν^*, (f) shift factors with WLF model

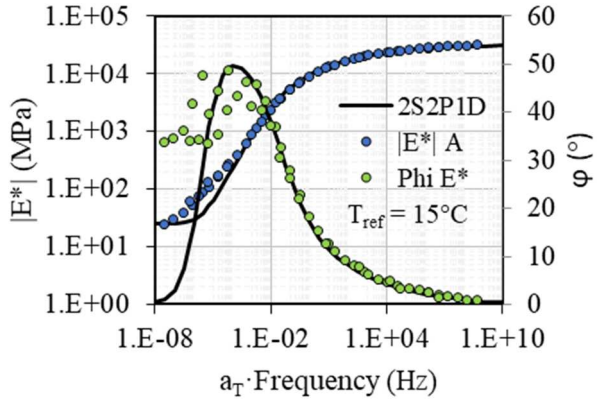

(a)

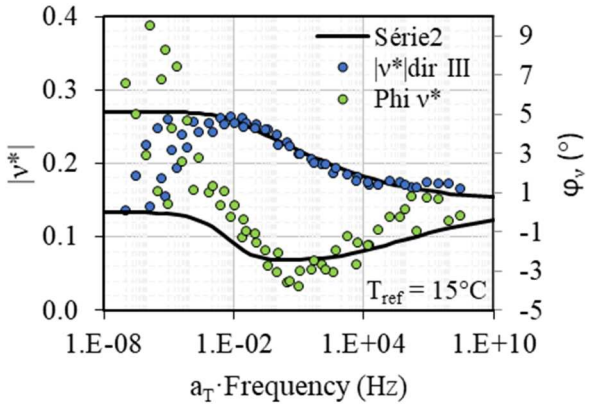

(b)

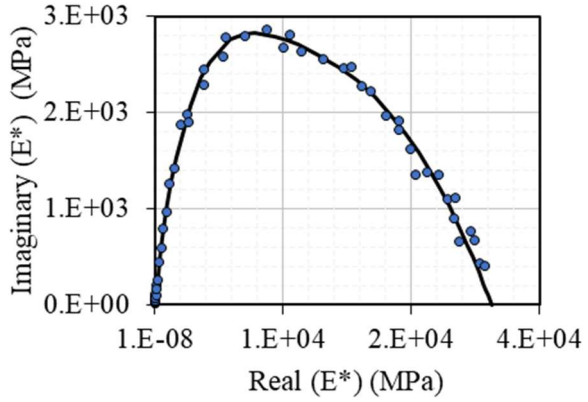

(c)

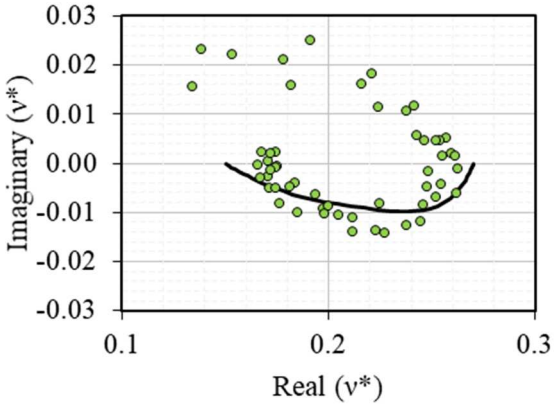

(d)

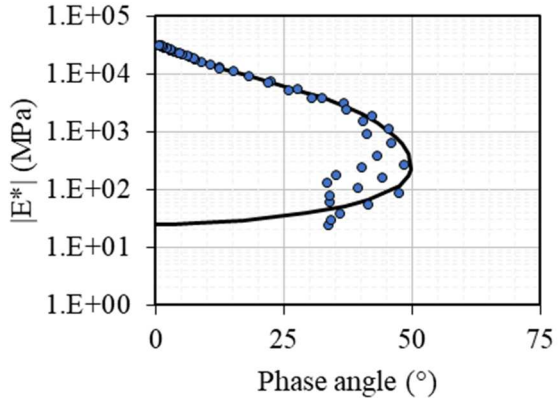

(e)

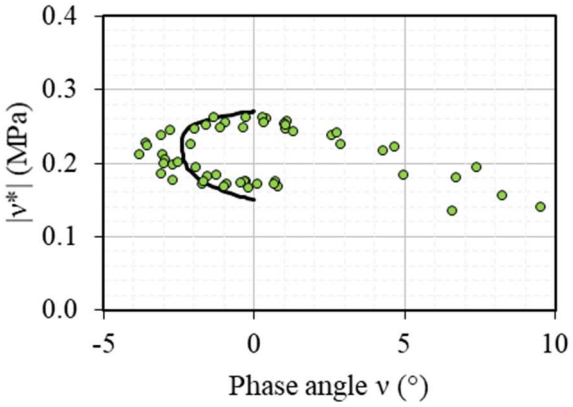

(f)

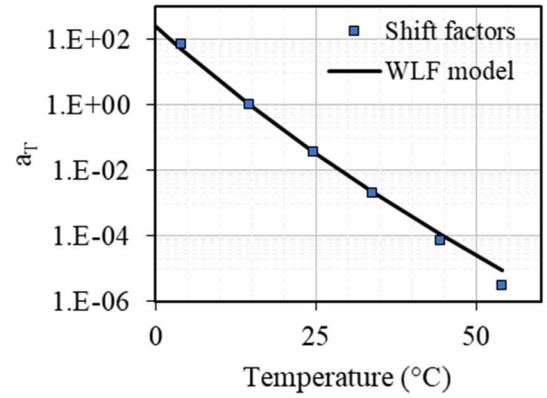

(g)

Figure A1-20. Complex modulus test results and 2S2P1D simulations for E2-V5 (bituminous mixture): (a) Master curves of $|E^*|$ and φ_E, (b) Master curves of $|\nu^*|$ and φ_ν, (c) Cole-Cole of E^*, (d) Cole-Cole of ν^*, (e) Black space of E^*, (e) Black space of ν^*, (f) shift factors with WLF model

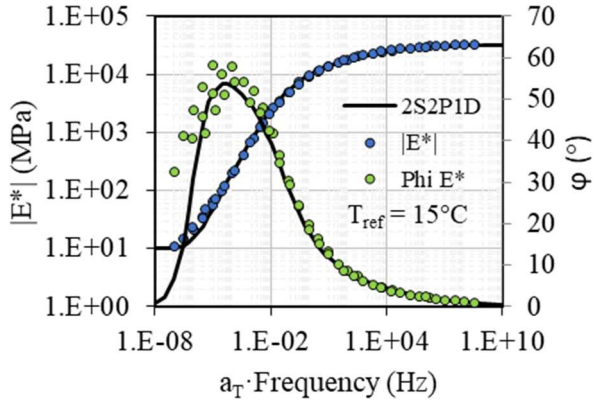

(a)

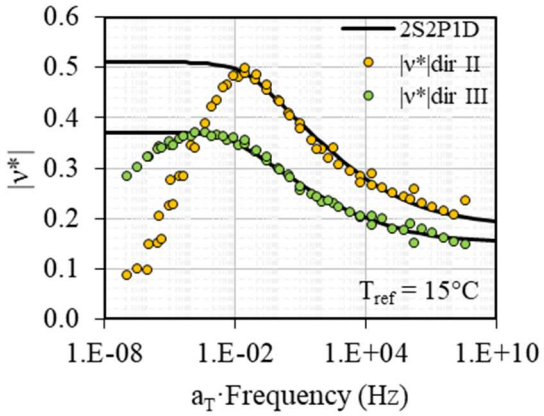

(b)

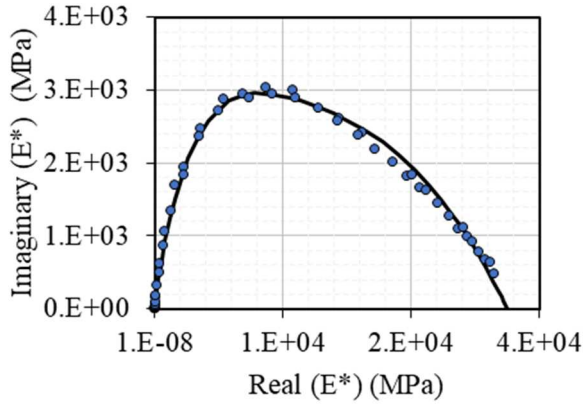

(c)

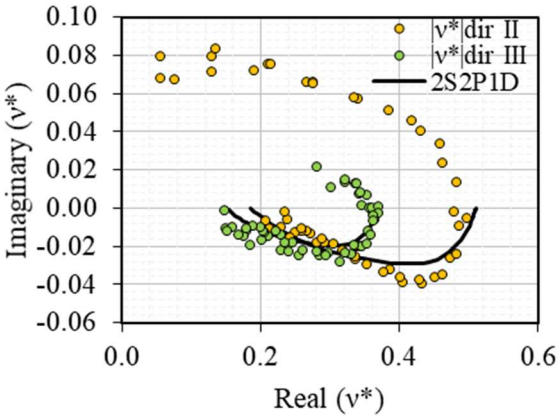

(d)

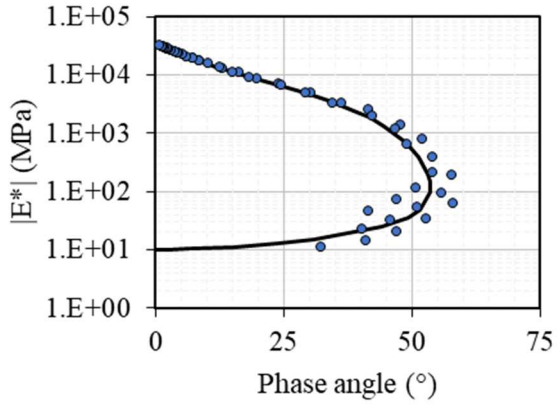

(e)

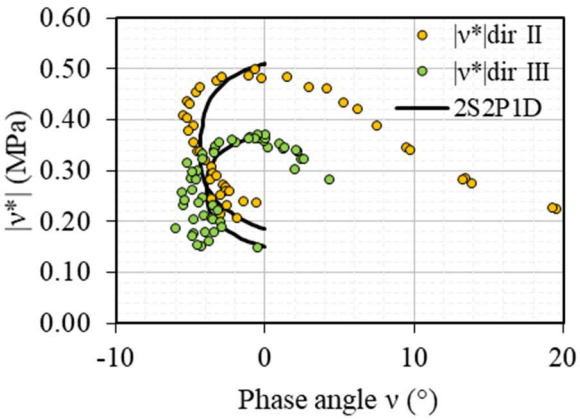

(f)

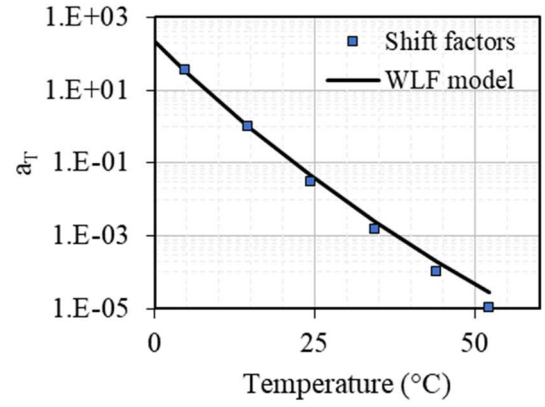

(g)

Figure A1-21. Complex modulus test results and 2S2P1D simulations for E1-H1: (a) Master curves of $|E^*|$ and φ_E, (b) Master curves of $|\nu^*|$, (c) Cole-Cole of E^*, (d) Cole-Cole of ν^*, (e) Black space of E^*, (e) Black space of ν^*, (f) shift factors with WLF model

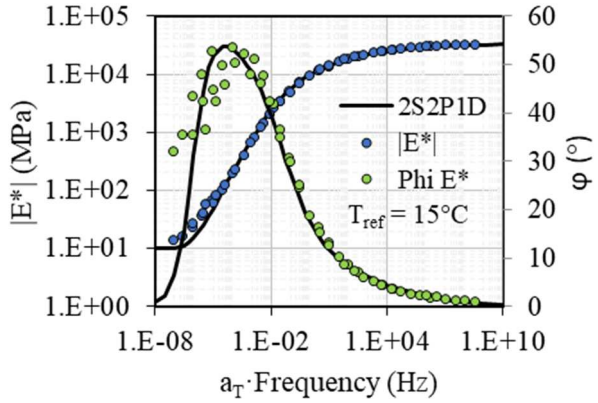

(a)

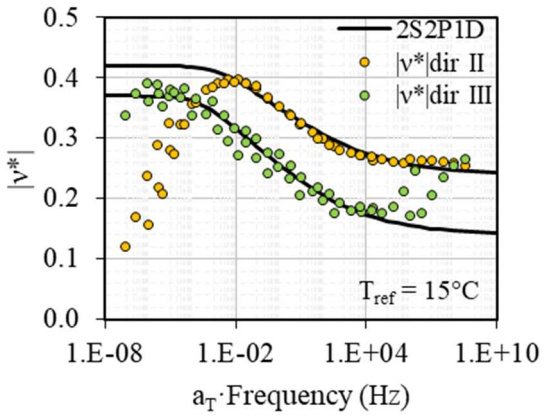

(b)

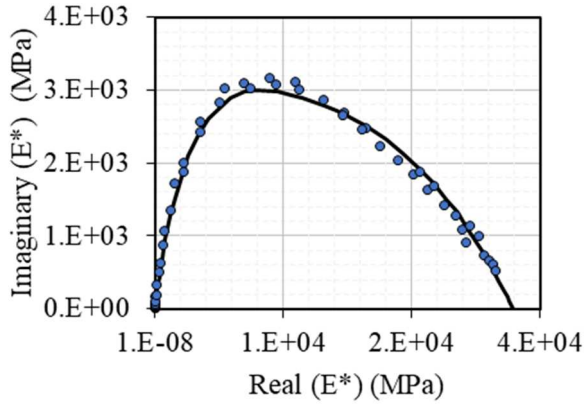

(c)

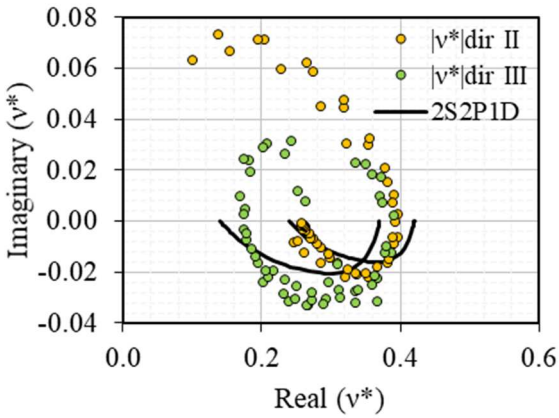

(d)

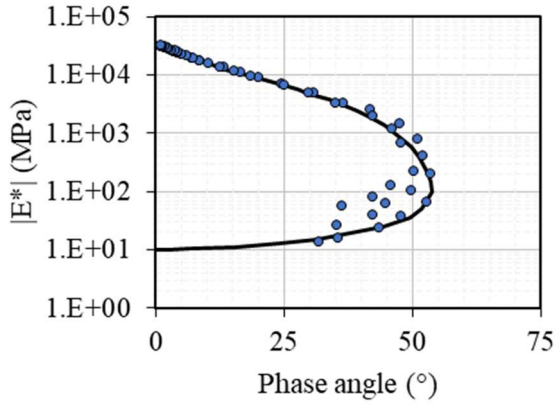

(e)

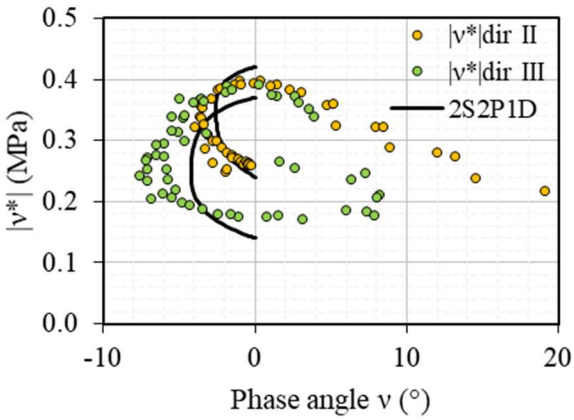

(f)

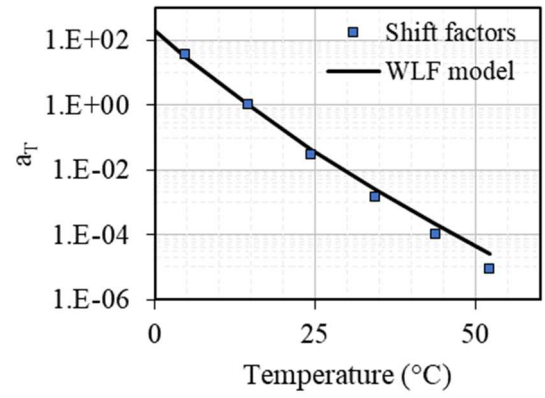

(g)

Figure A1-22. Complex modulus test results and 2S2P1D simulations for E1-H2: (a) Master curves of $|E^*|$ and φ_E, (b) Master curves of $|\nu^*|$, (c) Cole-Cole of E^*, (d) Cole-Cole of ν^*, (e) Black space of E^*, (e) Black space of ν^*, (f) shift factors with WLF model

APPENDIX A2 – COMPLEX MODULUS TEST RESULT: INTERFACES

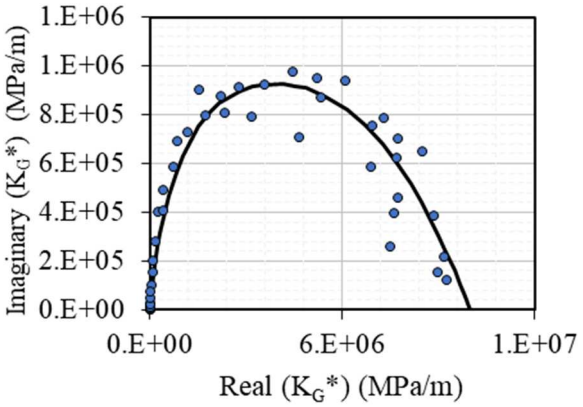

(a)

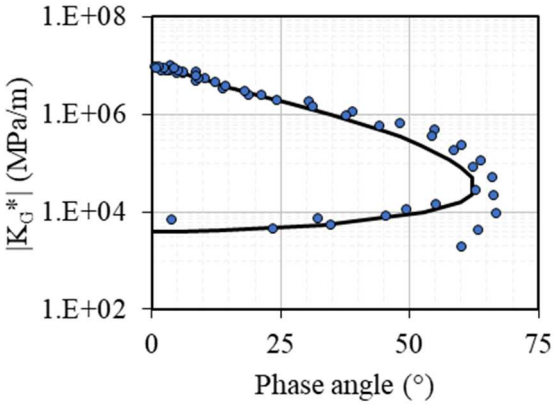

(b)

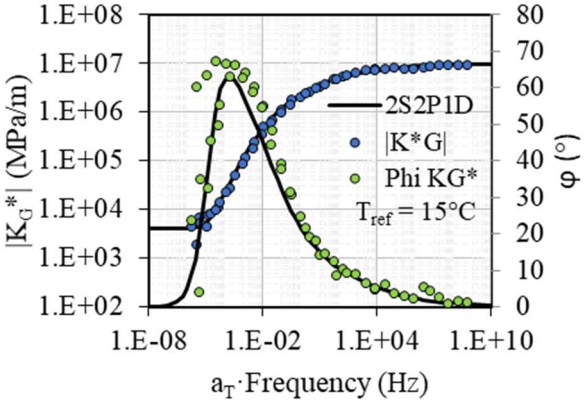

(c)

Figure A2-1. Complex modulus test results and 2S2P1D simulations of interface stiffness (K_G^*) for B2-V1: (a) Cole-Cole plot, (b) Black space, and (c) Master curves of $|K_G^*|$ and φ_{K_G}

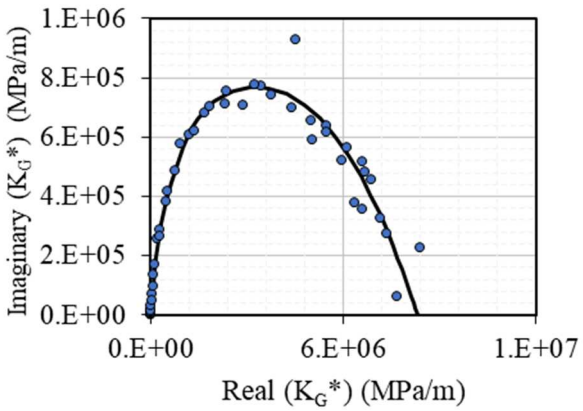

(a)

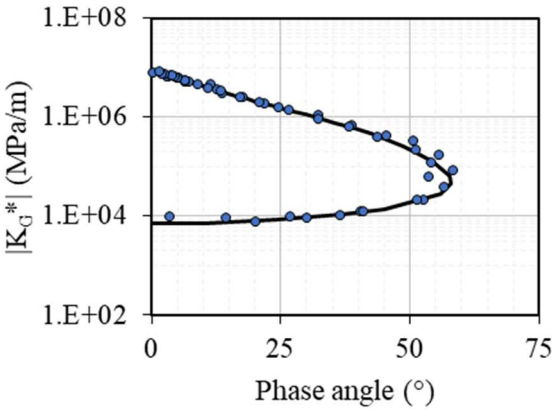

(b)

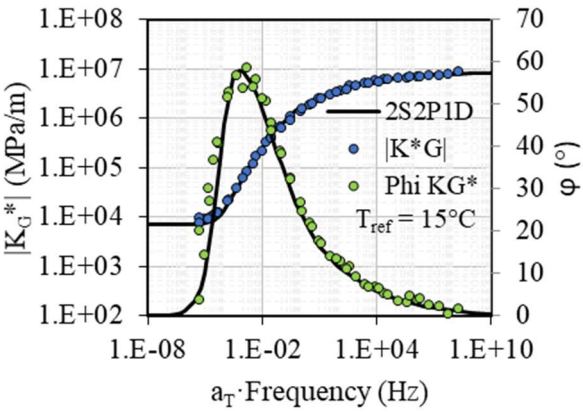

(c)

Figure A2-2. Complex modulus test results and 2S2P1D simulations of interface stiffness (K_G^*) for B2-V2: (a) Cole-Cole plot, (b) Black space, and (c) Master curves of $|K_G^*|$ and φ_{K_G}

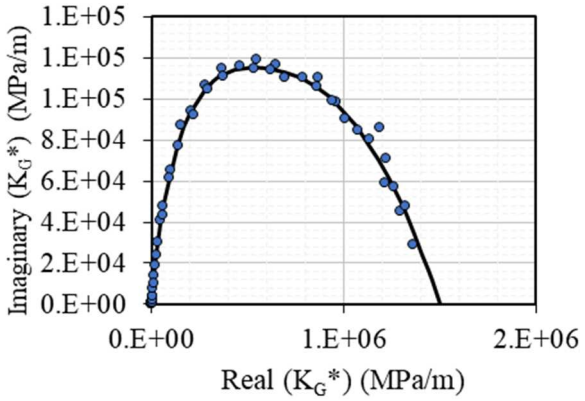

(a)

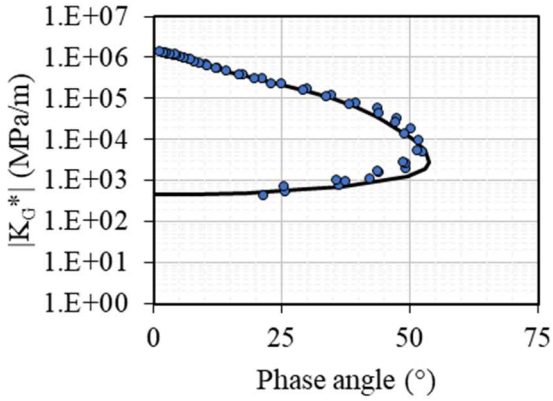

(b)

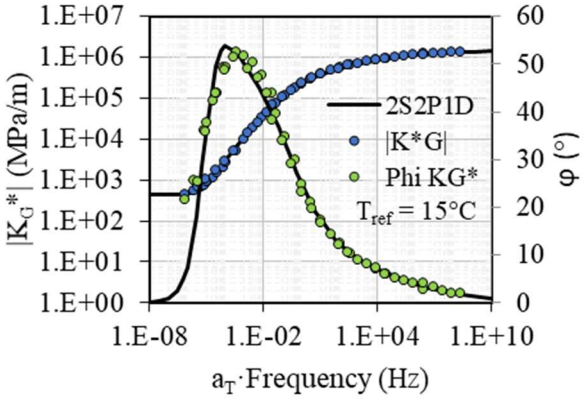

(c)

Figure A2-3. Complex modulus test results and 2S2P1D simulations of interface stiffness (K_G^*) for CE-V9: (a) Cole-Cole plot, (b) Black space, and (c) Master curves of $|K_G^*|$ and φ_{K_G}

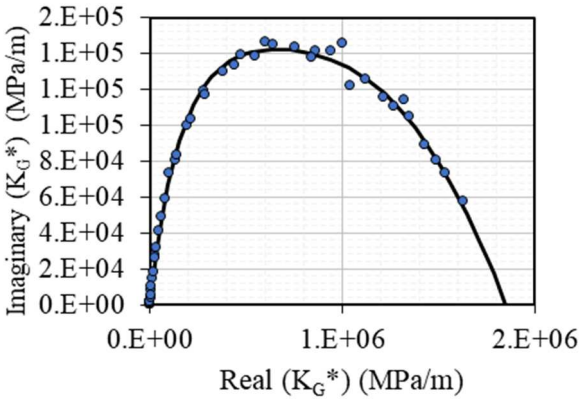

(a)

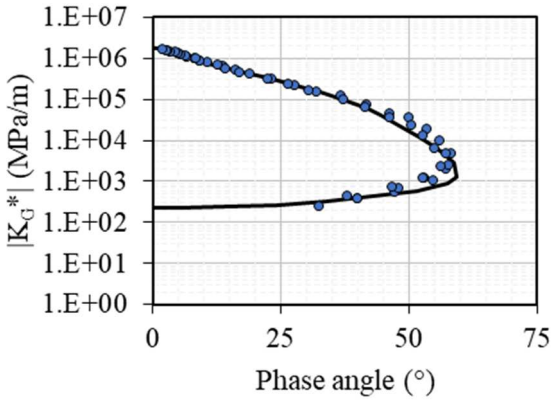

(b)

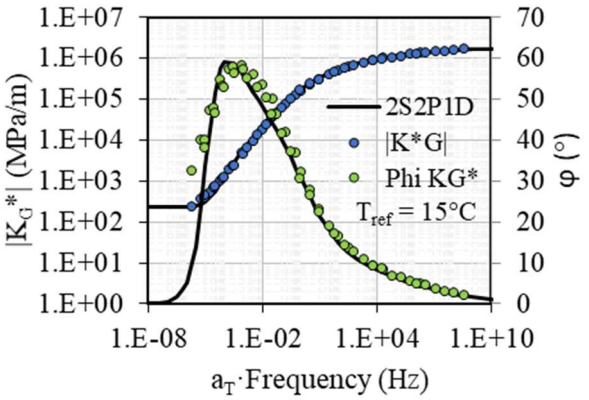

(c)

Figure A2-4. Complex modulus test results and 2S2P1D simulations of interface stiffness (K_G^*) for CE-V10: (a) Cole-Cole plot, (b) Black space, and (c) Master curves of $|K_G^*|$ and φ_{K_G}

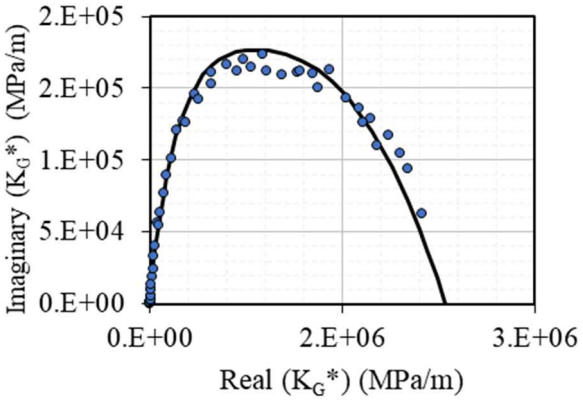

(a)

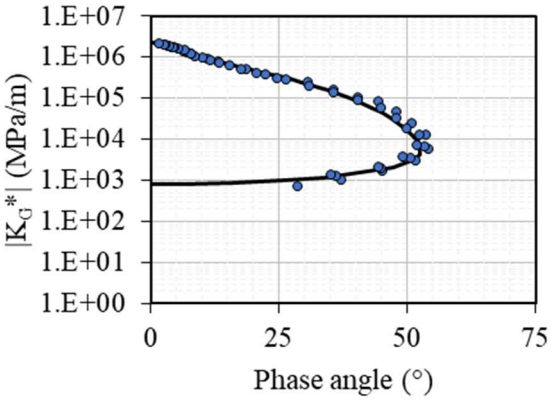

(b)

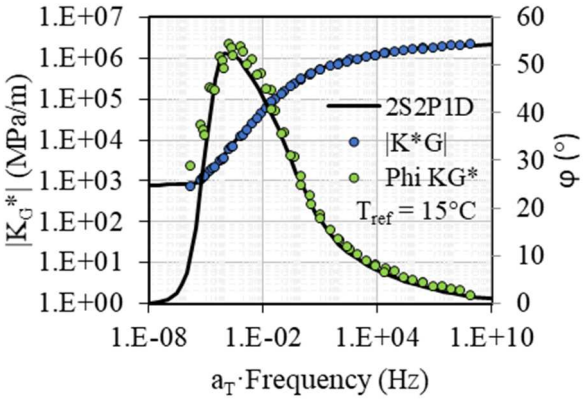

(c)

Figure A2-5. Complex modulus test results and 2S2P1D simulations of interface stiffness (K_G^*) for C1-V6: (a) Cole-Cole plot, (b) Black space, and (c) Master curves of $|K_G^*|$ and φ_{K_G}

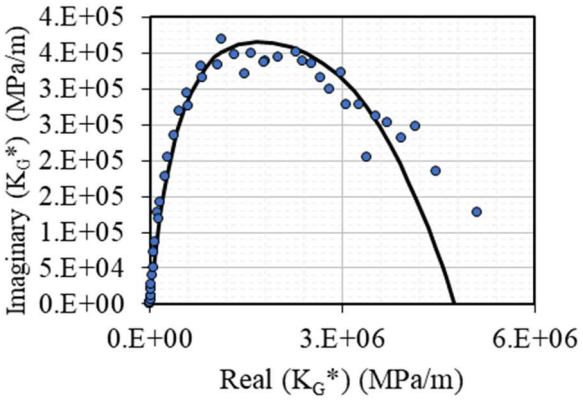

(a)

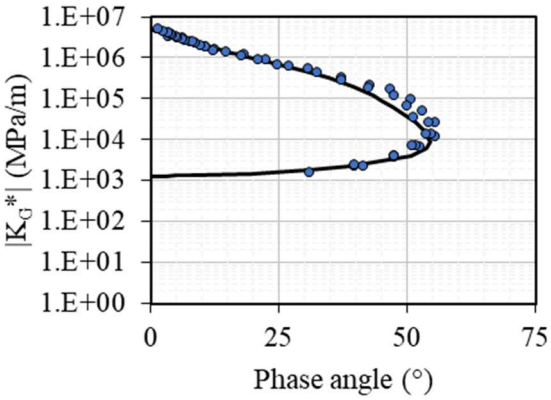

(b)

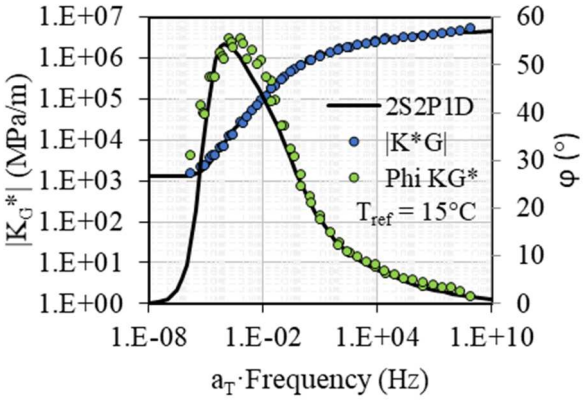

(c)

Figure A2-6. Complex modulus test results and 2S2P1D simulations of interface stiffness (K_G^*) for C2-V1: (a) Cole-Cole plot, (b) Black space, and (c) Master curves of $|K_G^*|$ and φ_{K_G}

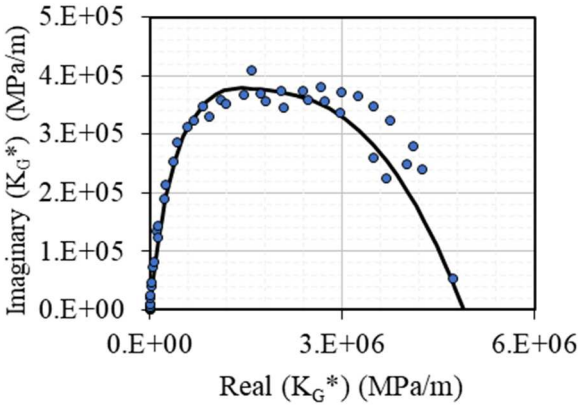

(a)

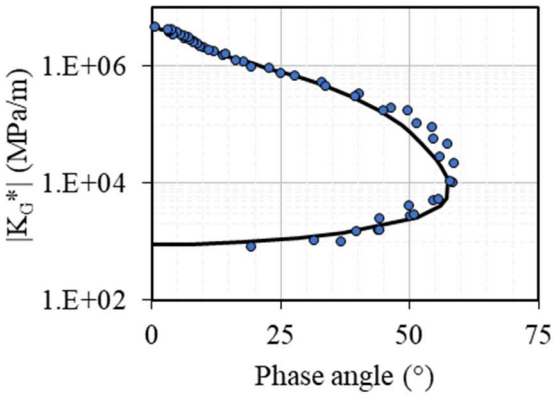

(b)

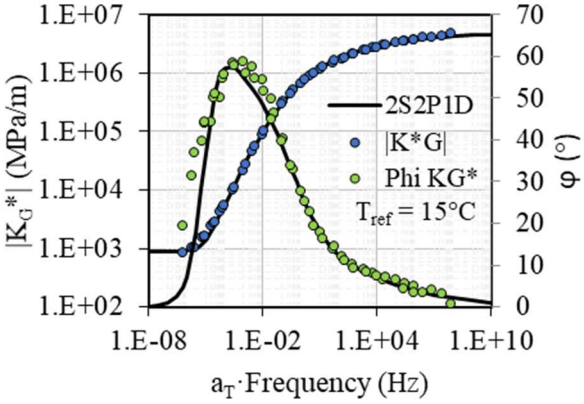

(c)

Figure A2-7. Complex modulus test results and 2S2P1D simulations of interface stiffness (K_G^*) for D2-V1: (a) Cole-Cole plot, (b) Black space, and (c) Master curves of $|K_G^*|$ and φ_{K_G}

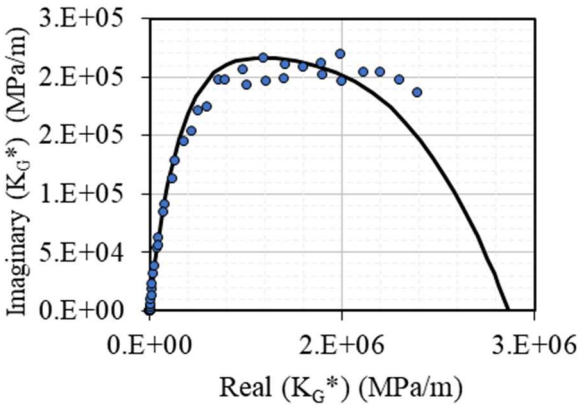

(a)

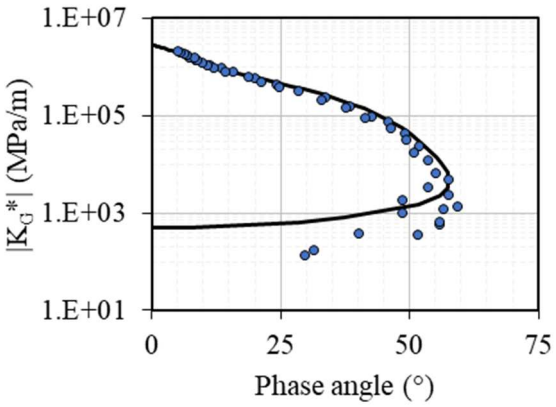

(b)

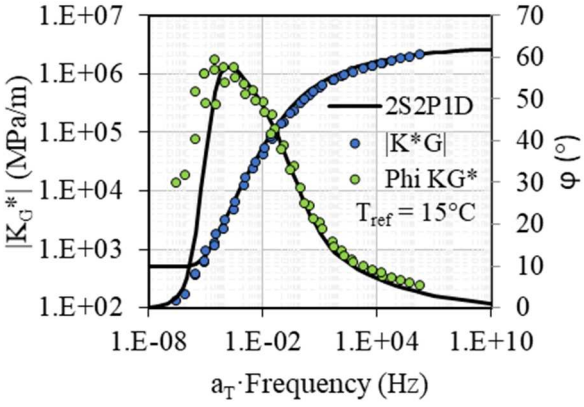

(c)

Figure A2-8. Complex modulus test results and 2S2P1D simulations of interface stiffness (K_G^*) for D2-V3: (a) Cole-Cole plot, (b) Black space, and (c) Master curves of $|K_G^*|$ and φ_{K_G}

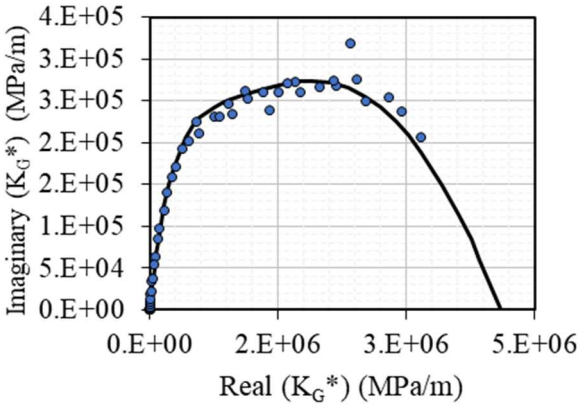

(a)

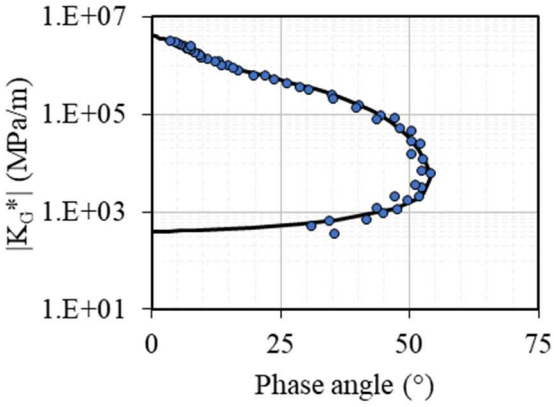

(b)

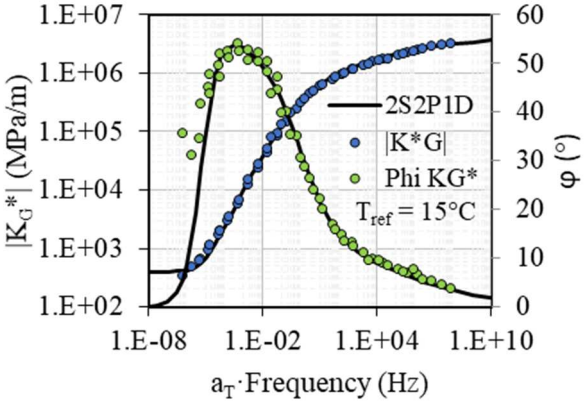

(c)

Figure A2-9. Complex modulus test results and 2S2P1D simulations of interface stiffness (K_G^*) for E2-V4: (a) Cole-Cole plot, (b) Black space, and (c) Master curves of $|K_G^*|$ and φ_{K_G}

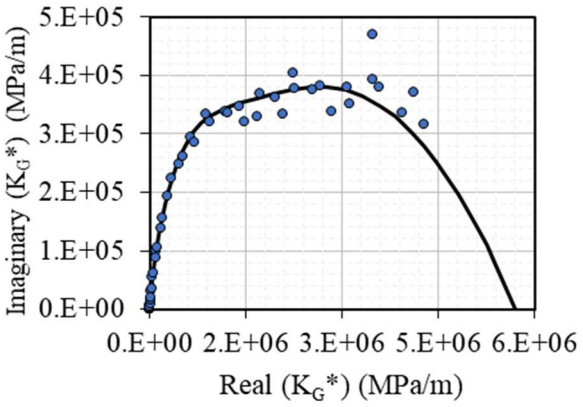

(a)

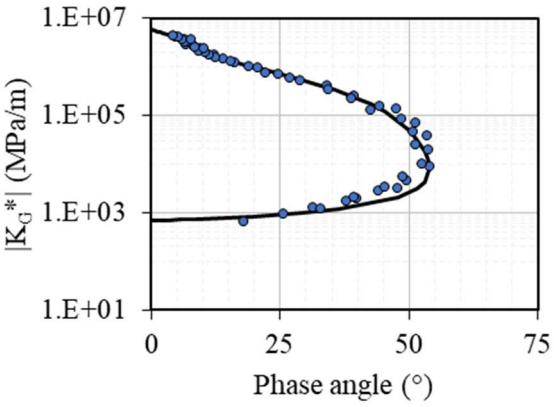

(b)

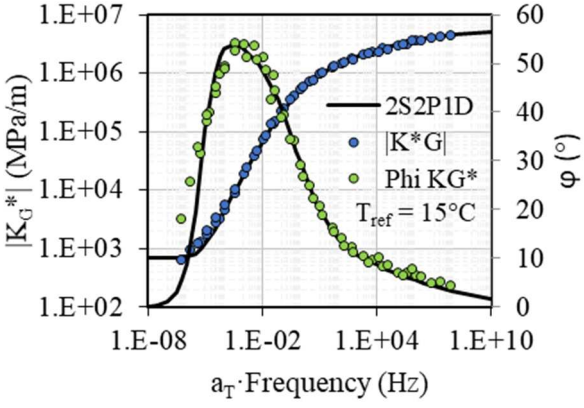

(c)

Figure A2-10. Complex modulus test results and 2S2P1D simulations of interface stiffness (K_G^*) for E2-V5: (a) Cole-Cole plot, (b) Black space, and (c) Master curves of $|K_G^*|$ and φ_{K_G}

APPENDIX B1 – TENSION TEST RESULTS

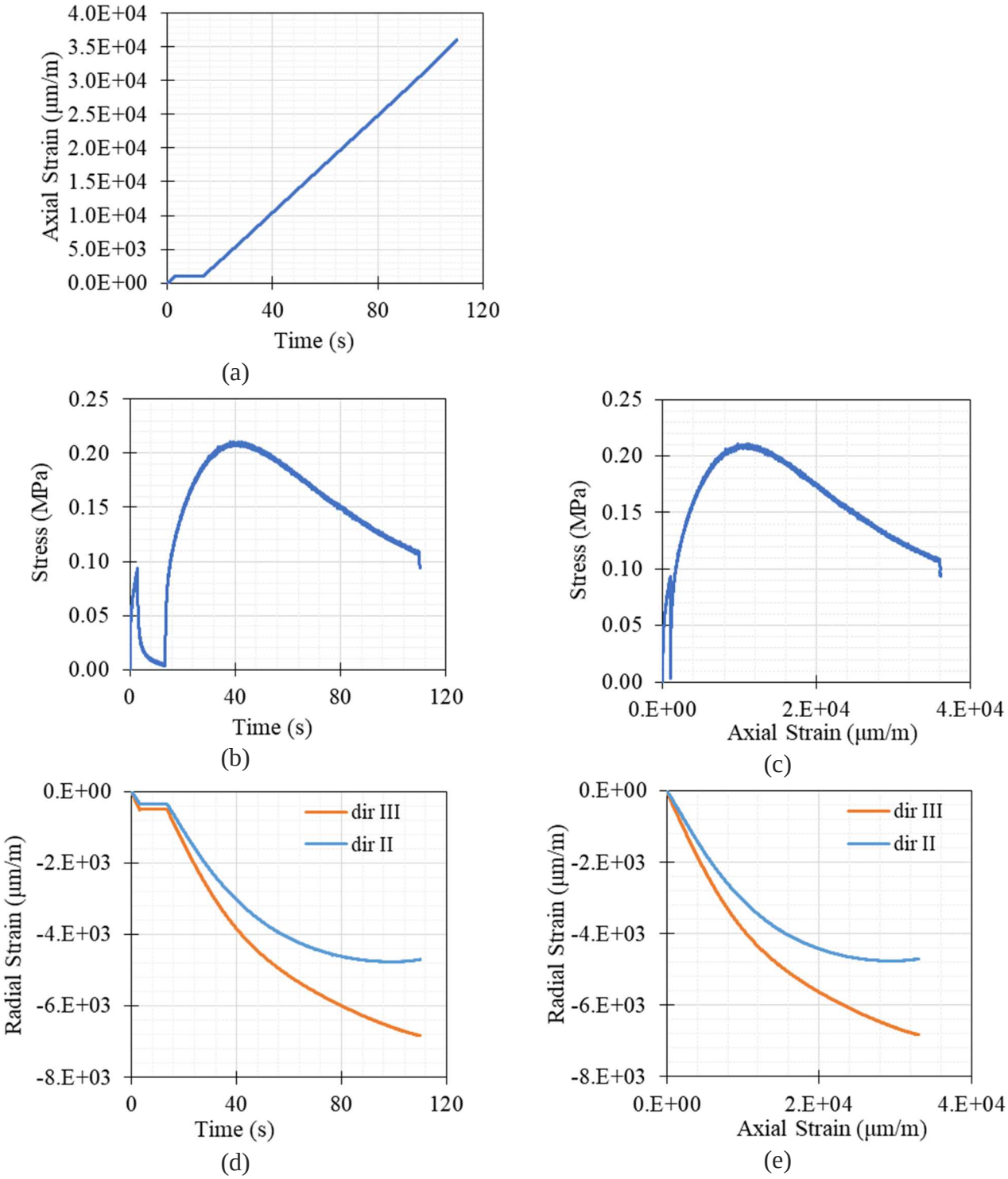

Figure B1-1. Tension test result of A1-H2 at 40°C and 2%/min strain rate

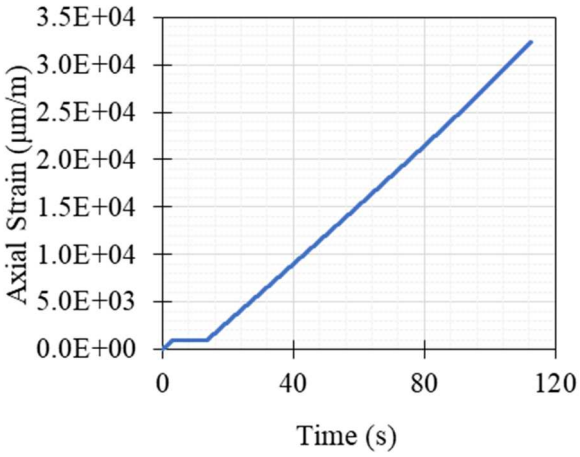

(a)

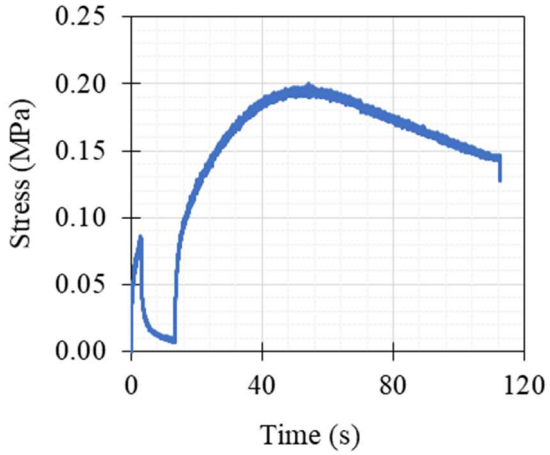

(b)

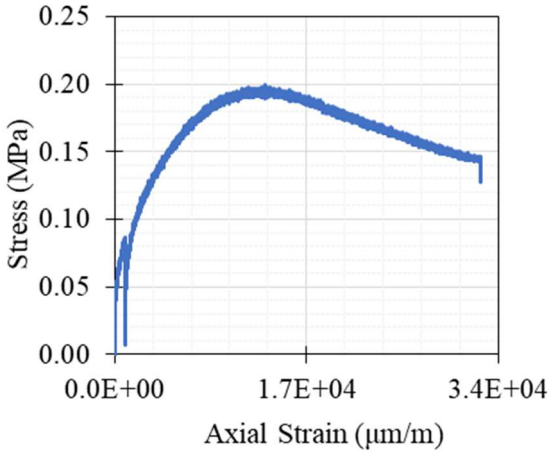

(c)

Figure B1-2. Tension test result of A1-H11 at 40°C and 2%/min strain rate

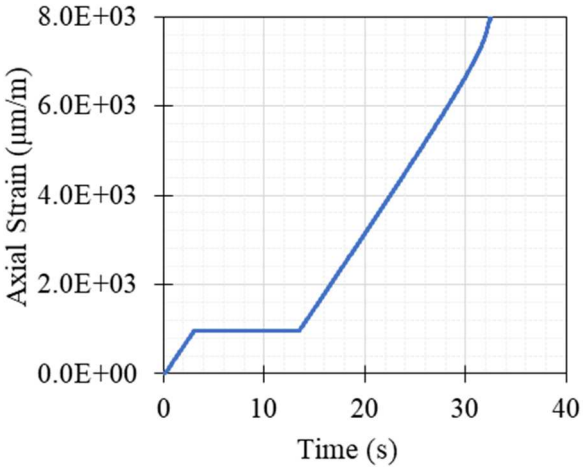

(a)

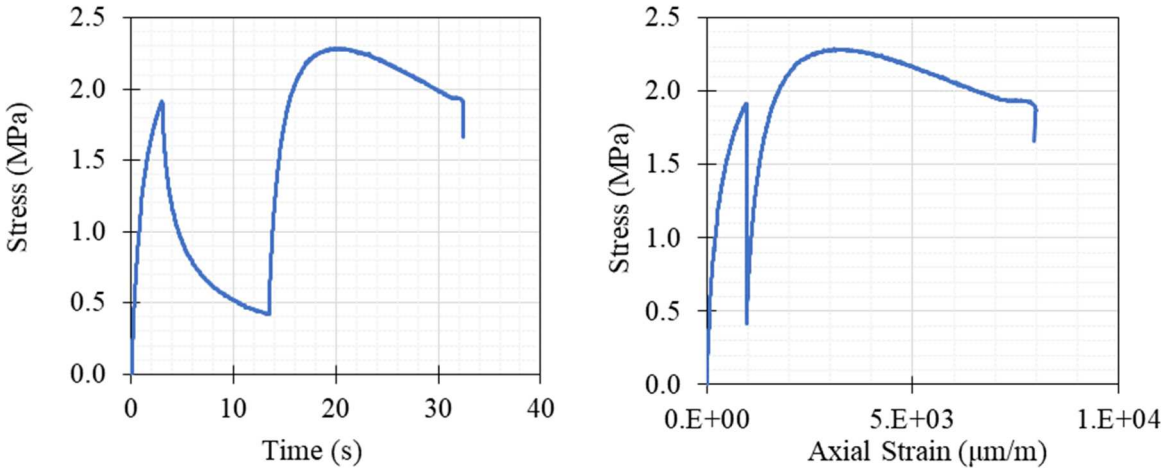

(b) (c)

Figure B1-3. Tension test result of A3-H4 at 19°C and 2%/min strain rate

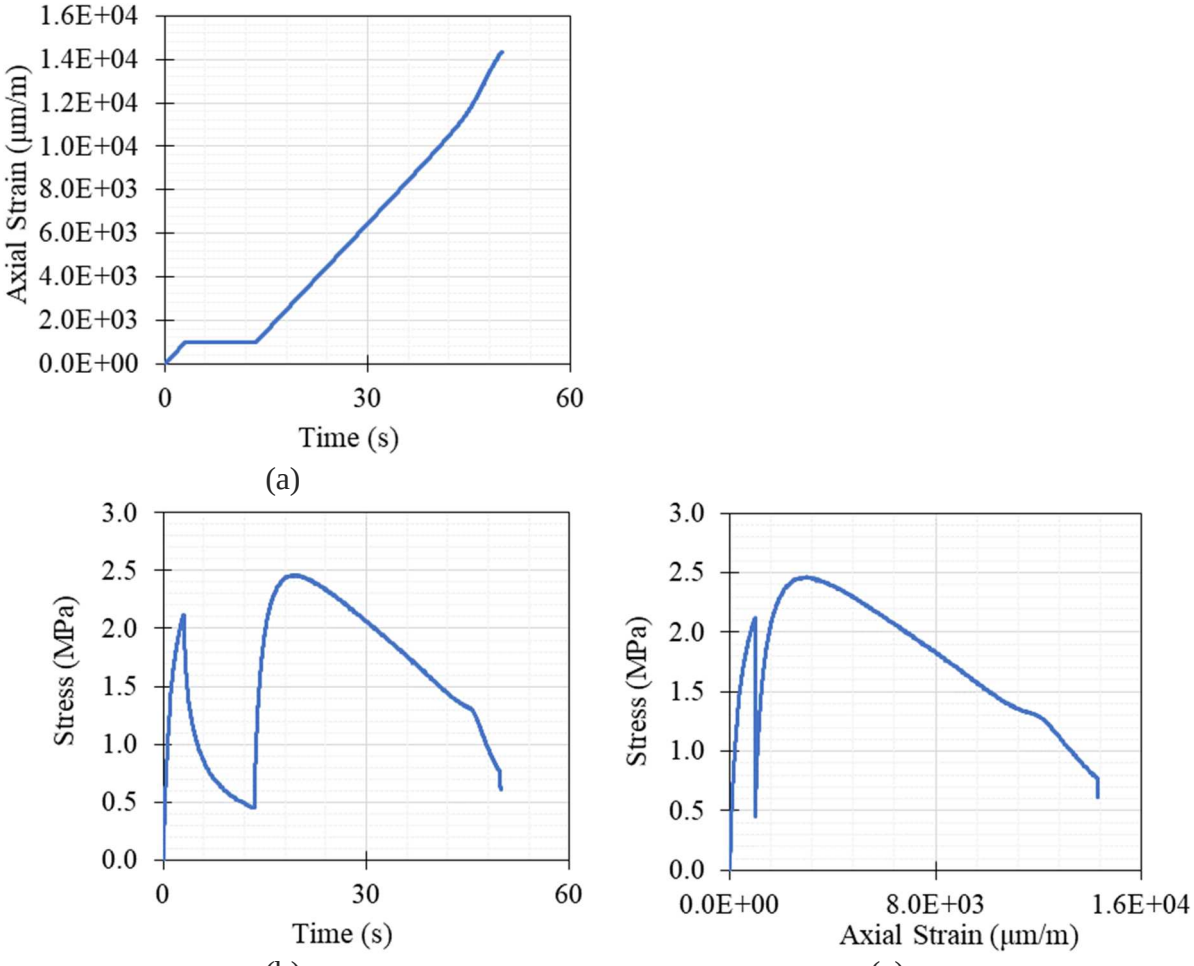

(a)

(b) (c)

Figure B1-4. Tension test result of A3-H7 at 19°C and 2%/min strain rate

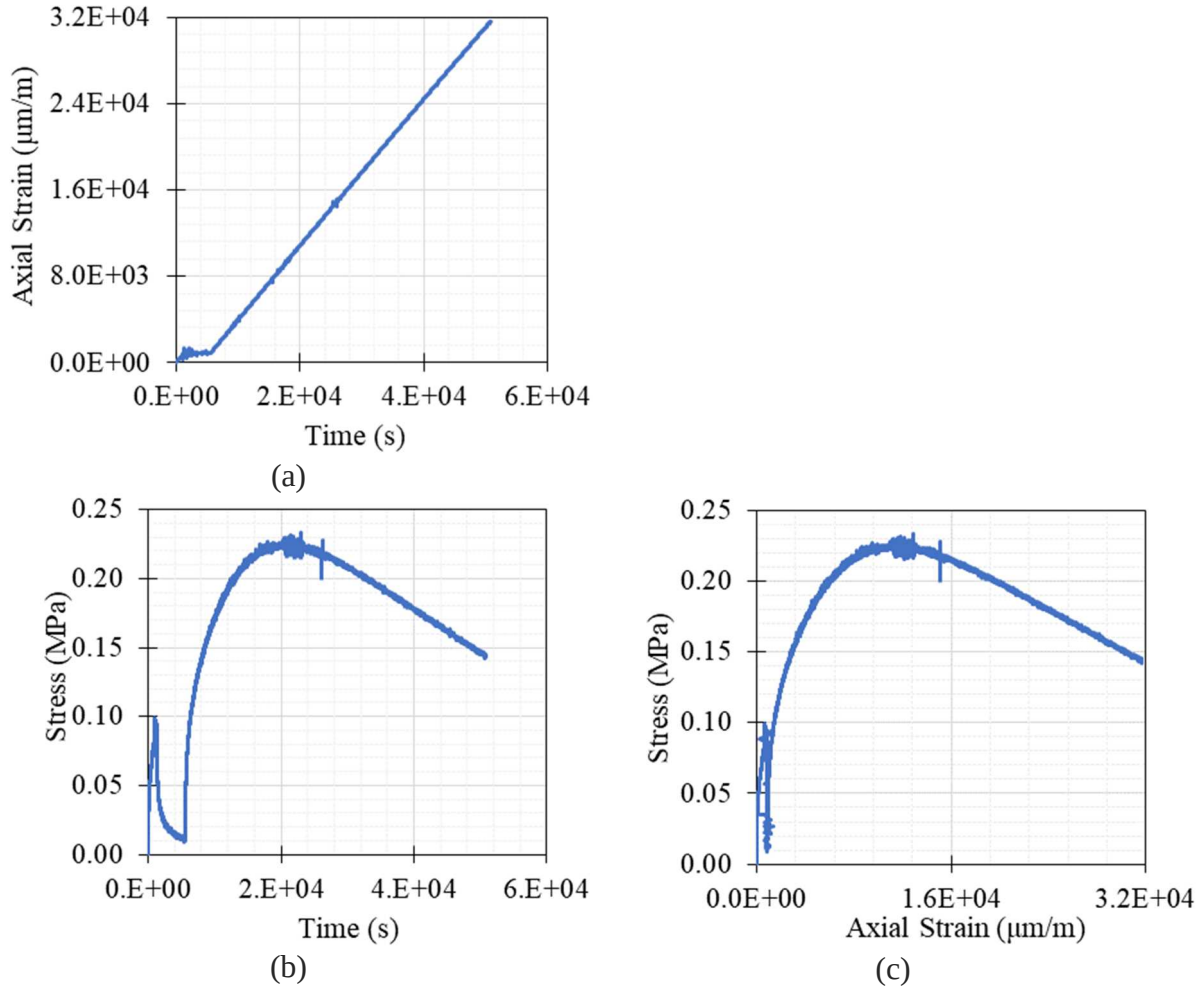

Figure B1-5. Tension test result of A3-H5 at 19°C and 0.005%/min strain rate

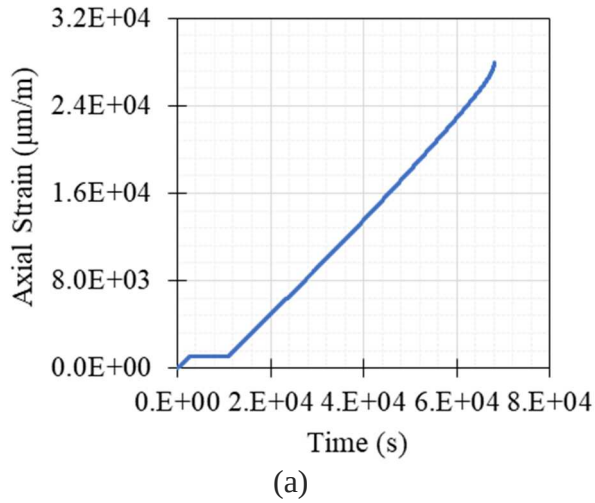

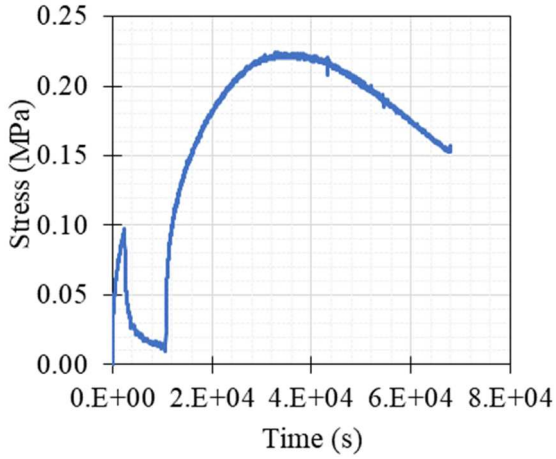

(b)

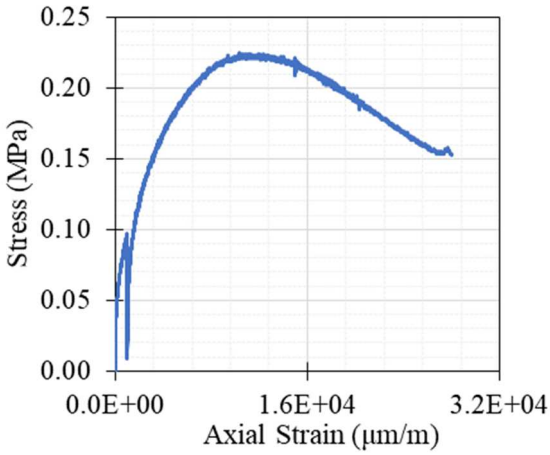

(c)

Figure B1-6. Tension test result of A3-H10 at 19°C and 0.002%/min strain rate

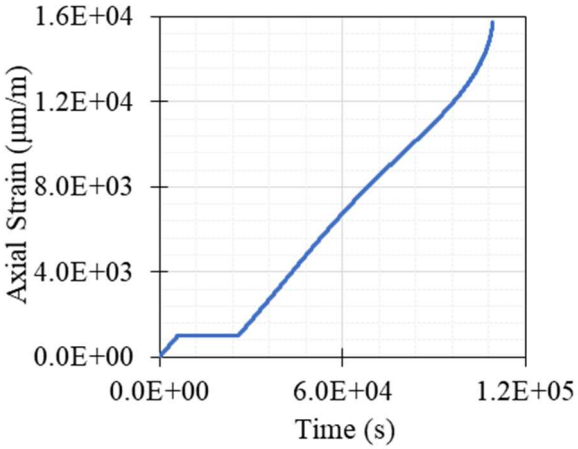

(a)

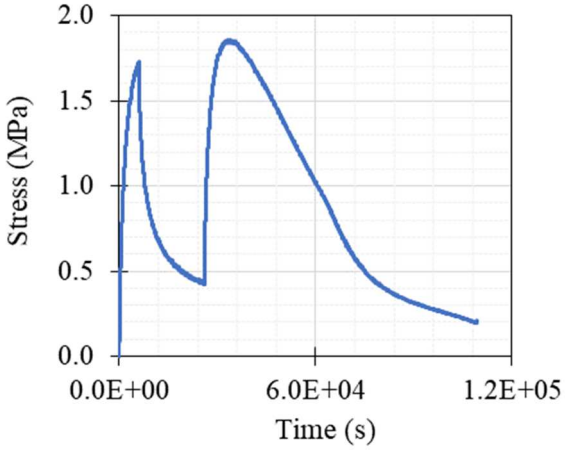

(b)

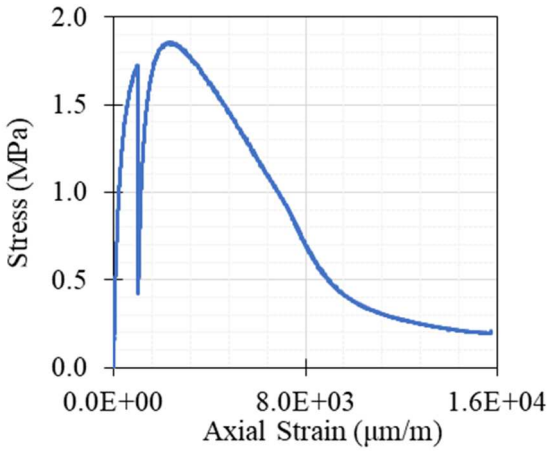

(c)

Figure B1-7. Tension test result of A3-H6 at 0°C and 0.001%/min strain rate

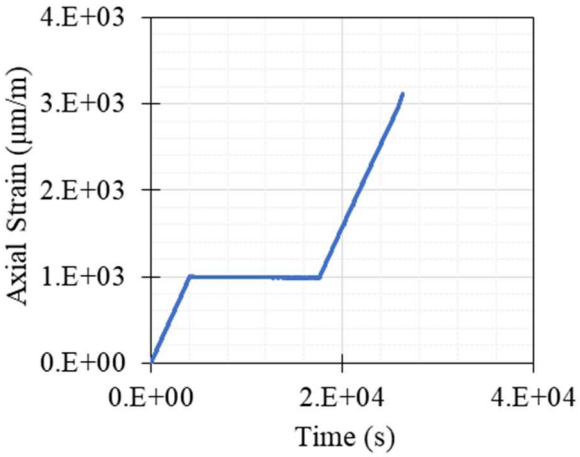

(a)

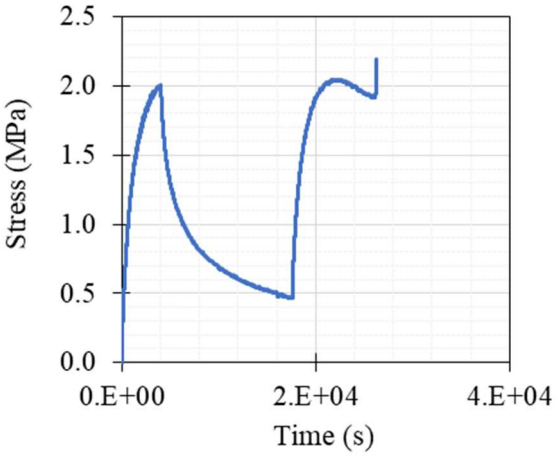

(b)

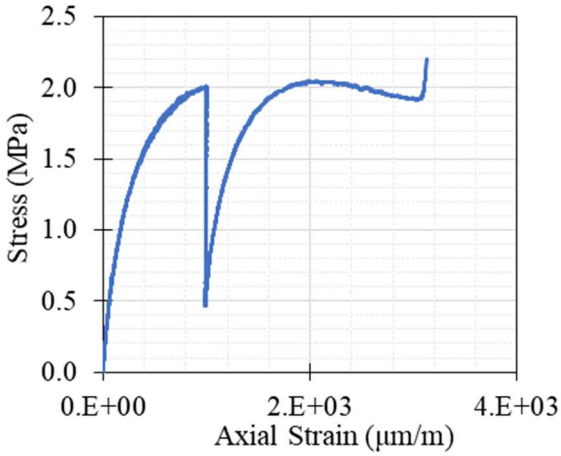

(c)

Figure B1-8. Tension test result of A3-H9 at 0°C and 0.002%/min strain rate

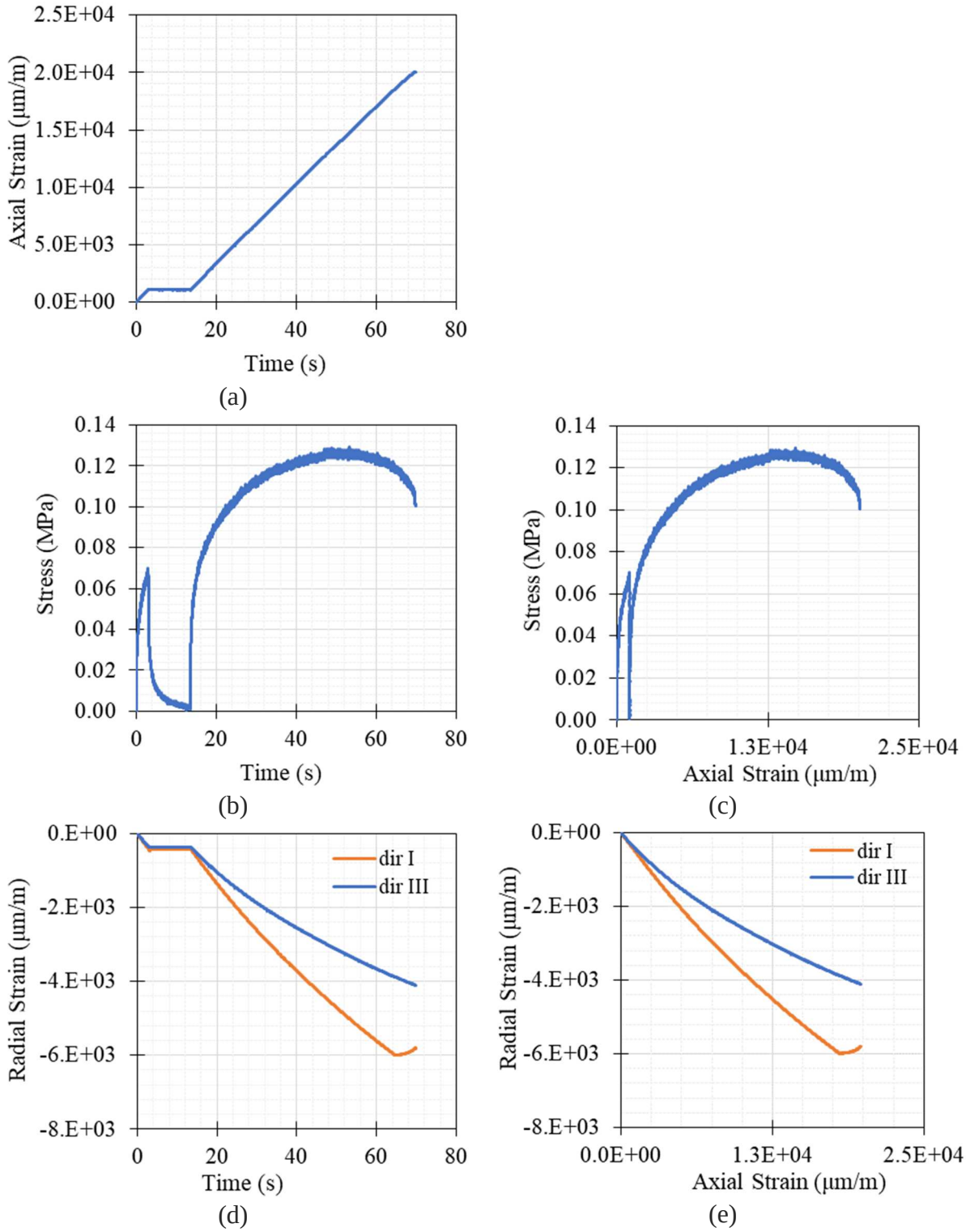

Figure B1-9. Tension test result of A1-V4 at 40°C and 2%/min strain rate

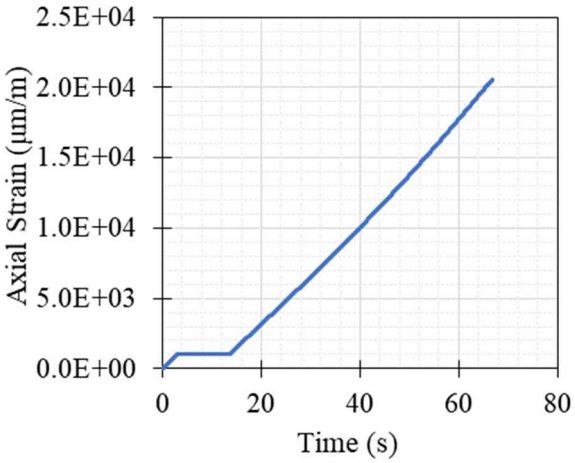

(a)

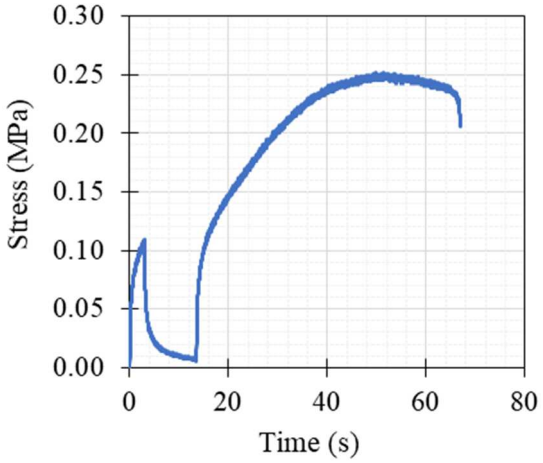

(b)

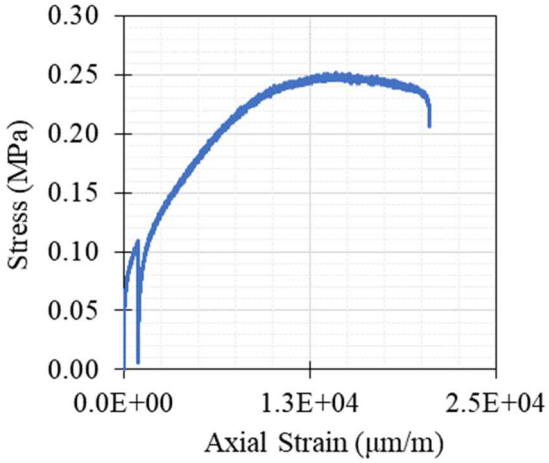

(c)

Figure B1-10. Tension test result of A1-V11 at 40°C and 2%/min strain rate

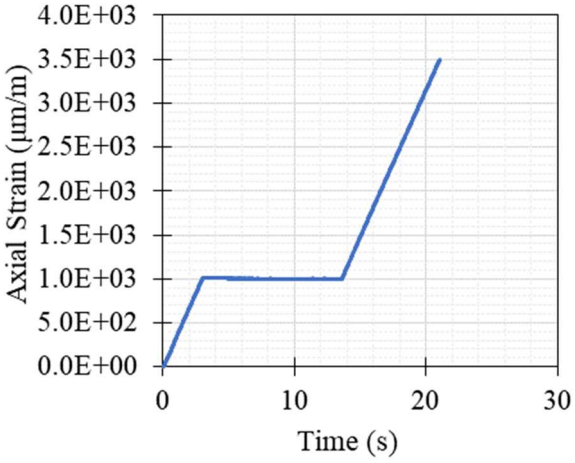

(a)

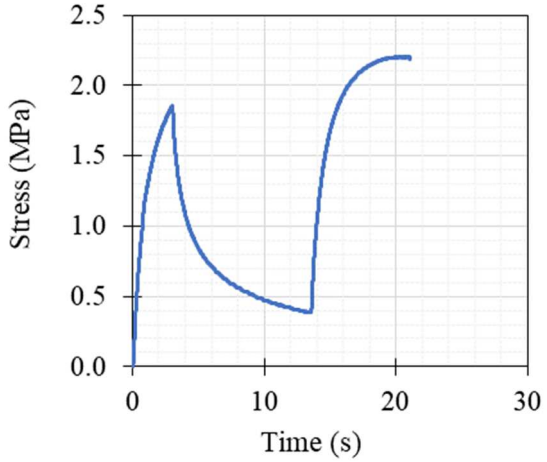

(b)

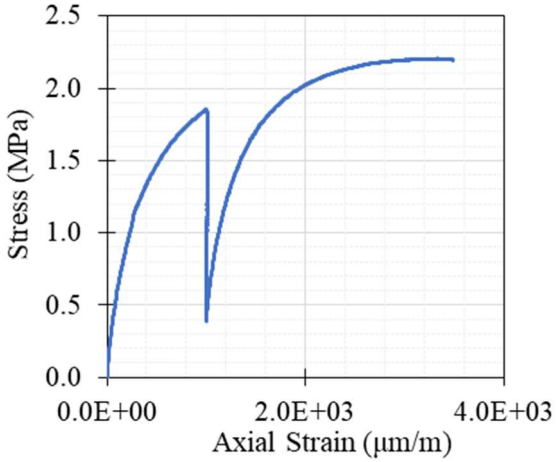

(c)

Figure B1-11. Tension test result of A1-V9 at 19°C and 2%/min strain rate

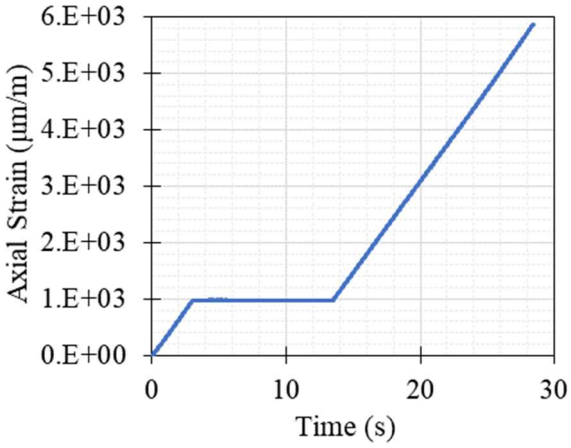

(a)

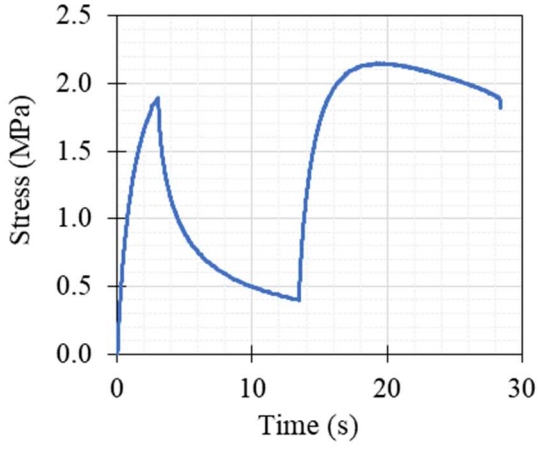

(b)

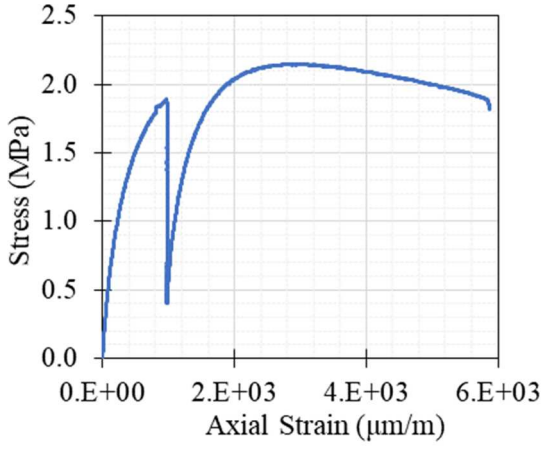

(c)

Figure B1-12. Tension test result of A4-V1 at 19°C and 2%/min strain rate

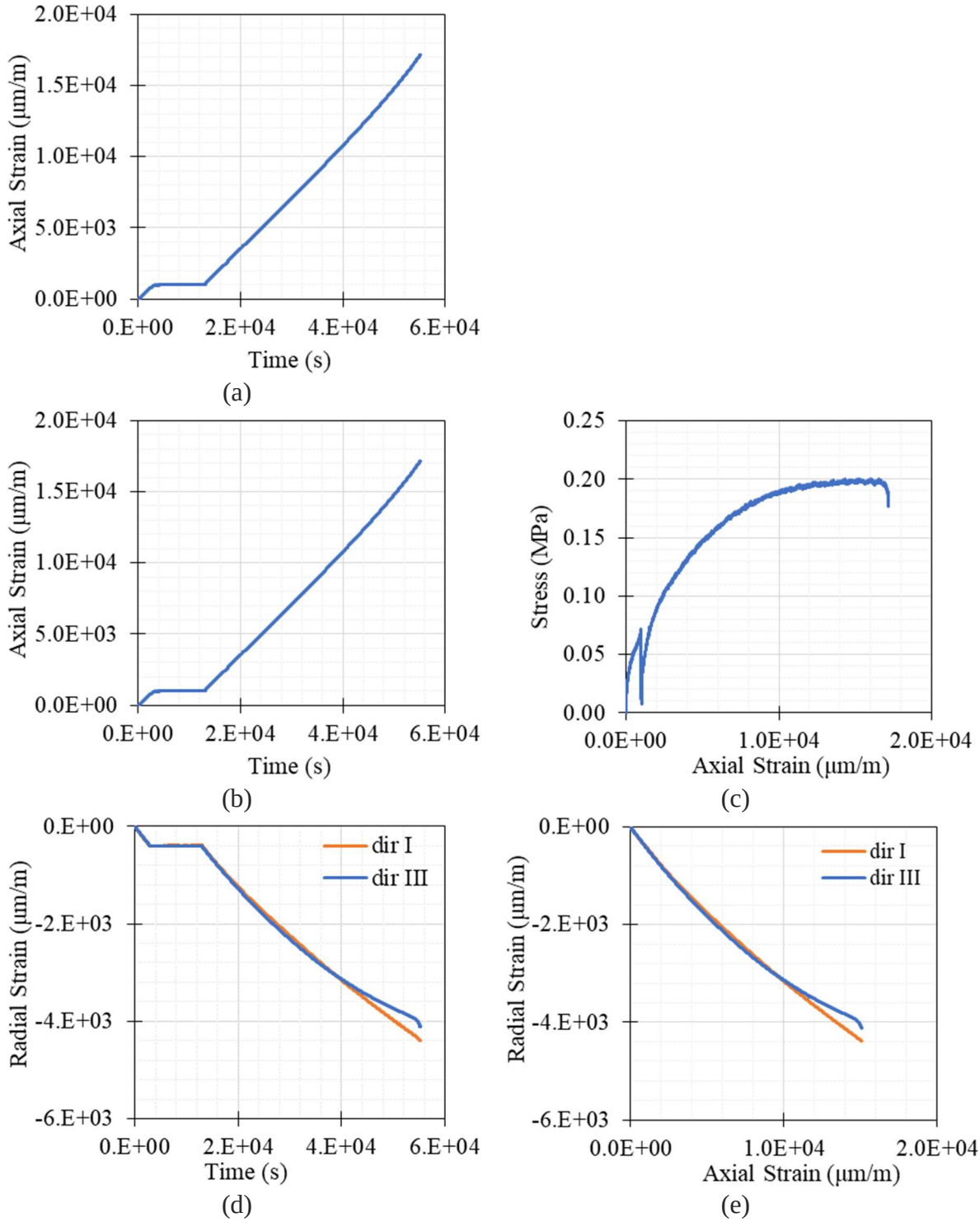

Figure B1-13. Tension test result of A1-V8 at 19°C and 0.002%/min strain rate

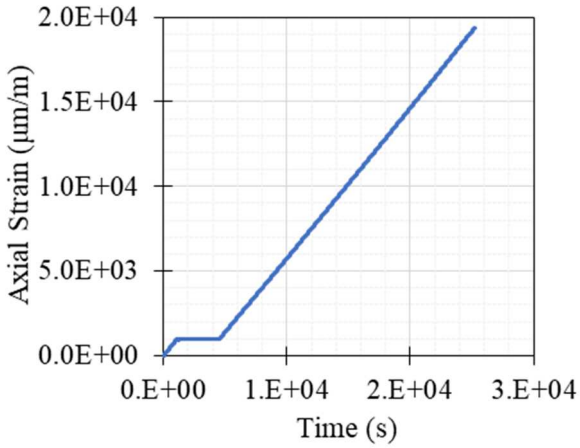

(a)

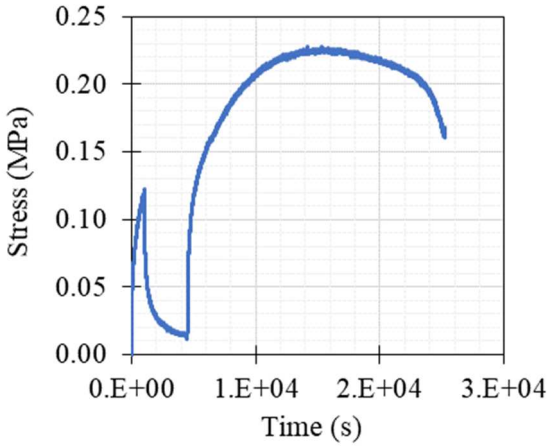

(b)

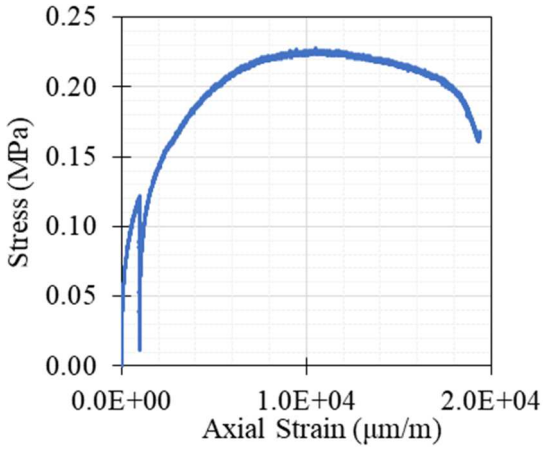

(c)

Figure B1-14. Tension test result of A2-V1 at 19°C and 0.006%/min strain rate

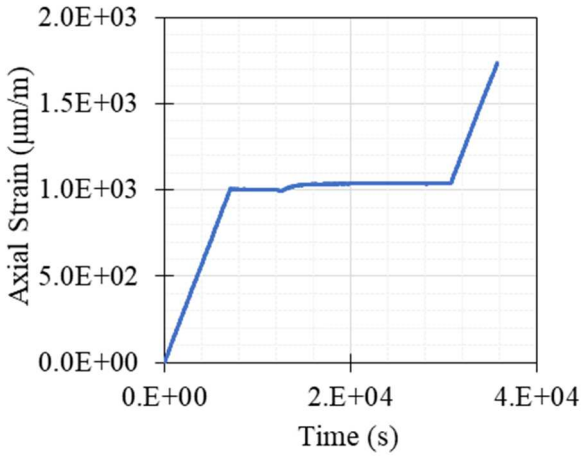

(a)

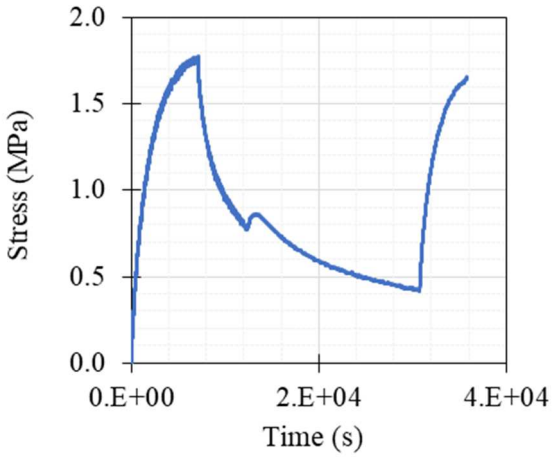

(b)

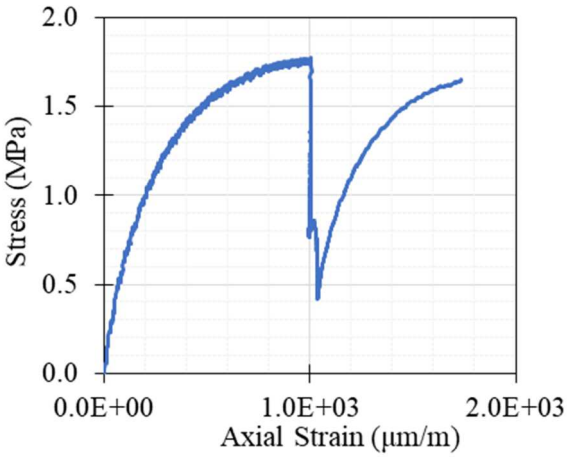

(c)

Figure B1-15. Tension test result of A1-V7 at 0°C and 0.001%/min strain rate

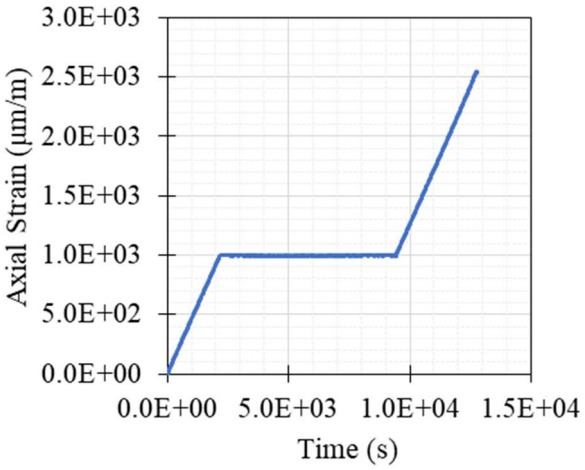

(a)

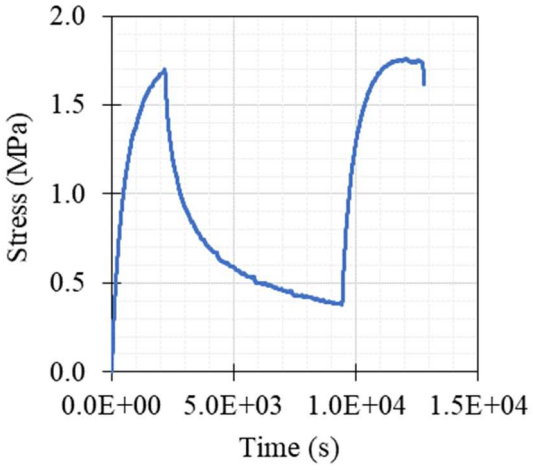

(b)

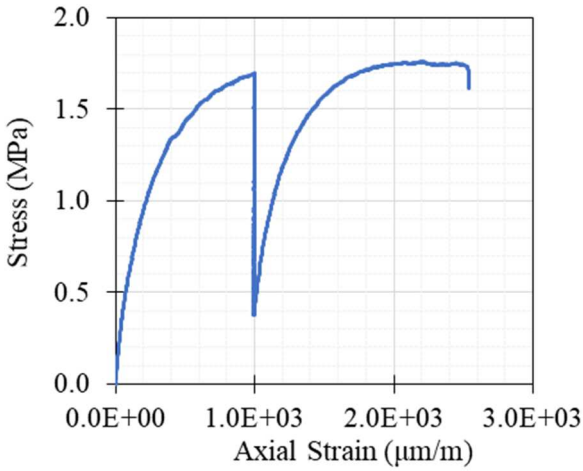

(c)

Figure B1-16. Tension test result of A4-V2 at 0°C and 0.003%/min strain rate

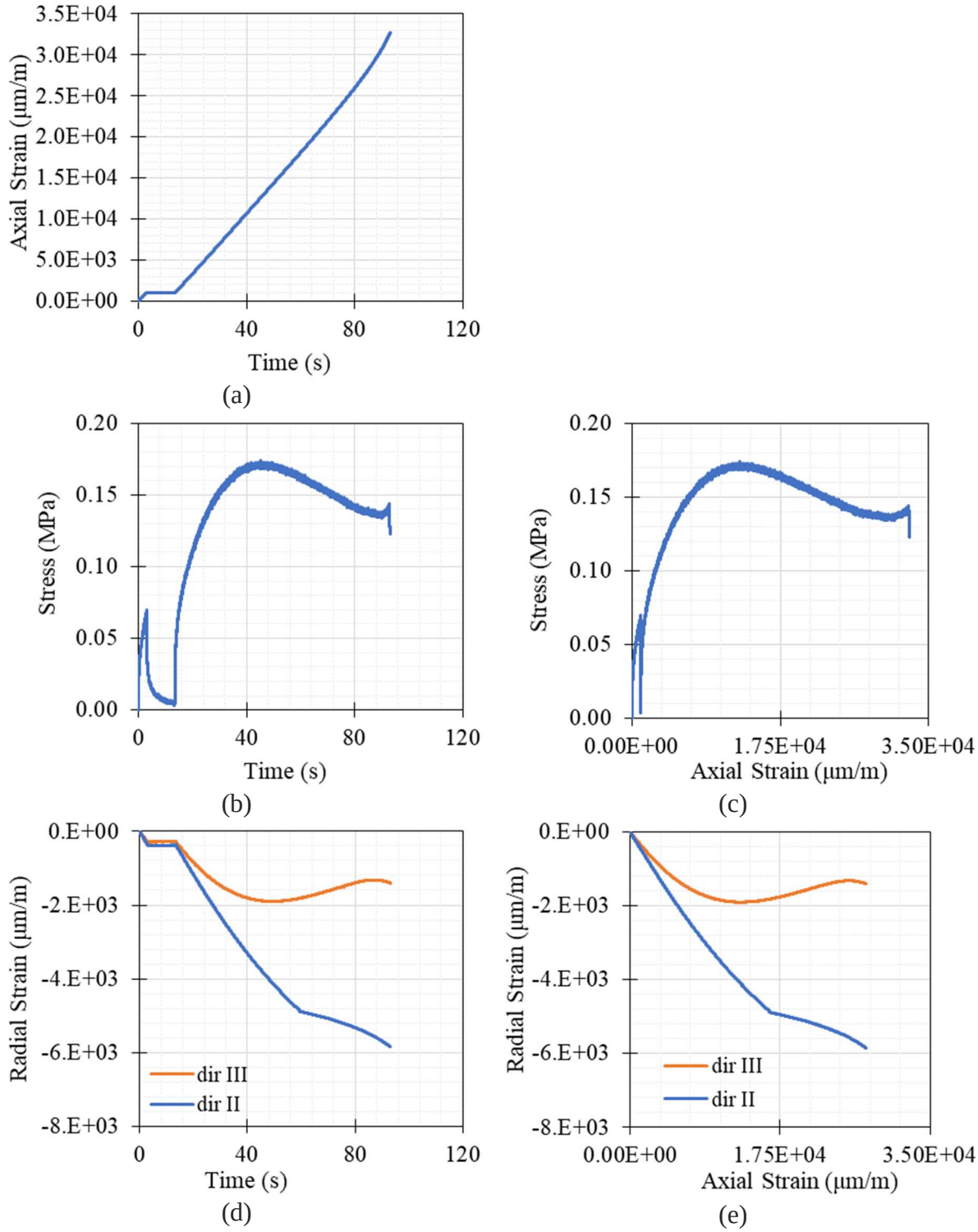

Figure B1-17. Tension test result of B1-H1 at 40°C and 2%/min strain rate

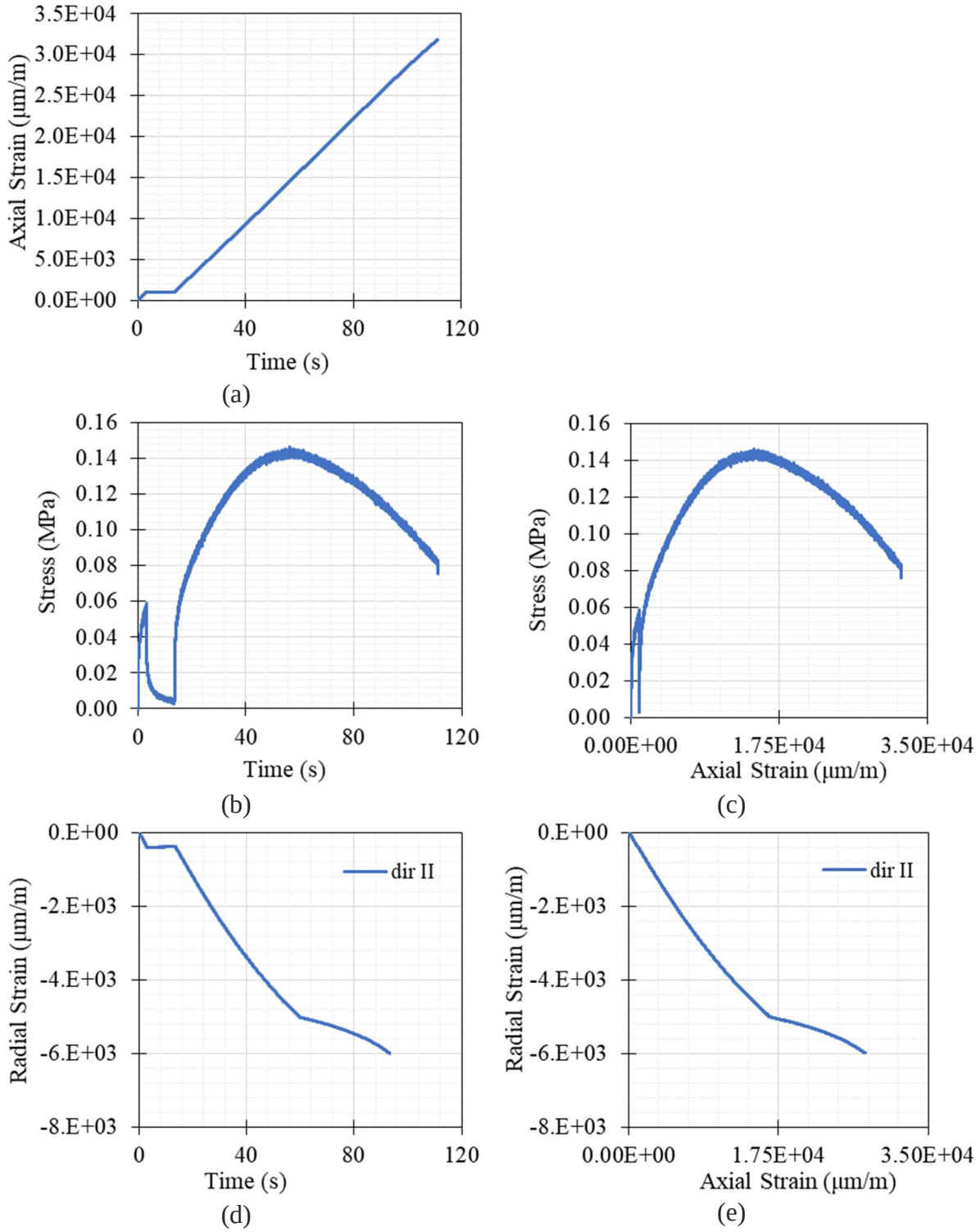

Figure B1-18. Tension test result of B2-H2 at 40°C and 2%/min strain rate

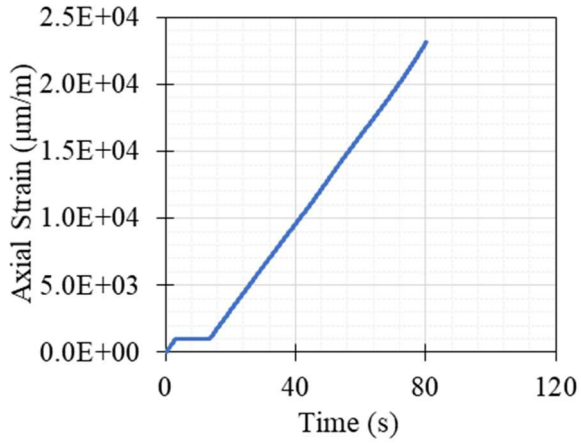

(a)

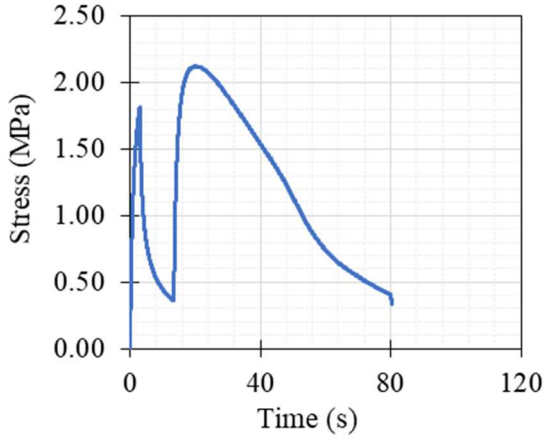

(b)

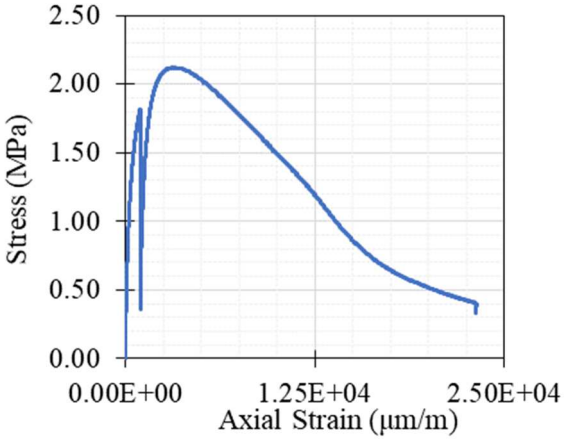

(c)

Figure B1-19. Tension test result of B1-H2 at 19°C and 2%/min strain rate

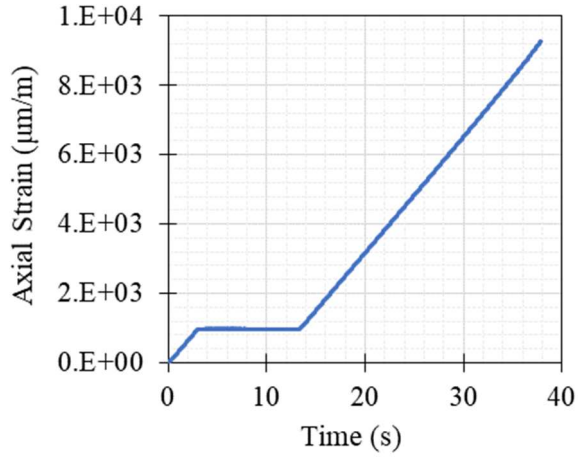

(a)

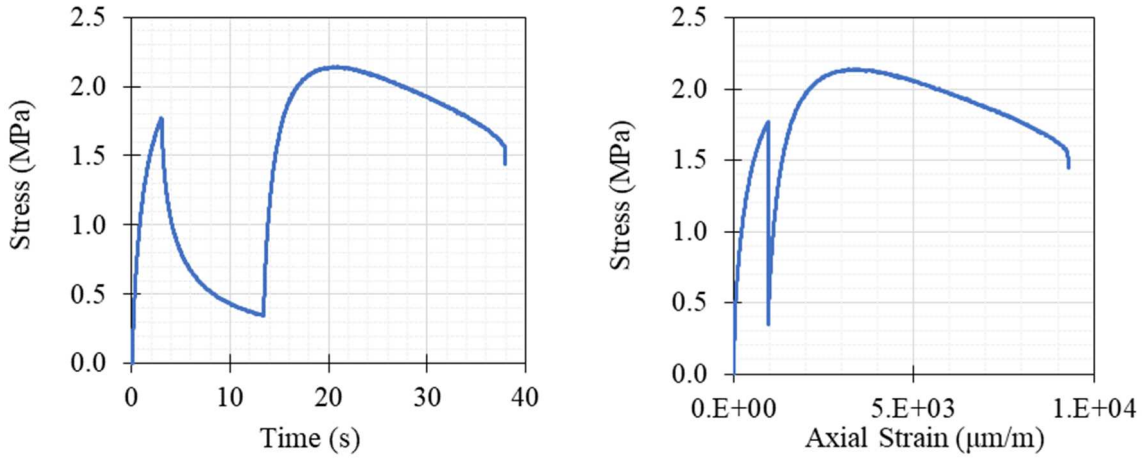

(b) (c)

Figure B1-20. Tension test result of B1-H1 at 40°C and 2%/min strain rate

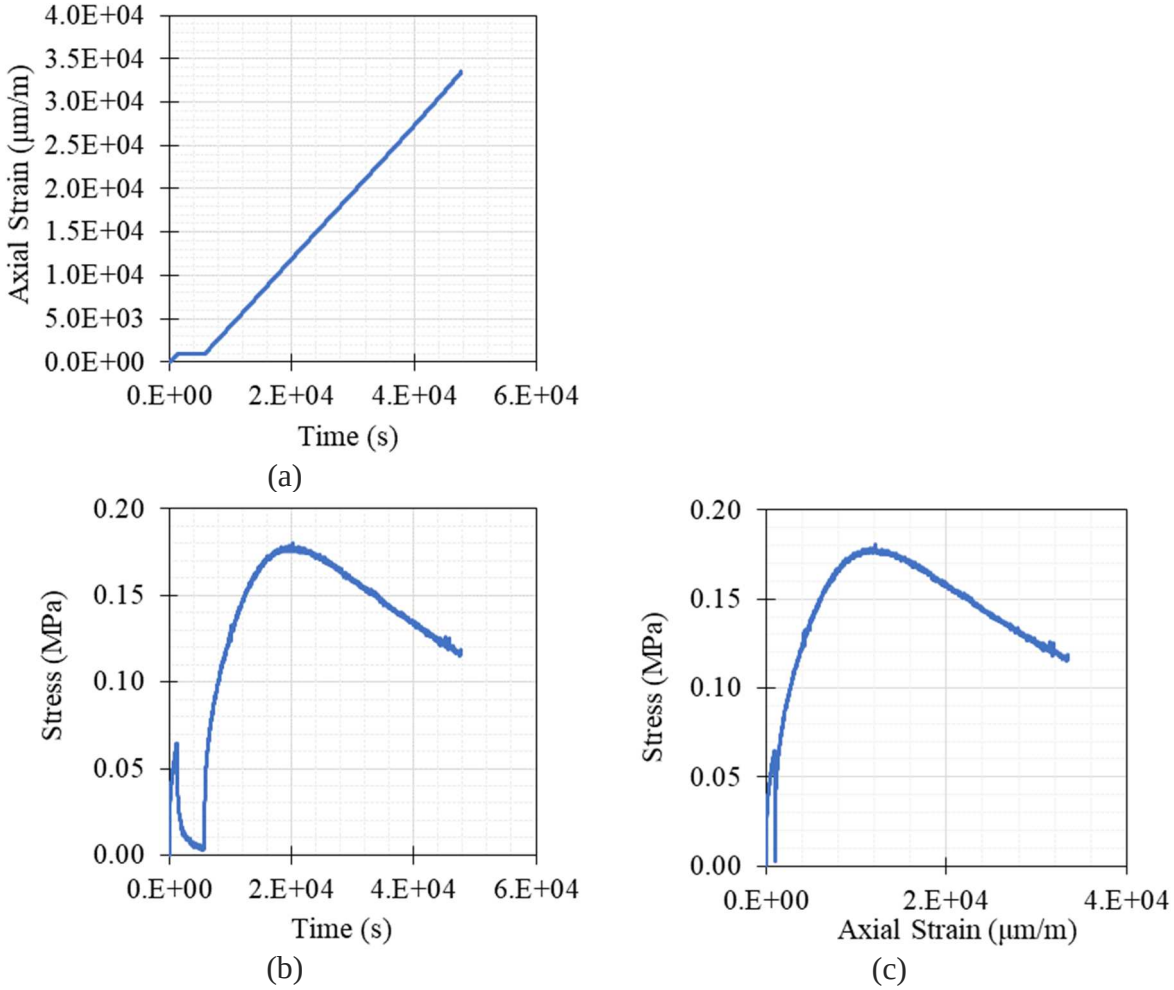

(a)

(b) (c)

Figure B1-21. Tension test result of B2-H1 at 19°C and 0.005%/min strain rate

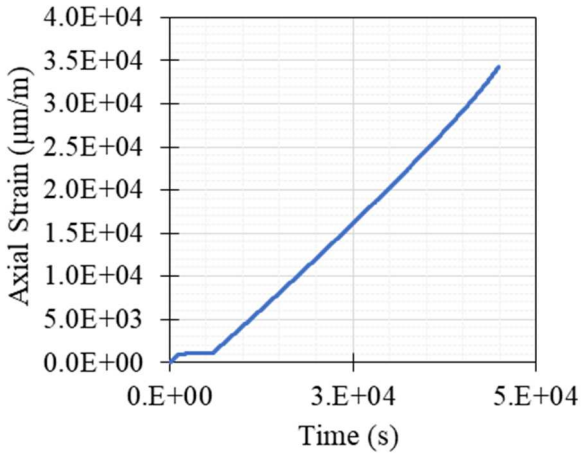

(a)

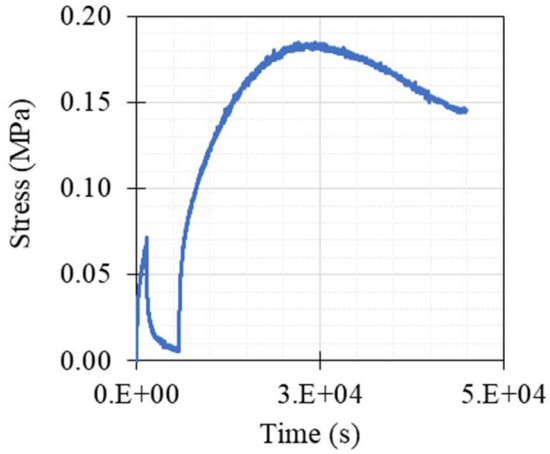

(b)

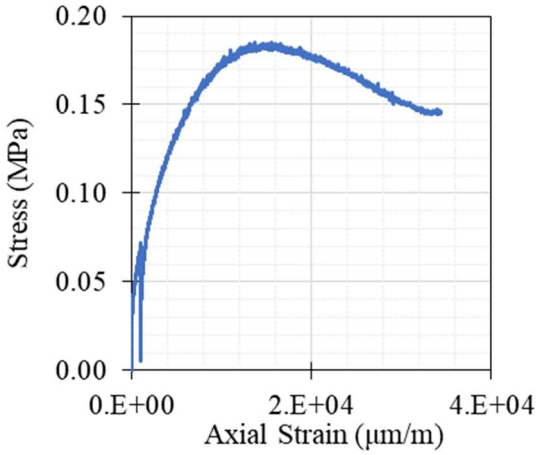

(c)

Figure B1-22. Tension test result of B2-H4 at 19°C and 0.004%/min strain rate

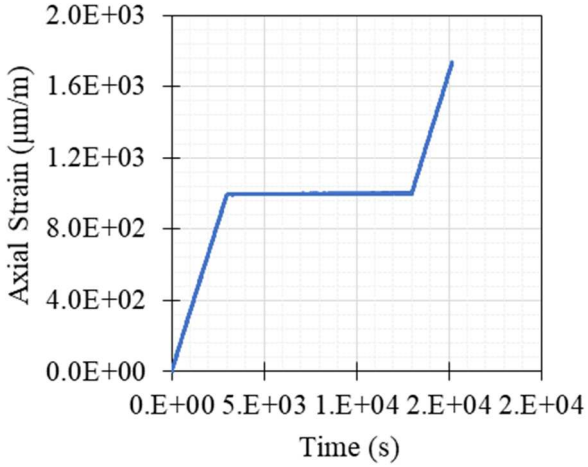

(a)

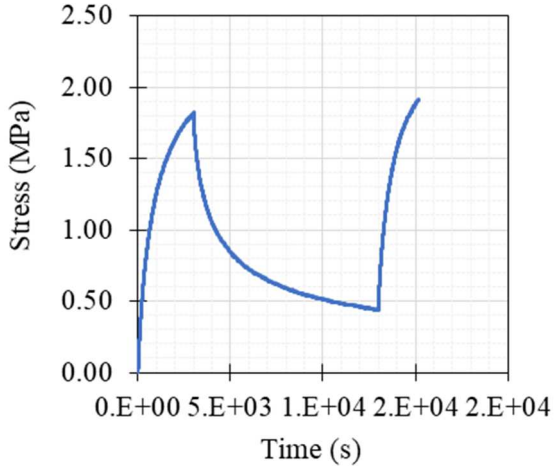

(b)

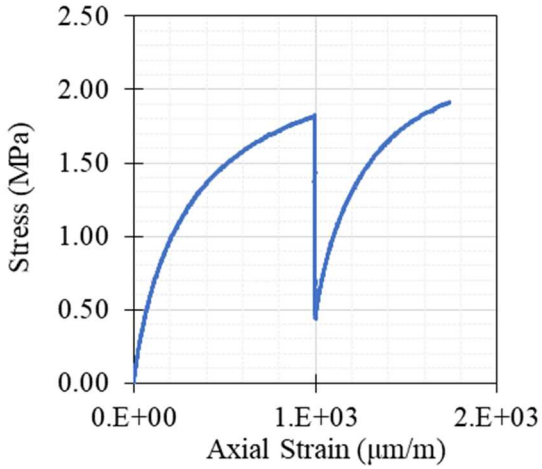

(c)

Figure B1-23. Tension test result of B1-H3 at 0°C and 0.002%/min strain rate

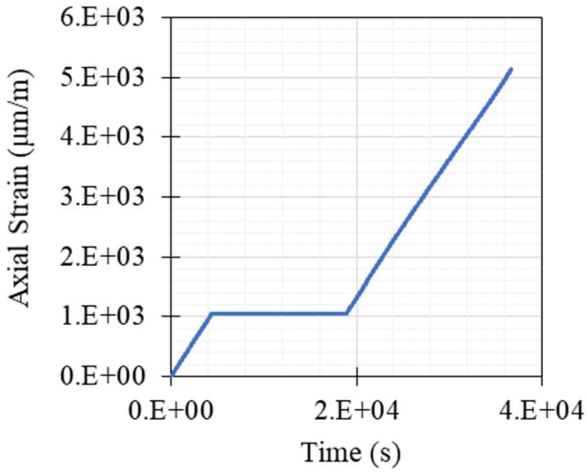

(a)

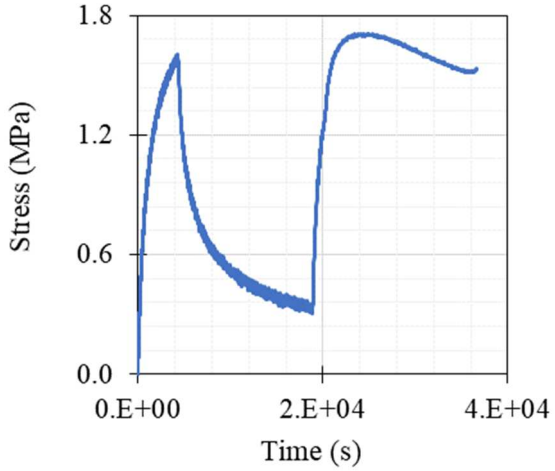

(b)

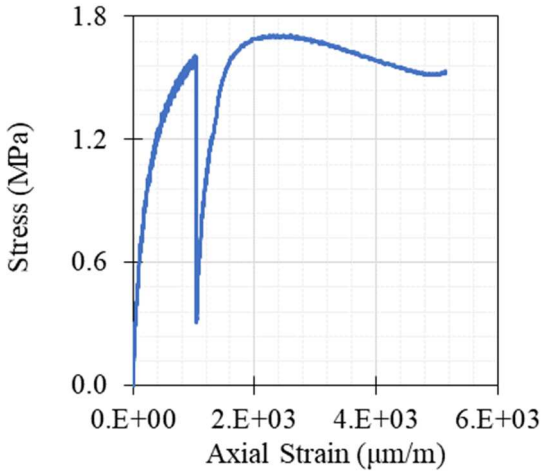

(c)

Figure B1-24. Tension test result of B3-H11 at 0°C and 0.001%/min strain rate

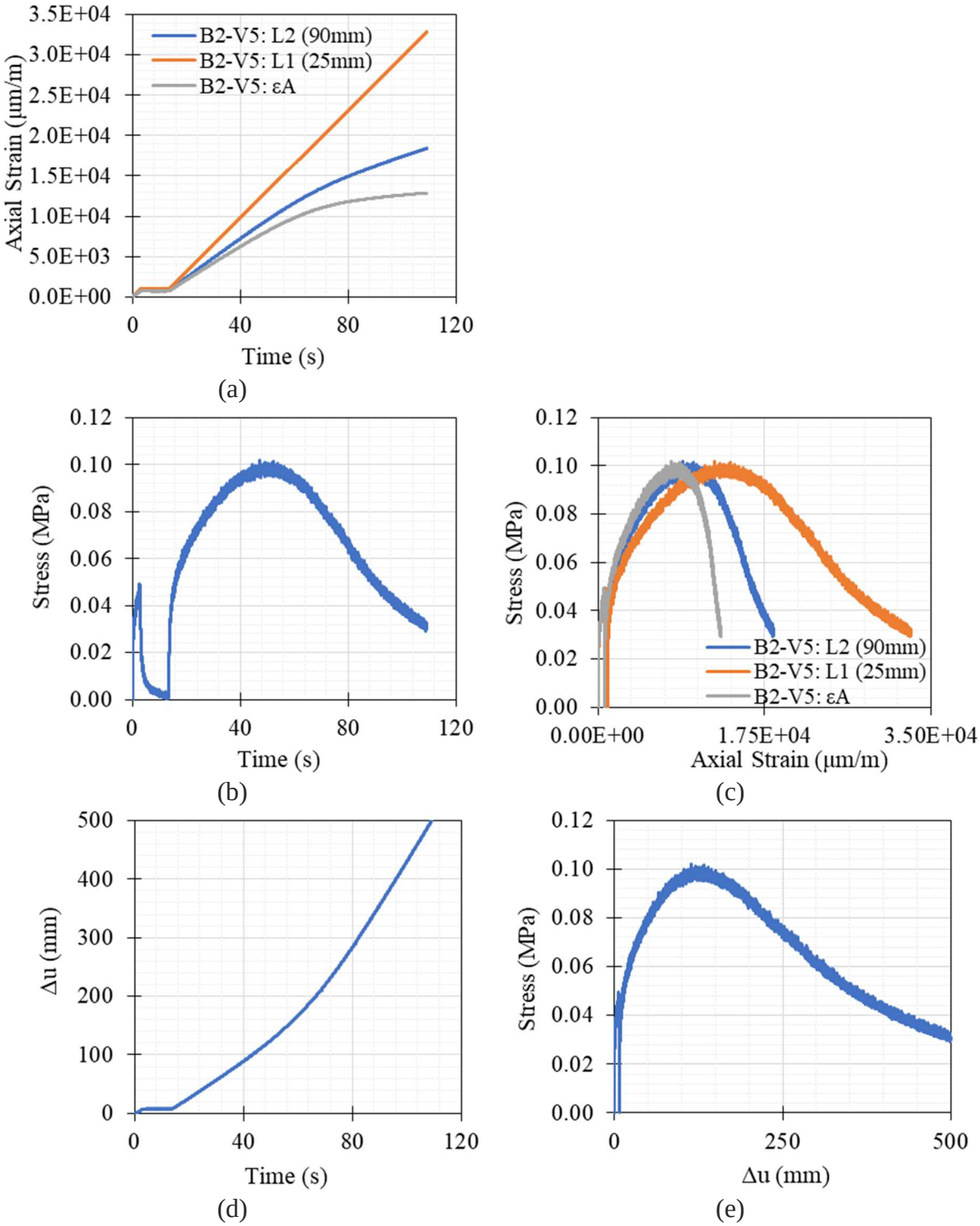

Figure B1-25. Tension test result of B2-V5 at 40°C and 2%/min strain rate

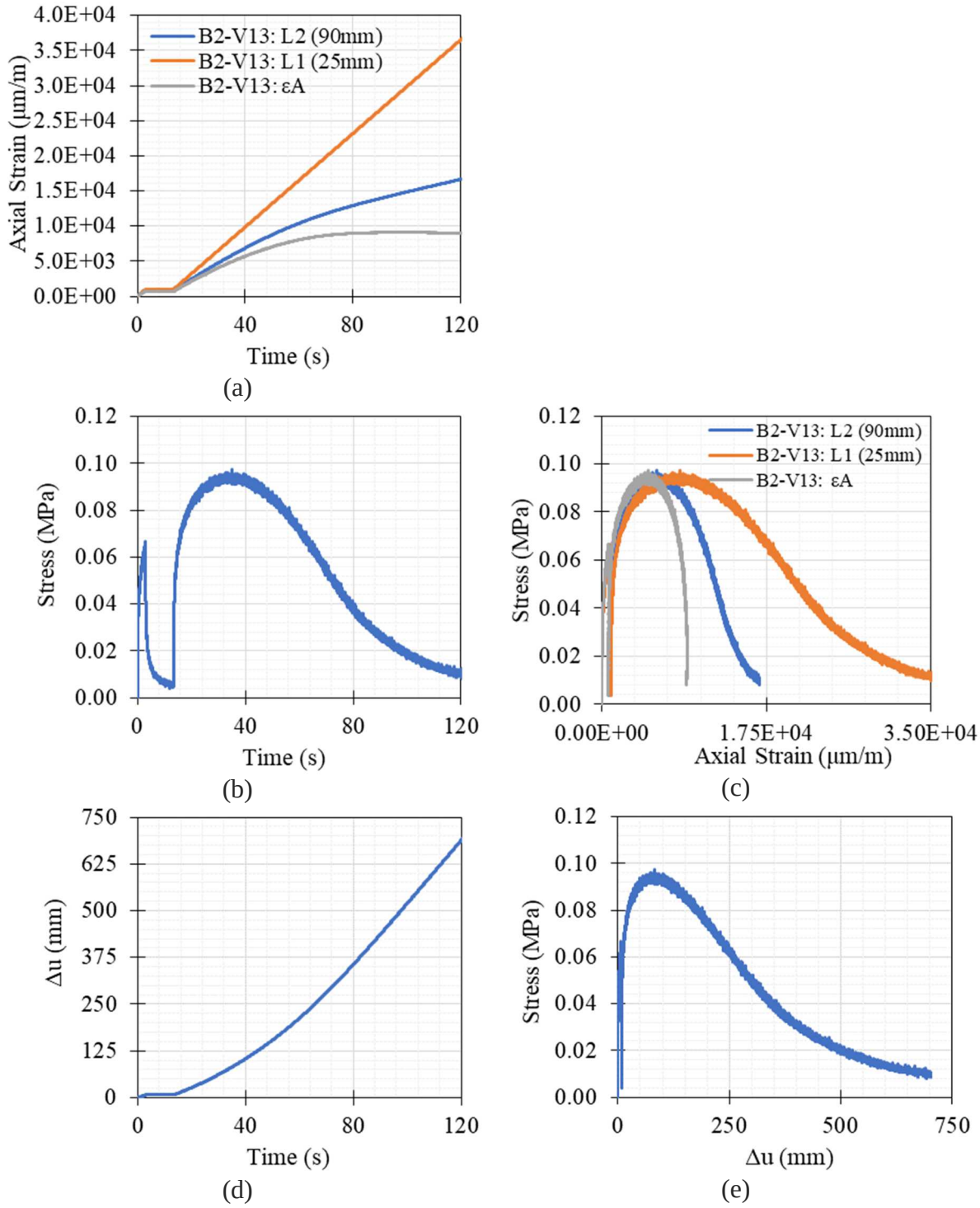

Figure B1-26. Tension test result of B3-V13 at 40°C and 2%/min strain rate

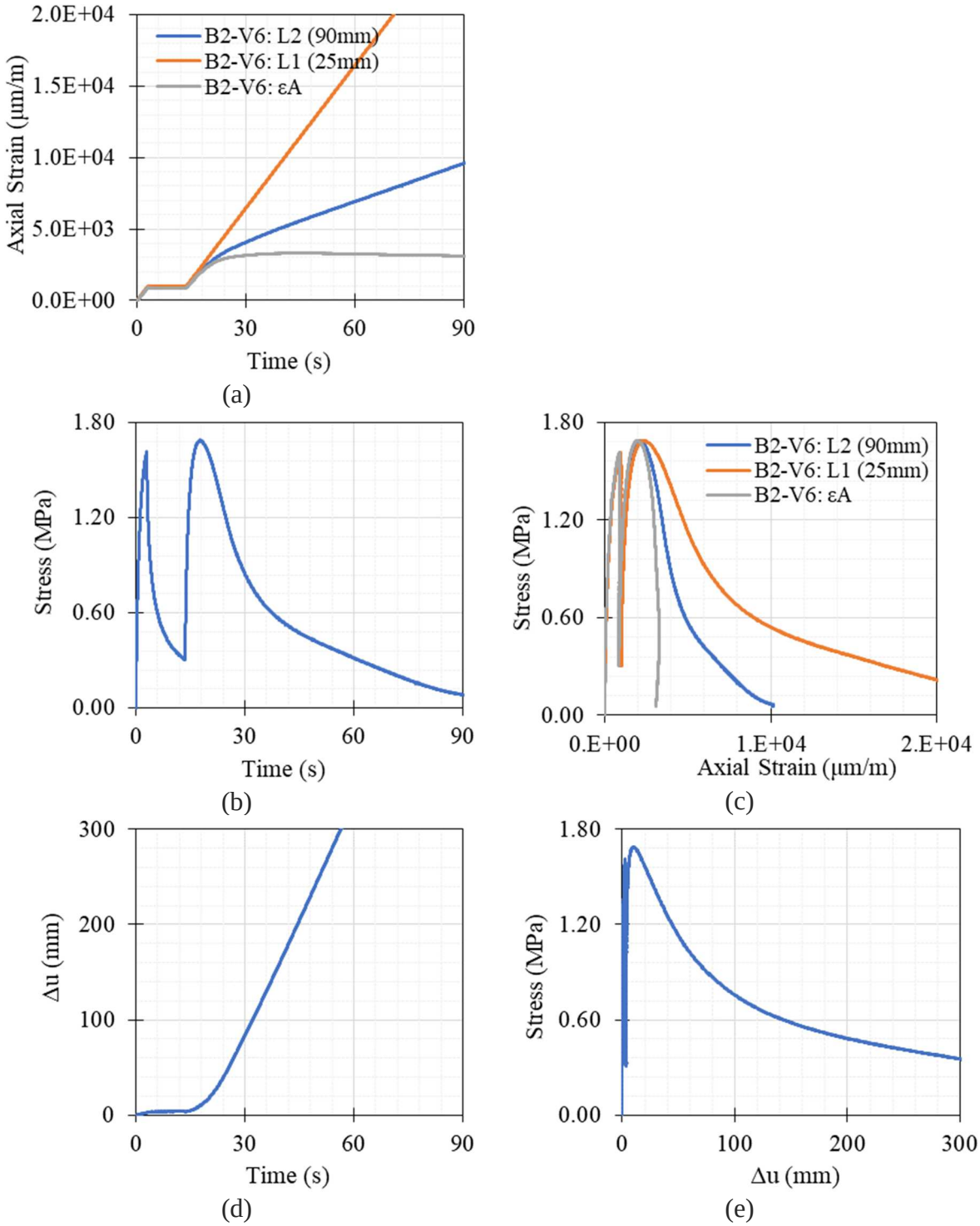

Figure B1-27. Tension test result of B2-V6 at 19°C and 2%/min strain rate

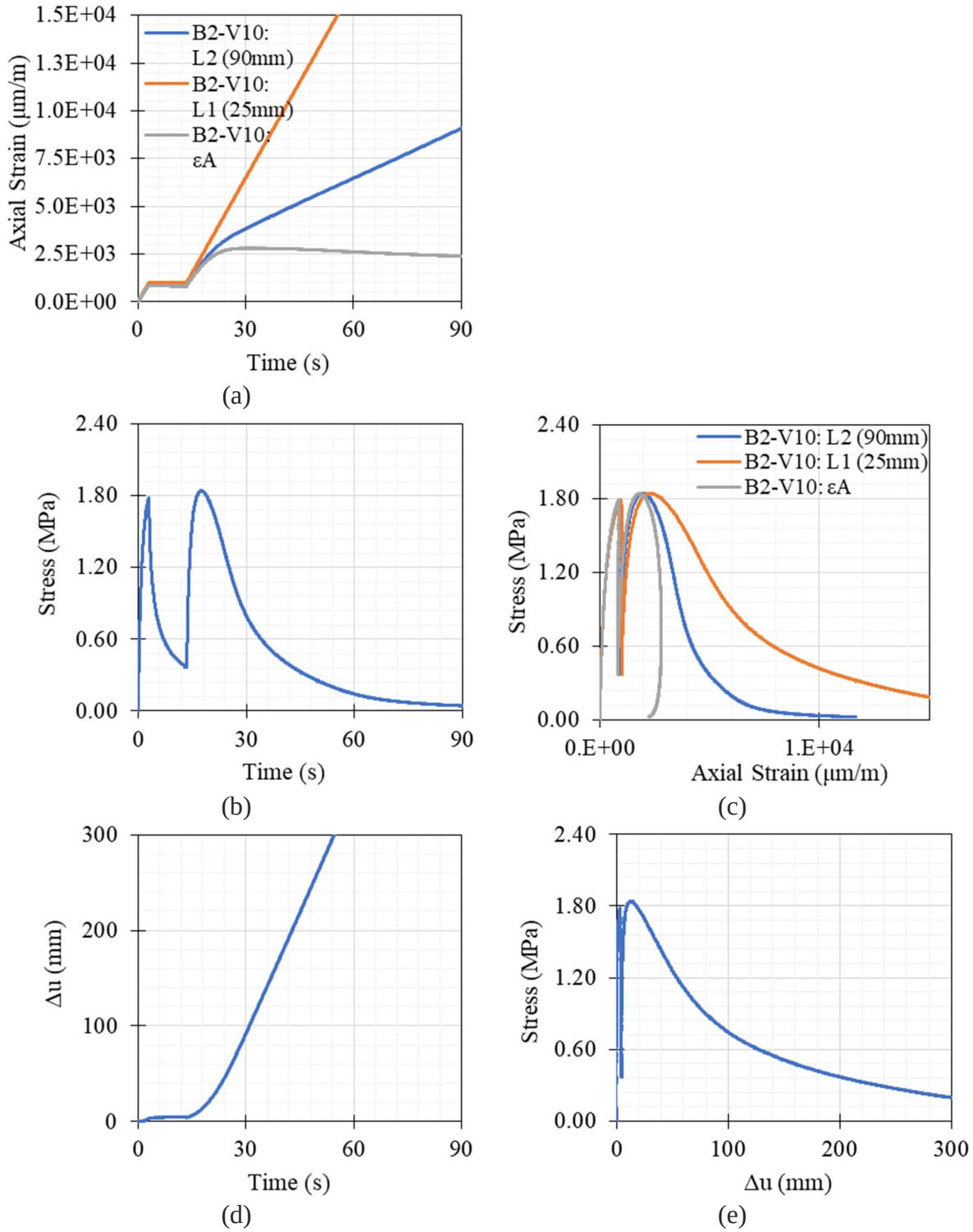

Figure B1-28. Tension test result of B2-V10 at 19°C and 2%/min strain rate

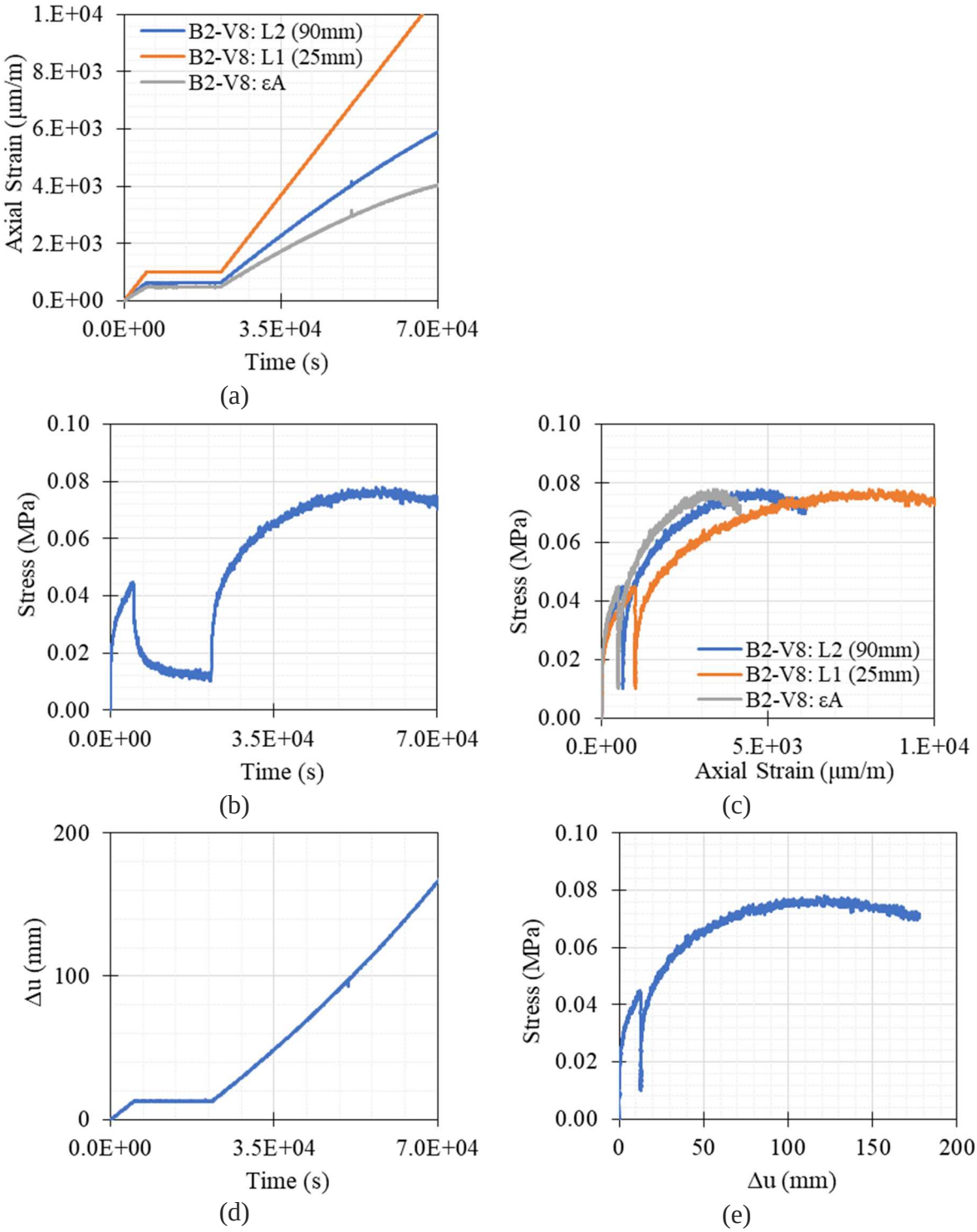

Figure B1-29. Tension test result of B2-V8 at 19°C and 0.001%/min strain rate

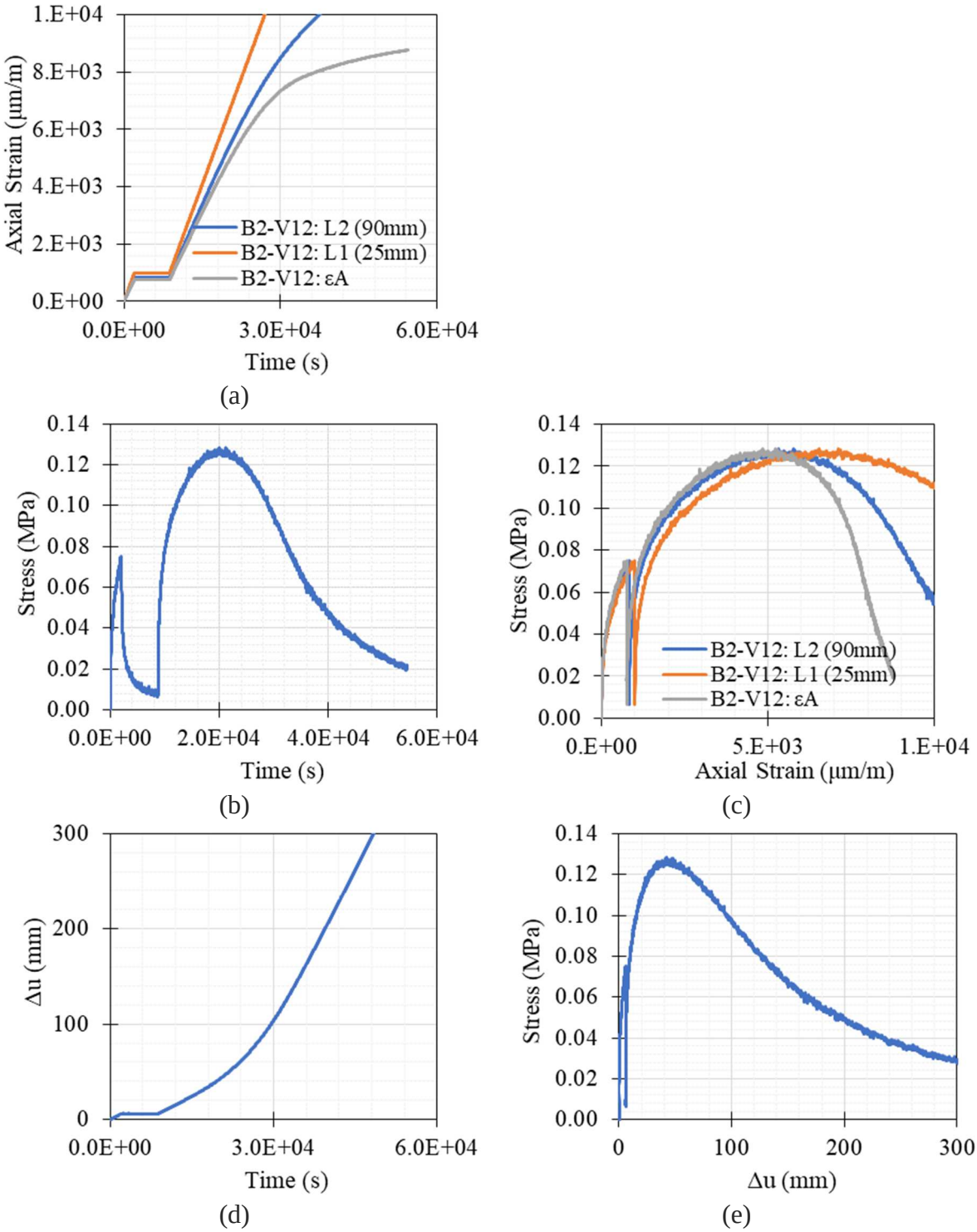

Figure B1-30. Tension test result of B2-V12 at 19°C and 0.003%/min strain rate

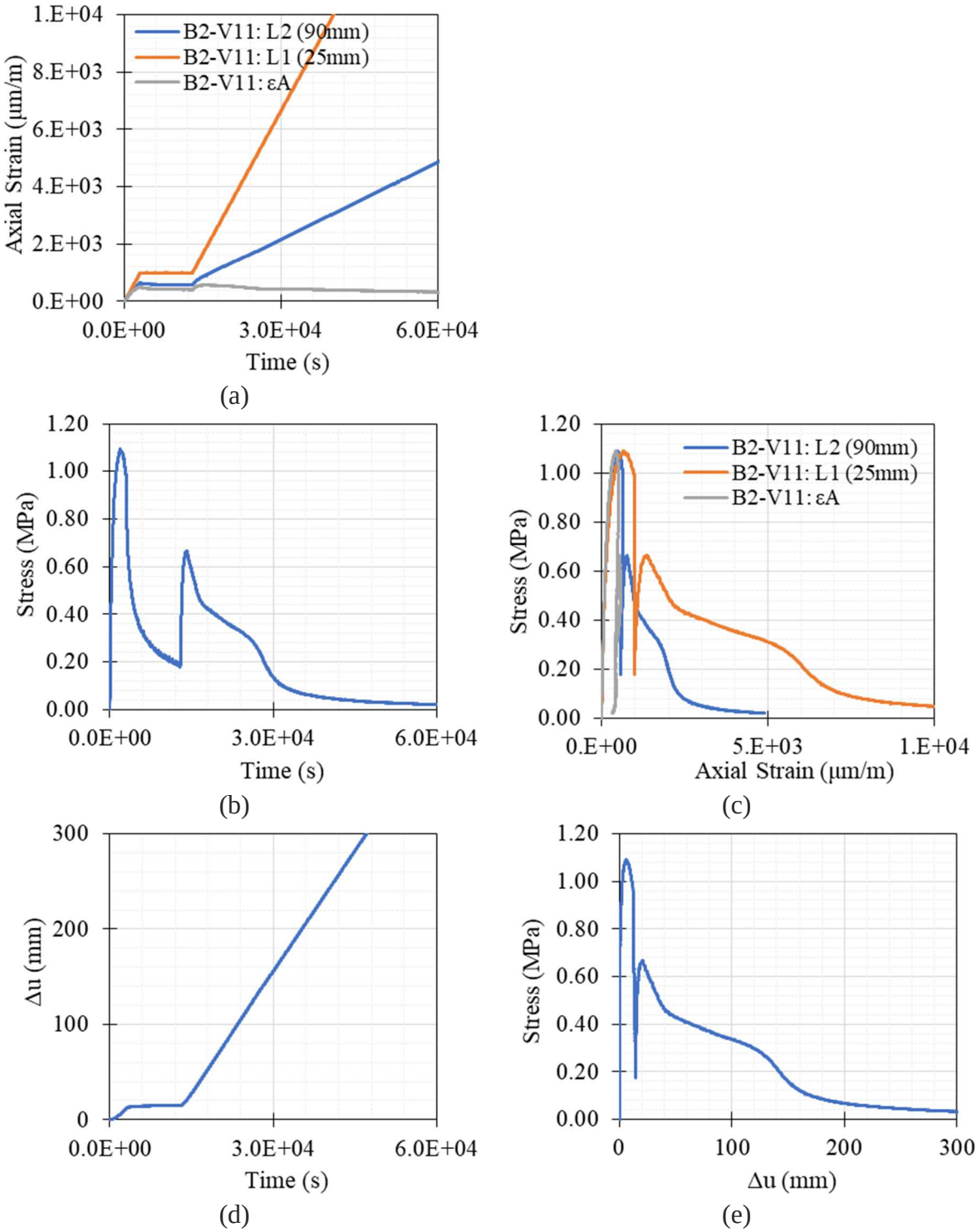

Figure B1-31. Tension test result of B2-V11 at 0°C and 0.002%/min strain rate

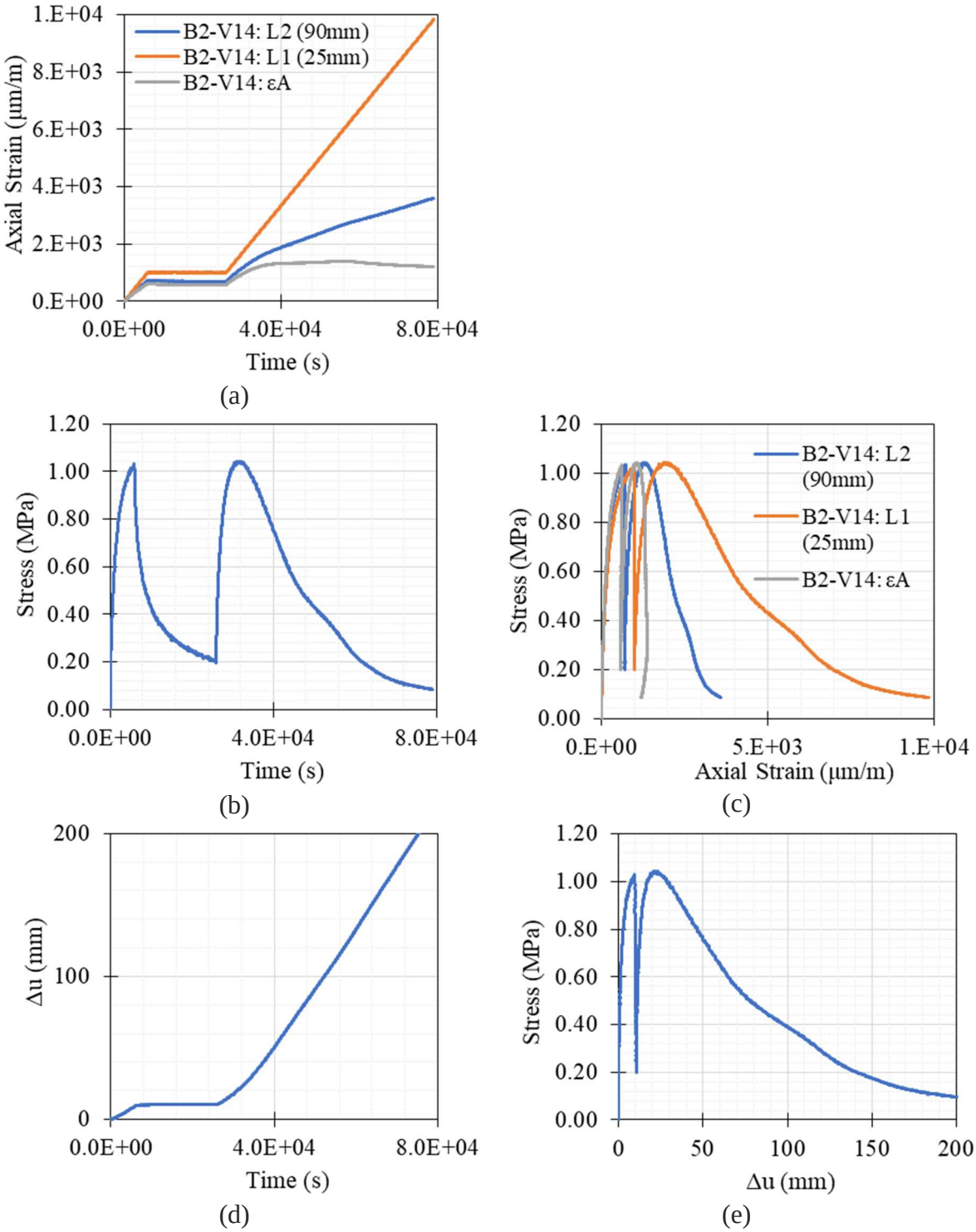

Figure B1-32. Tension test result of B2-V14 at 0°C and 0.001%/min strain rate

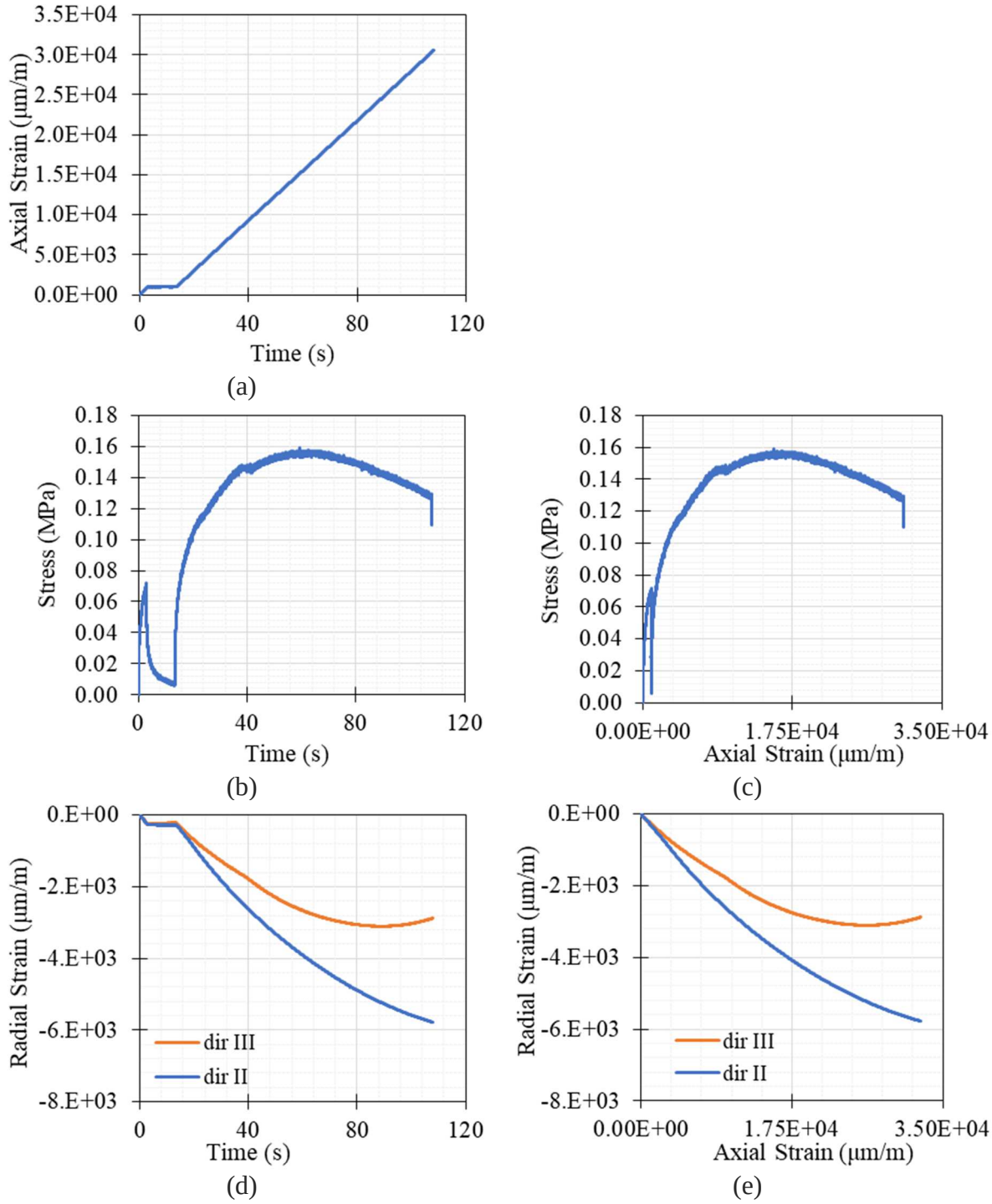

Figure B1-33. Tension test result of C2-H1 at 40°C and 2%/min strain rate

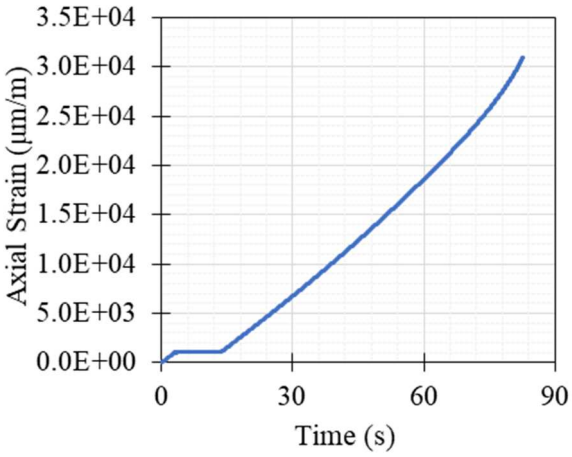

(a)

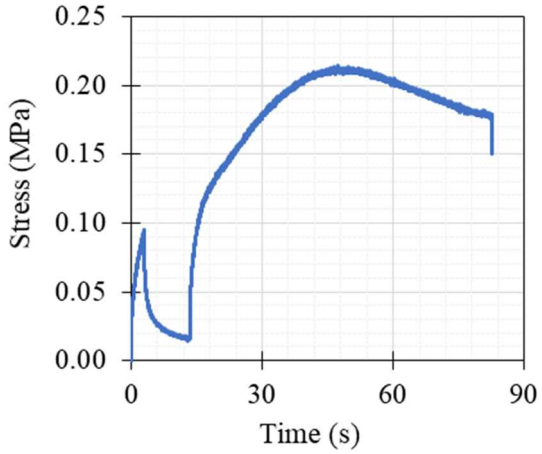

(b)

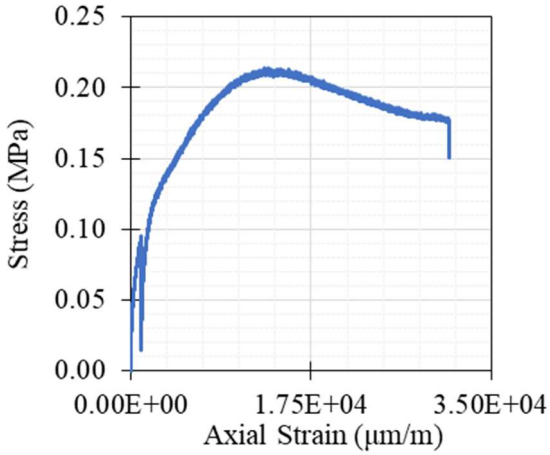

(c)

Figure B1-34. Tension test result of C3-H3 at 40°C and 2%/min strain rate

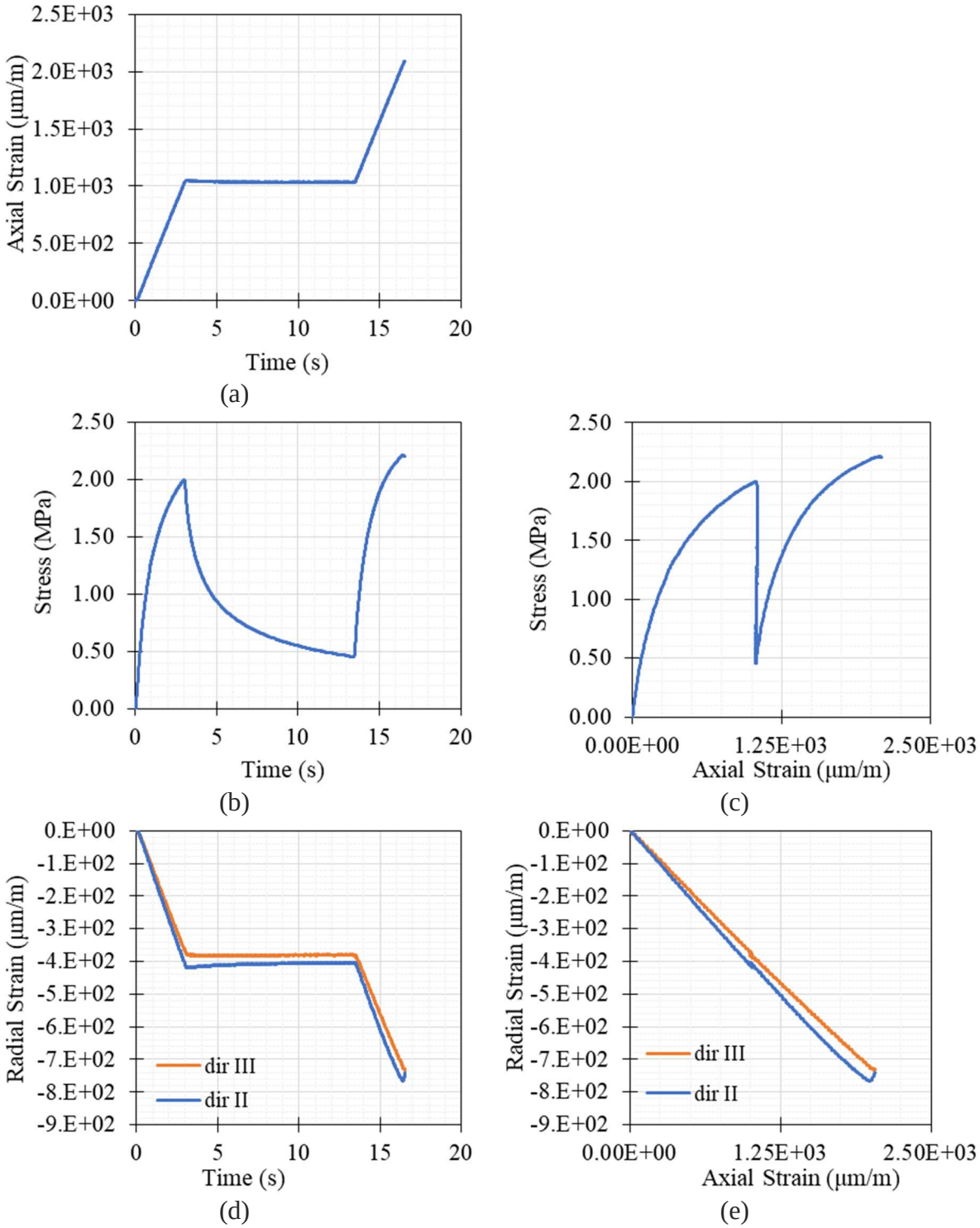

Figure B1-35. Tension test result of C2-H3 at 19°C and 2%/min strain rate

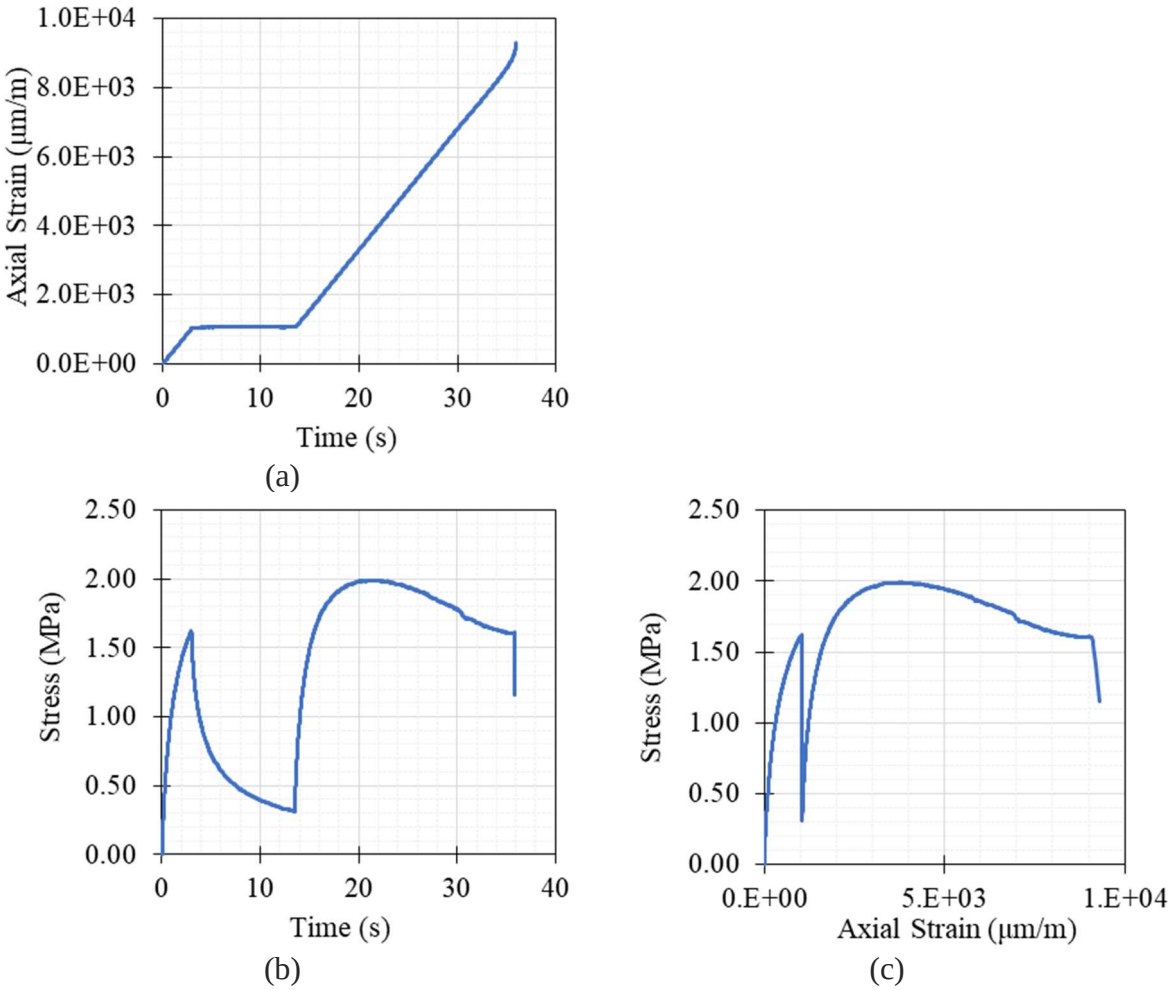

Figure B1-36. Tension test result of C3-H1 at 19°C and 2%/min strain rate

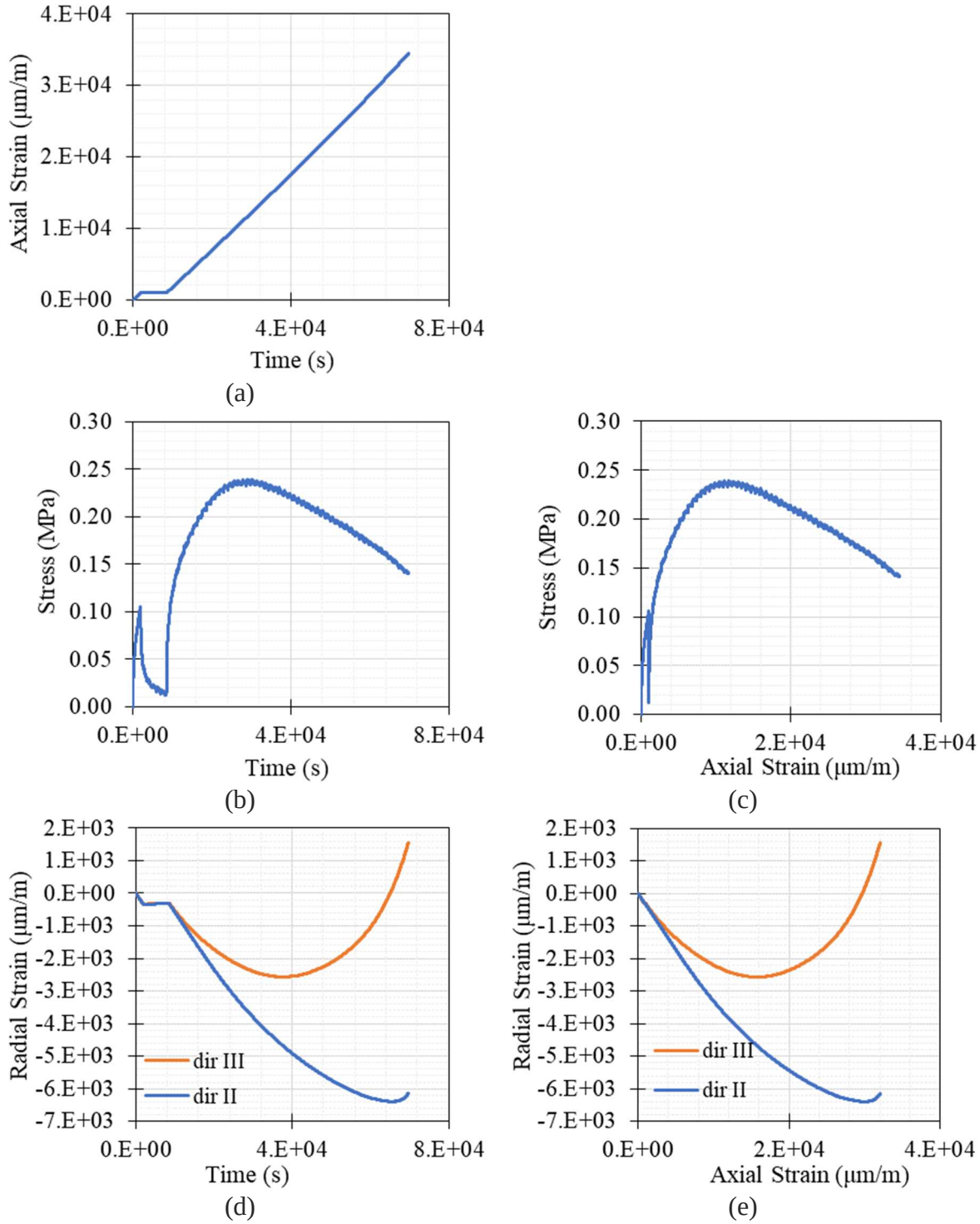

Figure B1-37. Tension test result of C2-H2 at 19°C and 0.003%/min strain rate

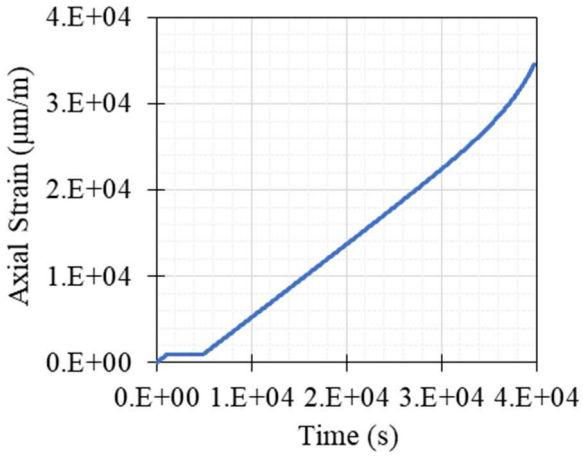

(a)

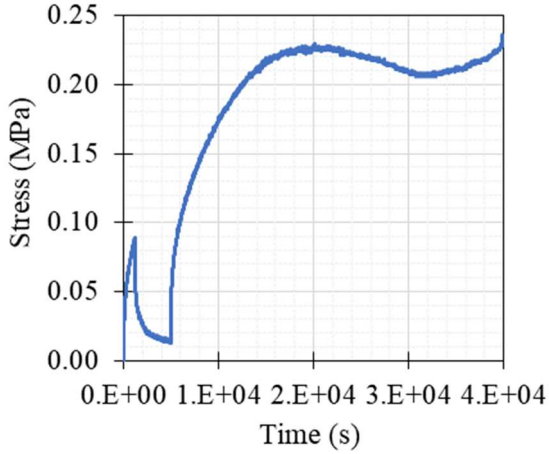

(b)

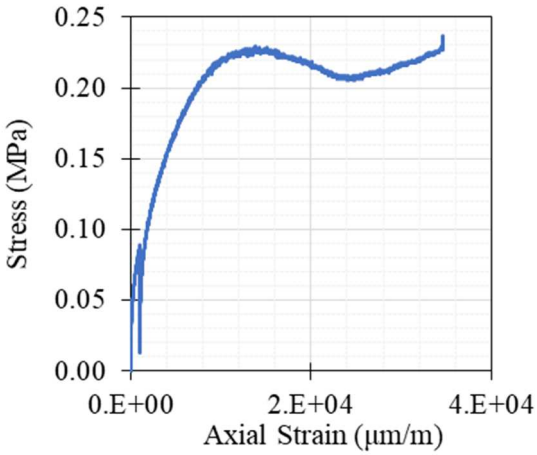

(c)

Figure B1-38. Tension test result of C4-H1 at 19°C and 0.005%/min strain rate

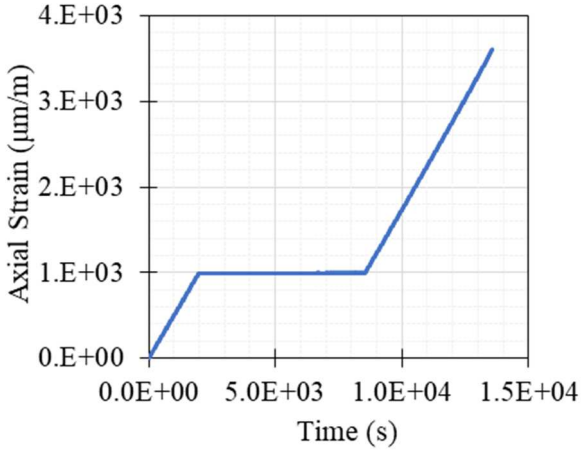

(a)

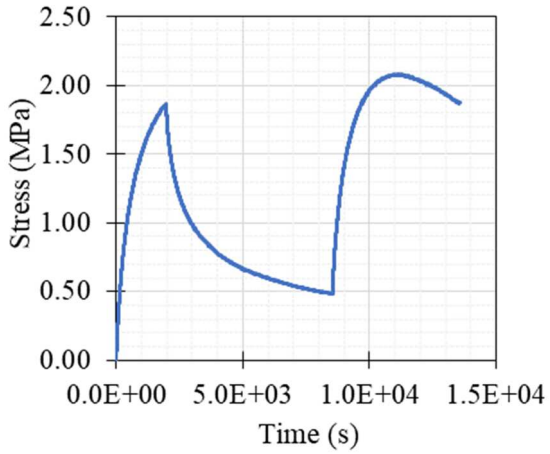

(b)

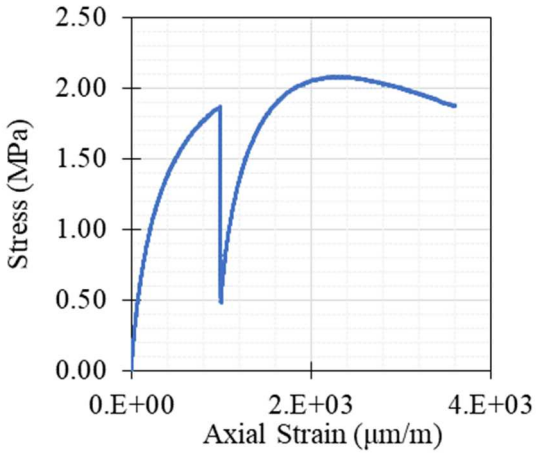

(c)

Figure B1-39. Tension test result of C2-H4 at 0°C and 0.003%/min strain rate

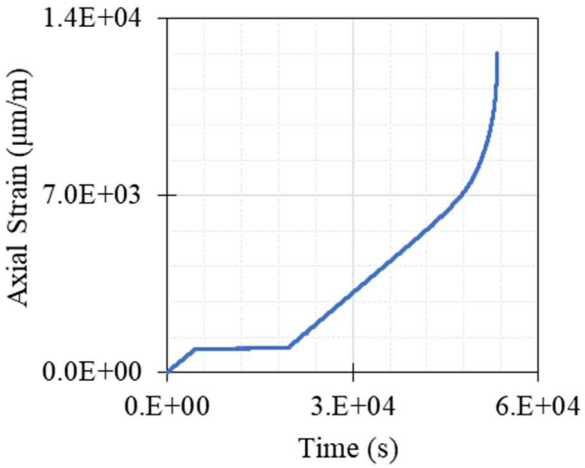

(a)

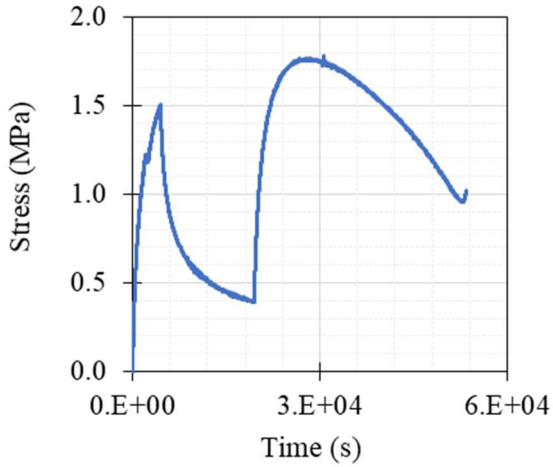

(b)

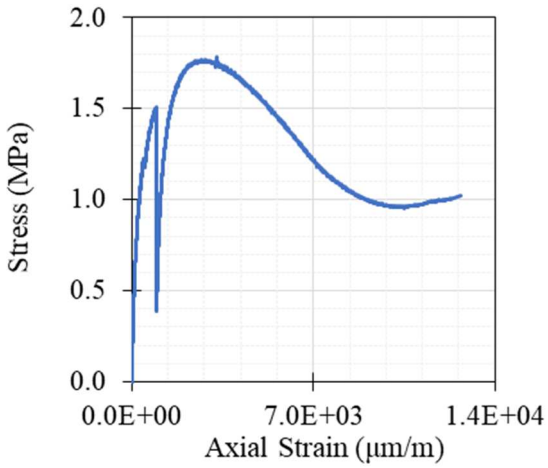

(c)

Figure B1-40. Tension test result of C3-H2 at 0°C and 0.001%/min strain rate

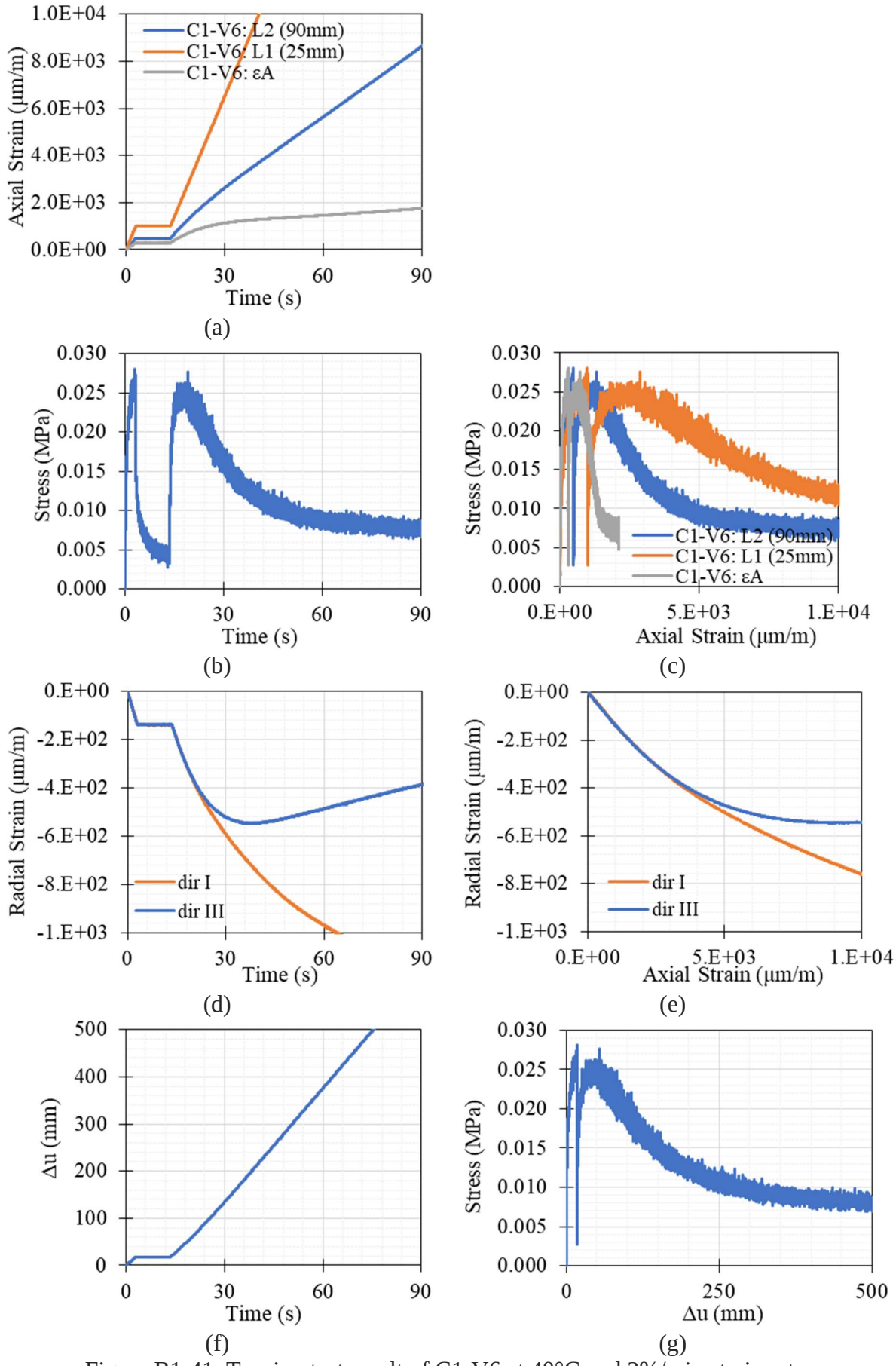

Figure B1-41. Tension test result of C1-V6 at 40°C and 2%/min strain rate

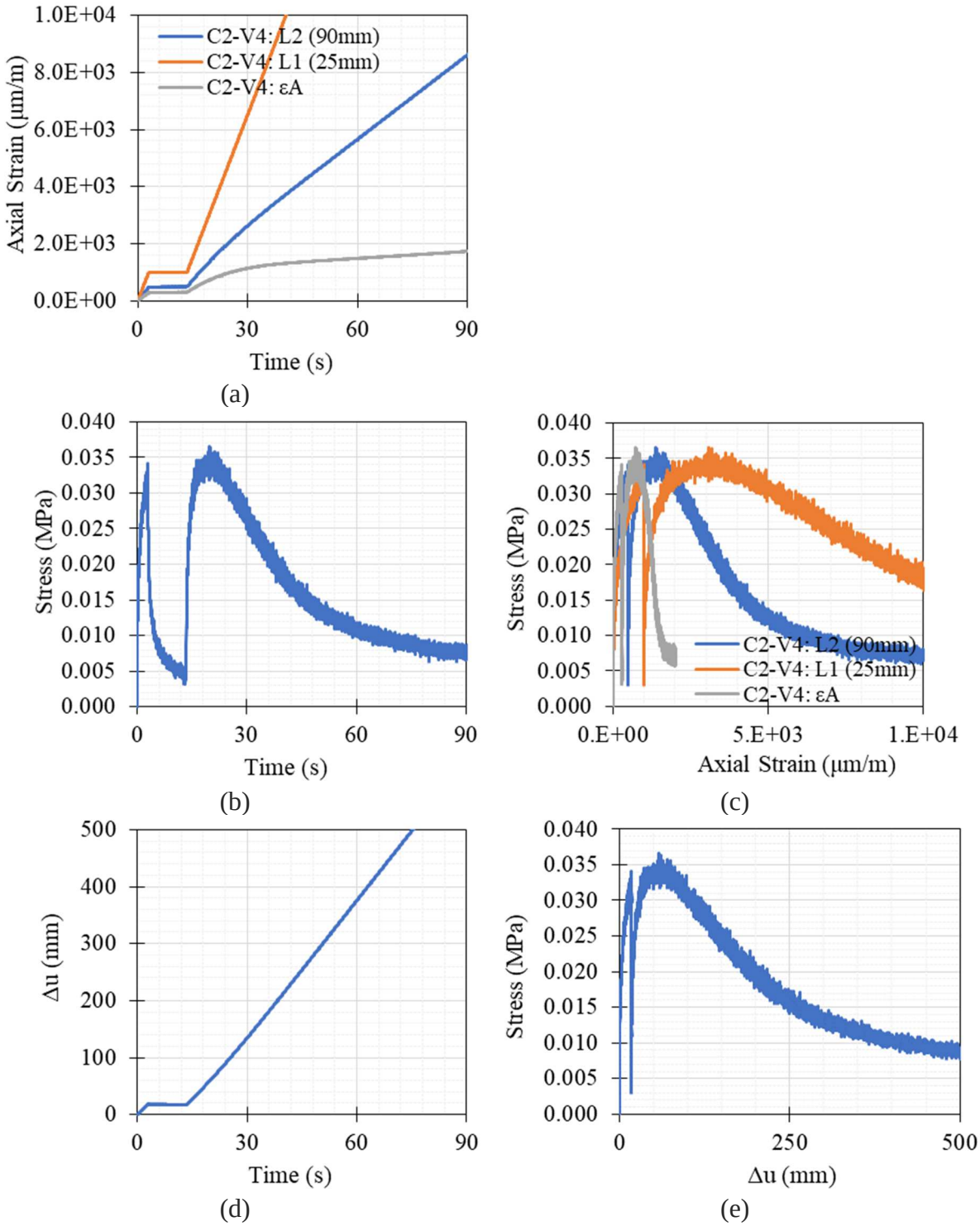

Figure B1-42. Tension test result of C2-V4 at 40°C and 2%/min strain rate

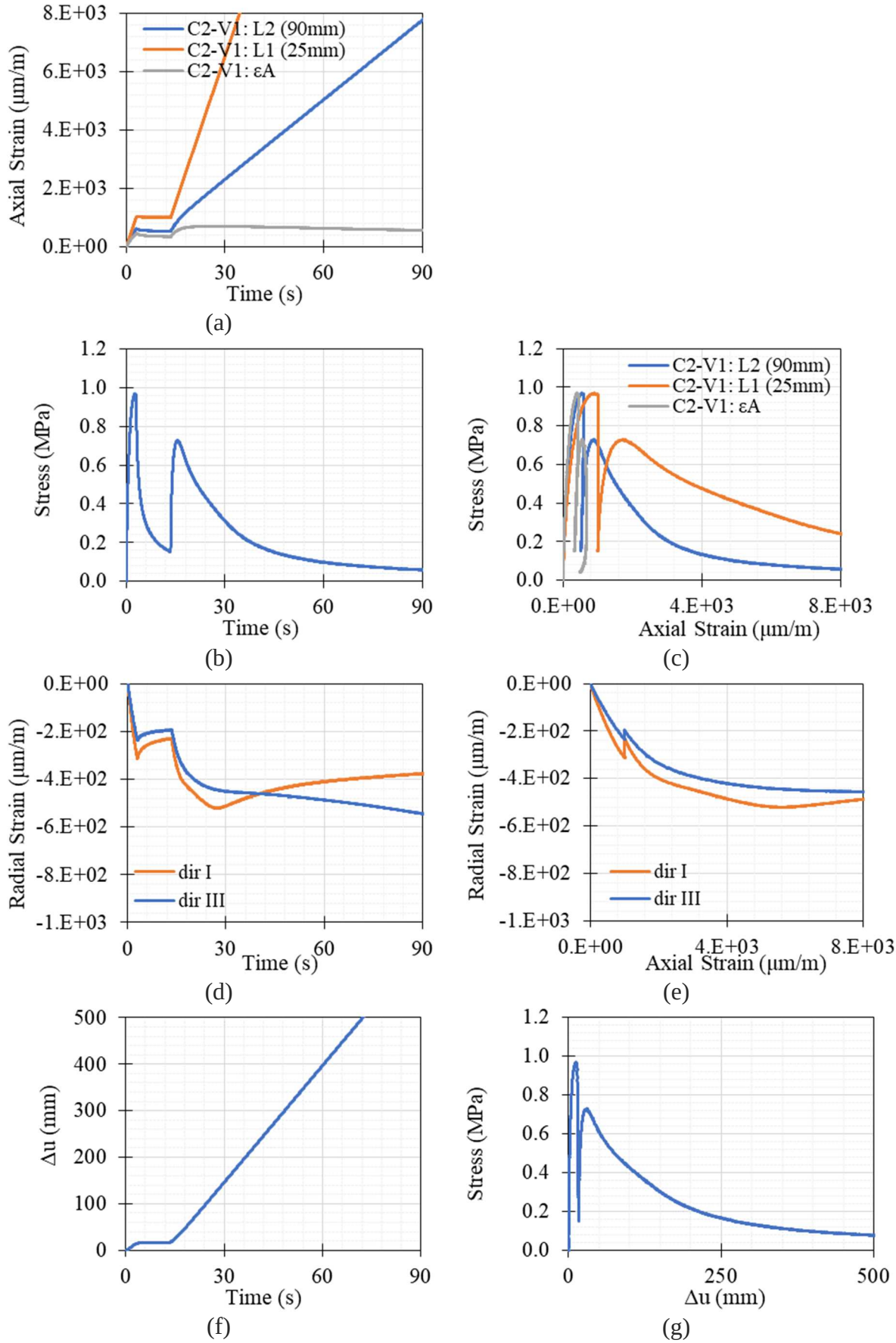

Figure B1-43. Tension test result of C2-V1 at 19°C and 2%/min strain rate

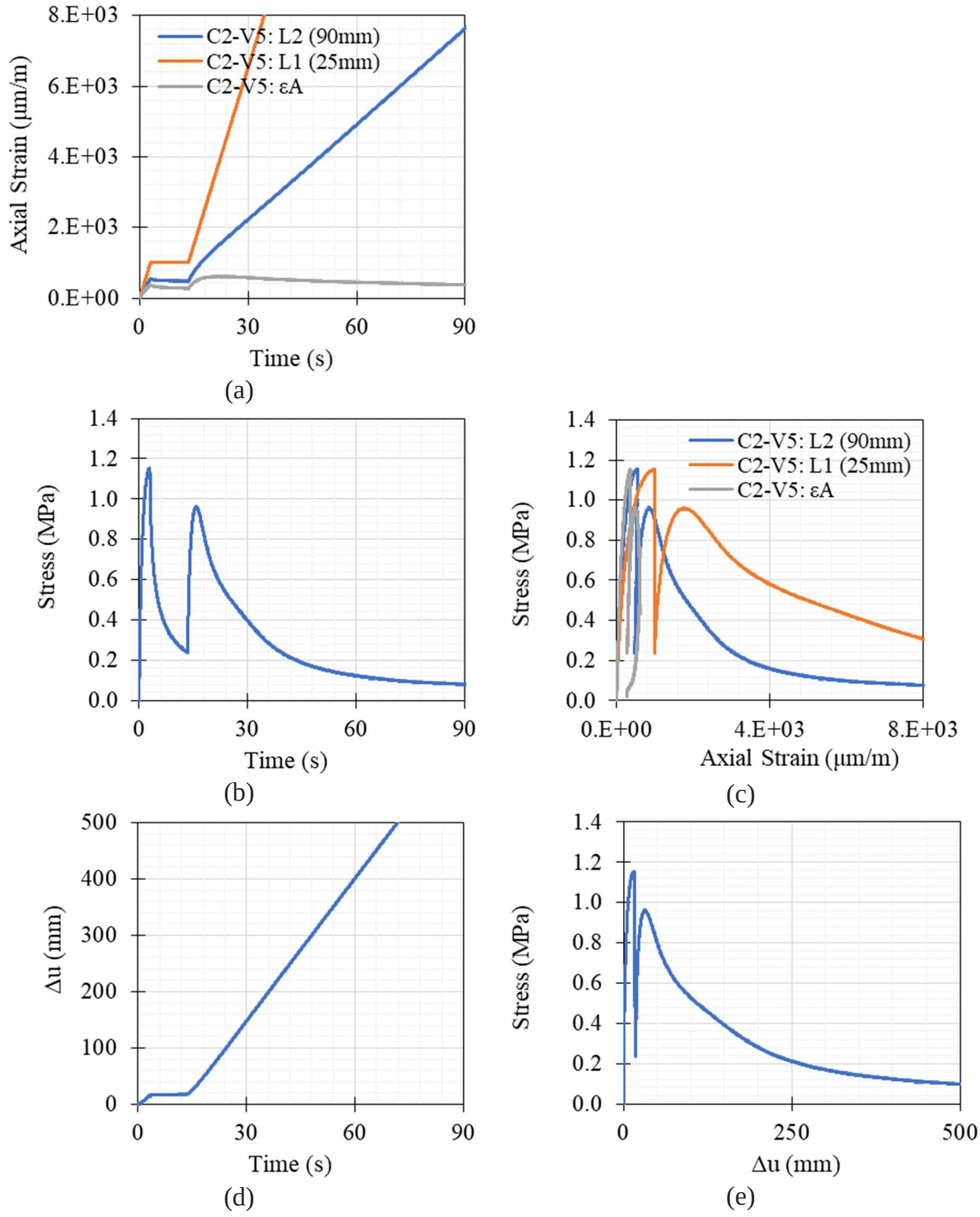

Figure B1-44. Tension test result of C2-V5 at 19°C and 2%/min strain rate

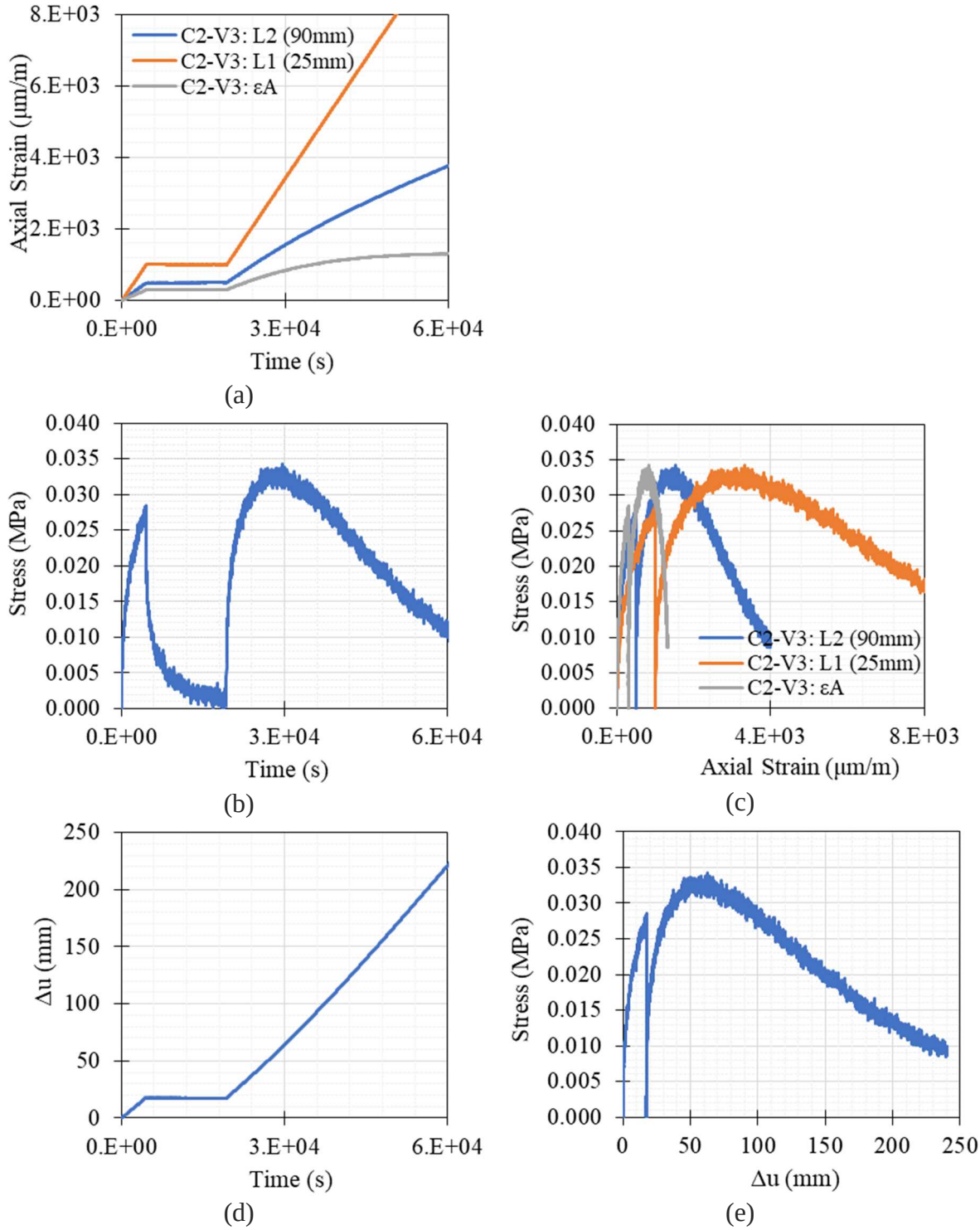

Figure B1-45. Tension test result of C2-V3 at 19°C and 0.001%/min strain rate

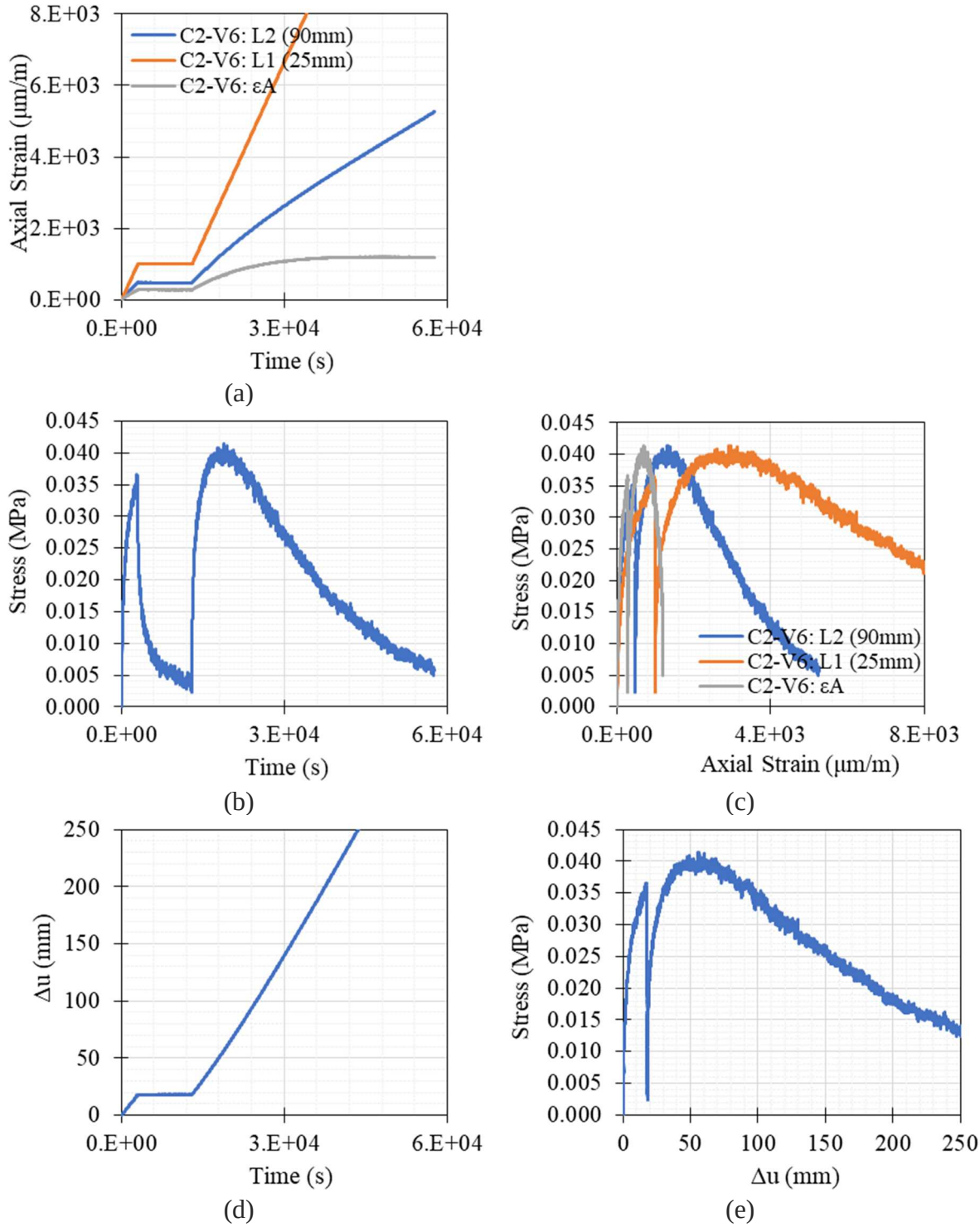

Figure B1-46. Tension test result of C2-V6 at 19°C and 0.002%/min strain rate

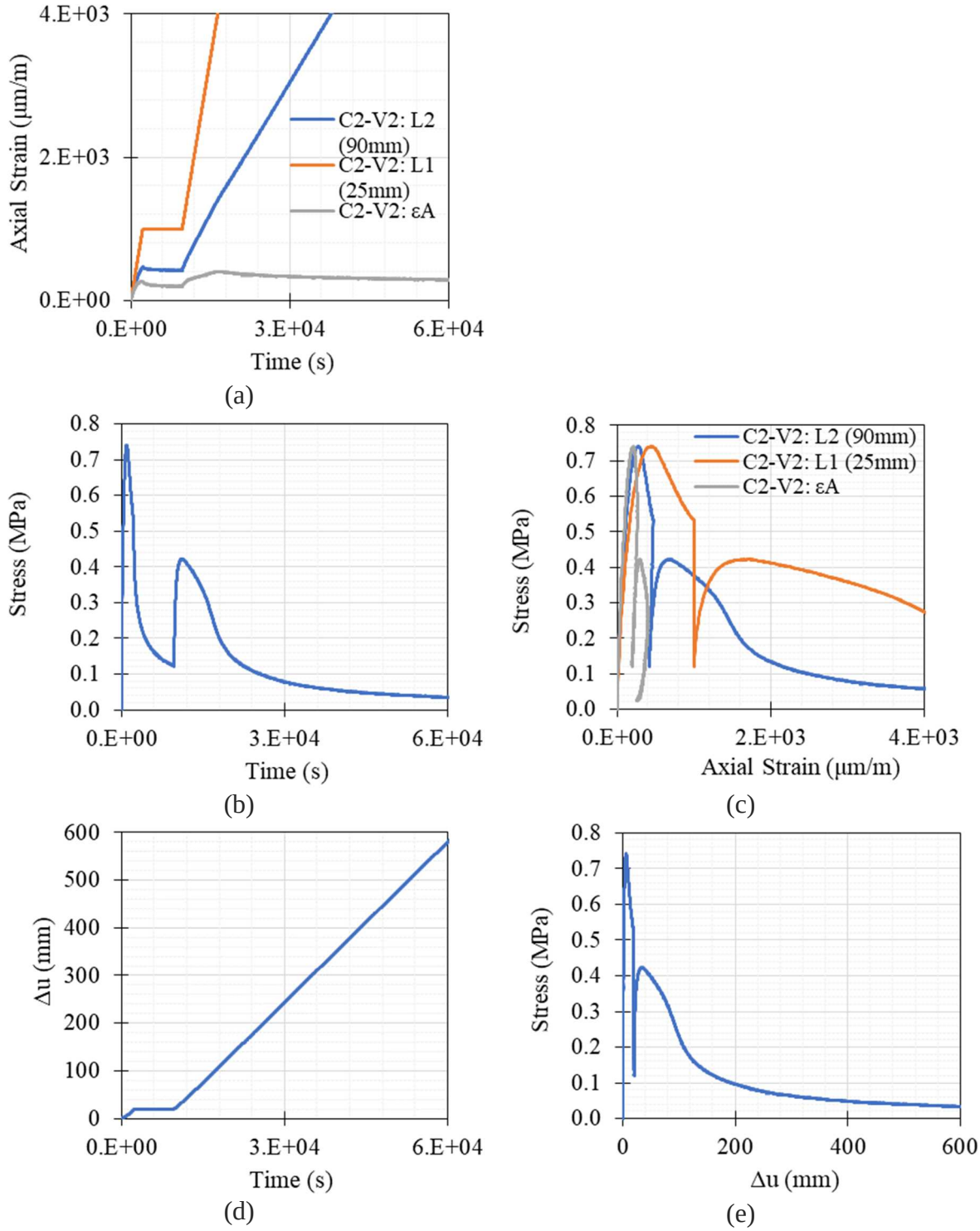

Figure B1-47. Tension test result of C2-V2 at 0°C and 0.003%/min strain rate

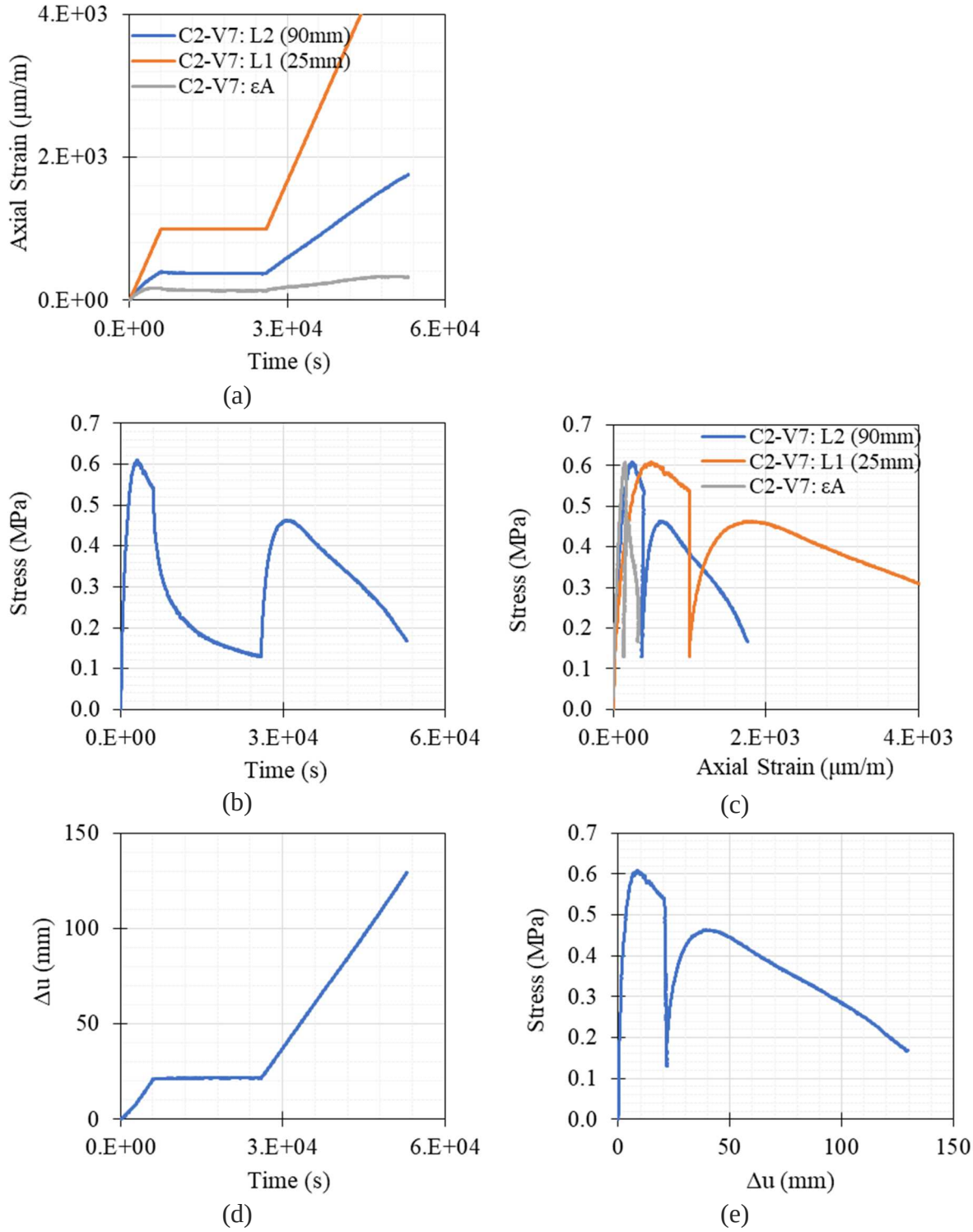

Figure B1-48. Tension test result of C2-V7 at 0°C and 0.001%/min strain rate

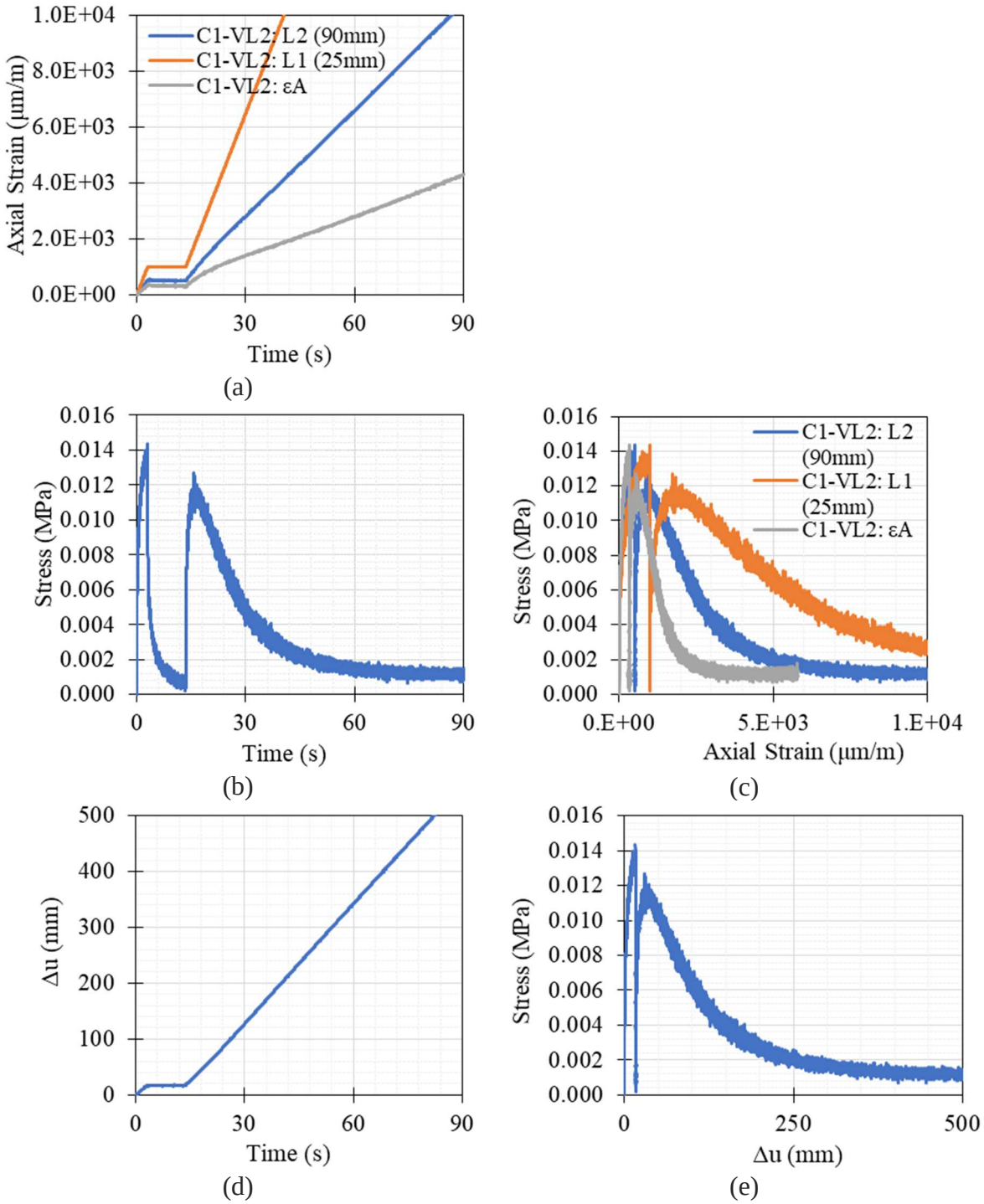

Figure B1-49. Tension test result of C1-VL2 at 40°C and 2%/min strain rate

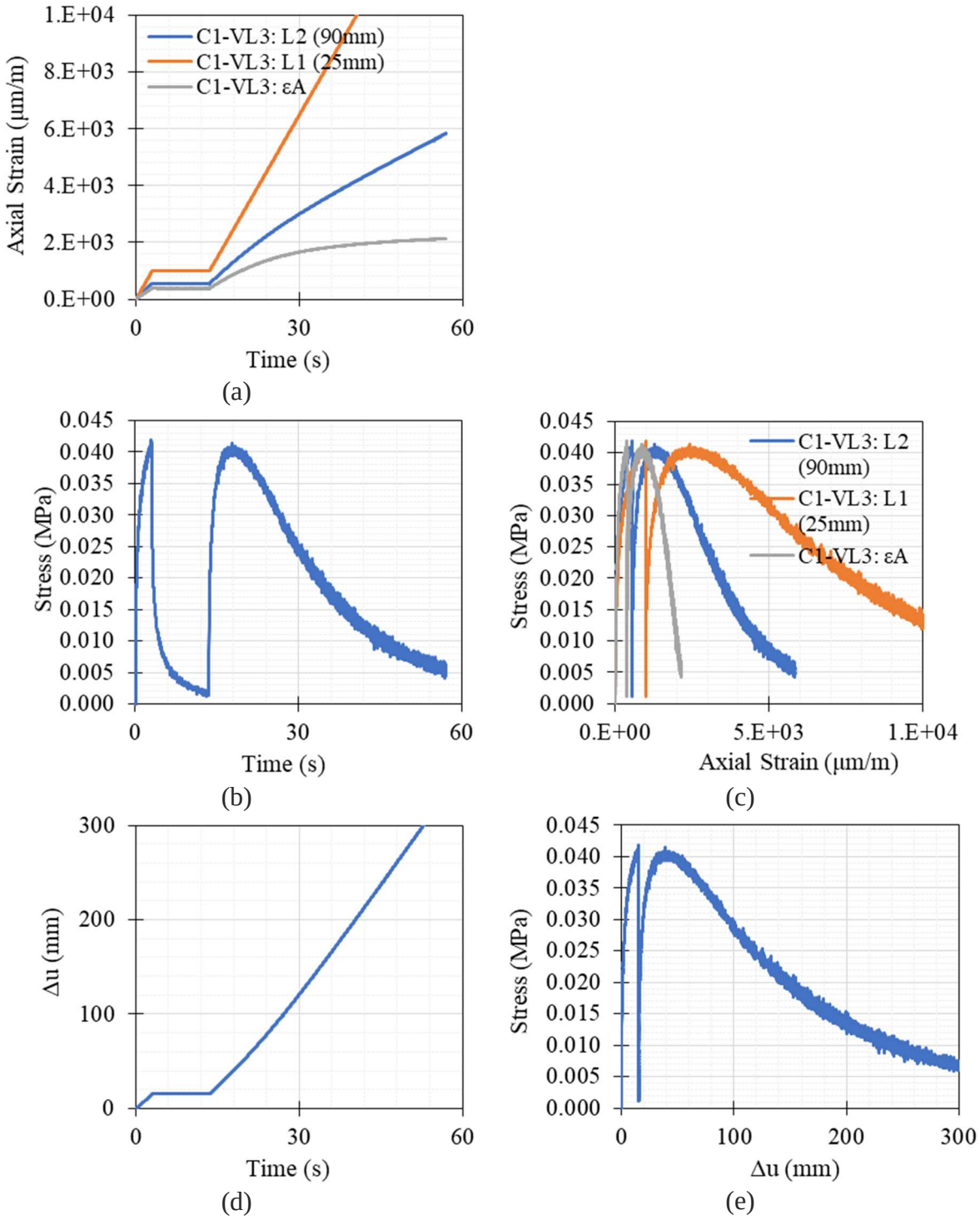

Figure B1-50. Tension test result of C1-VL3 at 40°C and 2%/min strain rate

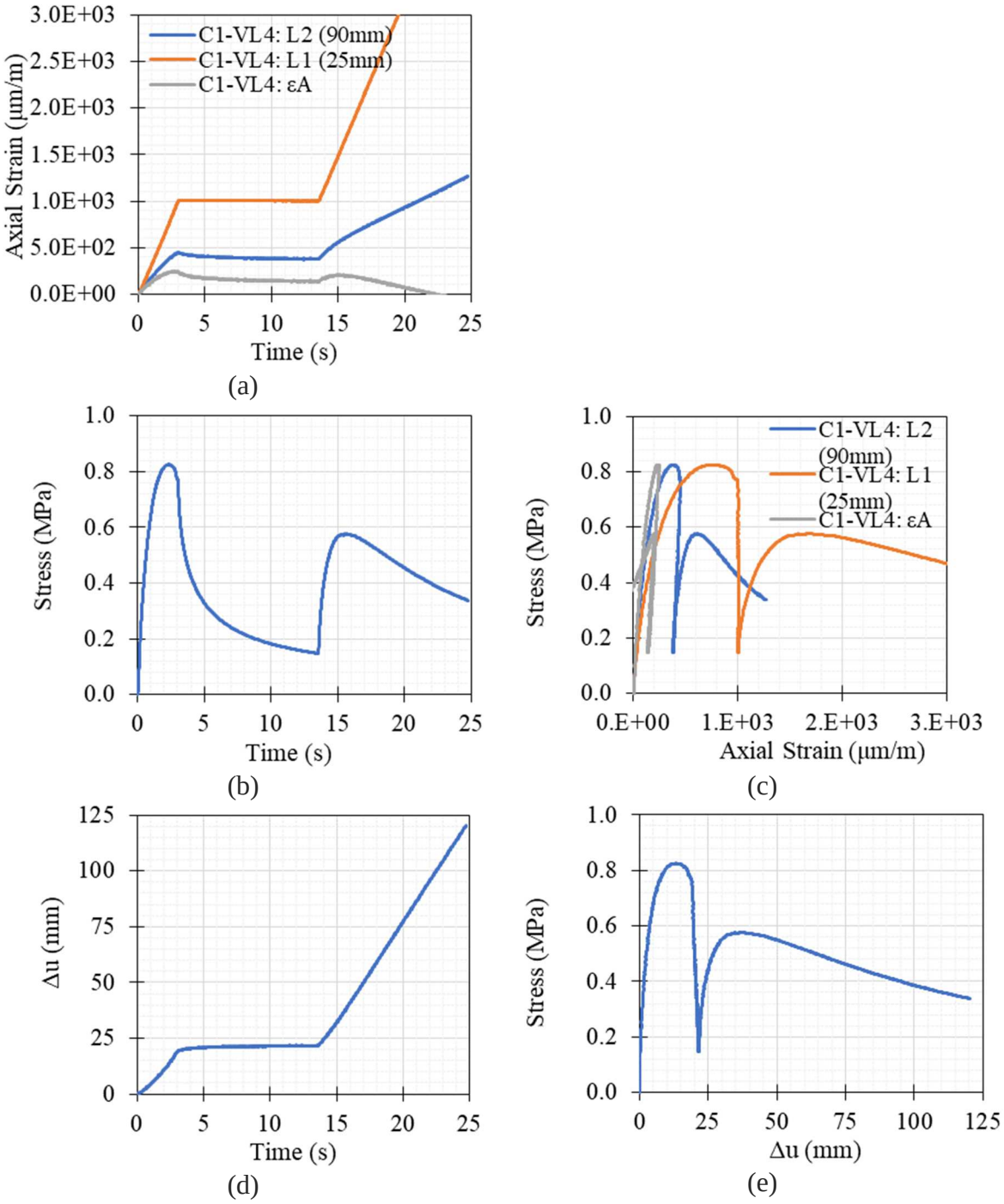

Figure B1-51. Tension test result of C1-VL4 at 19°C and 2%/min strain rate

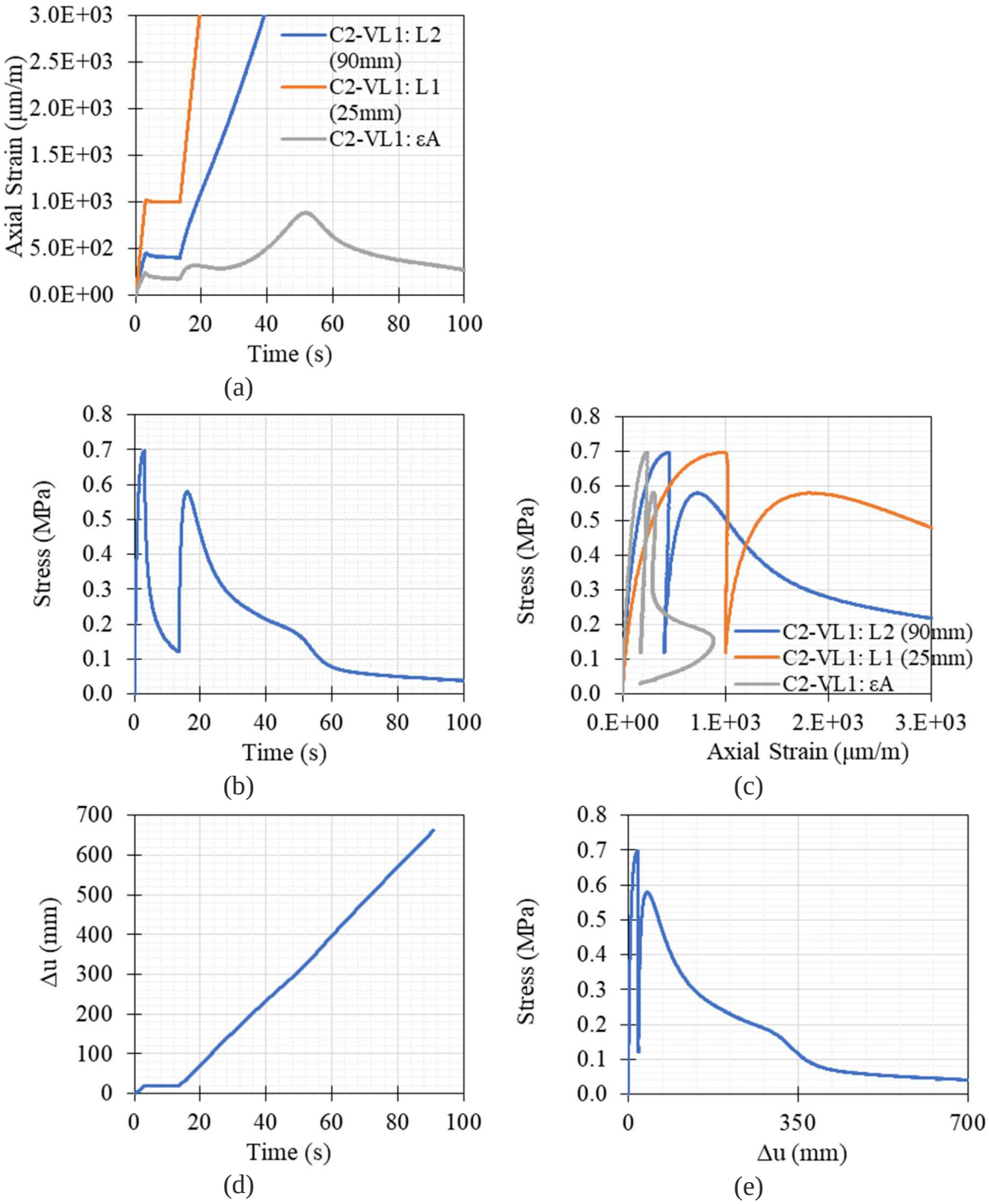

Figure B1-52. Tension test result of C2-VL1 at 19°C and 2%/min strain rate

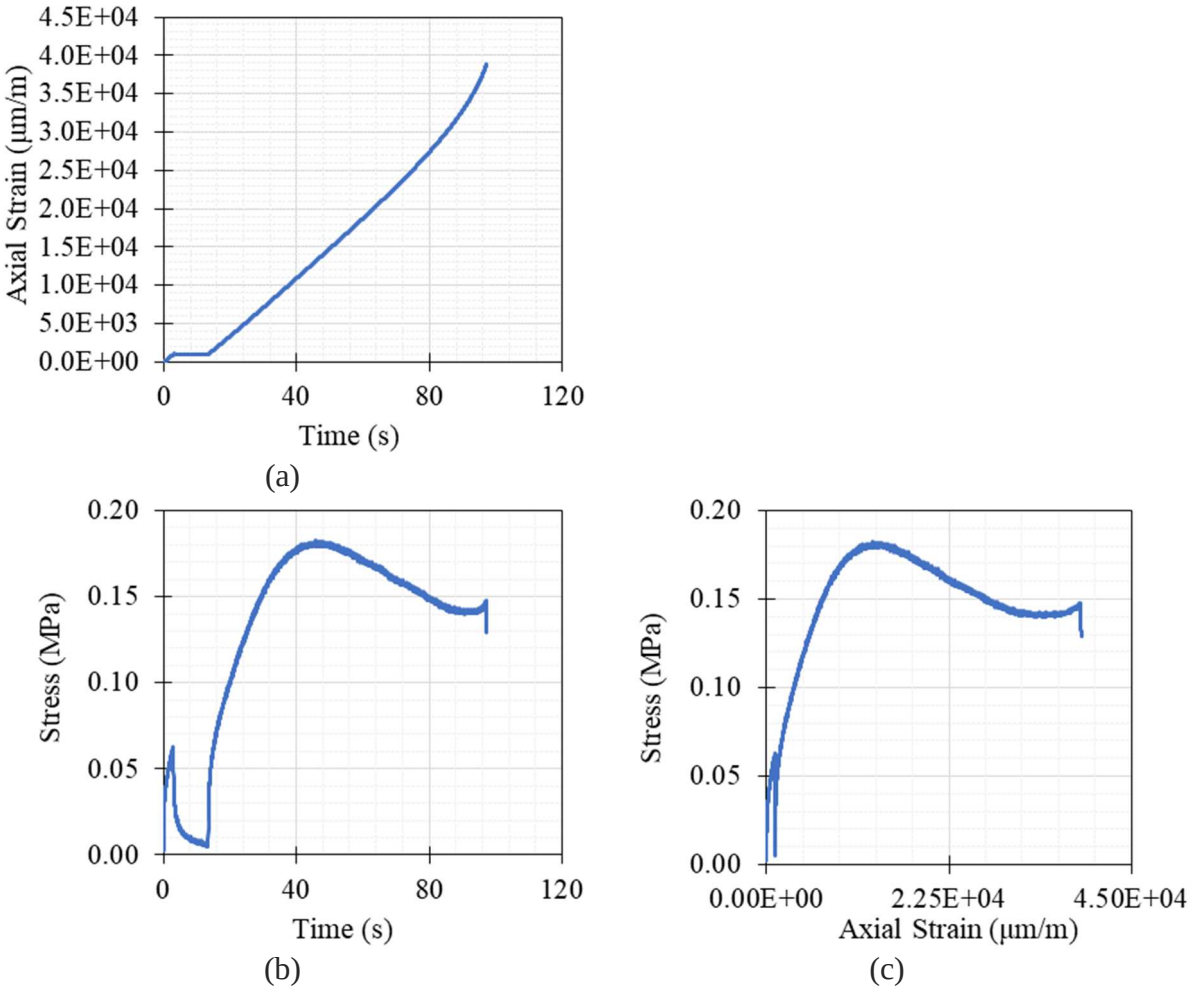

Figure B1-53. Tension test result of D2-H3 at 40°C and 2%/min strain rate

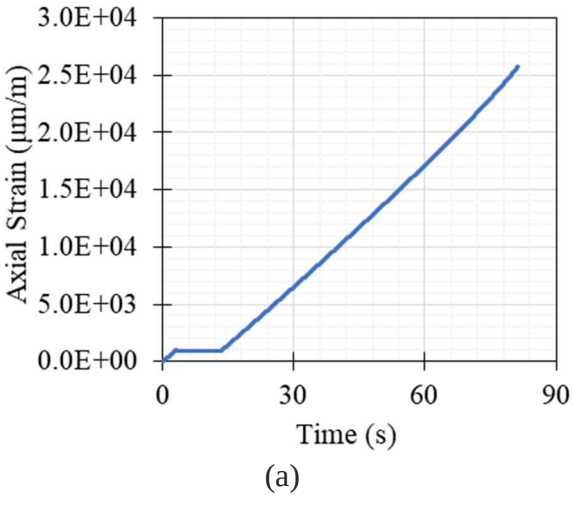

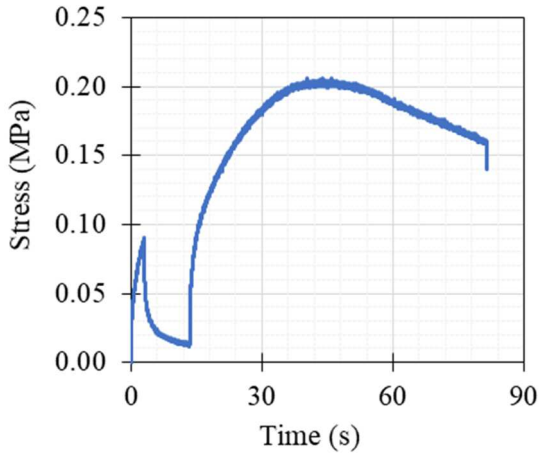

(b)

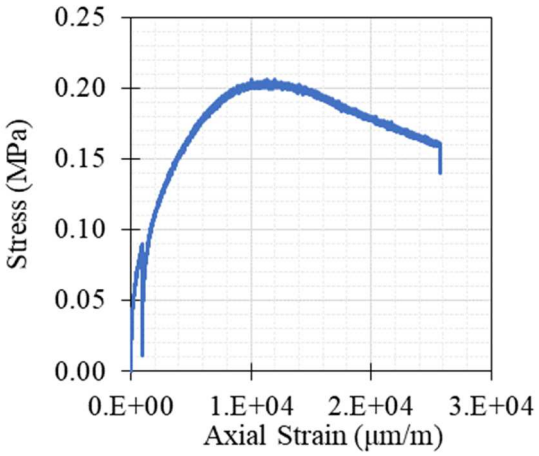

(c)

Figure B1-54. Tension test result of D3-H11 at 40°C and 2%/min strain rate

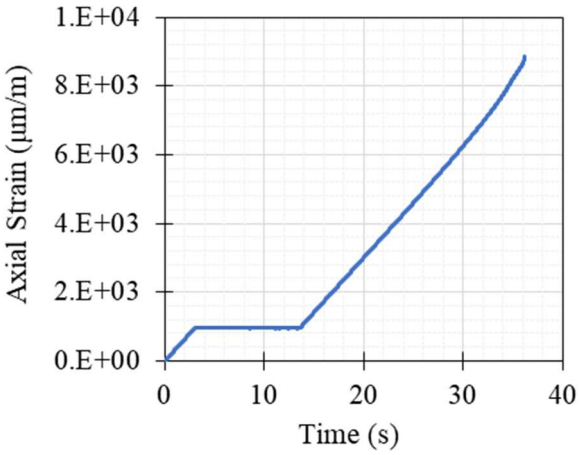

(a)

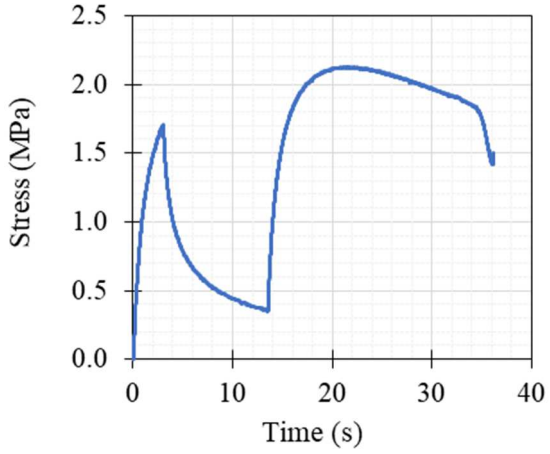

(b)

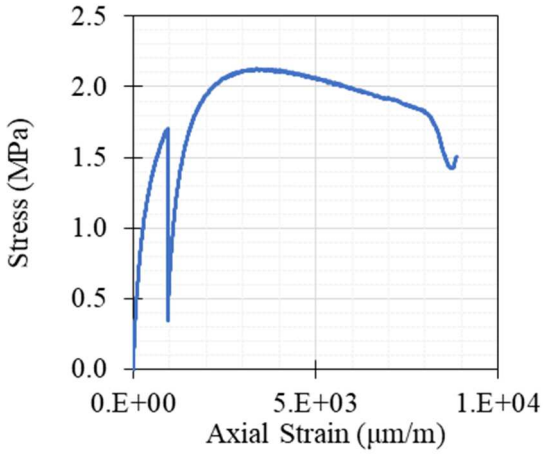

(c)

Figure B1-55. Tension test result of D1-H1 at 19°C and 2%/min strain rate

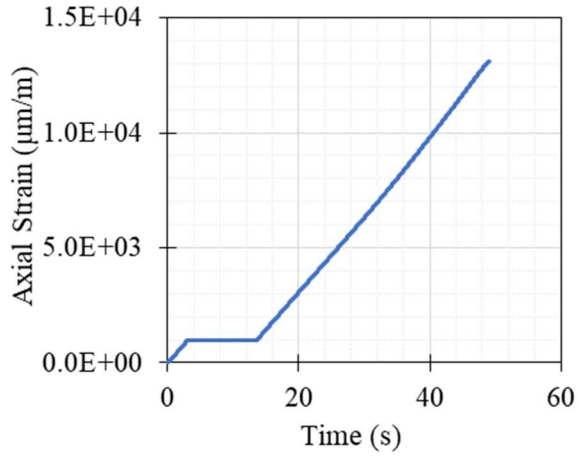

(a)

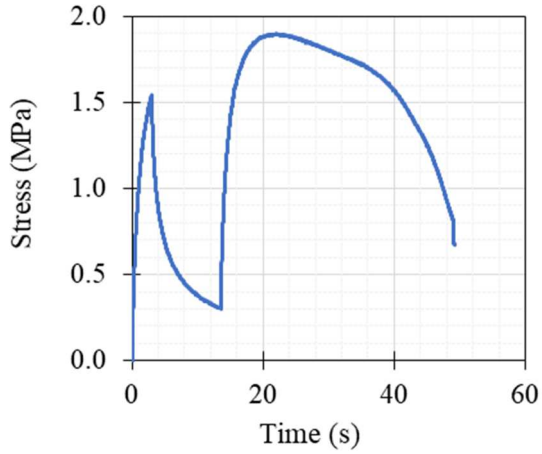

(b)

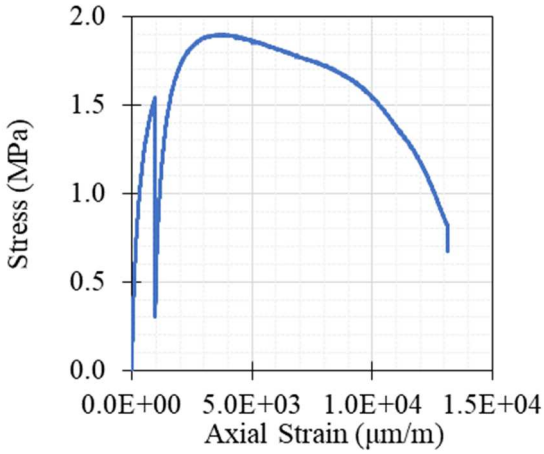

(c)

Figure B1-56. Tension test result of D2-H5 at 19°C and 2%/min strain rate

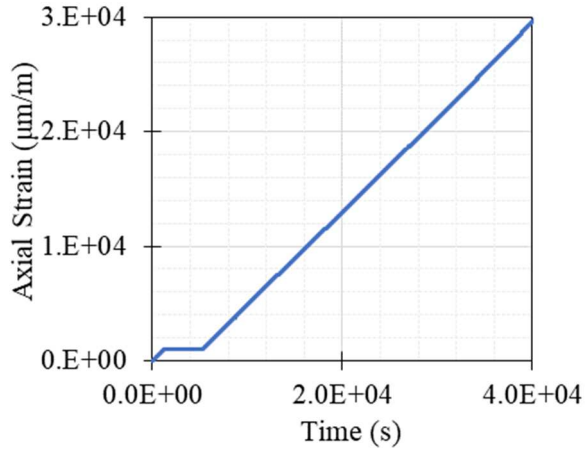

(a)

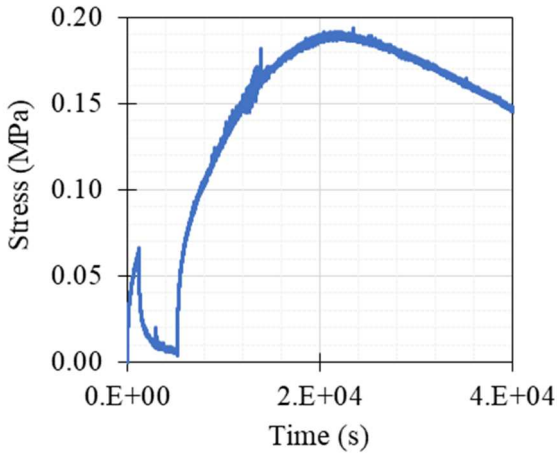

(b)

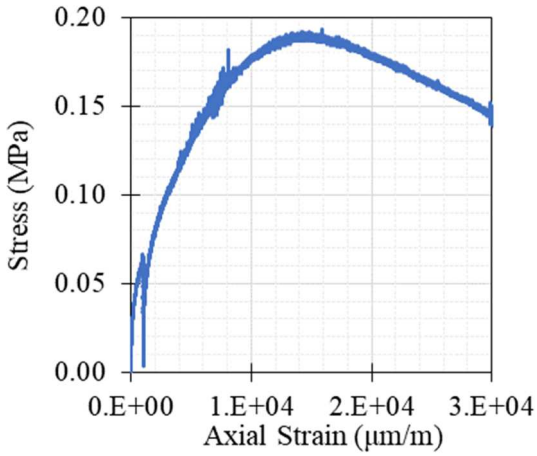

(c)

Figure B1-57. Tension test result of D2-H4 at 40°C and 0.005%/min strain rate

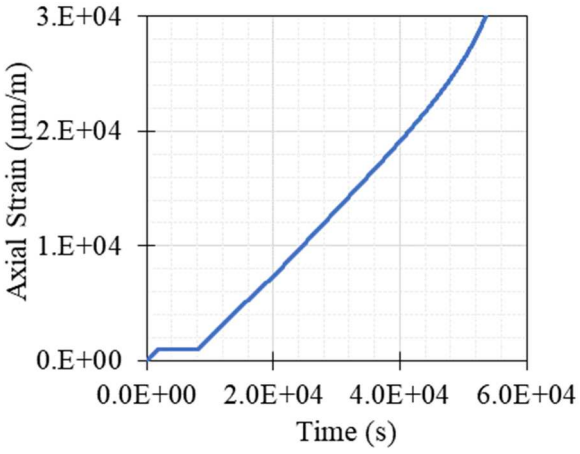

(a)

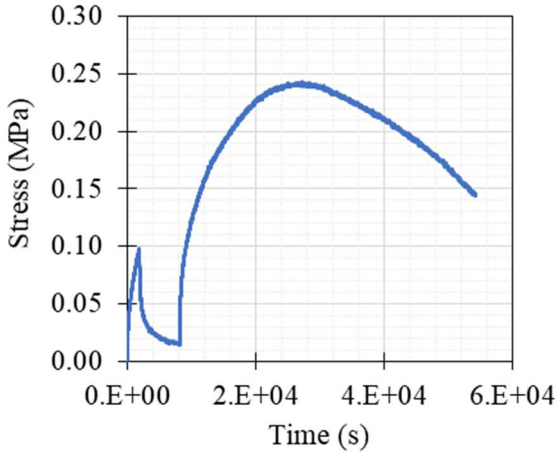

(b)

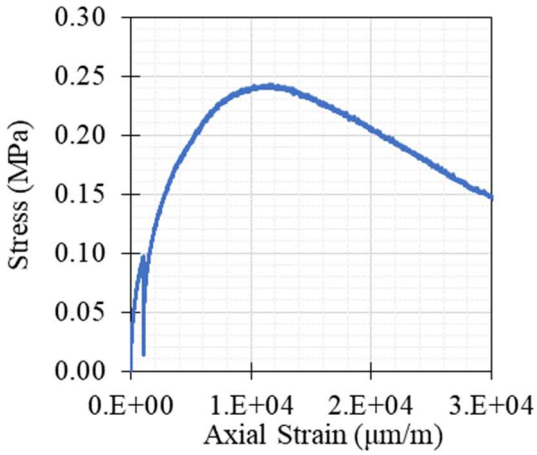

(c)

Figure B1-58. Tension test result of D3-H12 at 19°C and 0.003%/min strain rate

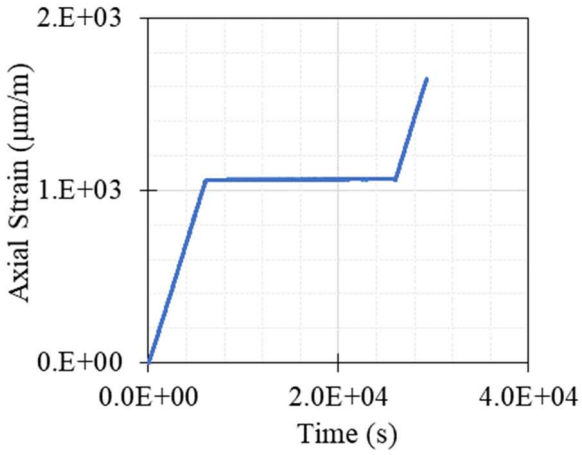

(a)

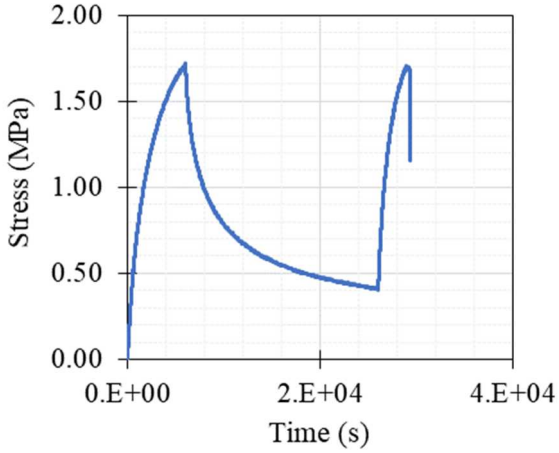

(b)

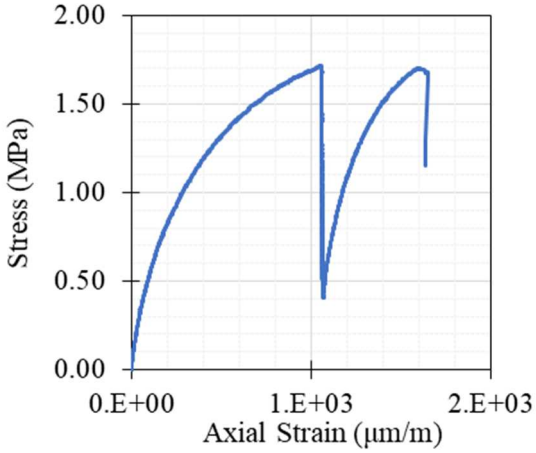

(c)

Figure B1-59. Tension test result of D1-H3 at 0°C and 0.001%/min strain rate

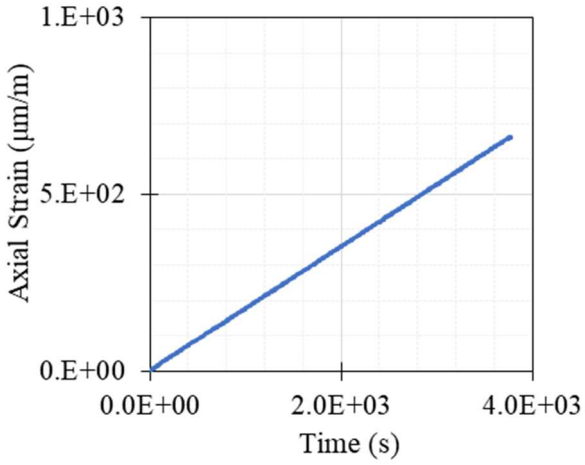

(a)

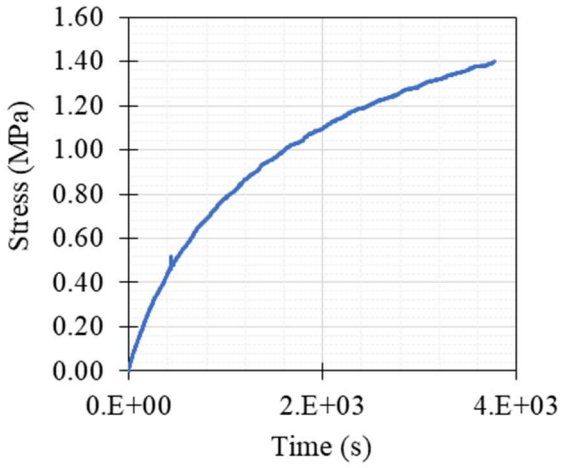

(b)

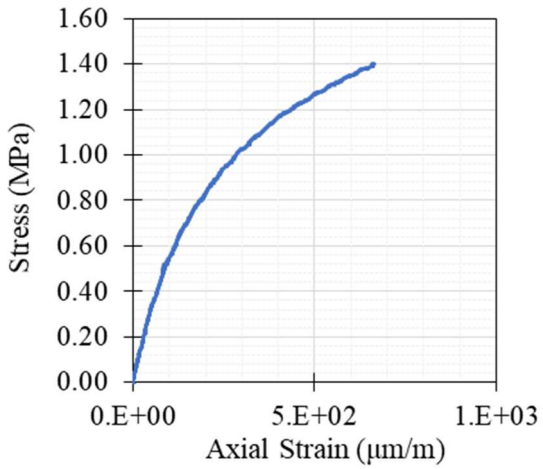

(c)

Figure B1-60. Tension test result of D2-H6 at 0°C and 0.001%/min strain rate

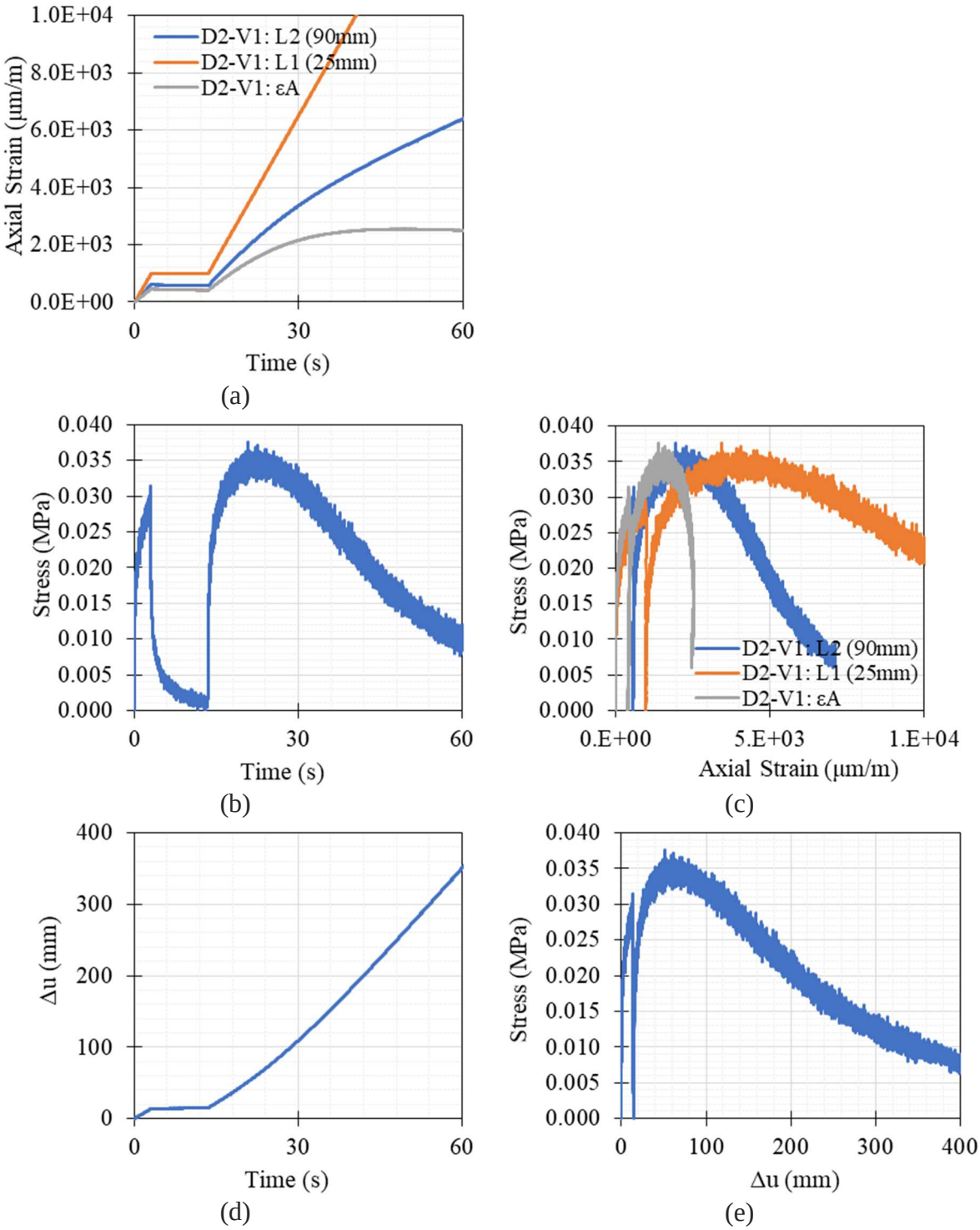

Figure B1-61. Tension test result of D2-V1 at 40°C and 2%/min strain rate

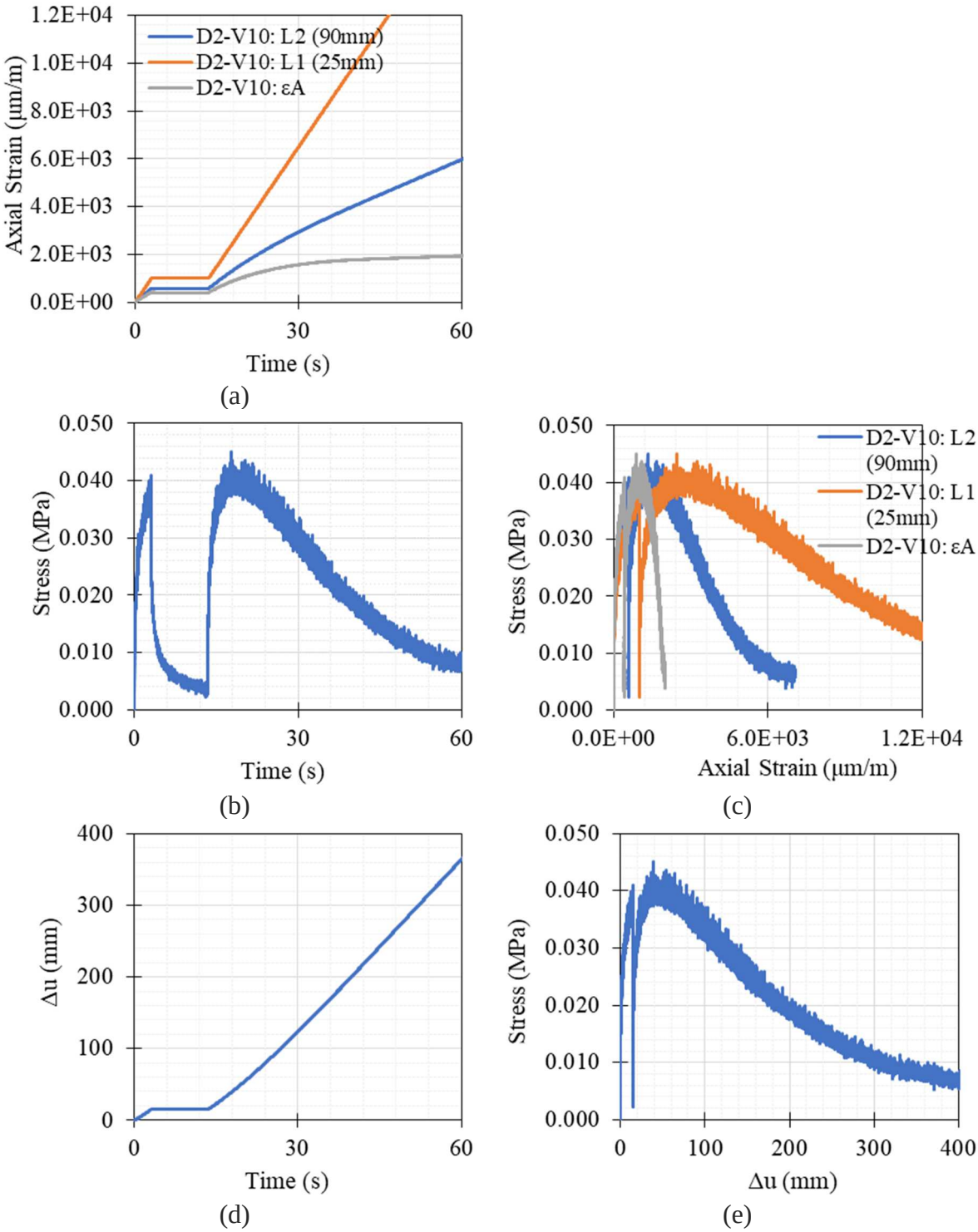

Figure B1-62. Tension test result of D2-V10 at 40°C and 2%/min strain rate

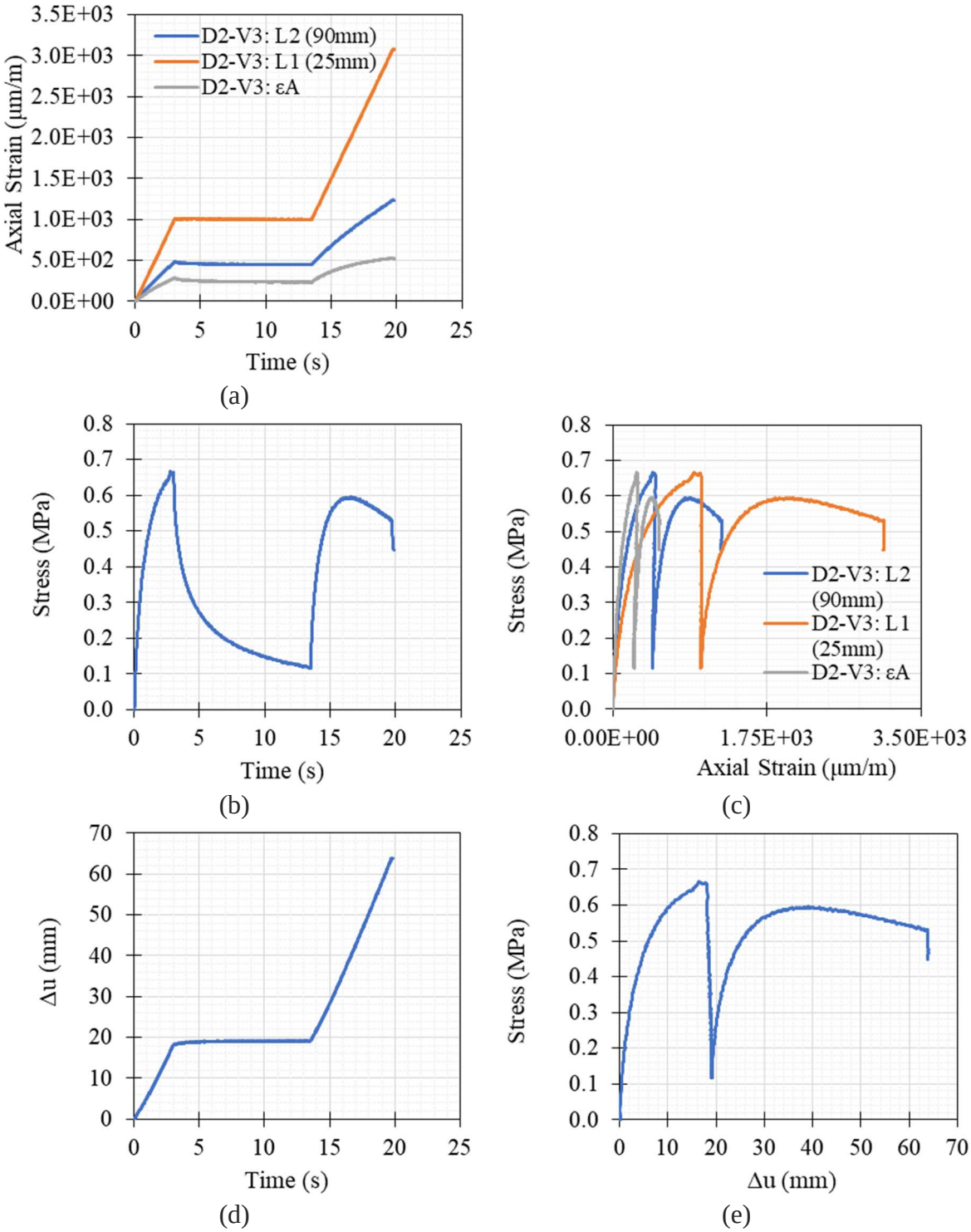

Figure B1-63. Tension test result of D2-V3 at 19°C and 2%/min strain rate

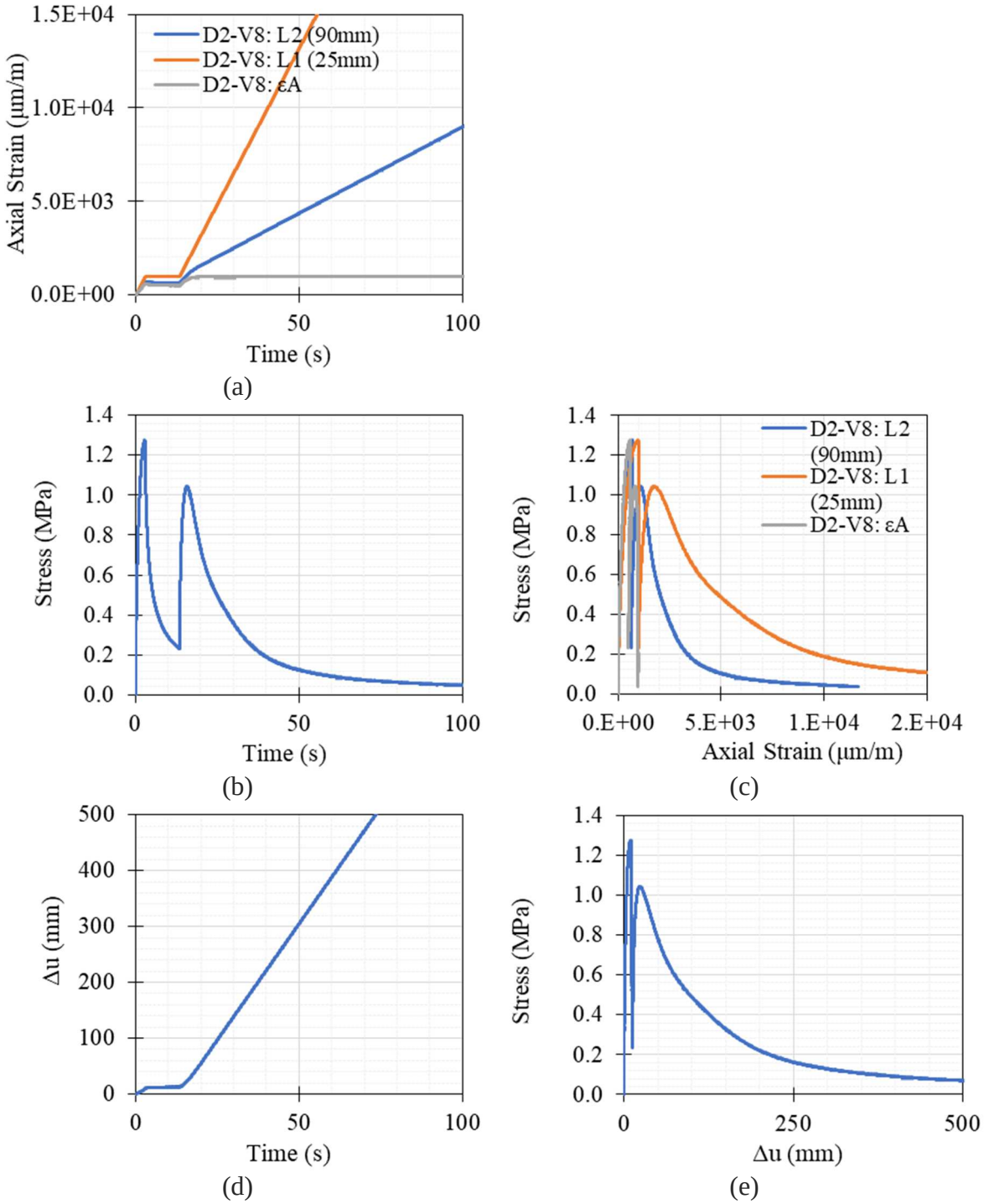

Figure B1-64. Tension test result of D2-V8 at 19°C and 2%/min strain rate

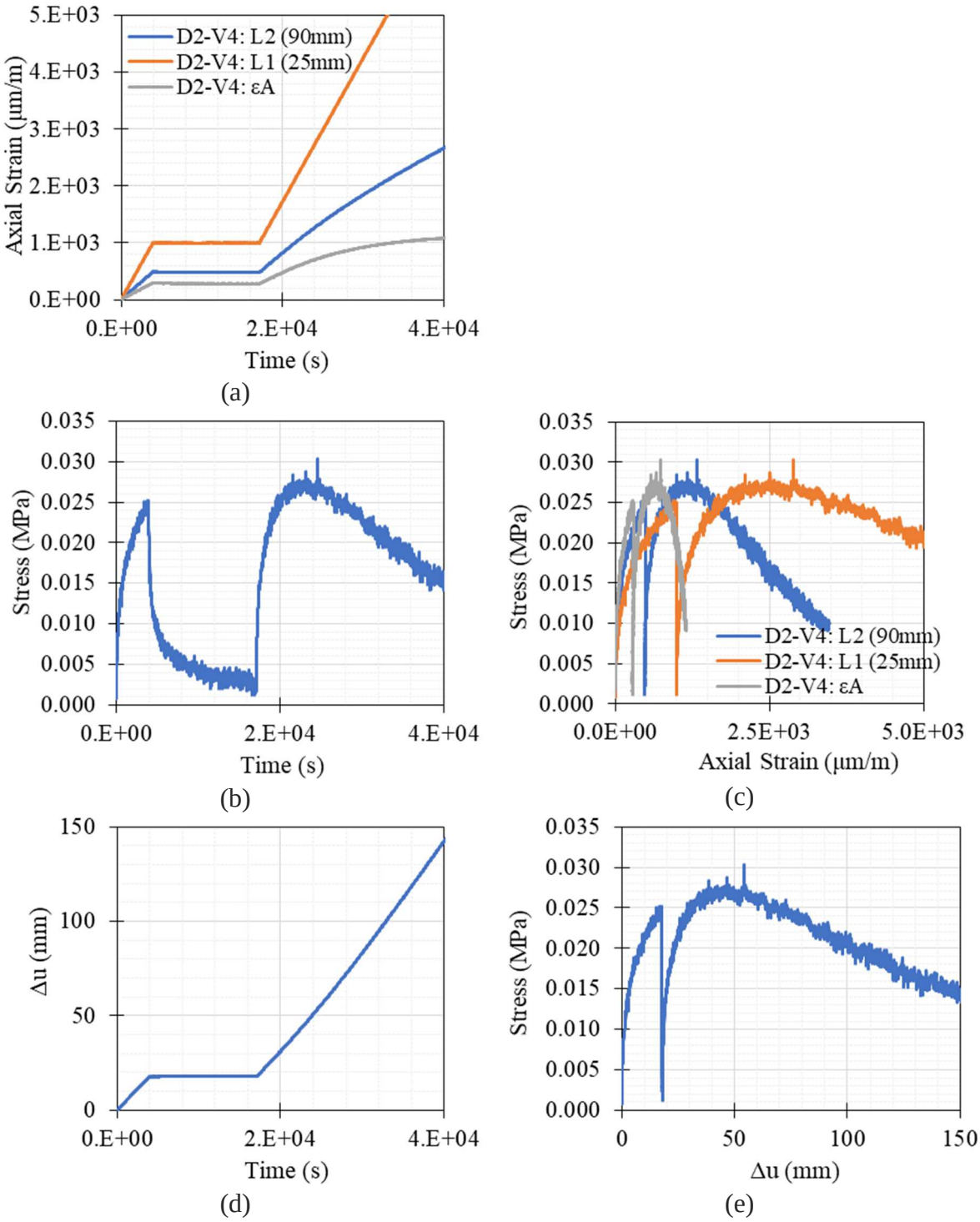

Figure B1-65. Tension test result of D2-V4 at 19°C and 0.002%/min strain rate

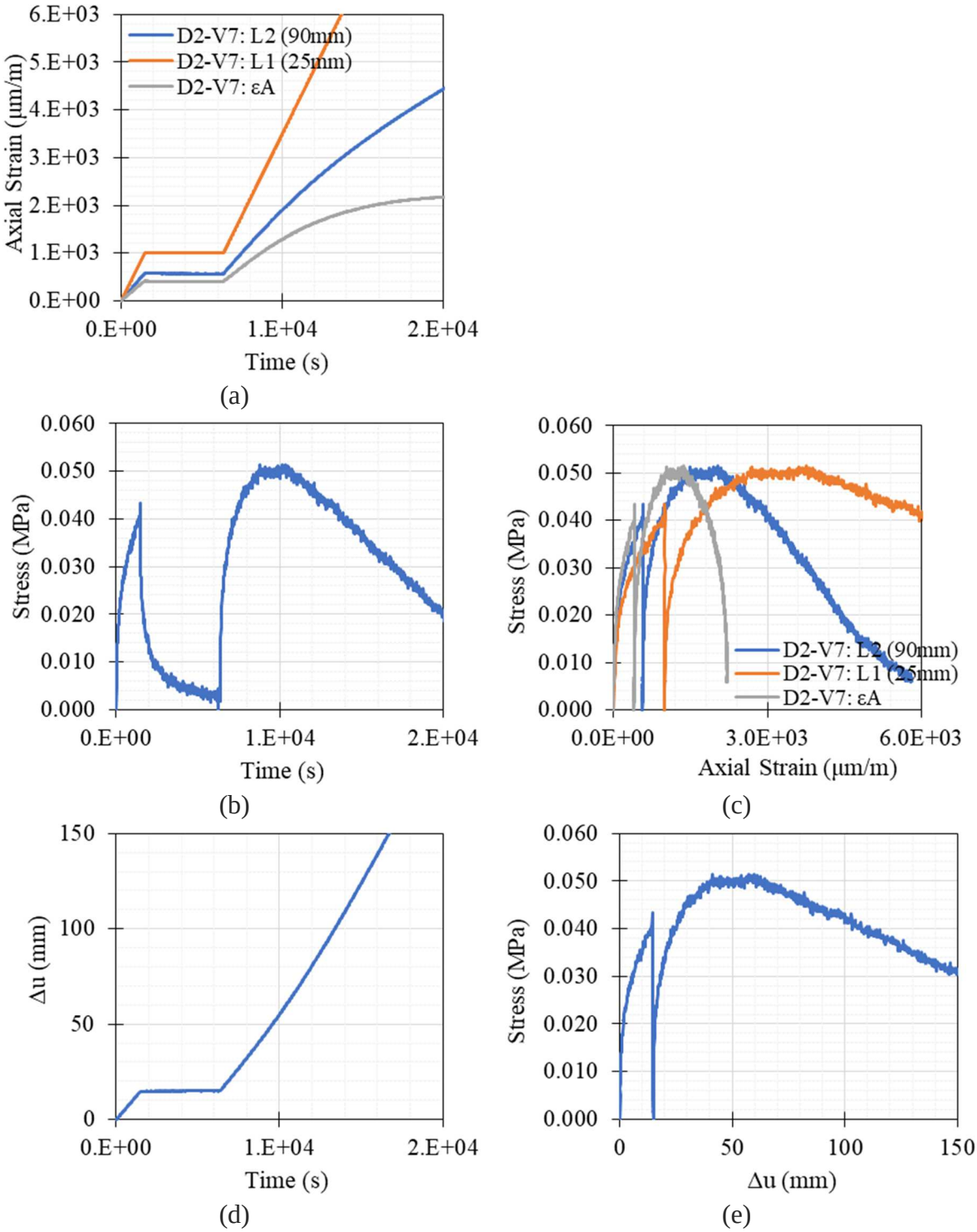

Figure B1-66. Tension test result of D2-V7 at 0°C and 0.004%/min strain rate

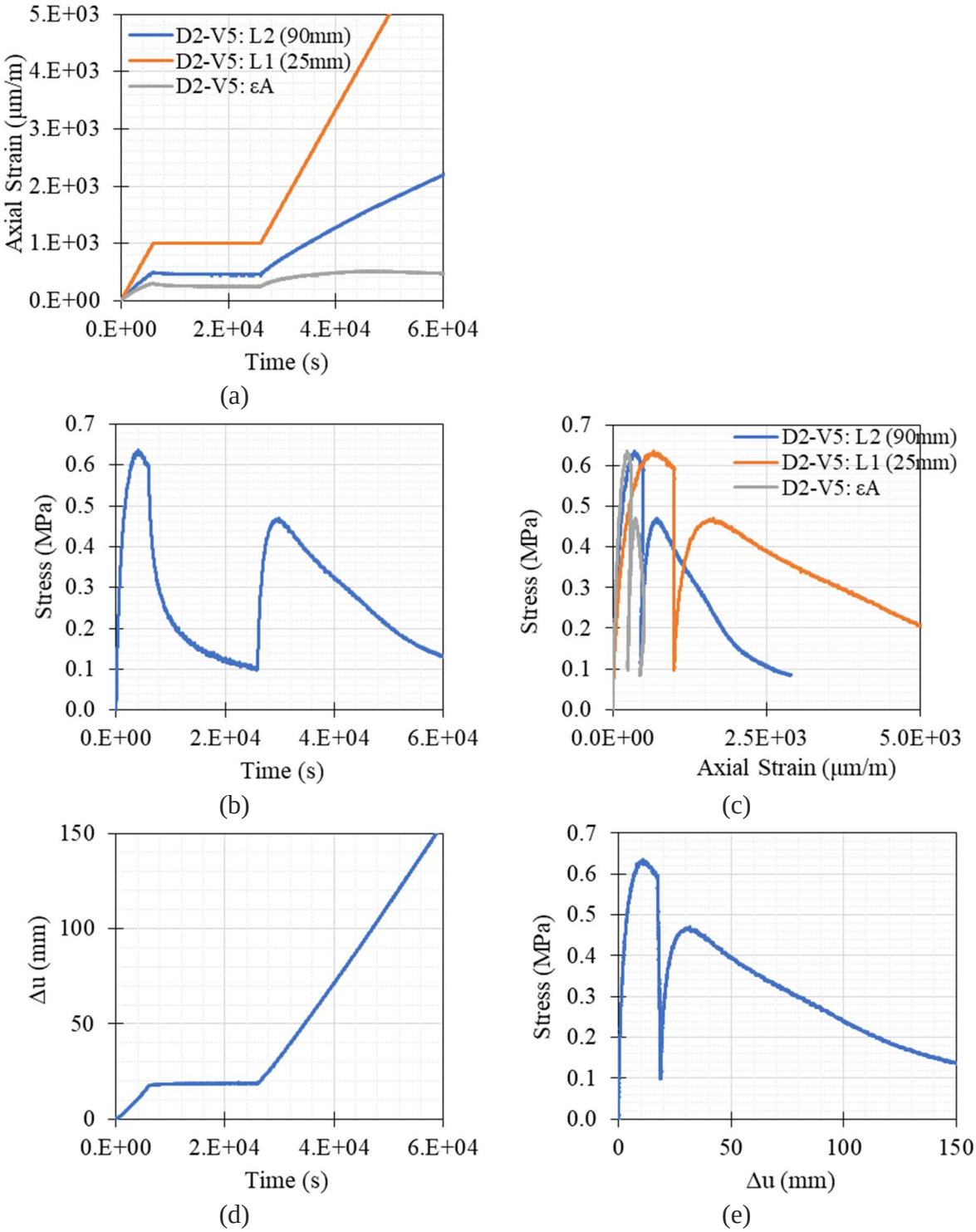

Figure B1-67. Tension test result of D2-V5 at 0°C and 0.001%/min strain rate

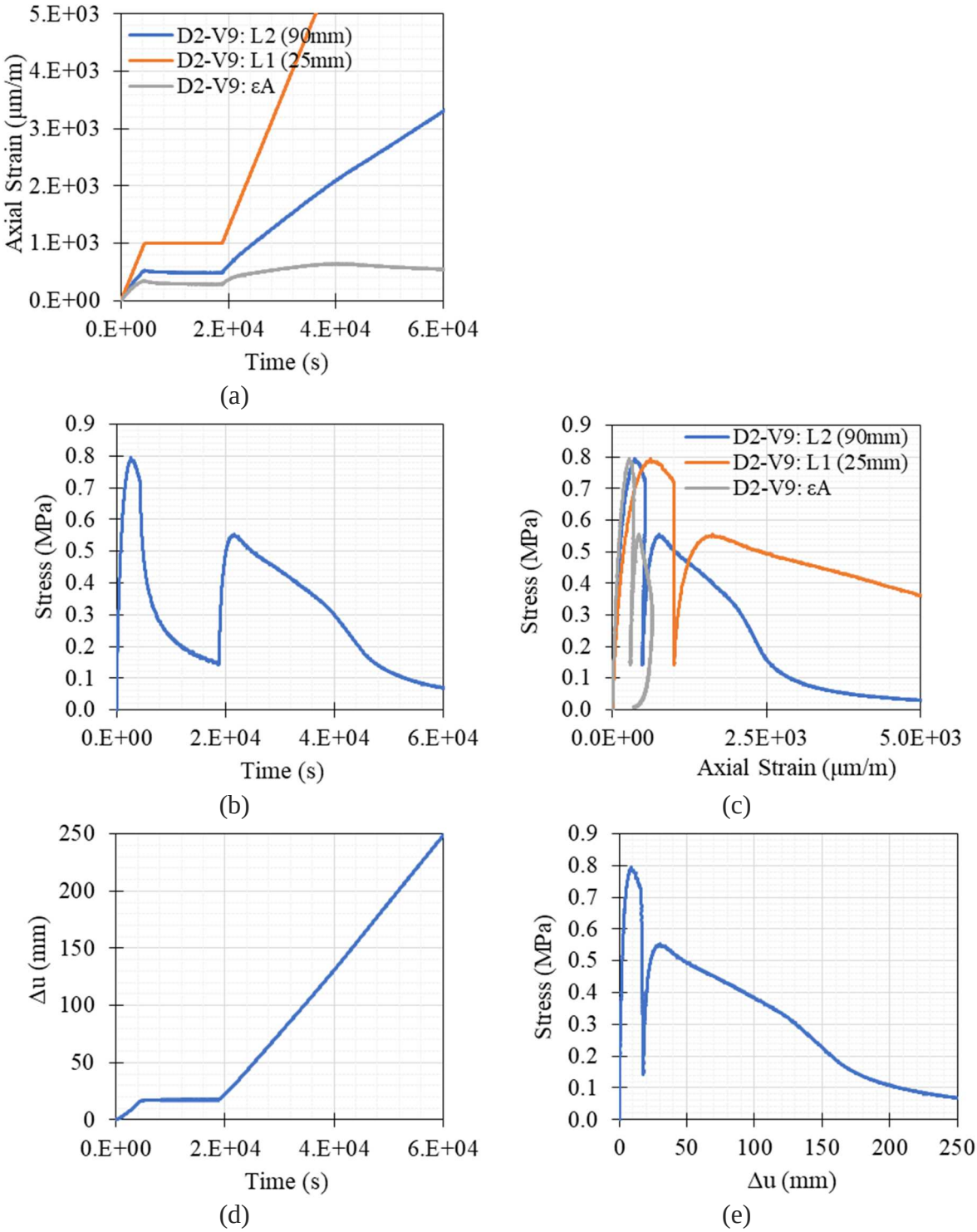

Figure B1-68. Tension test result of D2-V9 at 0°C and 0.001%/min strain rate

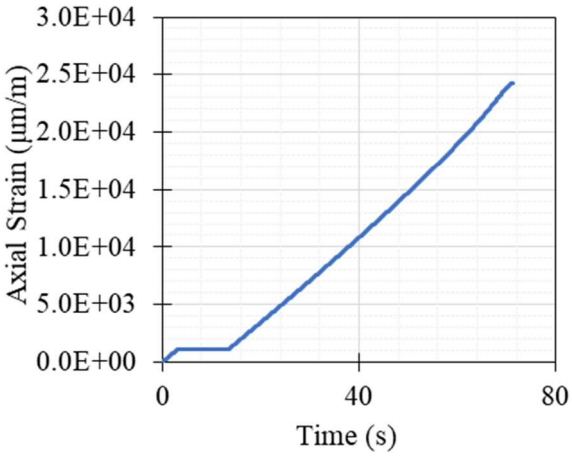

(a)

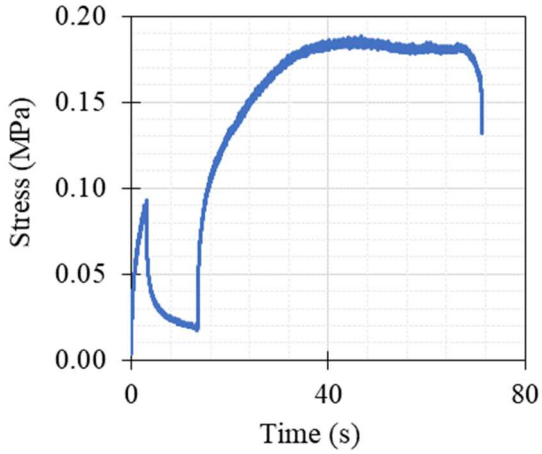

(b)

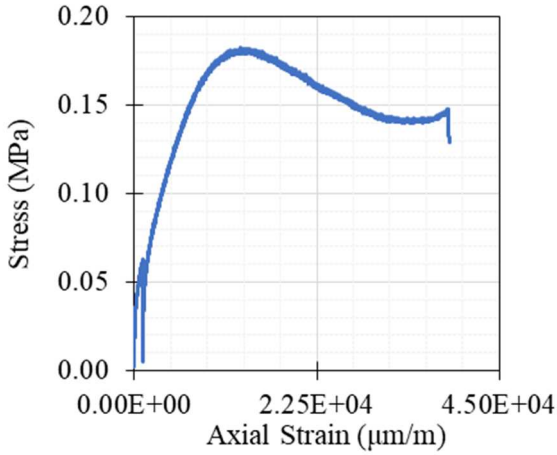

(c)

Figure B1-69. Tension test result of E1-H3 at 40°C and 2%/min strain rate

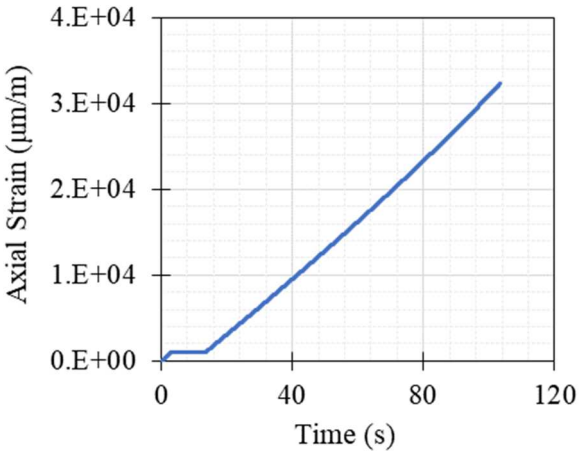

(a)

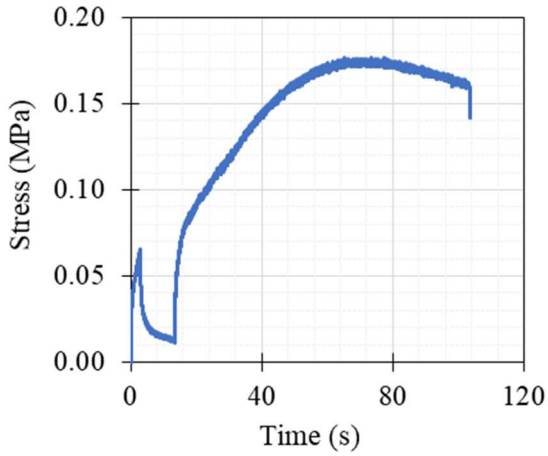

(b)

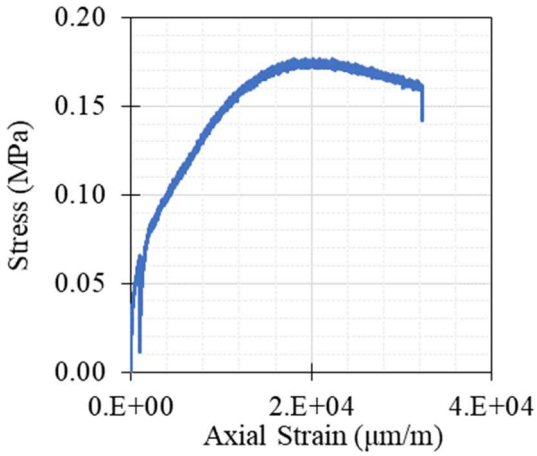

(c)

Figure B1-70. Tension test result of E3-H3 at 40°C and 2%/min strain rate

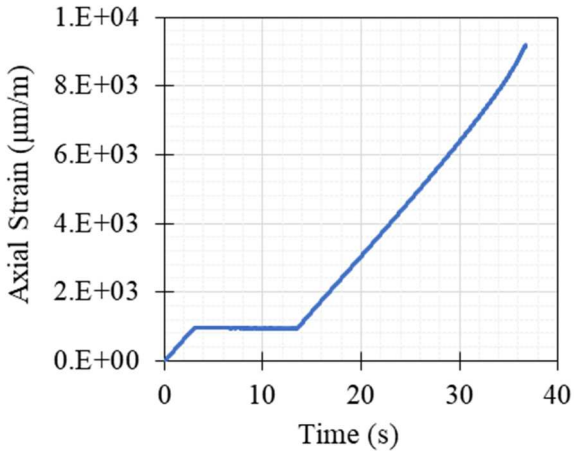

(a)

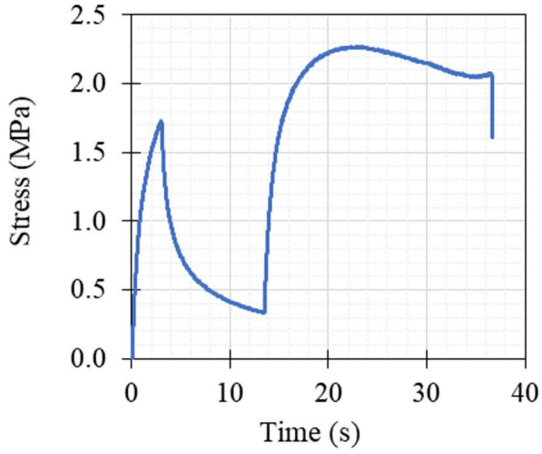

(b)

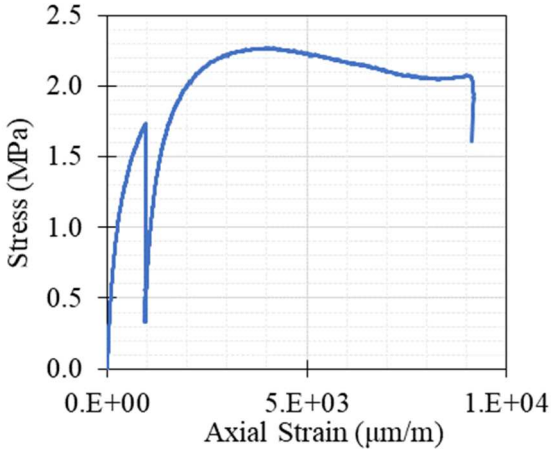

(c)

Figure B1-71. Tension test result of E1-H2 at 19°C and 2%/min strain rate

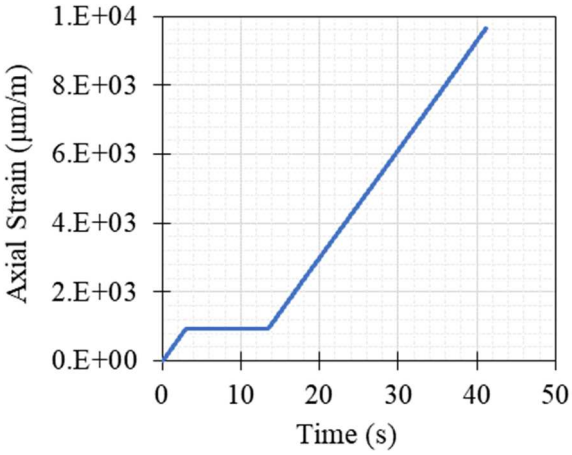

(a)

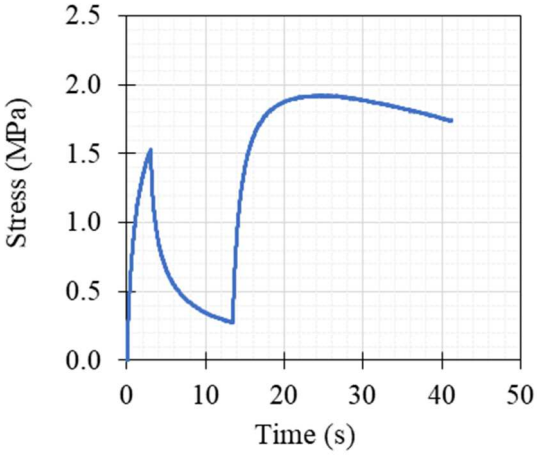

(b)

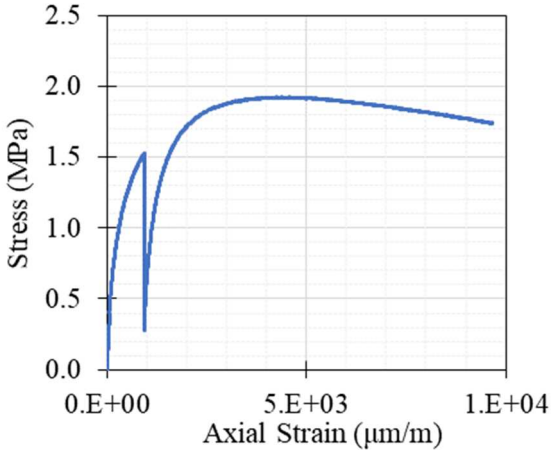

(c)

Figure B1-72. Tension test result of E2-H3 at 19°C and 2%/min strain rate

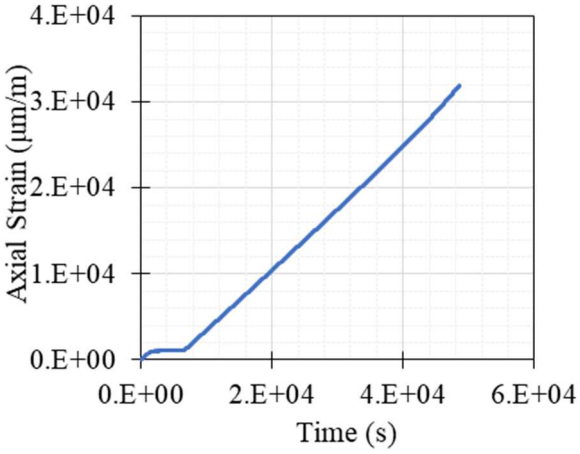

(a)

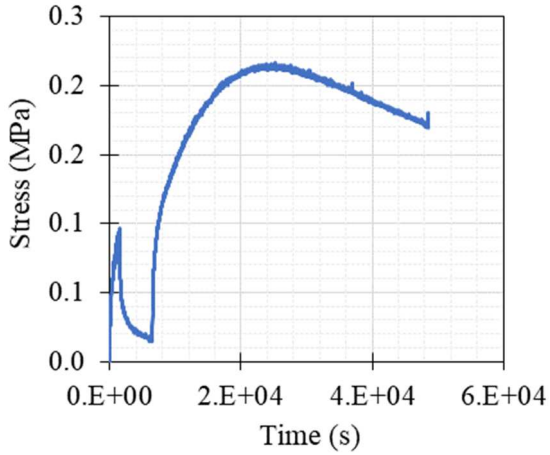

(b)

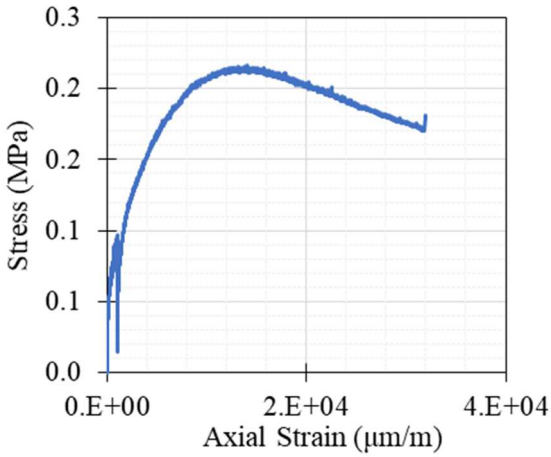

(c)

Figure B1-73. Tension test result of E2-H2 at 19°C and 0.004%/min strain rate

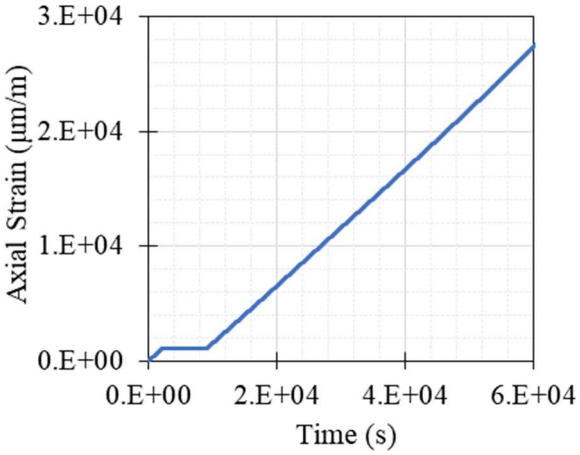

(a)

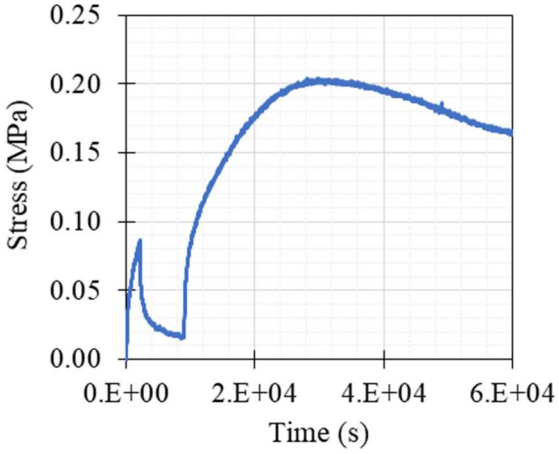

(b)

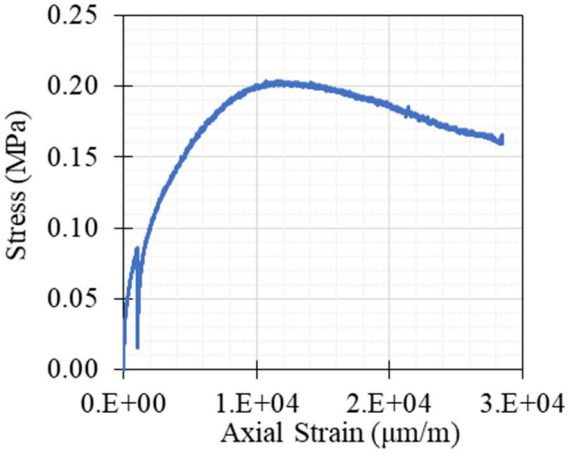

(c)

Figure B1-74. Tension test result of E3-H2 at 19°C and 0.003%/min strain rate

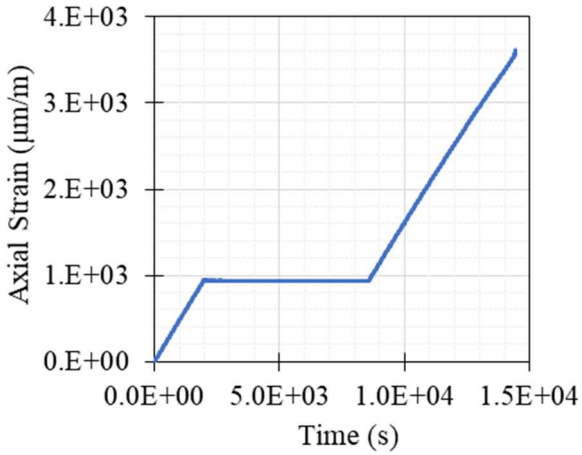

(a)

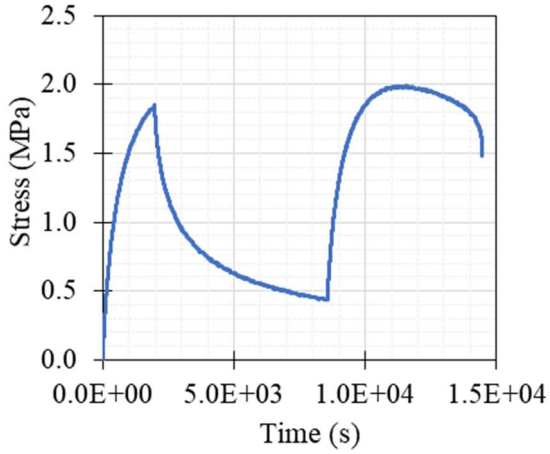

(b)

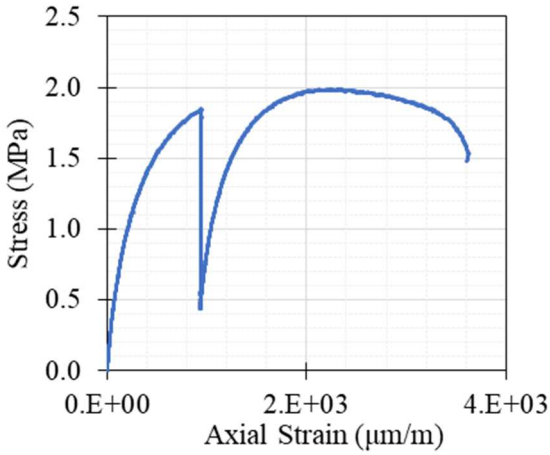

(c)

Figure B1-75. Tension test result of E2-H4 at 0°C and 0.003%/min strain rate

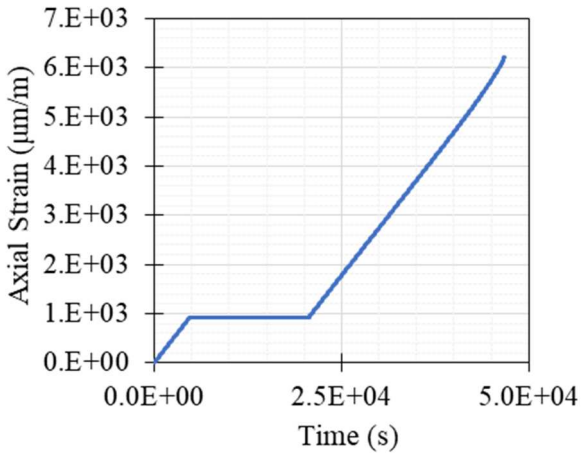

(a)

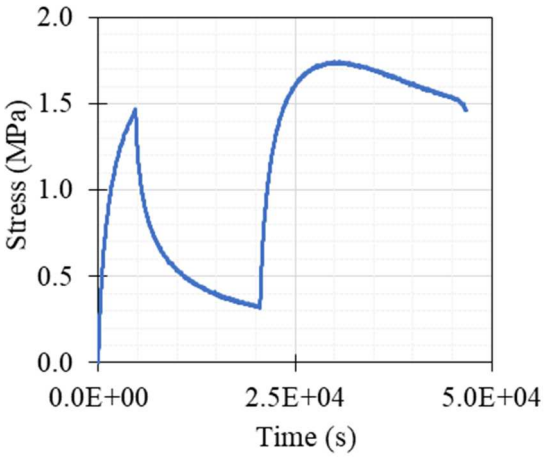

(b)

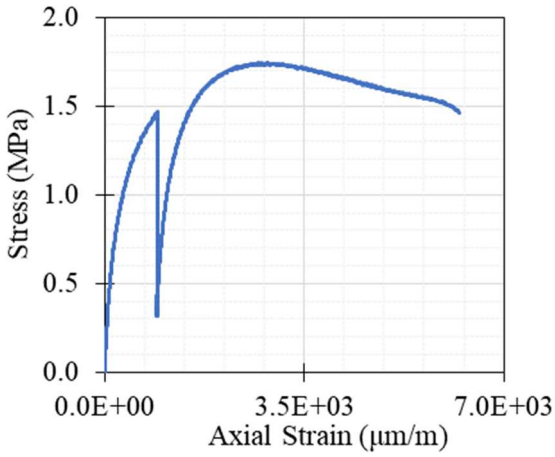

(c)

Figure B1-76. Tension test result of E2-H5 at 0°C and 0.001%/min strain rate

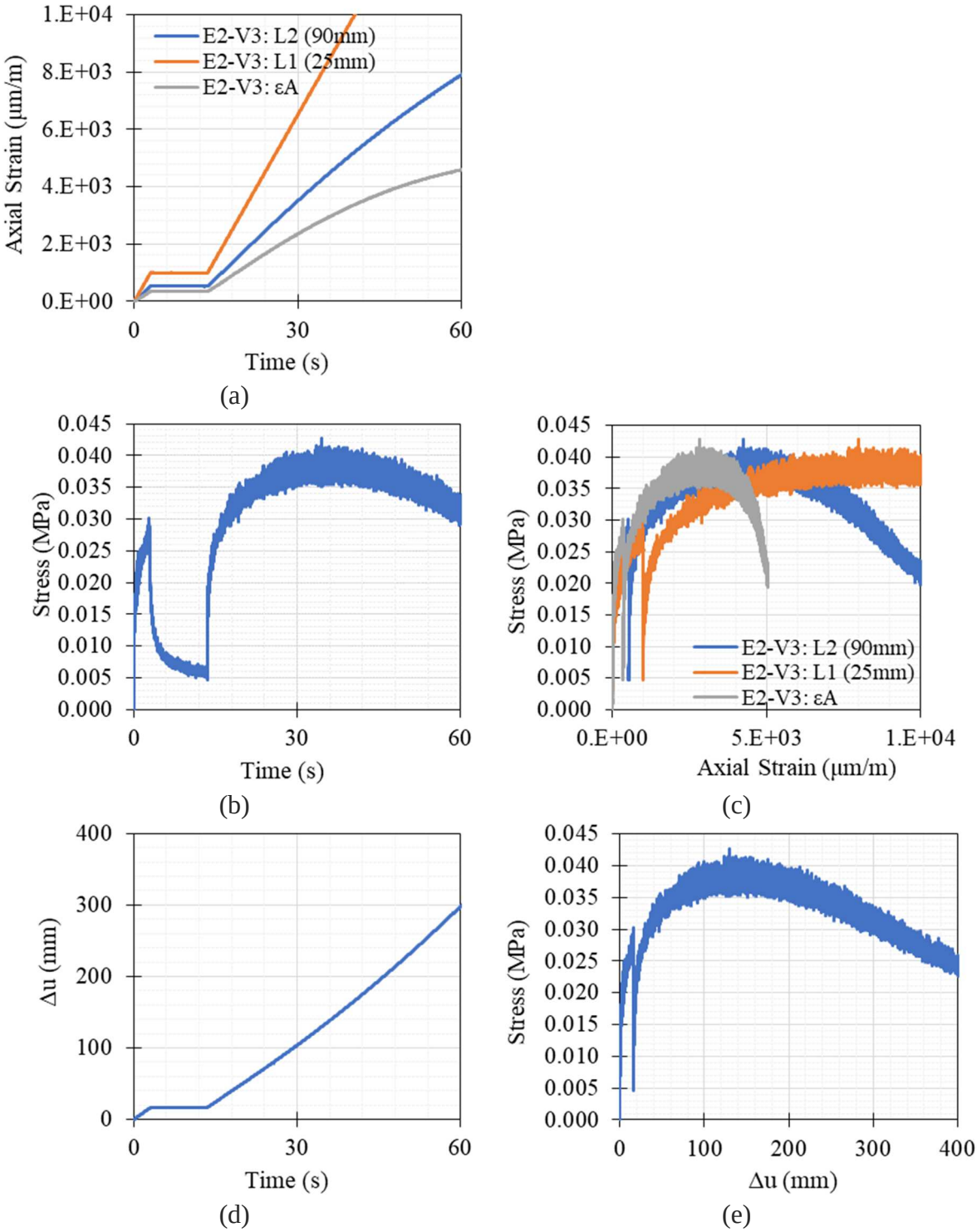

Figure B1-77. Tension test result of E2-V3 at 40°C and 2%/min strain rate

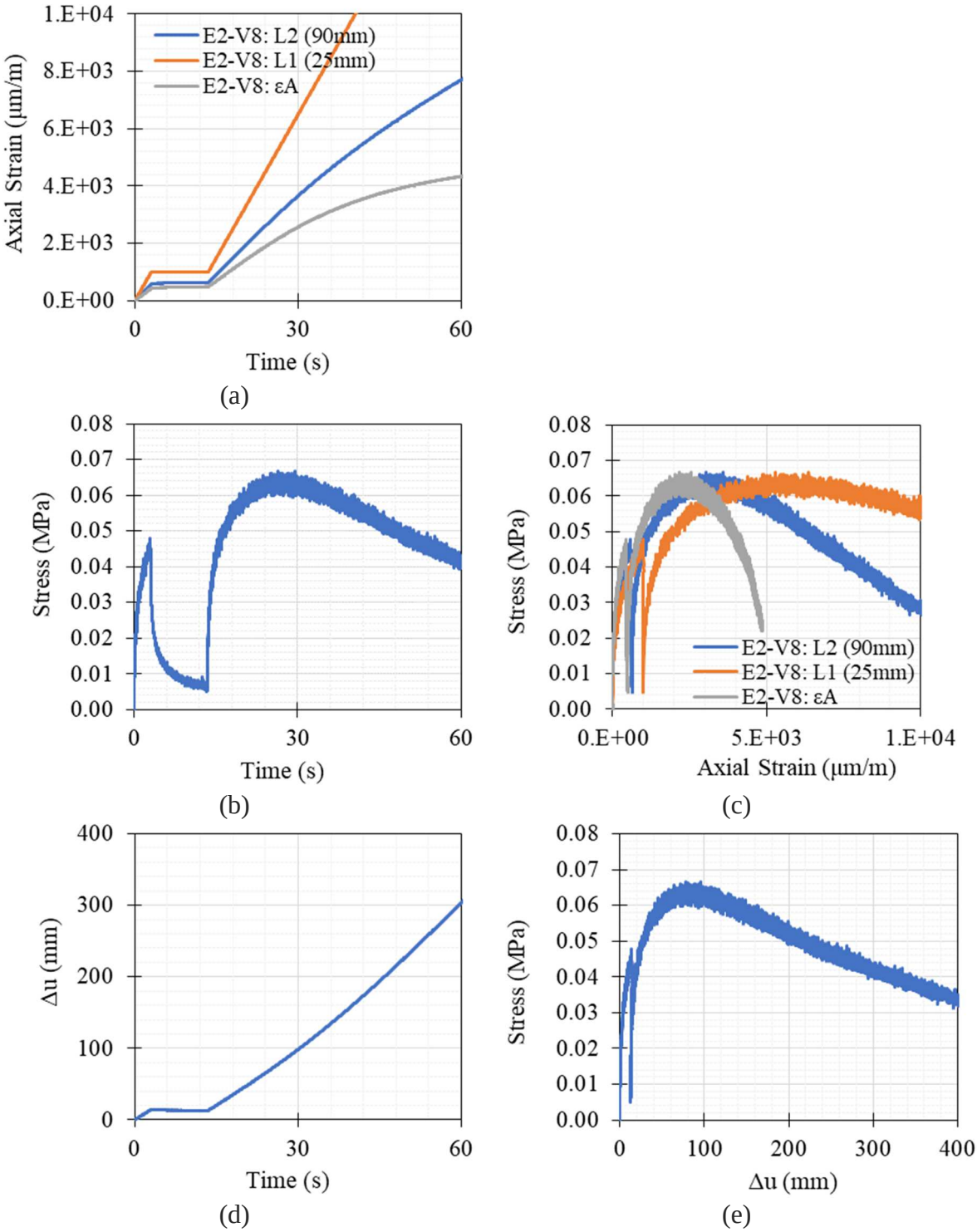

Figure B1-78. Tension test result of E2-V8 at 40°C and 2%/min strain rate

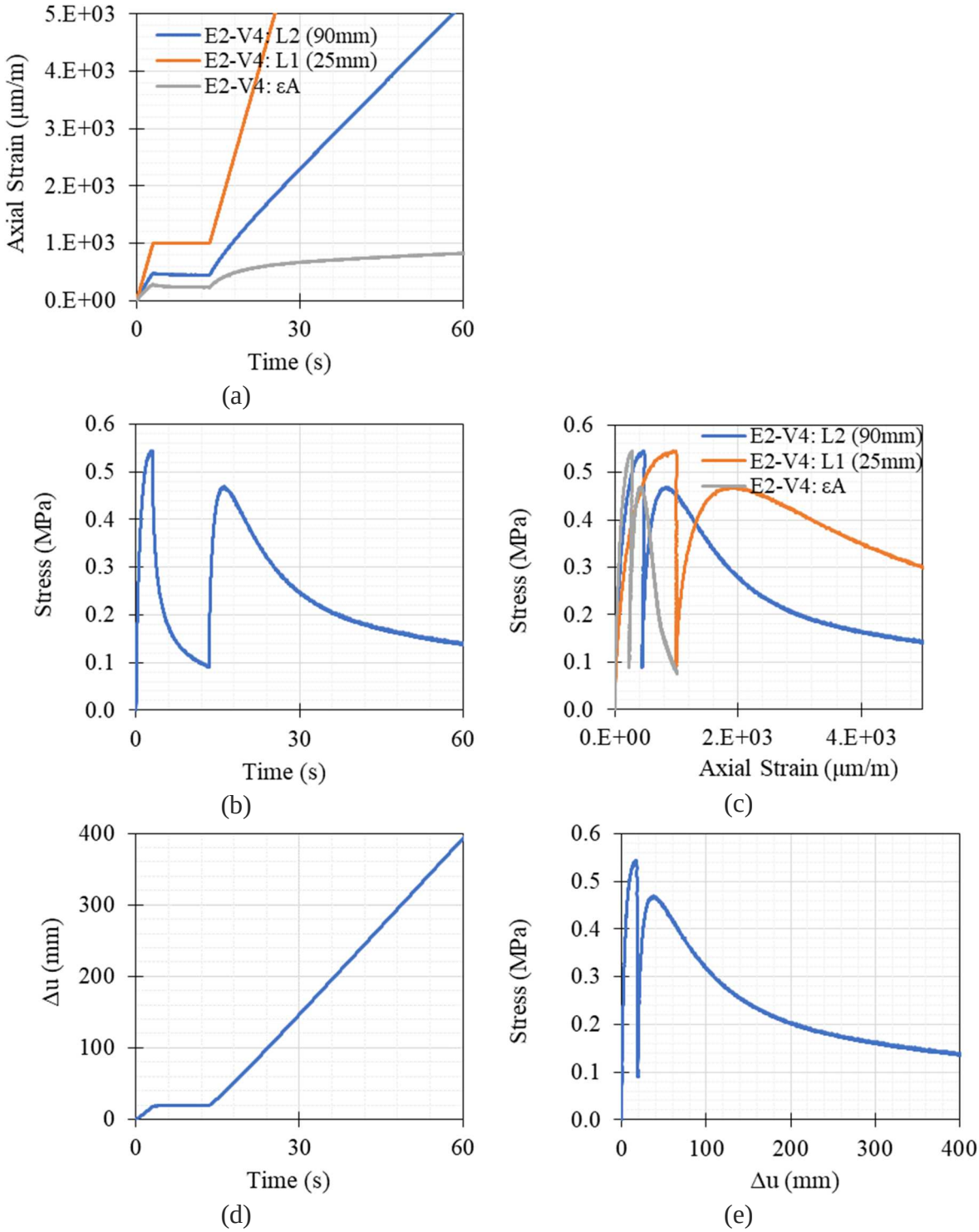

Figure B1-79. Tension test result of E2-V4 at 19°C and 2%/min strain rate

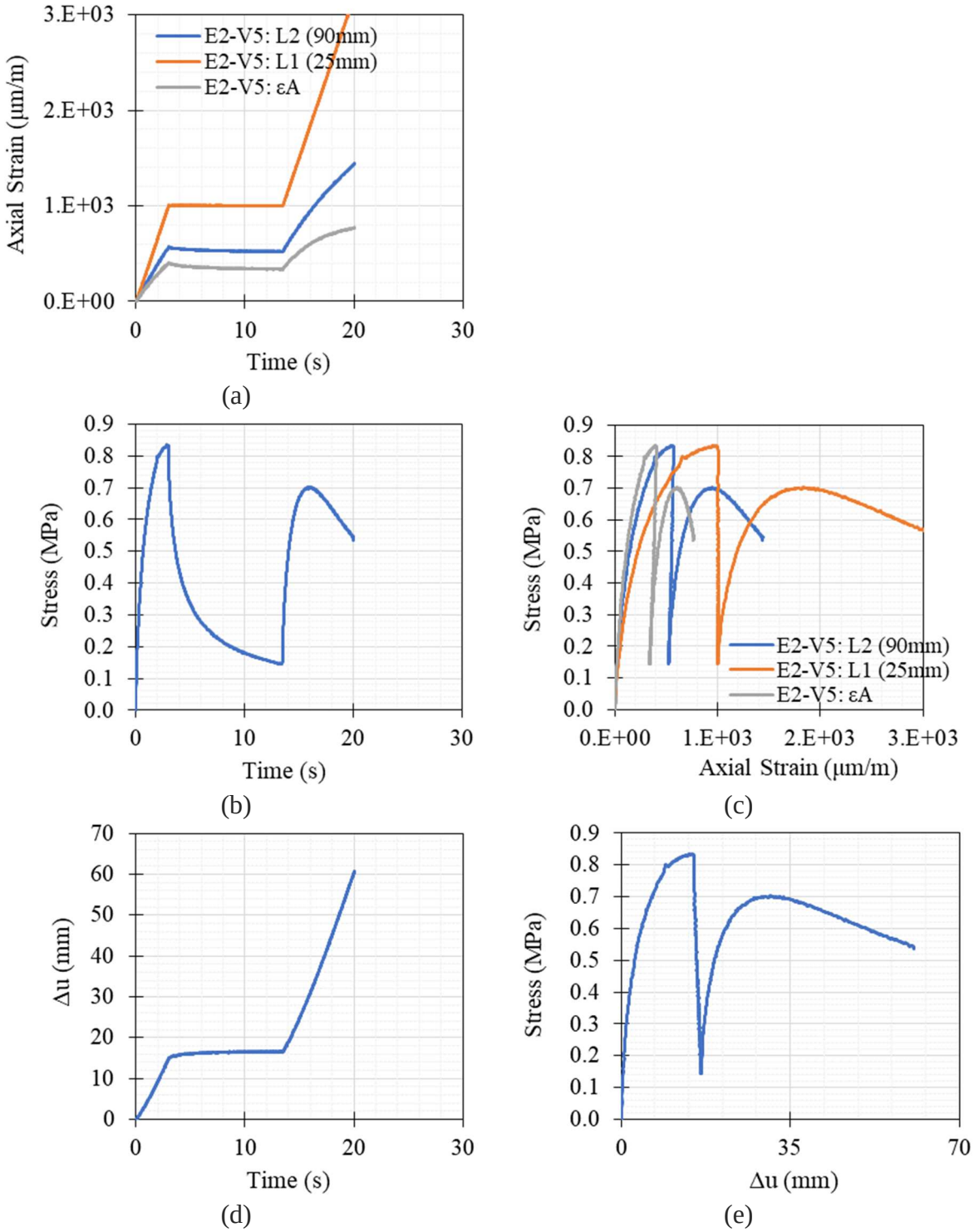

Figure B1-80. Tension test result of E2-V5 at 19°C and 2%/min strain rate

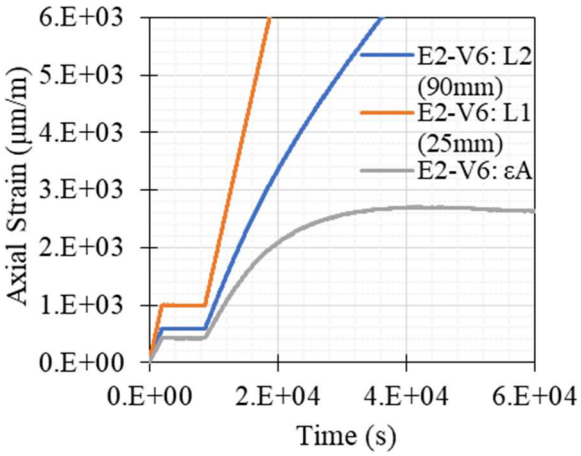

(a)

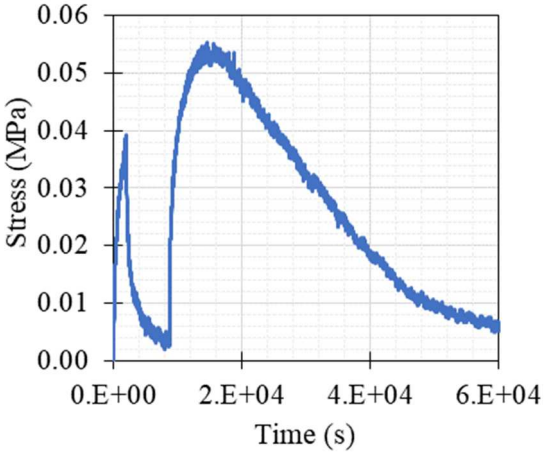

(b)

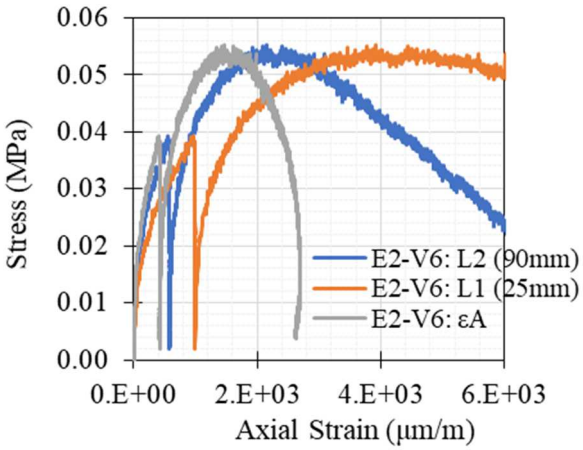

(c)

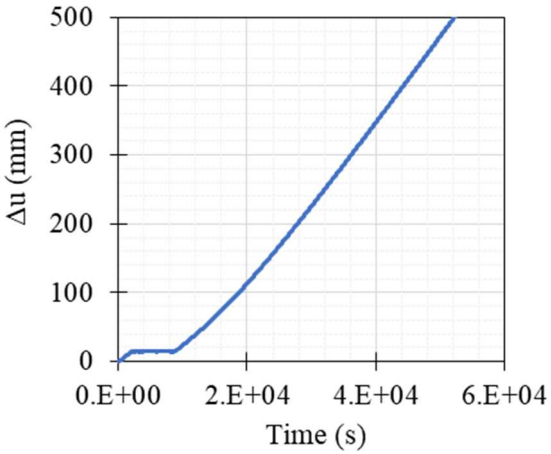

(d)

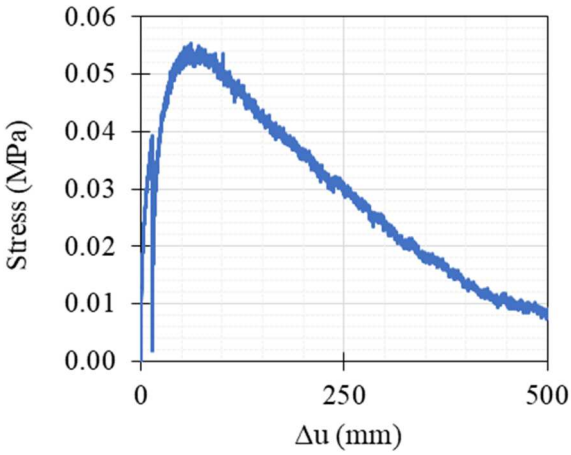

(e)

Figure B1-81. Tension test result of E2-V6 at 19°C and 0.003%/min strain rate

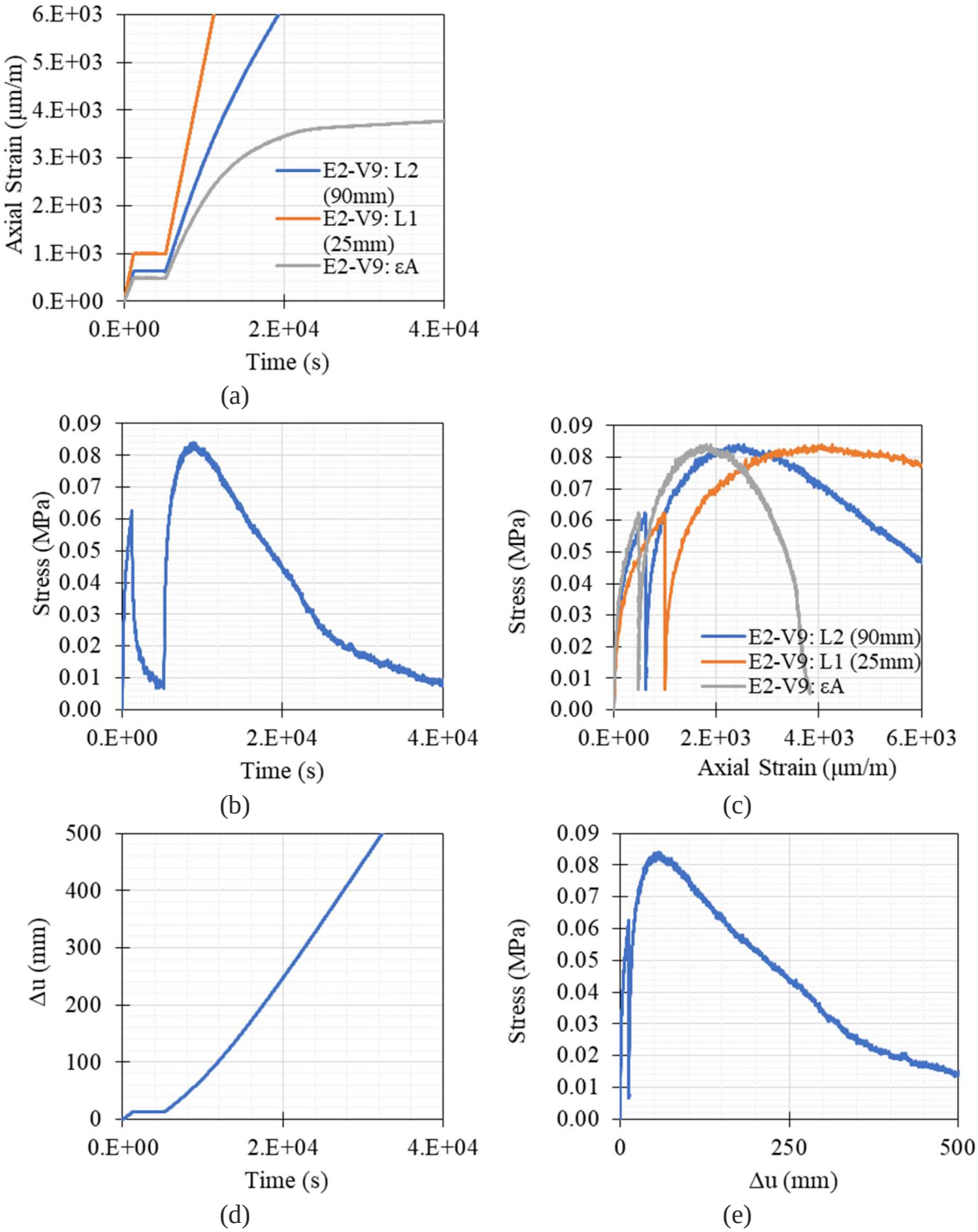

Figure B1-82. Tension test result of E2-V9 at 19°C and 0.005%/min strain rate

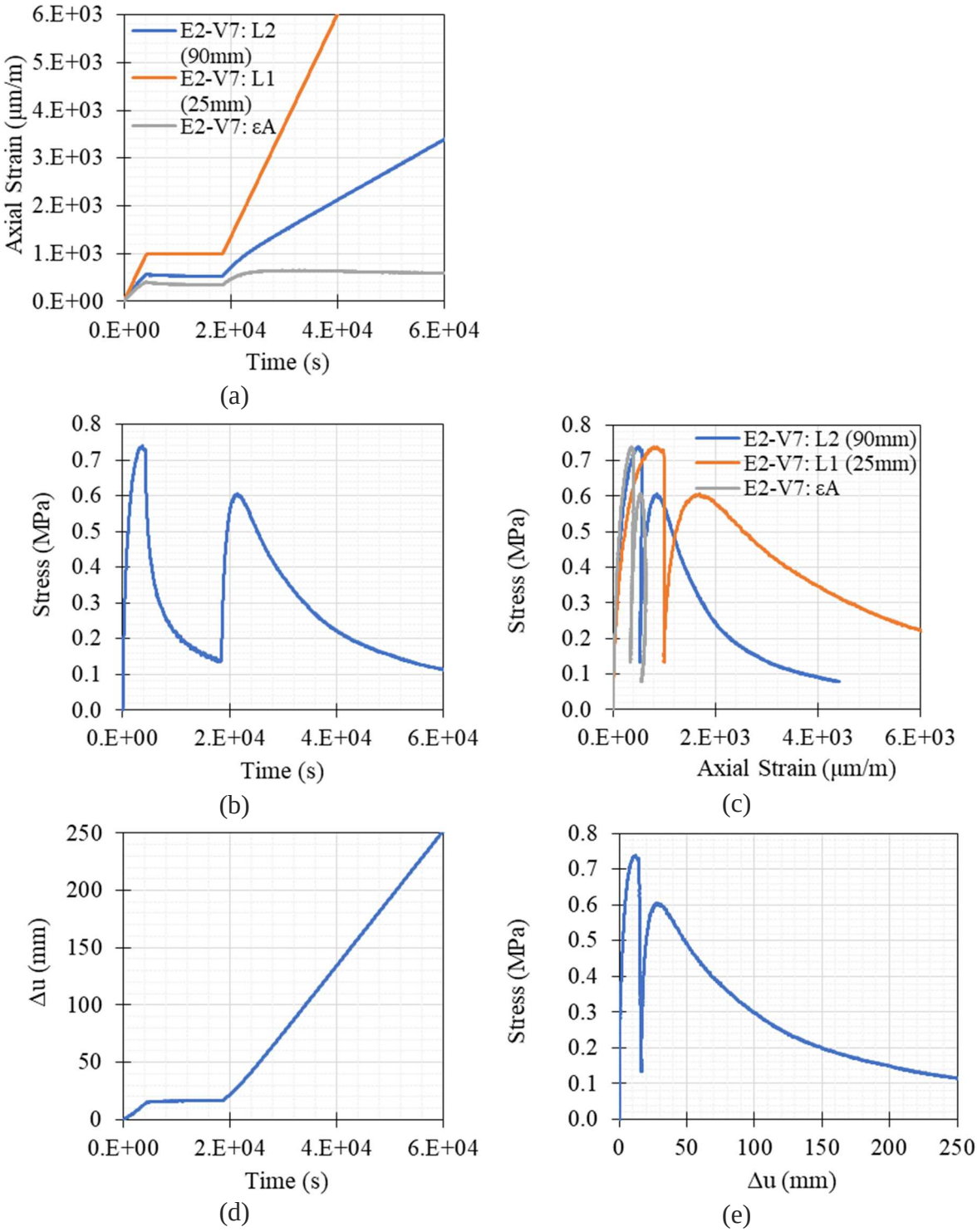

Figure B1-83. Tension test result of E2-V7 at 0°C and 0.001%/min strain rate

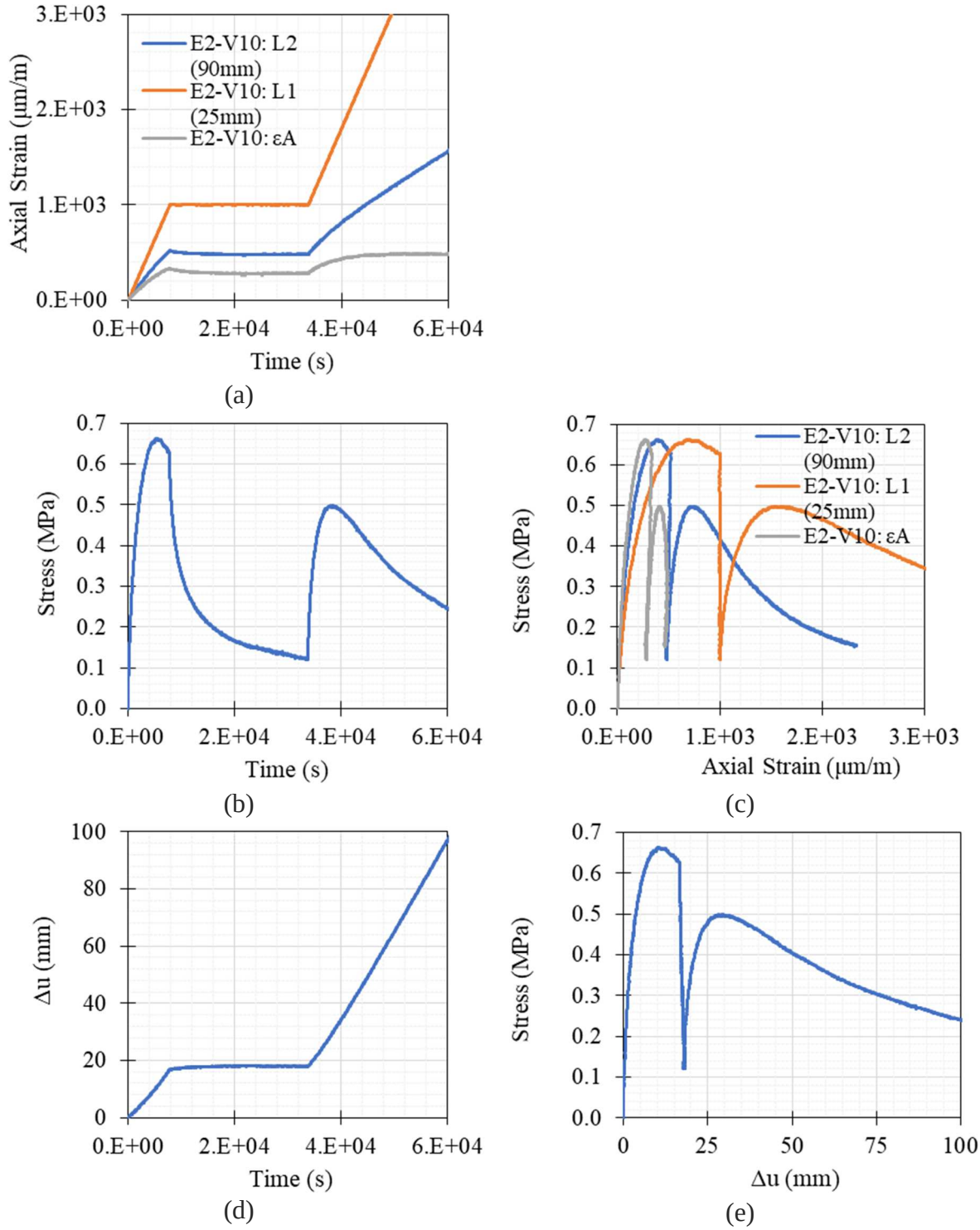

Figure B1-84. Tension test result of E2-V10 at 0°C and 0.001%/min strain rate

APPENDIX B2 – TENSION TEST: PICTURES OF TESTED SPECIMENS

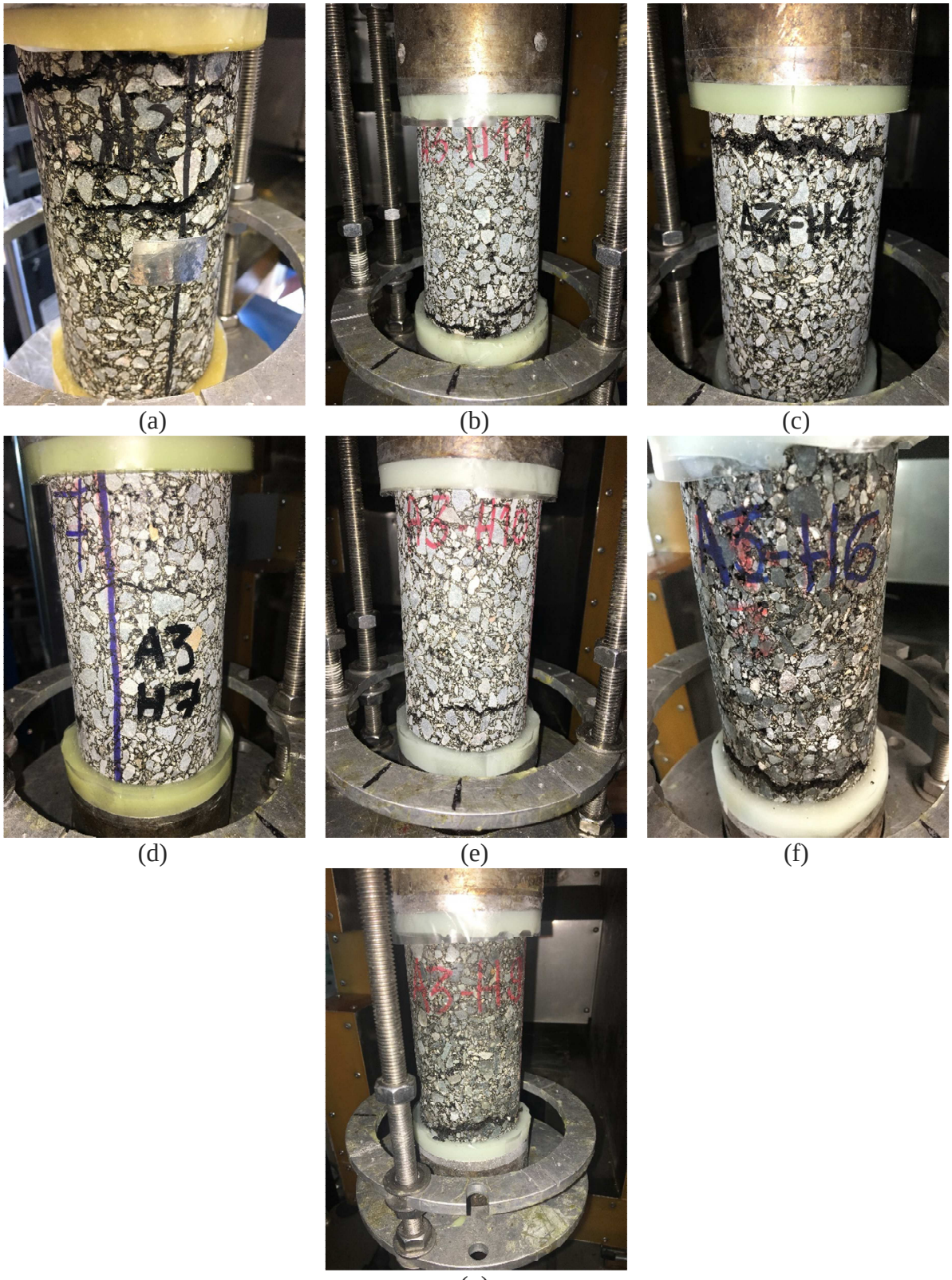

(a) (b) (c)

(d) (e) (f)

(g)

Figure B2-1. Tested specimens of configuration A, type H: (a) A1-H2, 40°C and 2%/min, (b) A3-H11, 40°C and 2%/min, (c) A3-H4, 19°C and 2%/min, (d) A3-H7, 19°C and 2%, (e) A3-H10, 19°C and 0.002%/min, (f) A3-H6, 0°C and 0.001%/min, (g) A3-H9, 0°C and 0.002%/min

(a)

(b)

(c)

(d)

Figure B2-2. Tested specimens of configuration A, type V: (a) A1-V11, 40°C and 2%/min, (b) A1-V8, 40°C and %/min, (c) A2-V1, 19°C and 0.006%/min, (d) A1-V7, 0°C and 0.001%/min

(a) (b) (c)

(d) (e) (f)

(g)

Figure B2-3. Tested specimens of configuration B, type H: (a) B1-H1, 40°C and 2%/min, (b) B2-H2, 40°C and 2%/min, (c) B1-H2, 19°C and 2%/min, (d) B2-H3, 19°C and 2%, (e) B2-H1, 19°C and 0.005%/min, (f) B2-H4, 19°C and 0.004%/min, (g) B3-H11, 0°C and 0.001%/min

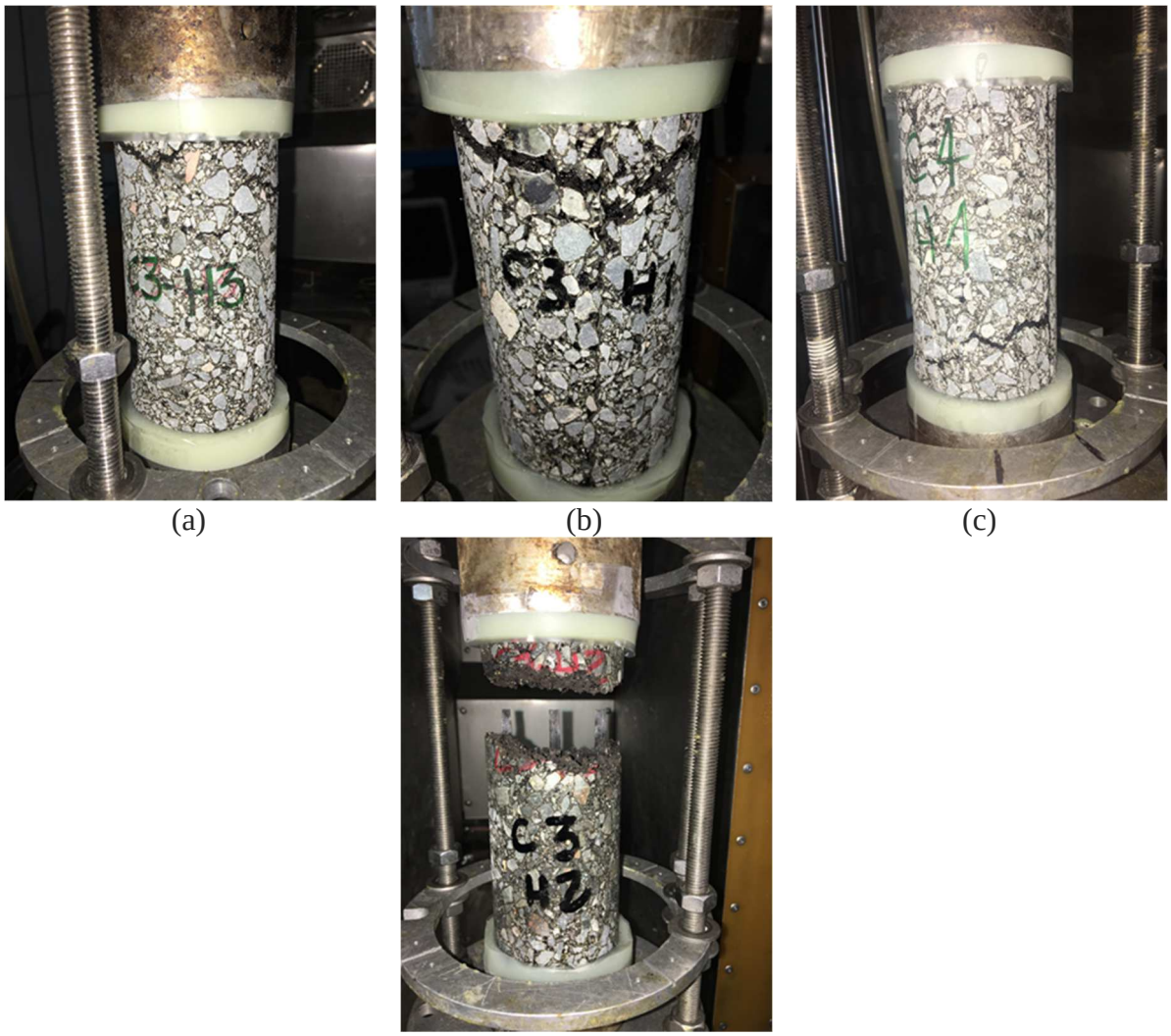

(a) (b) (c)

(d)

Figure B2-4. Tested specimens of configuration C, type H: (a) C3-H3, 40°C and 2%/min, (b) C3-H1, 19°C and 2%/min, (c) C4-H1, 19°C and 0.005%/min, (d) C3-H2, 0°C and 0.001%/min

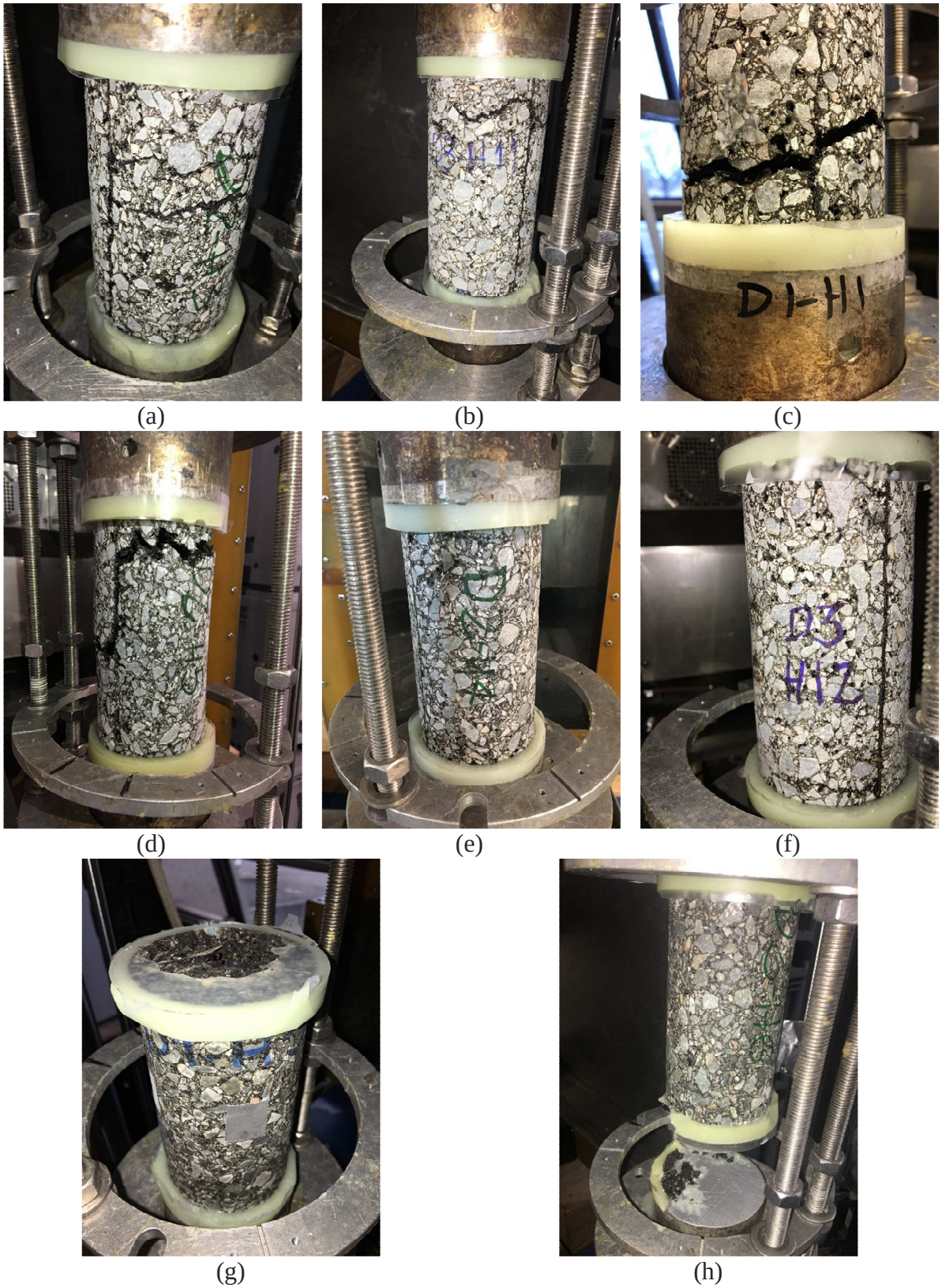

(a) (b) (c)

(d) (e) (f)

(g) (h)

Figure B2-5. Tested specimens of configuration D, type H: (a) D2-H3, 40°C and 2%/min, (b) D3-H11, 40°C and 2%/min, (c) D1-H1, 19°C and 2%/min, (d) D2-H5, 19°C and 2%/min, (e) D2-H4, 19°C and 0.005%/min, (f) D3-H12, 19°C and 0.003%/min, (g) D1-H3, 0°C and 0.001%/min, (h) D2-H6, 0°C and 0.001%/min

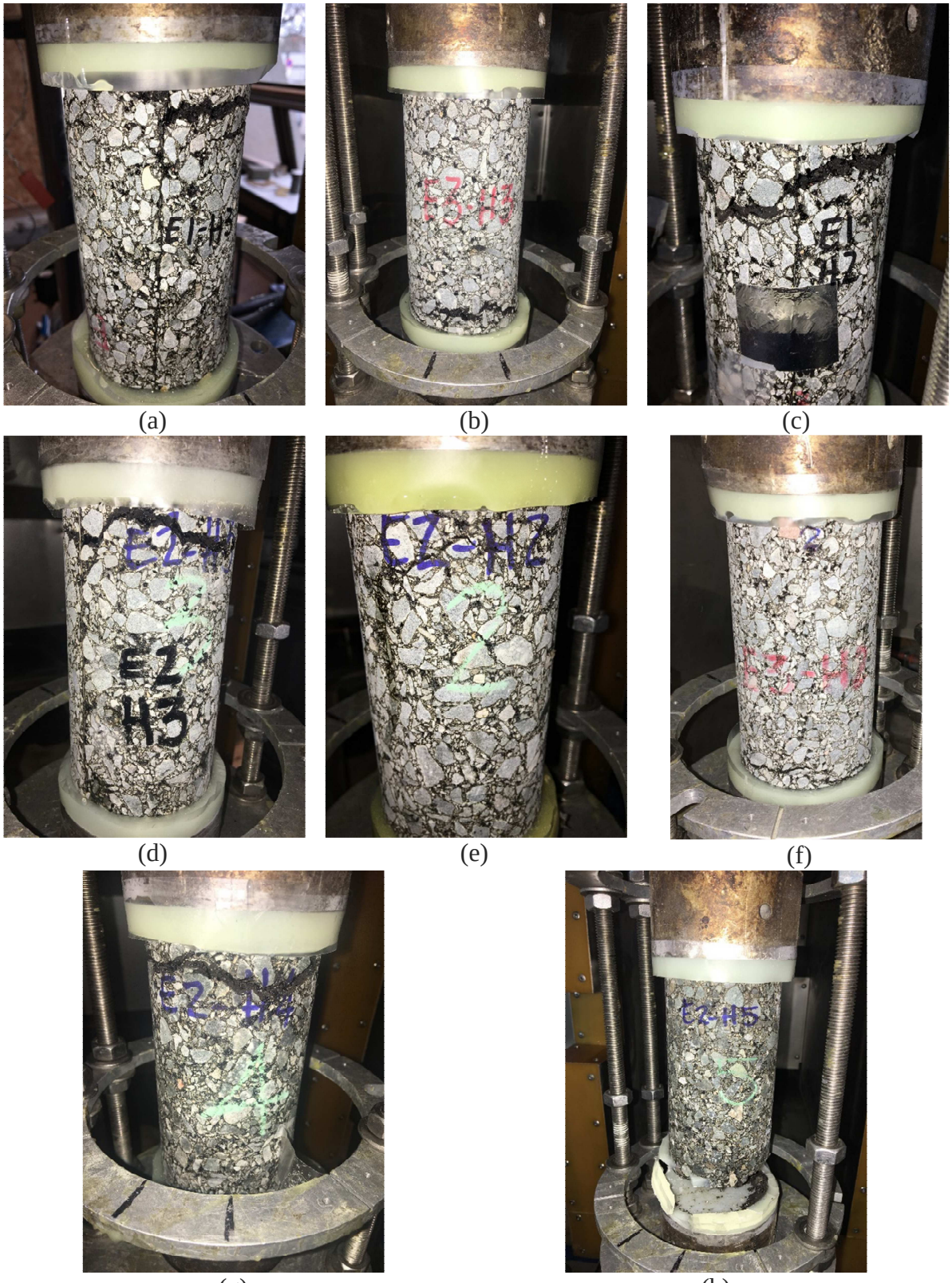

(a) (b) (c)

(d) (e) (f)

(g) (h)

Figure B2-6. Tested specimens of configuration E, type H: (a) E1-H3, 40°C and 2%/min, (b) E3-H3, 40°C and 2%/min, (c) E1-H2, 19°C and 2%/min, (d) E2-H3, 19°C and 2%/min, (e) E2-H2, 19°C and 0.004%/min, (f) E3-H2, 19°C and 0.003%/min, (g) E2-H4, 0°C and 0.003%/min, (h) E2-H5, 0°C and 0.001%/min

APPENDIX C – FATIGUE TEST RESULTS

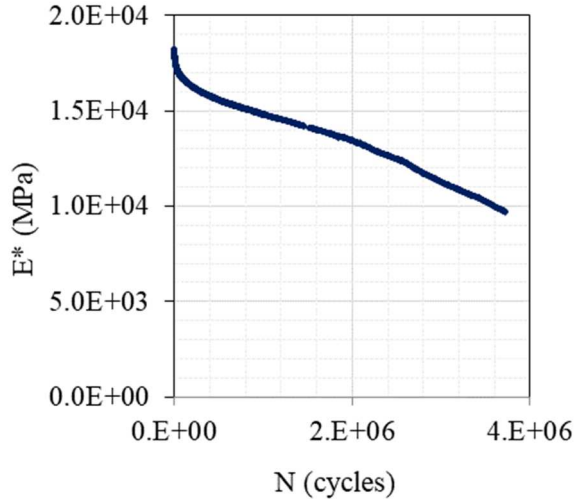

(a)

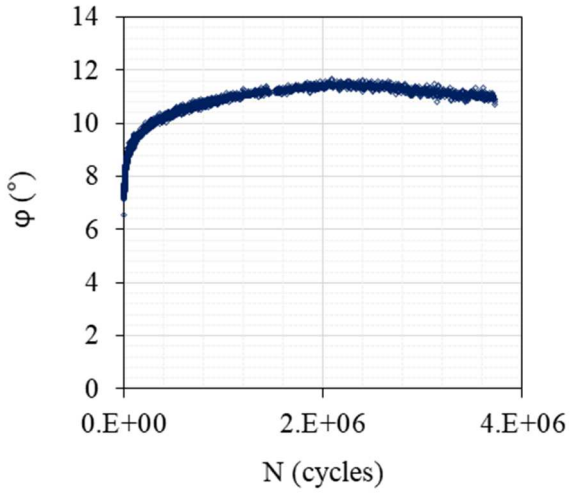

(b)

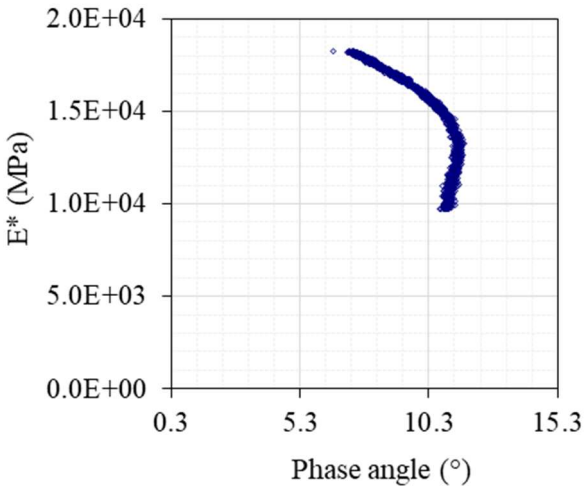

(c)

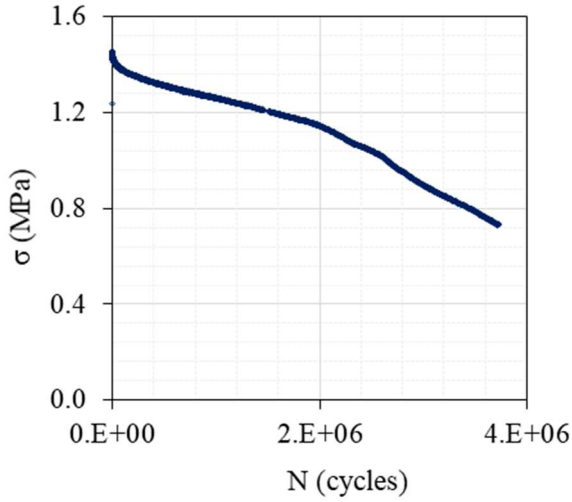

(d)

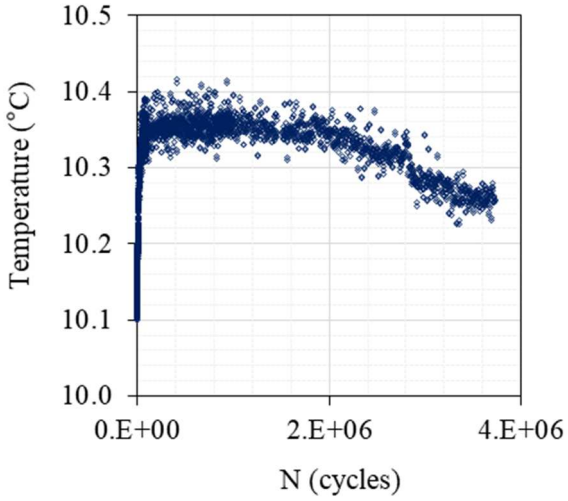

(e)

Figure C-1. Fatigue result of A2-H2 tested at 83μm/m of controlled strain amplitude

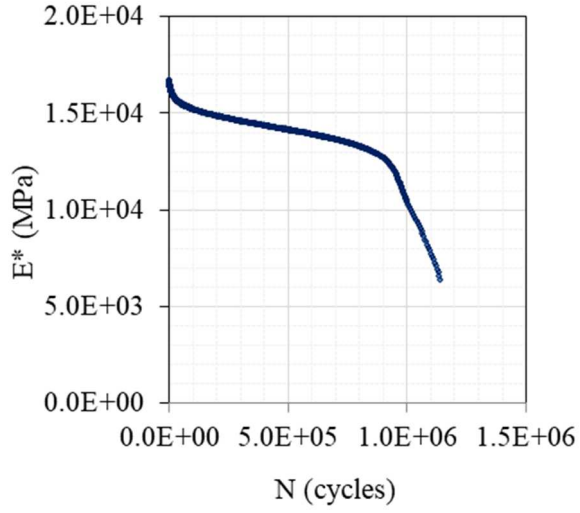

(a)

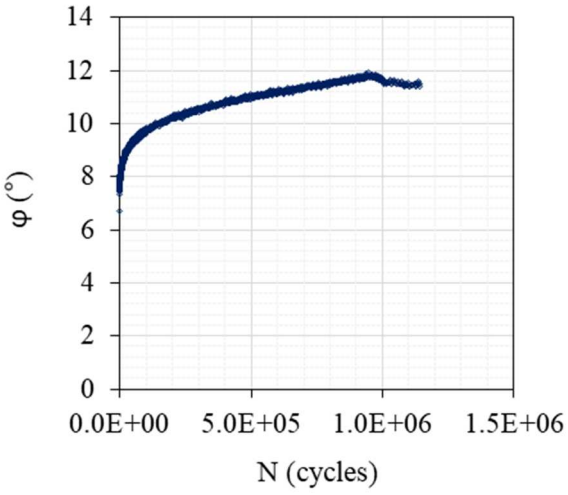

(b)

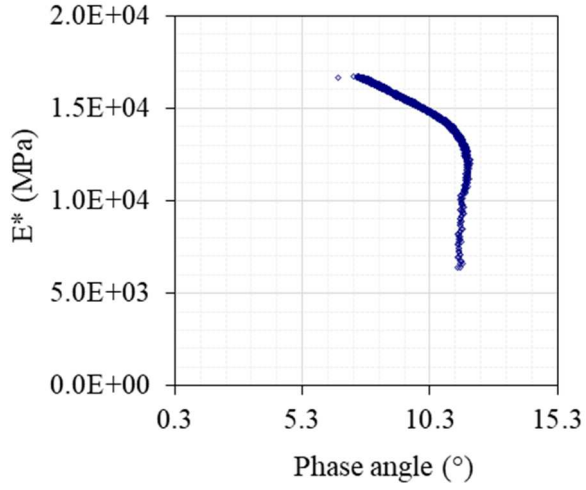

(c)

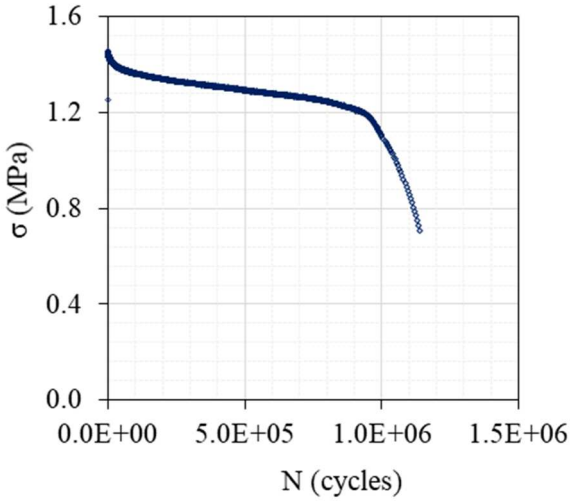

(d)

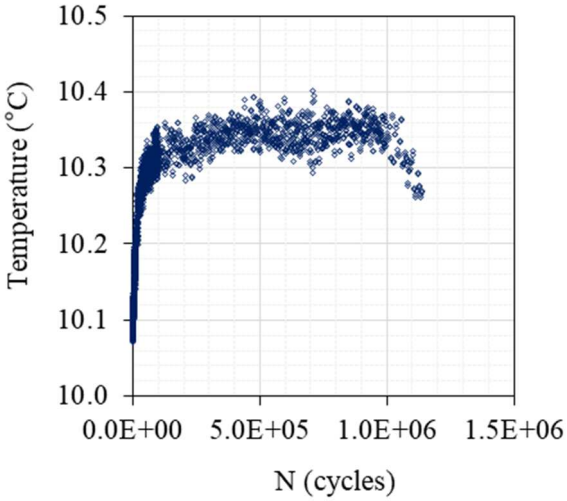

(e)

Figure C-2. Fatigue result of A3-H12 tested at 92μm/m of controlled strain amplitude

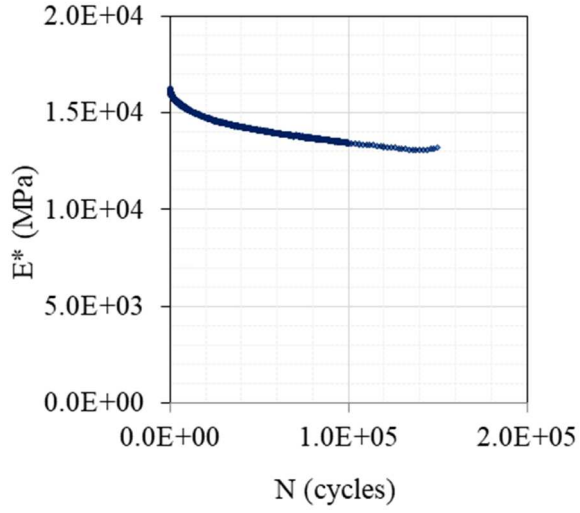

(a)

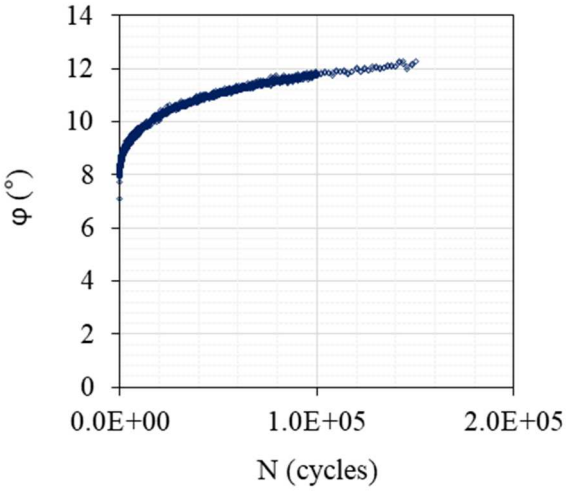

(b)

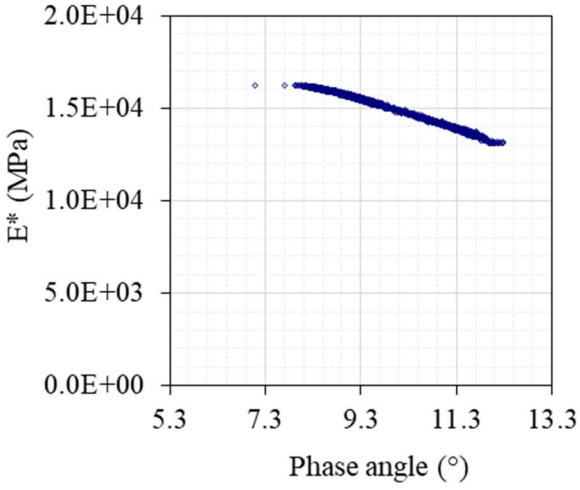

(c)

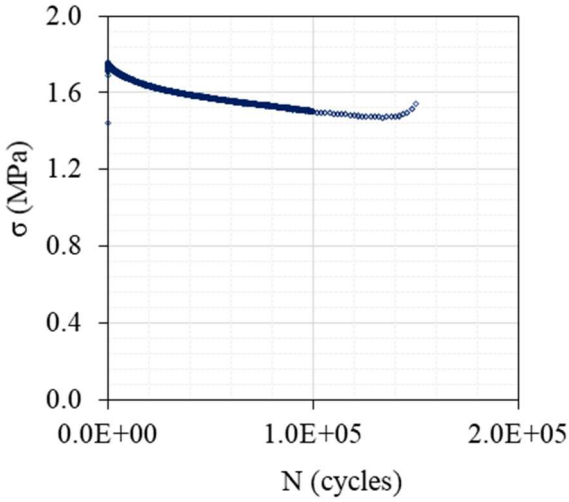

(d)

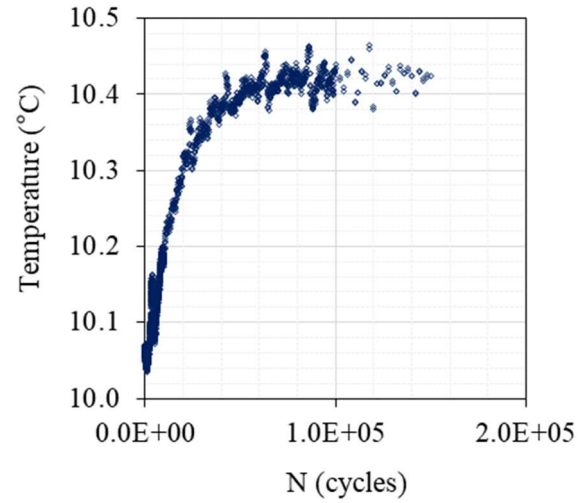

(e)

Figure C-3. Fatigue result of A4-H1 tested at 112μm/m of controlled strain amplitude

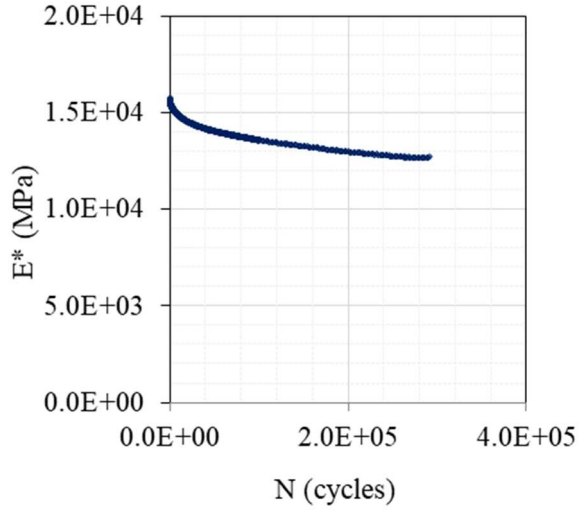

(a)

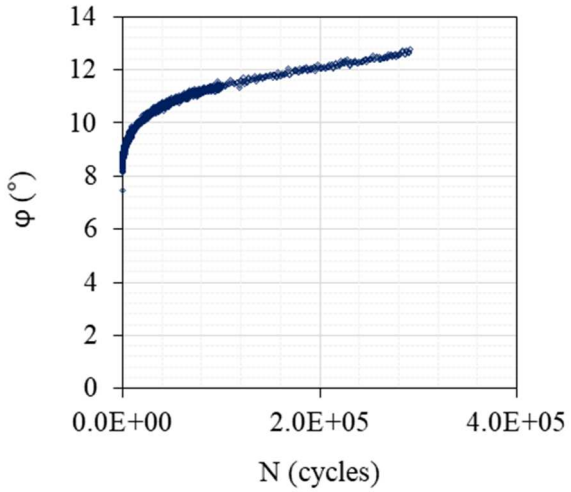

(b)

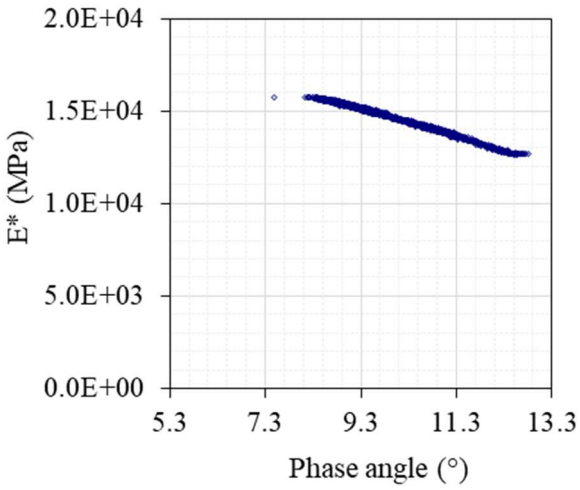

(c)

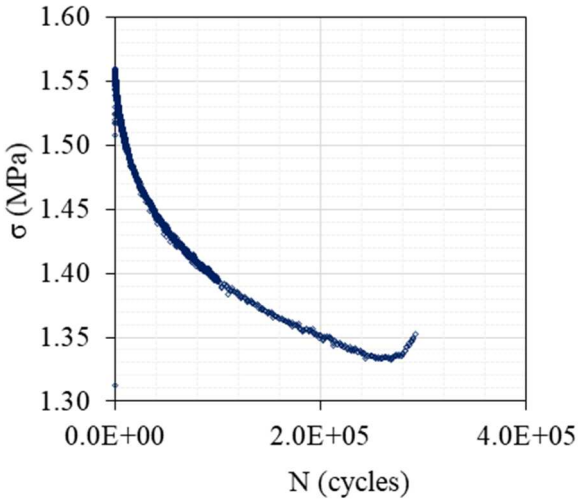

(d)

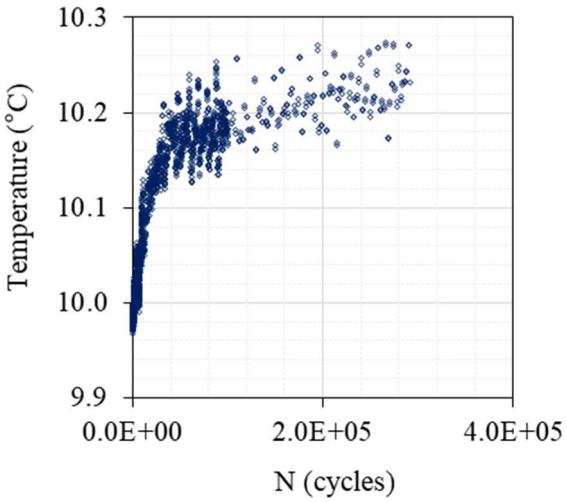

(e)

Figure C-4. Fatigue result of A4-H2 tested at 104μm/m of controlled strain amplitude

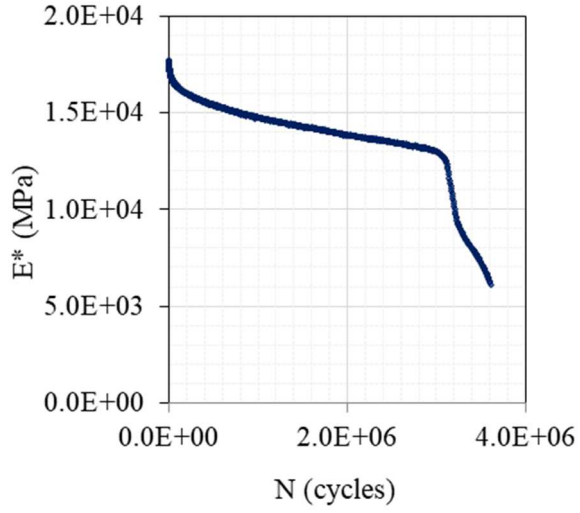

(a)

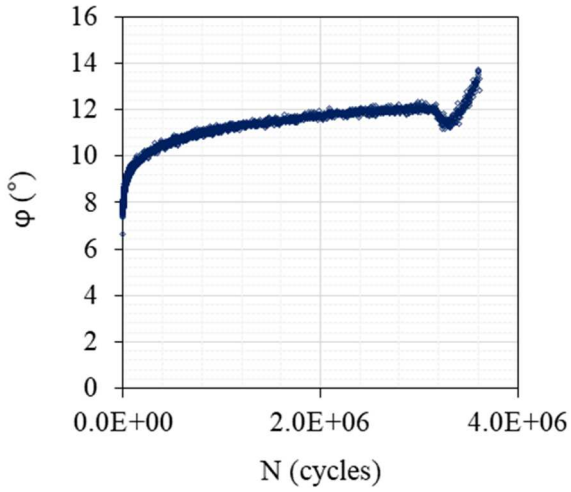

(b)

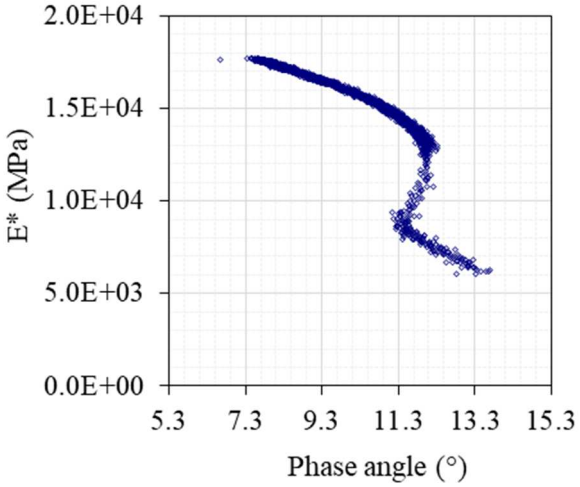

(c)

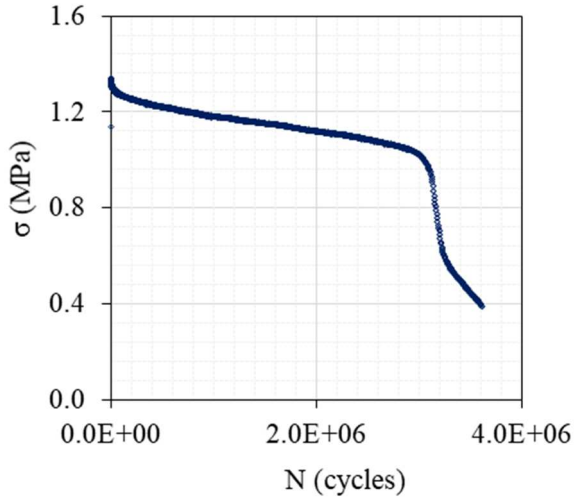

(d)

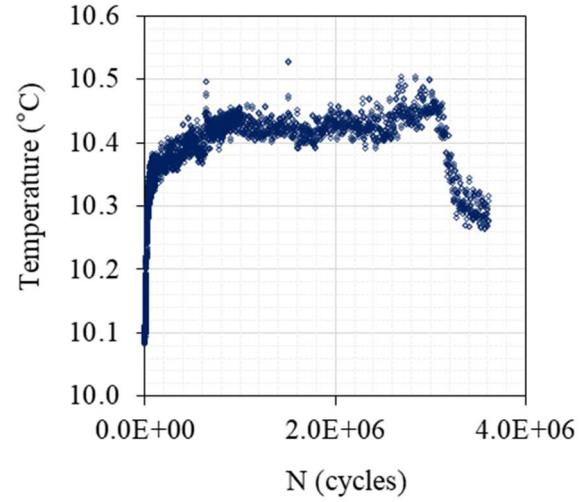

(e)

Figure C-5. Fatigue result of A4-H4 tested at 79μm/m of controlled strain amplitude

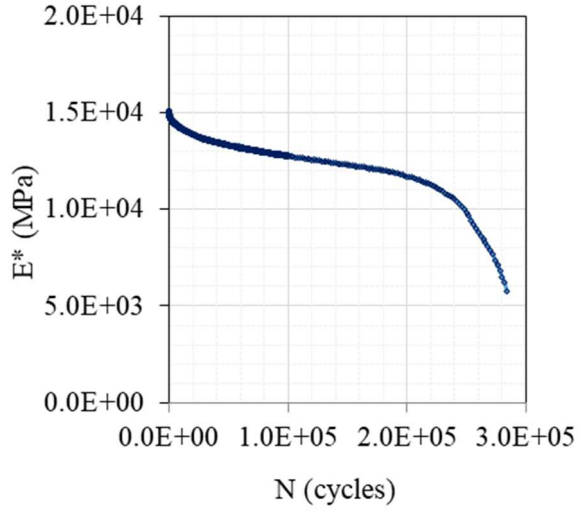

(a)

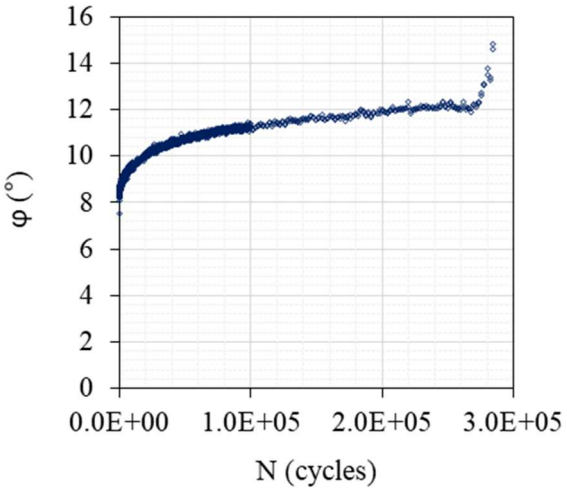

(b)

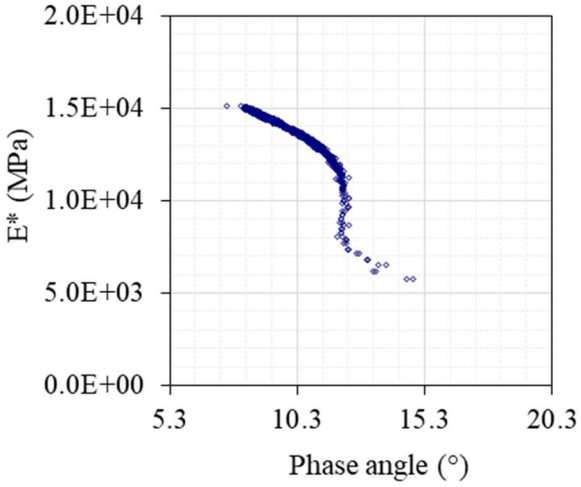

(c)

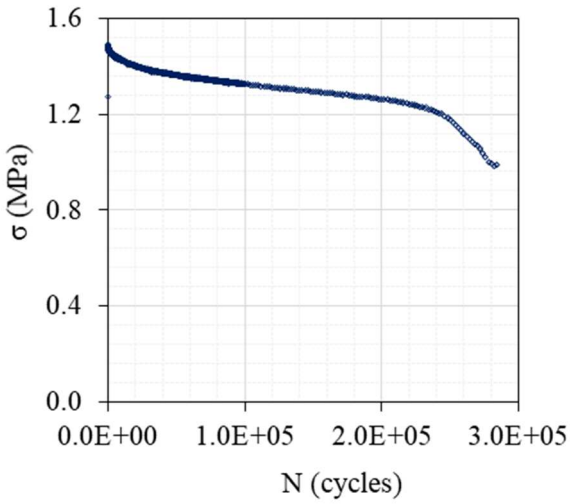

(d)

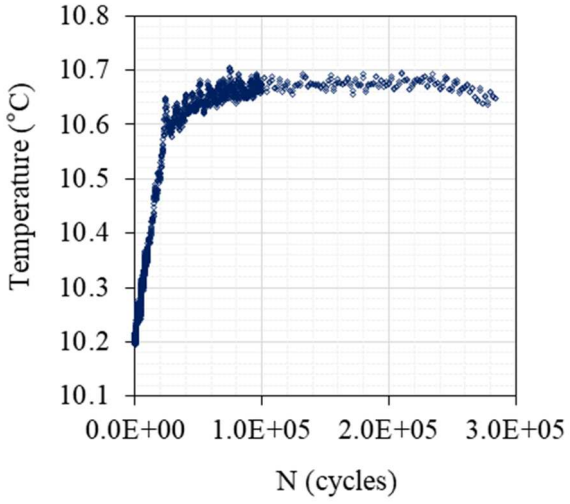

(e)

Figure C-6. Fatigue result of A4-H5 tested at 108μm/m of controlled strain amplitude

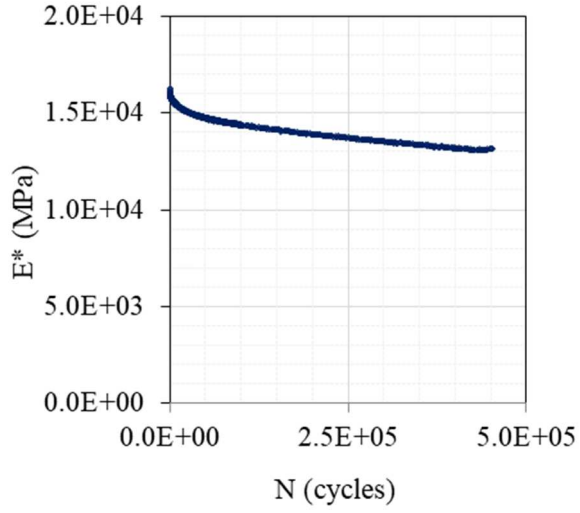

(a)

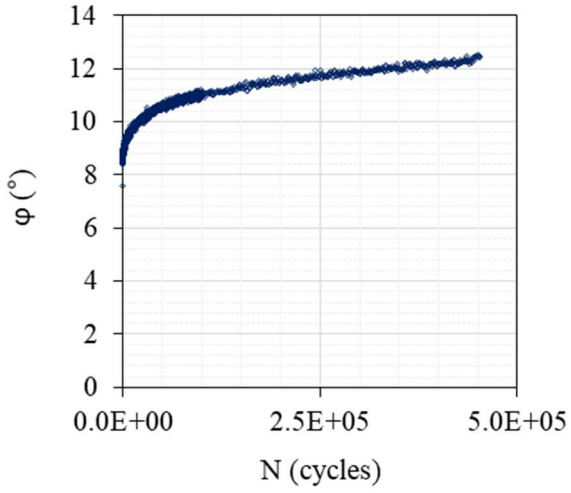

(b)

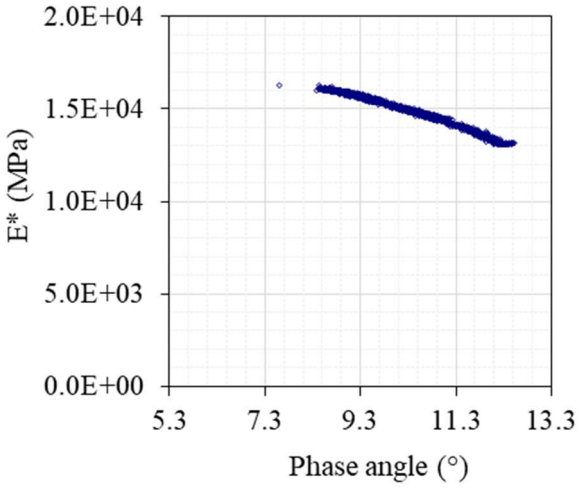

(c)

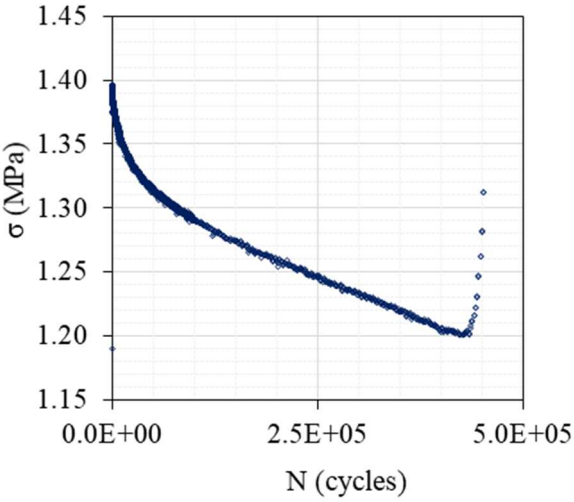

(d)

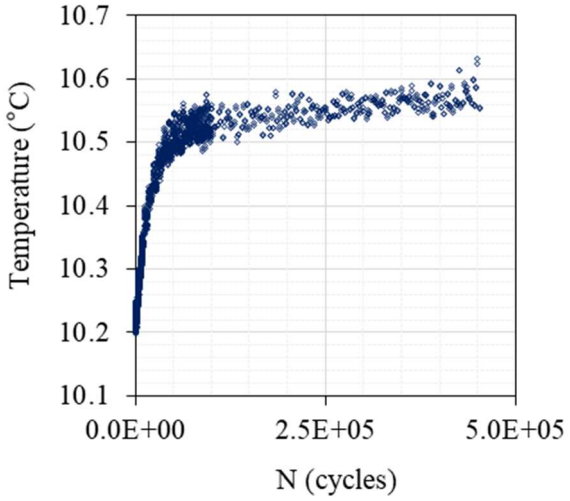

(e)

Figure C-7. Fatigue result of A4-H6 tested at 91μm/m of controlled strain amplitude

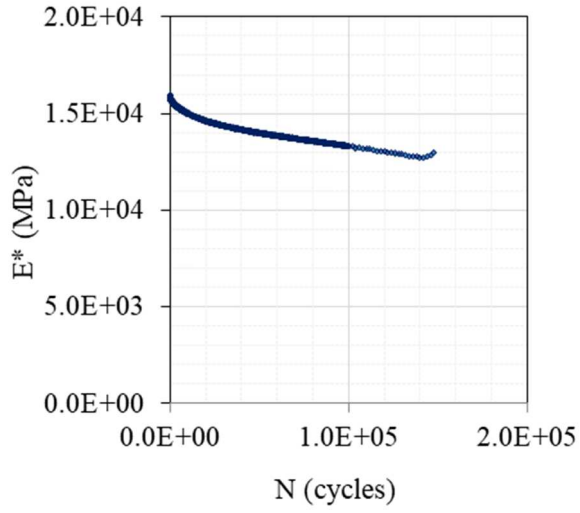

(a)

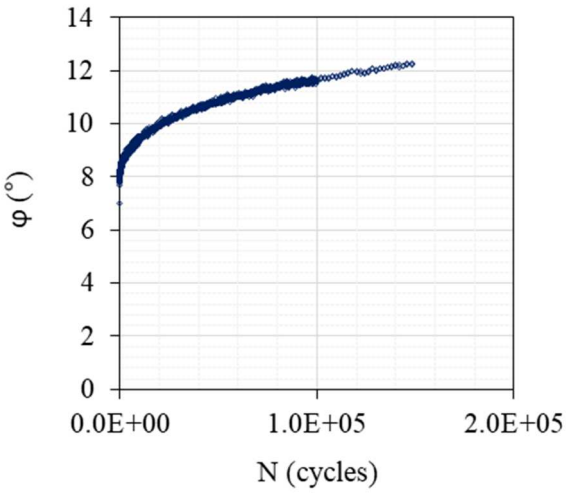

(b)

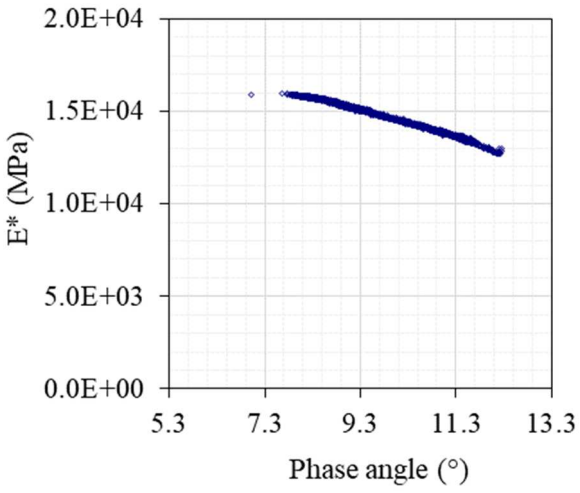

(c)

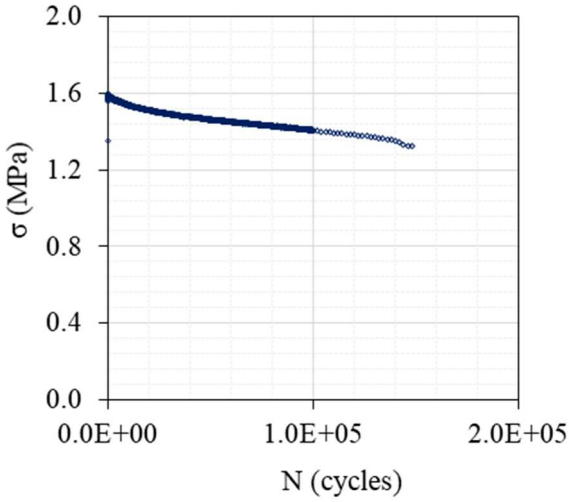

(d)

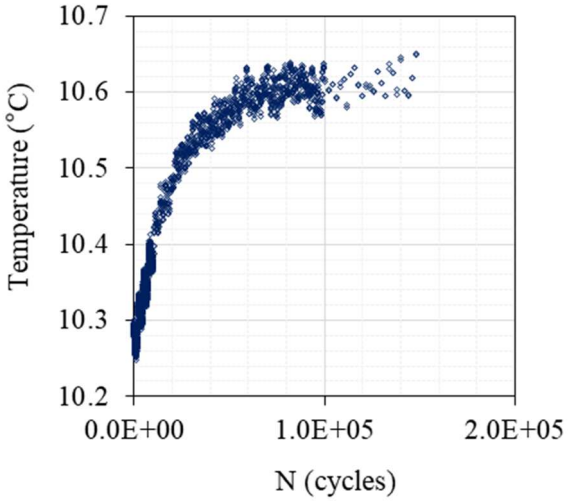

(e)

Figure C-8. Fatigue result of A4-H7 tested at 105μm/m of controlled strain amplitude

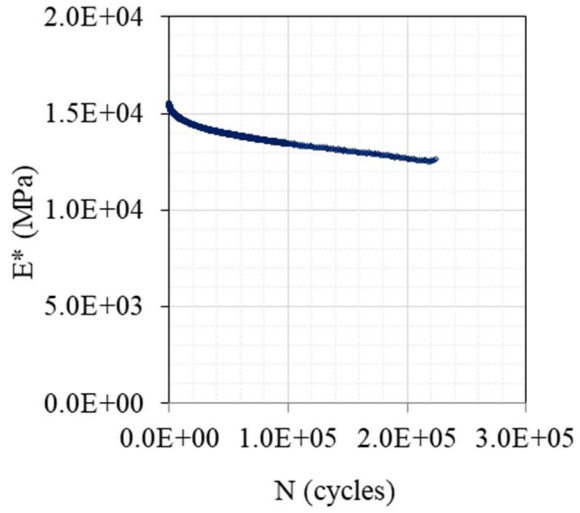

(a)

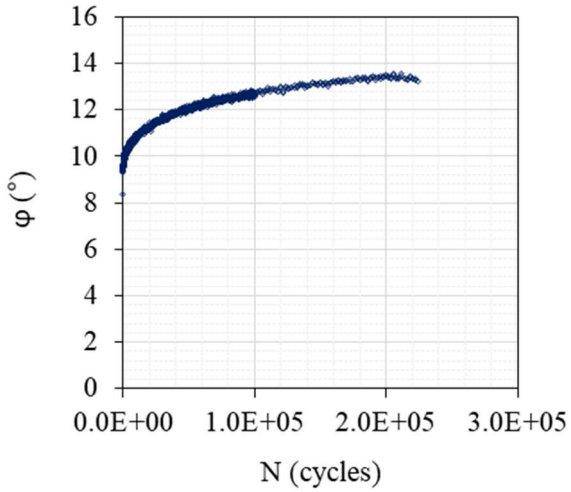

(b)

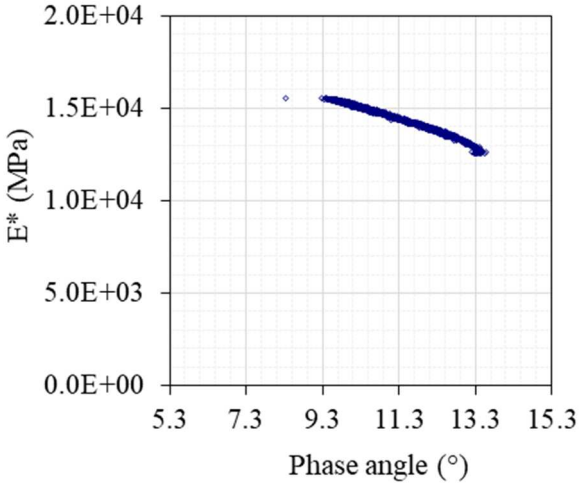

(c)

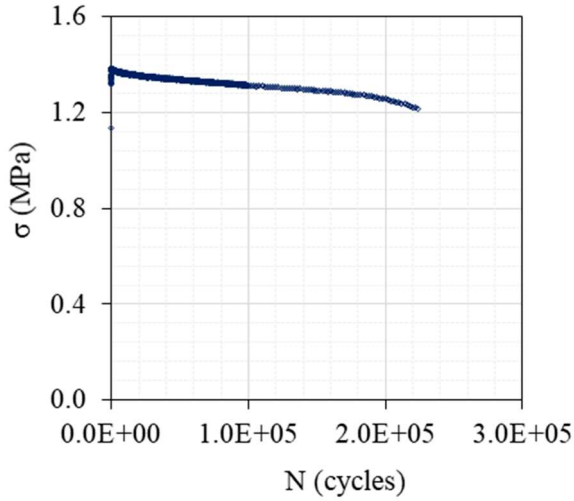

(d)

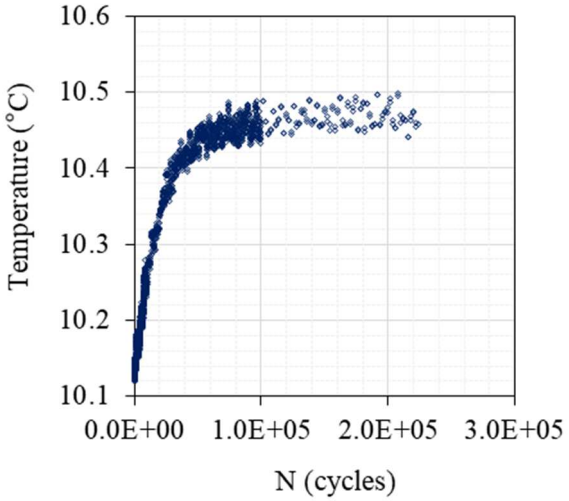

(e)

Figure C-9. Fatigue result of B3-H2 tested at 97μm/m of controlled strain amplitude

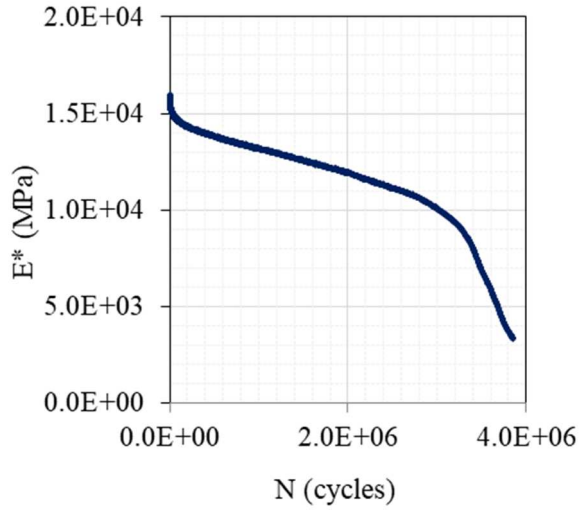

(a)

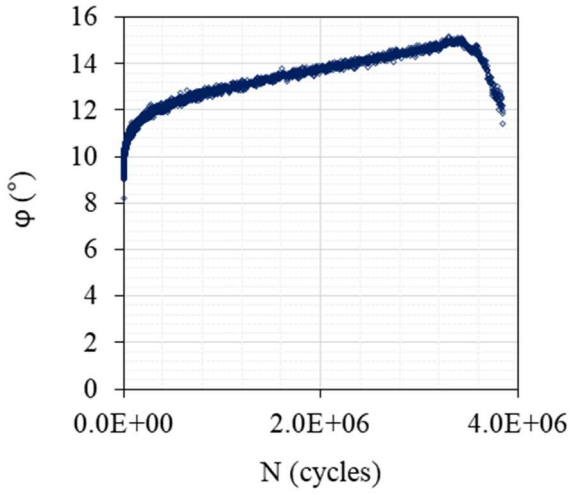

(b)

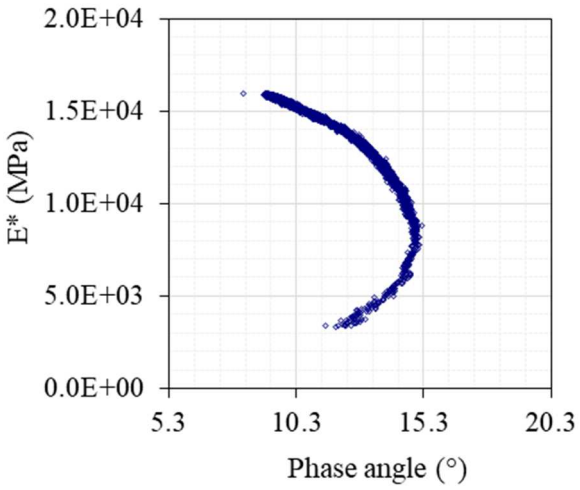

(c)

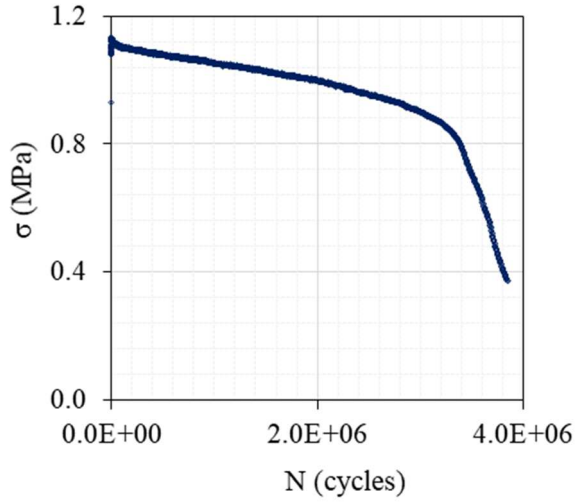

(d)

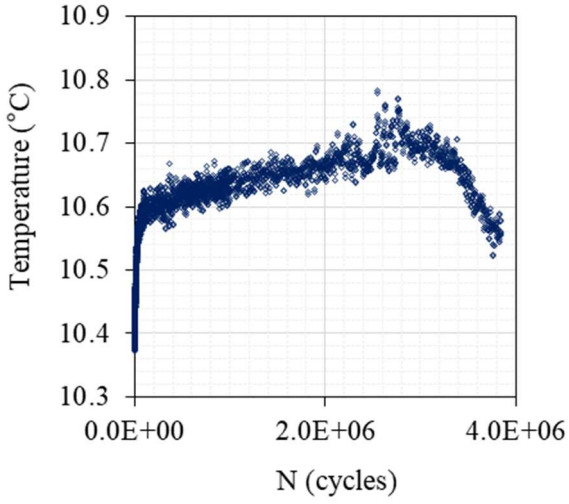

(e)

Figure C-10. Fatigue result of B3-H3 tested at 85μm/m of controlled strain amplitude

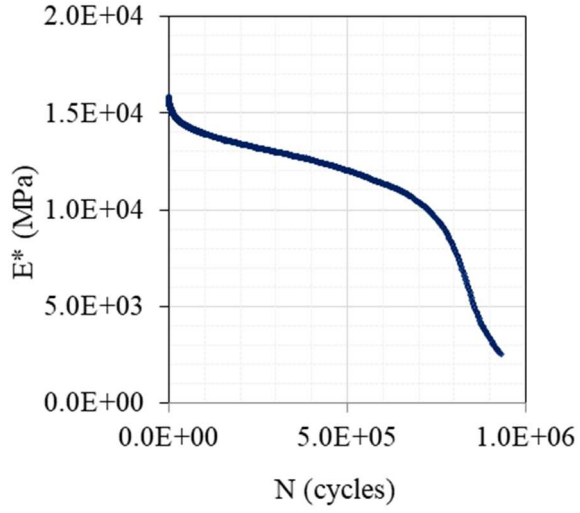

(a)

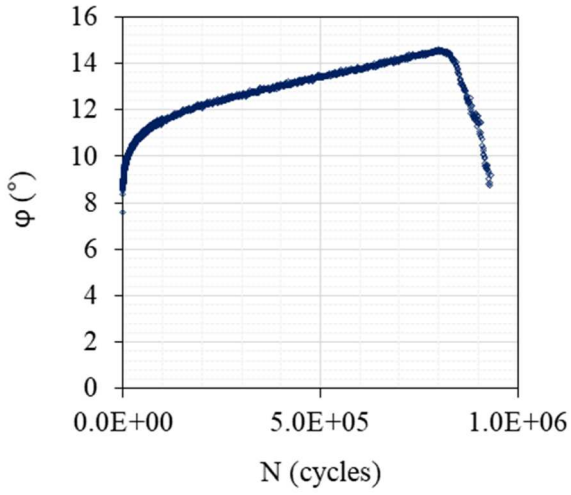

(b)

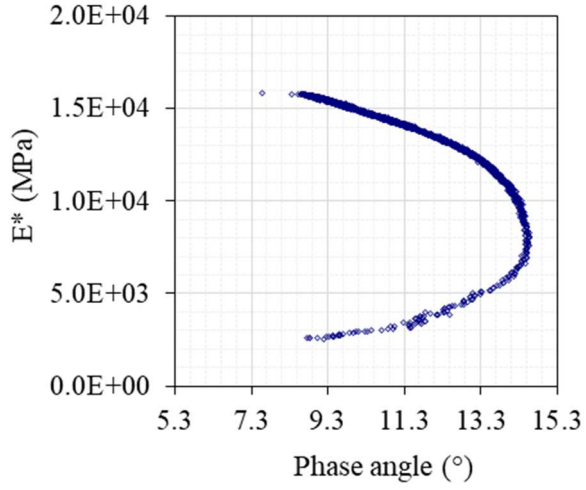

(c)

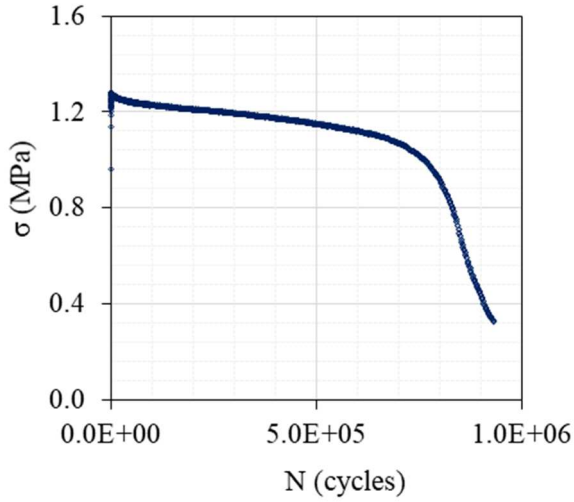

(d)

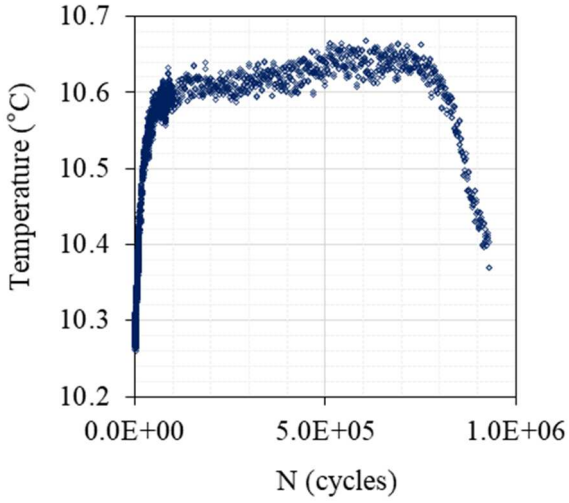

(e)

Figure C-11. Fatigue result of B3-H4 tested at 95μm/m of controlled strain amplitude

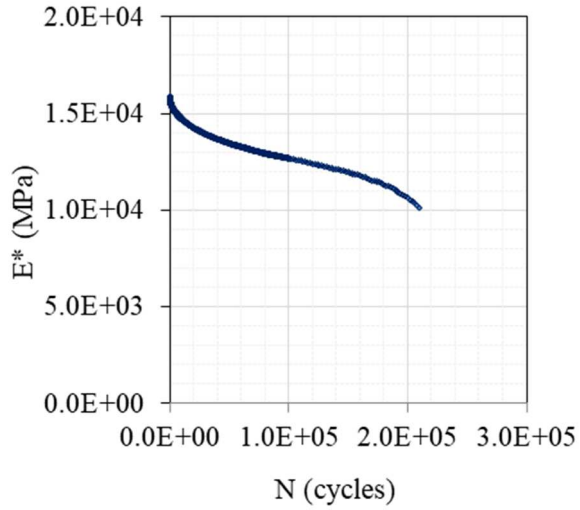

(a)

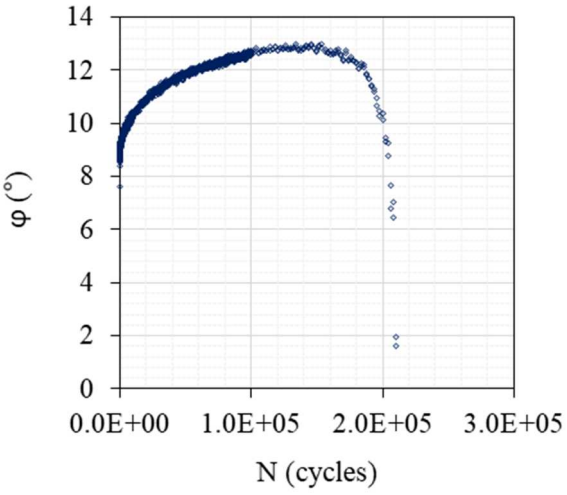

(b)

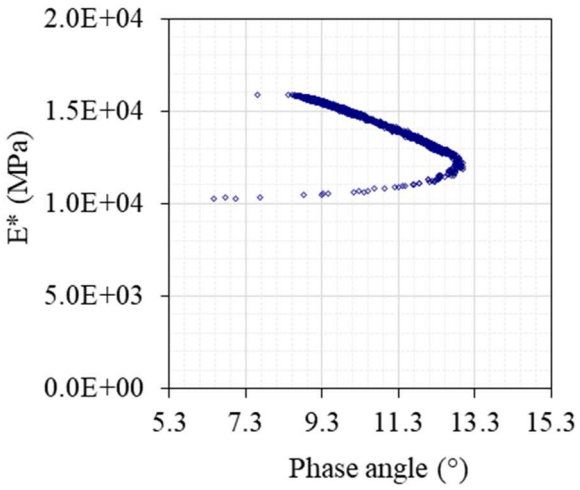

(c)

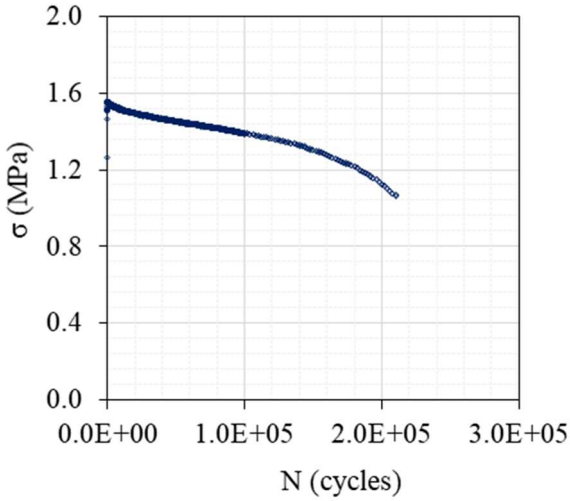

(d)

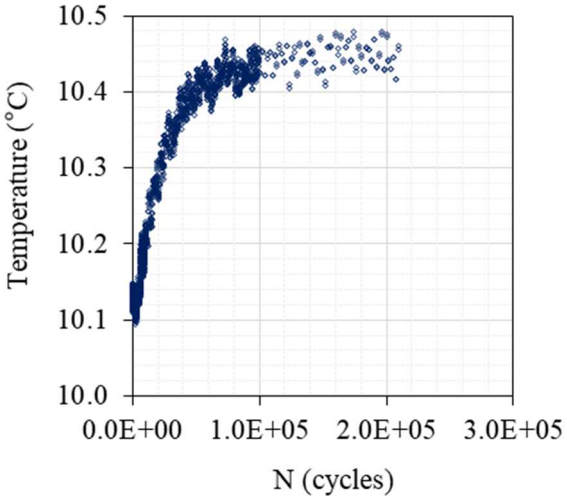

(e)

Figure C-12. Fatigue result of B3-H5 tested at 108μm/m of controlled strain amplitude

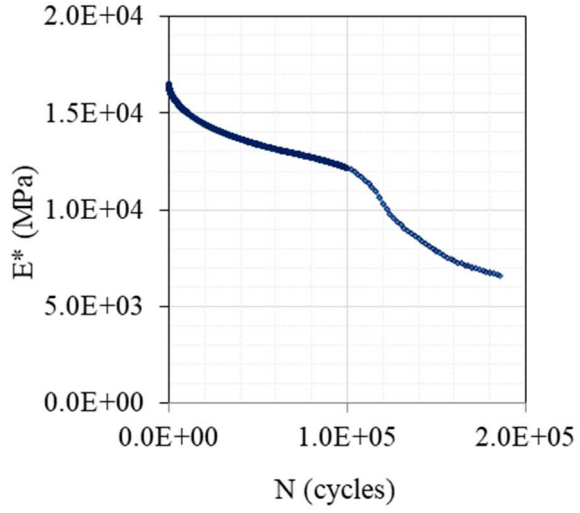

(a)

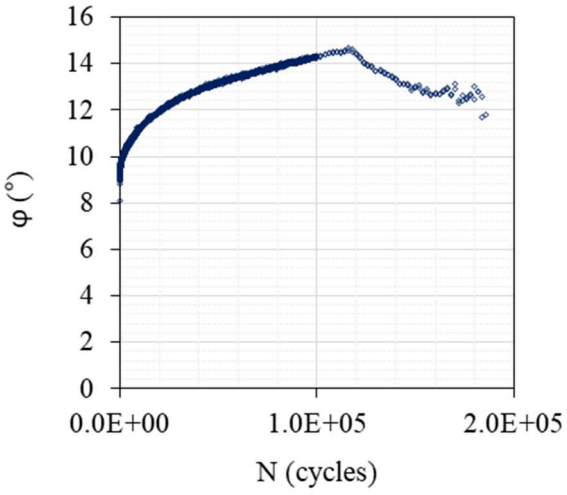

(b)

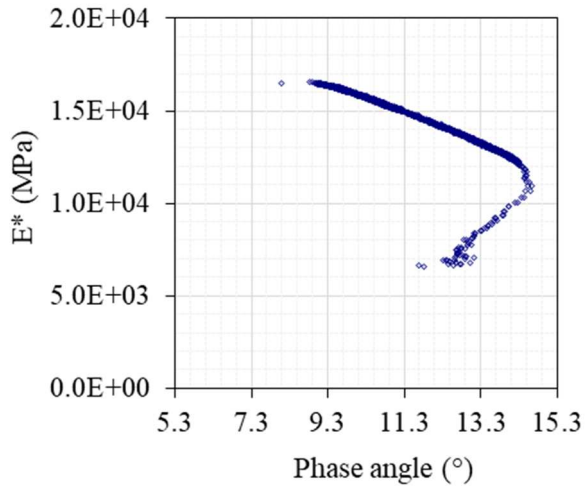

(c)

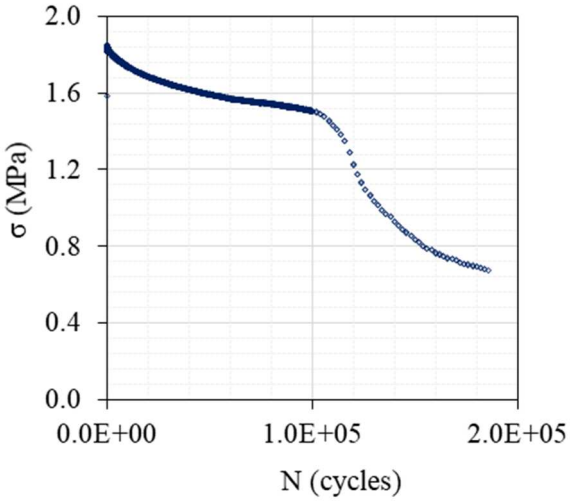

(d)

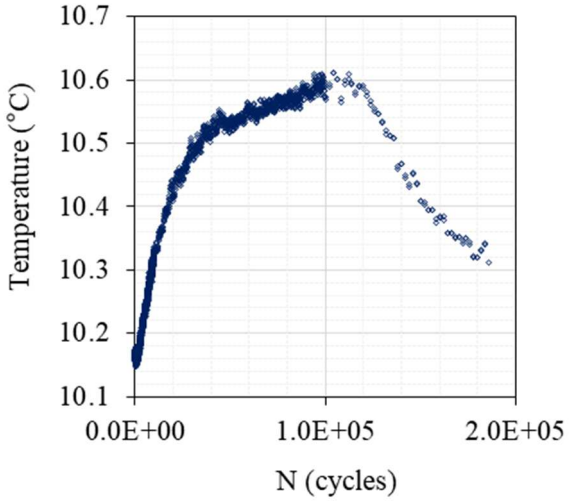

(e)

Figure C-13. Fatigue result of B3-H6 tested at 115μm/m of controlled strain amplitude

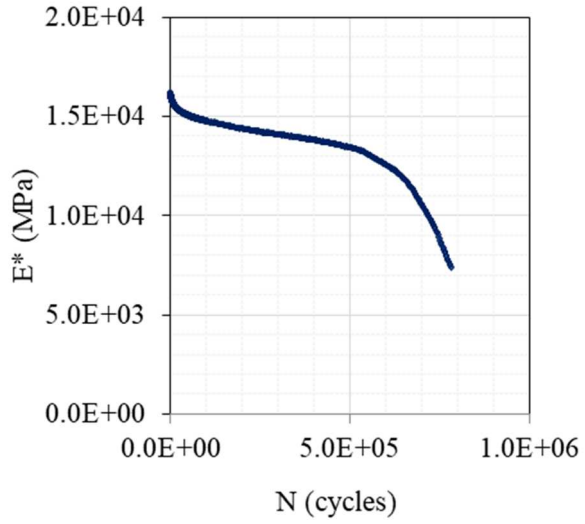

(a)

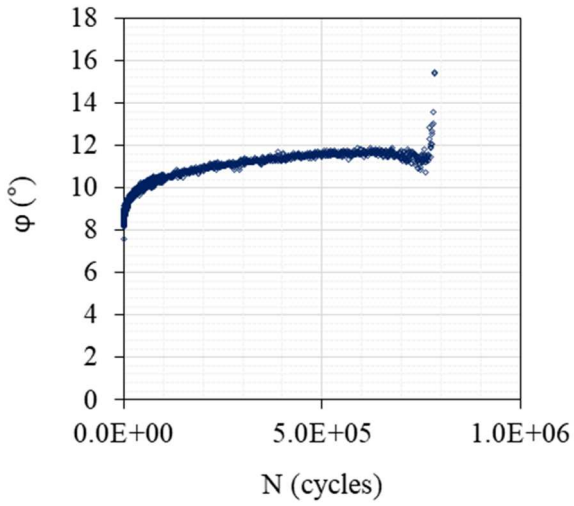

(b)

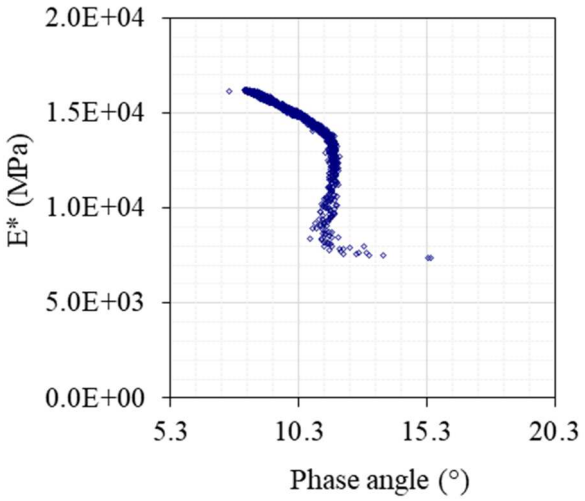

(c)

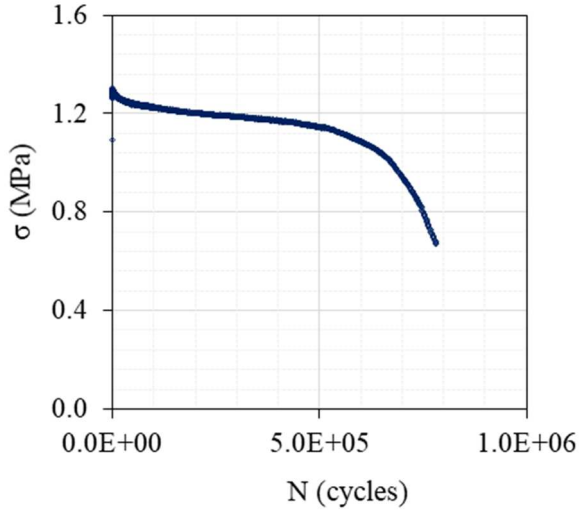

(d)

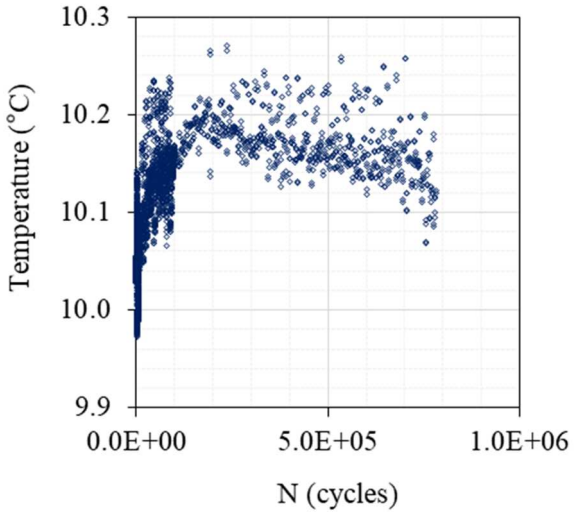

(e)

Figure C-14. Fatigue result of B3-H7 tested at 85μm/m of controlled strain amplitude

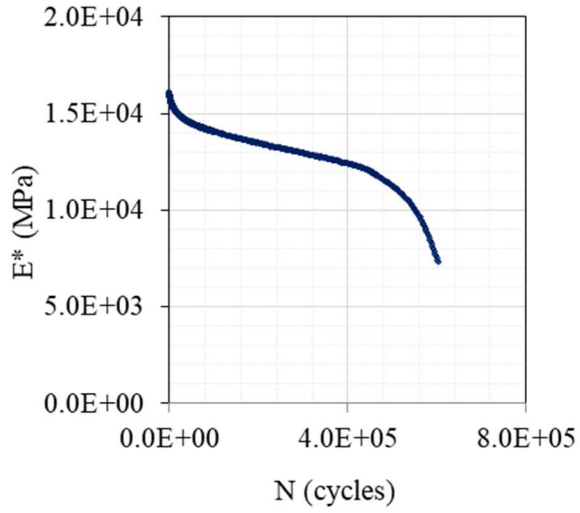

(a)

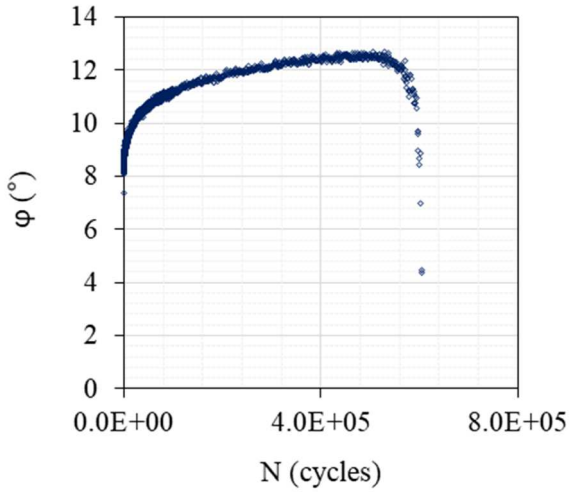

(b)

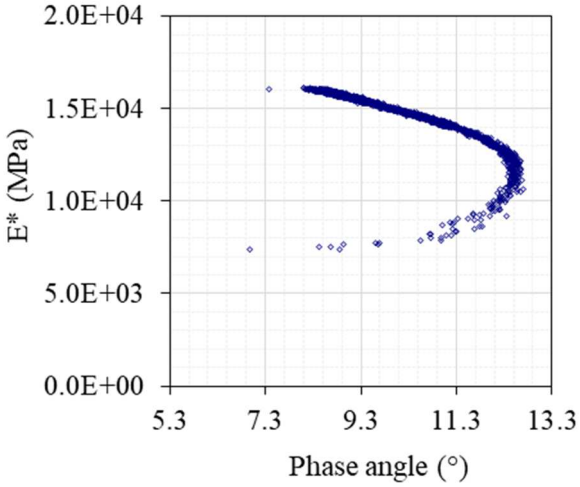

(c)

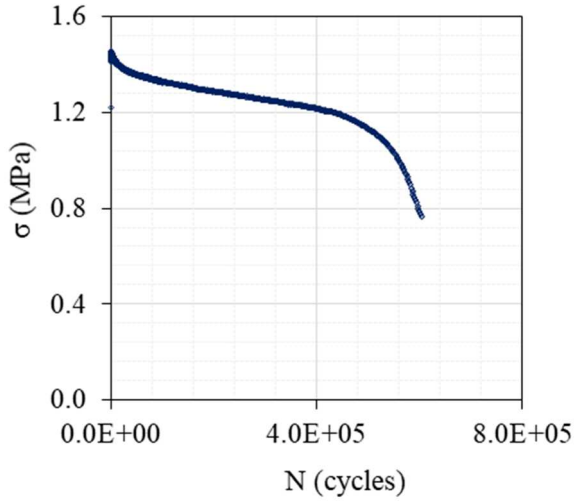

(d)

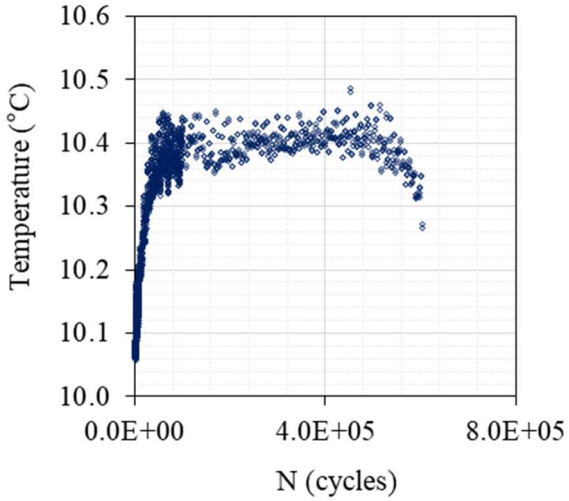

(e)

Figure C-15. Fatigue result of B3-H8 tested at 97μm/m of controlled strain amplitude

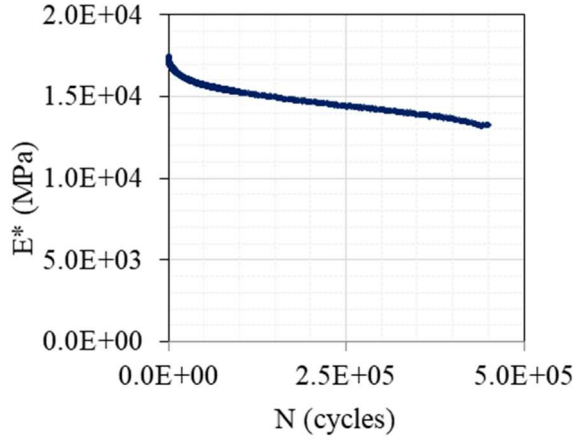

(a)

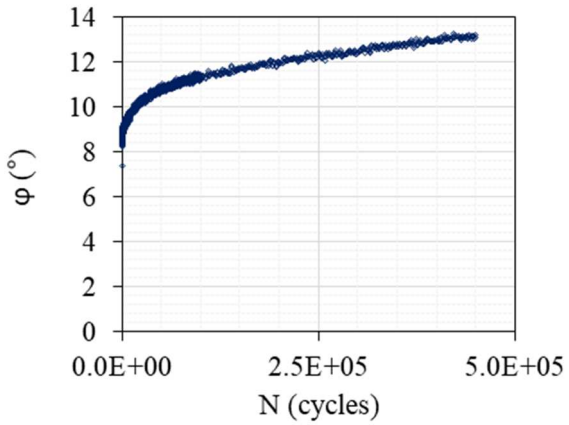

(b)

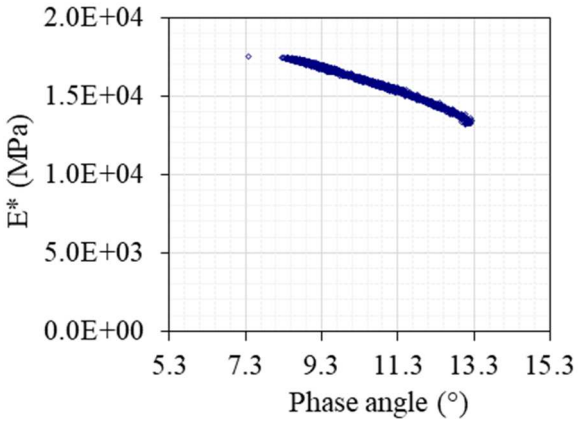

(c)

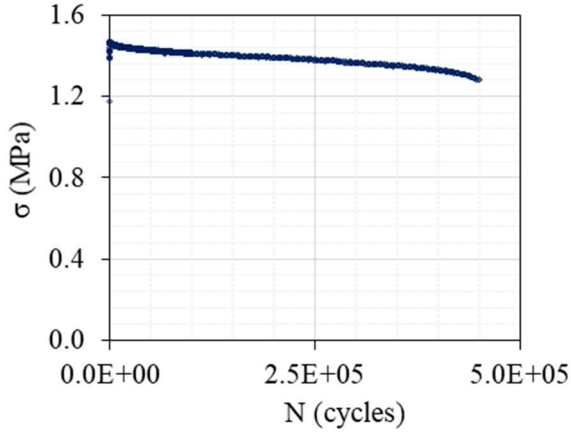

(d)

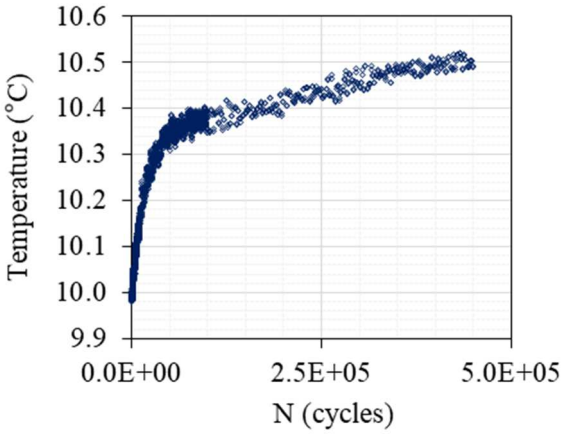

(e)

Figure C-16. Fatigue result of C4-H2 tested at 94μm/m of controlled strain amplitude

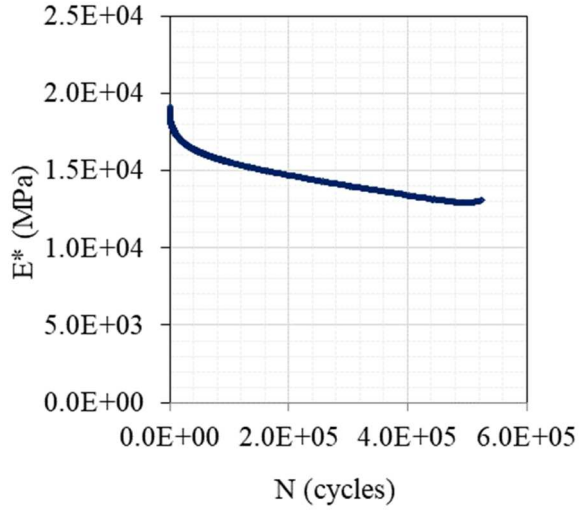

(a)

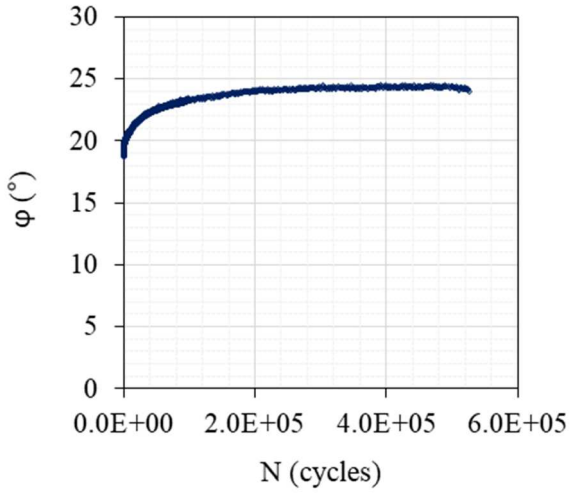

(b)

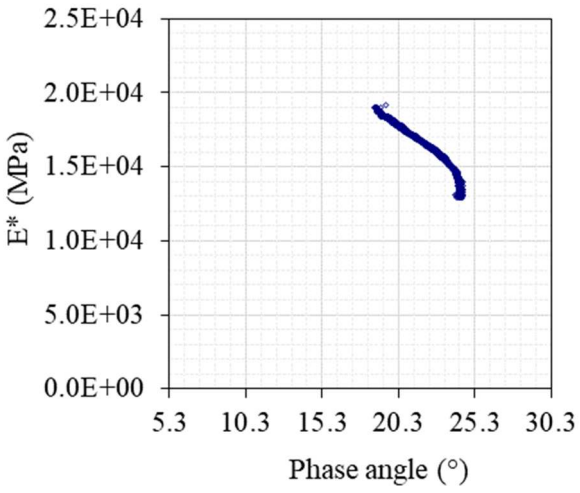

(c)

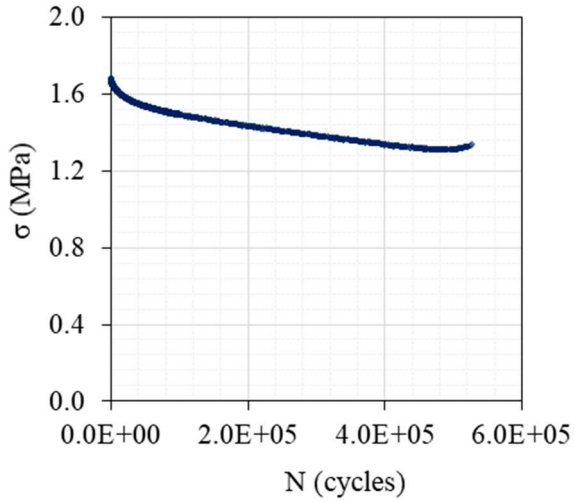

(d)

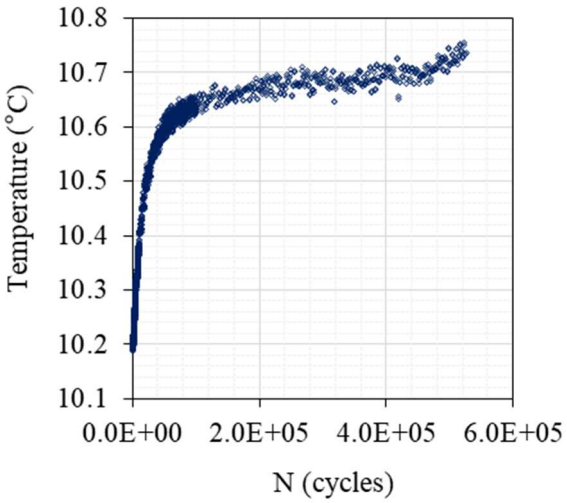

(e)

Figure C-17. Fatigue result of C4-H4 tested at 98μm/m of controlled strain amplitude

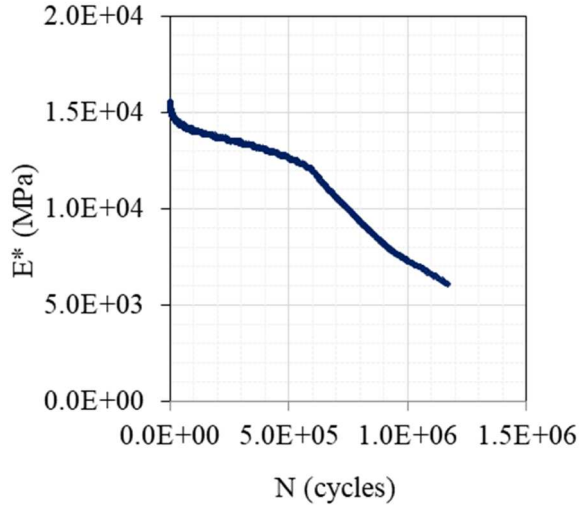

(a)

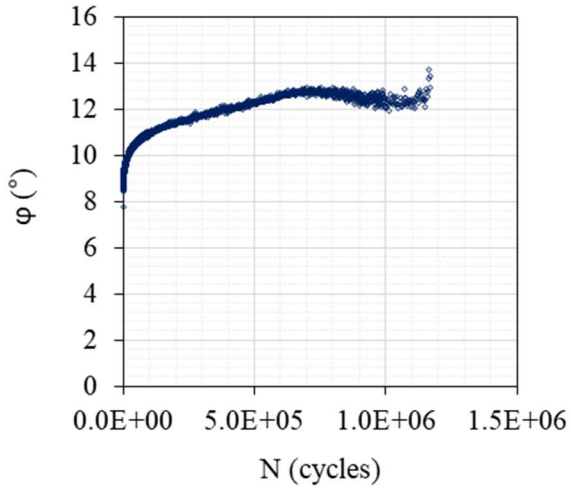

(b)

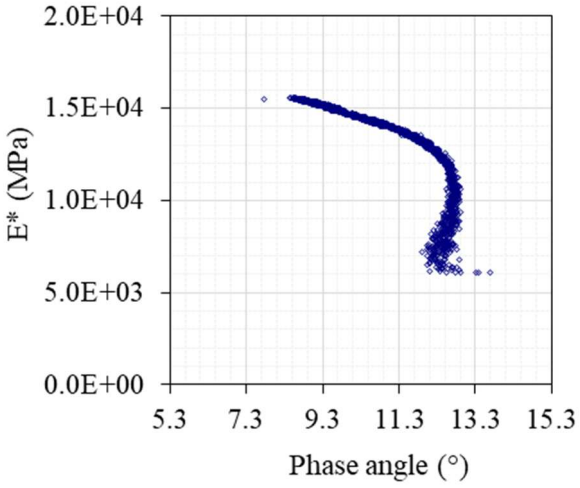

(c)

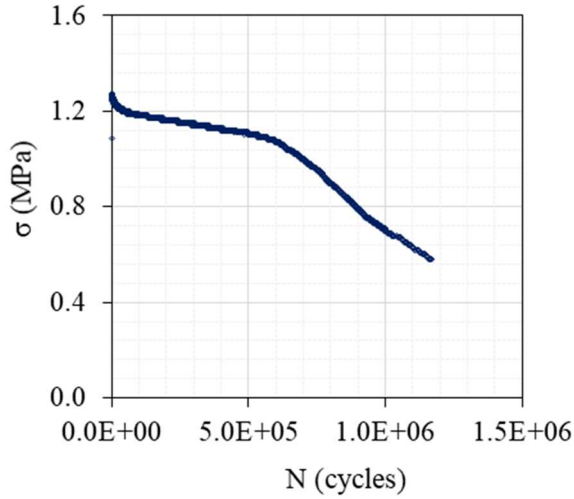

(d)

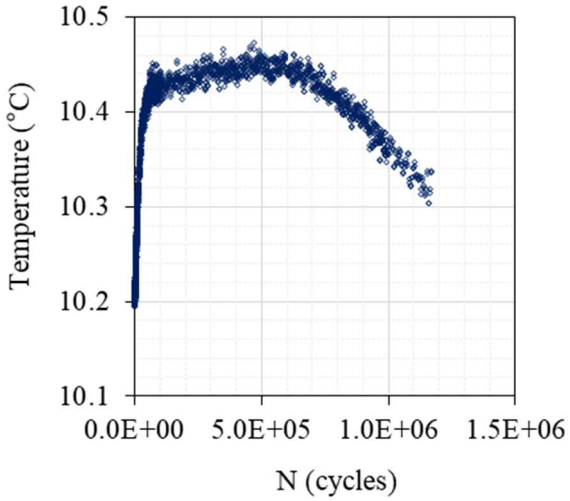

(e)

Figure C-18. Fatigue result of C4-H5 tested at 89μm/m of controlled strain amplitude

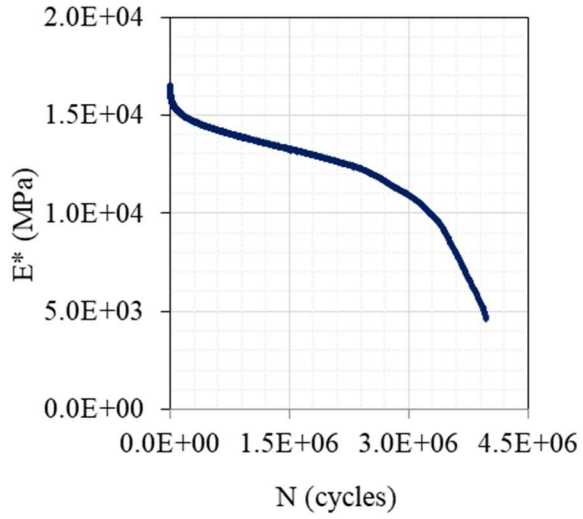

(a)

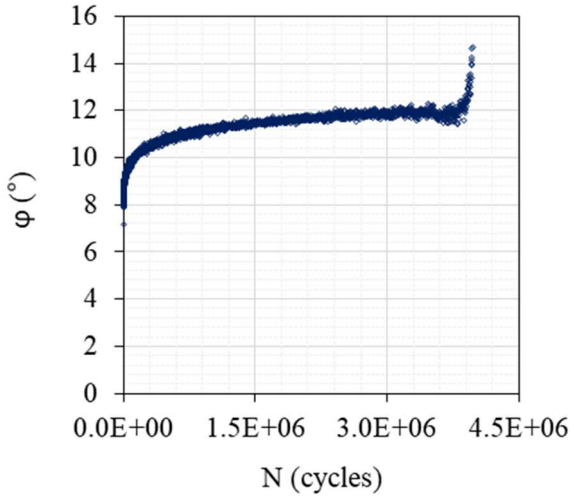

(b)

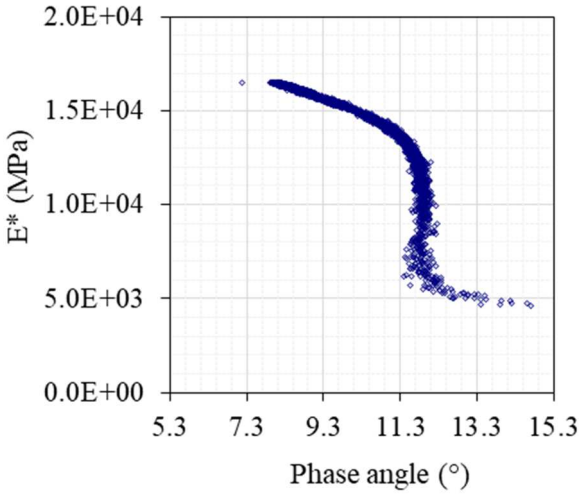

(c)

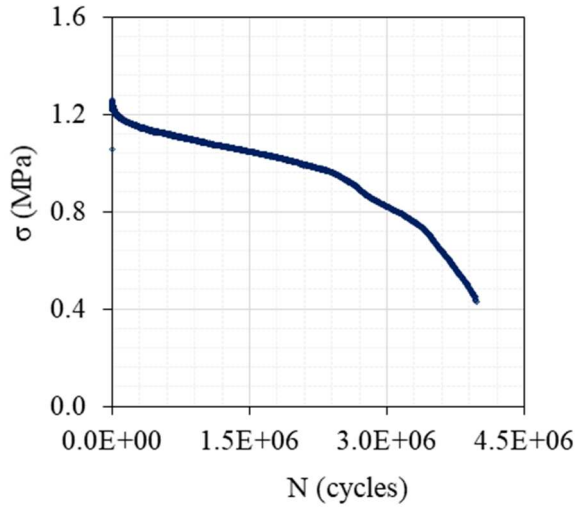

(d)

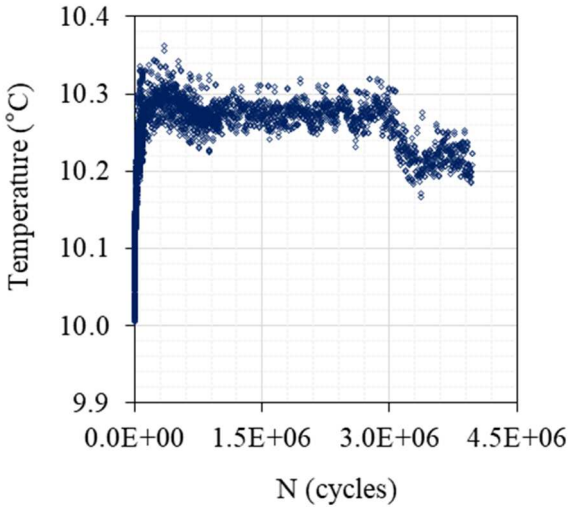

(e)

Figure C-19. Fatigue result of C4-H7 tested at 79μm/m of controlled strain amplitude

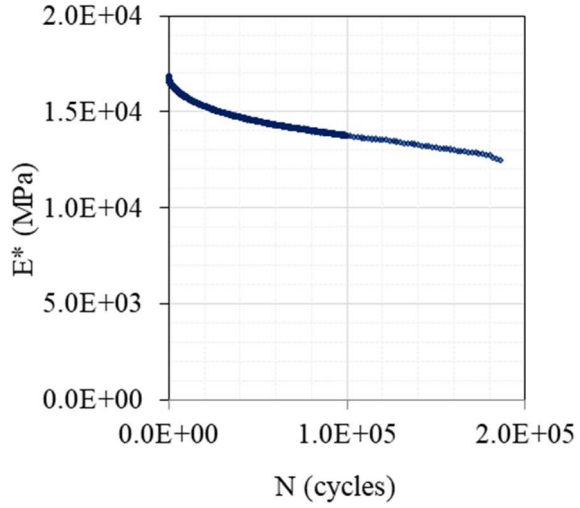

(a)

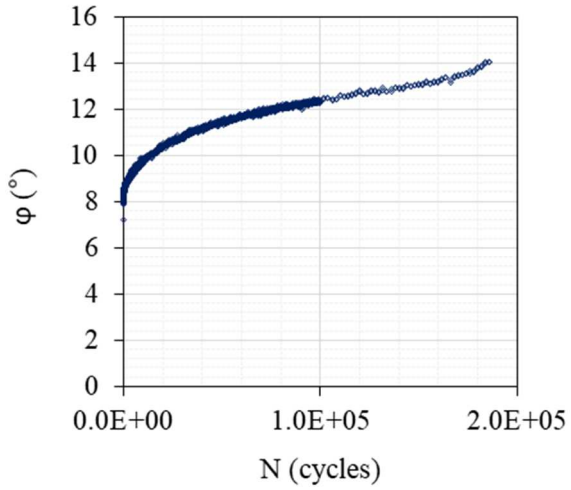

(b)

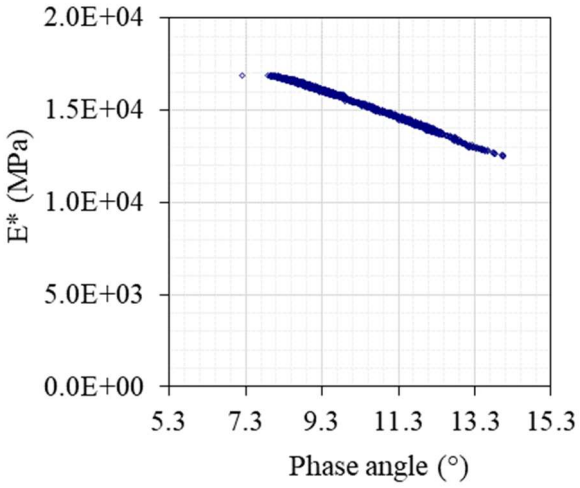

(c)

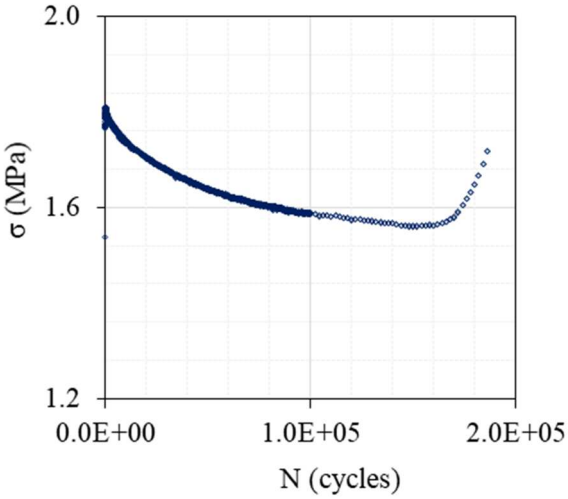

(d)

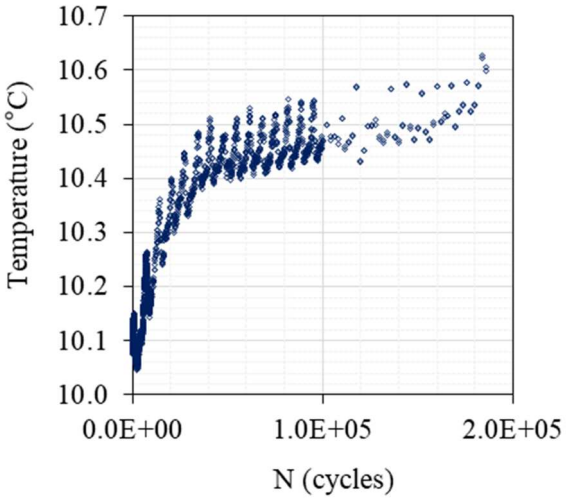

(e)

Figure C-20. Fatigue result of C4-H8 tested at 116μm/m of controlled strain amplitude

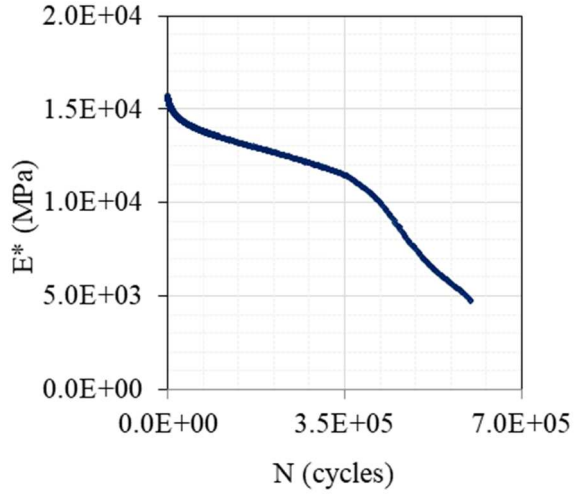

(a)

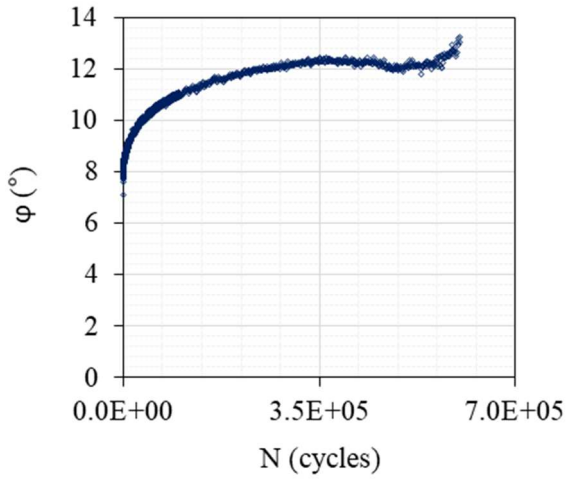

(b)

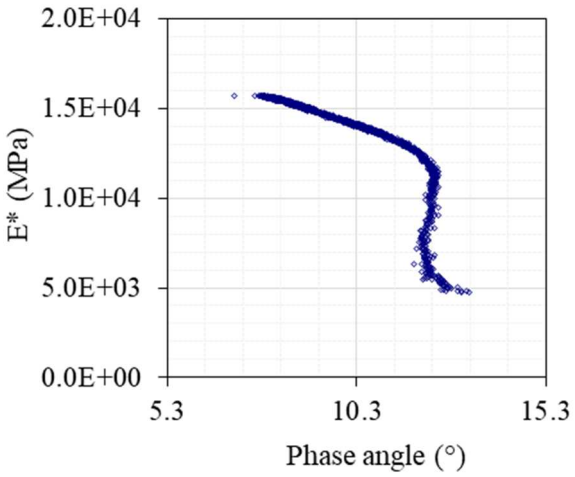

(c)

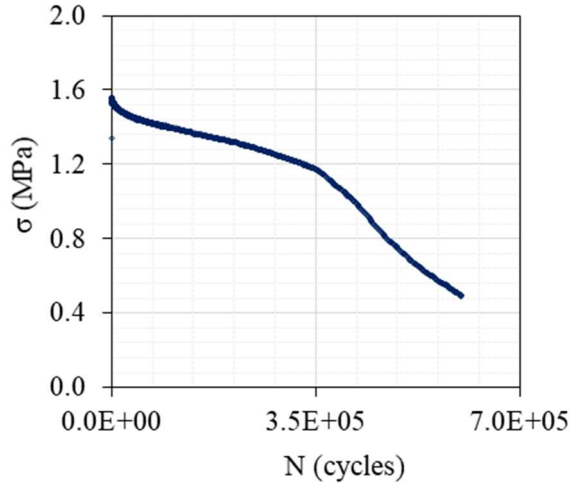

(d)

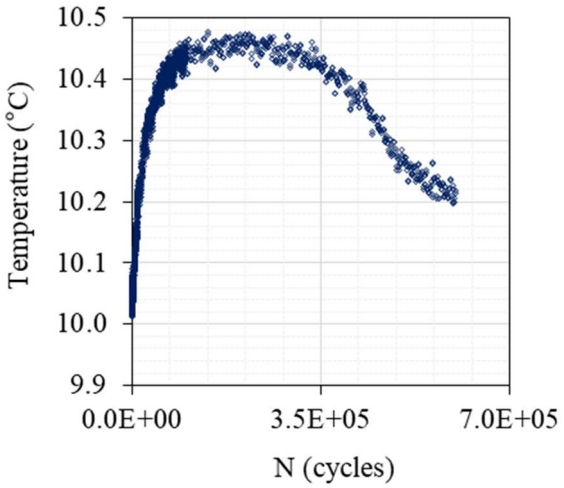

(e)

Figure C-21. Fatigue result of C4-H9 tested at 102μm/m of controlled strain amplitude

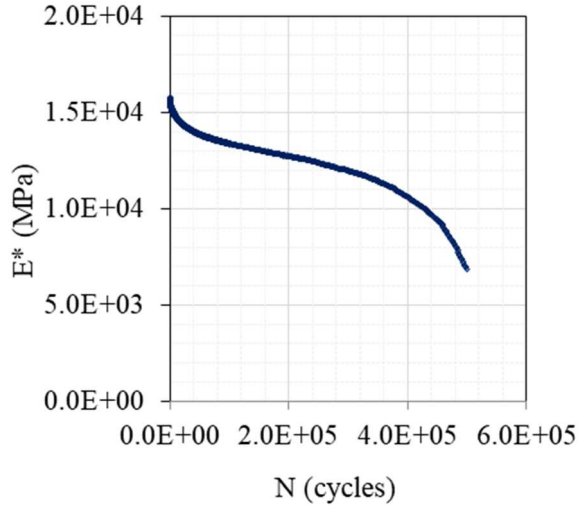

(a)

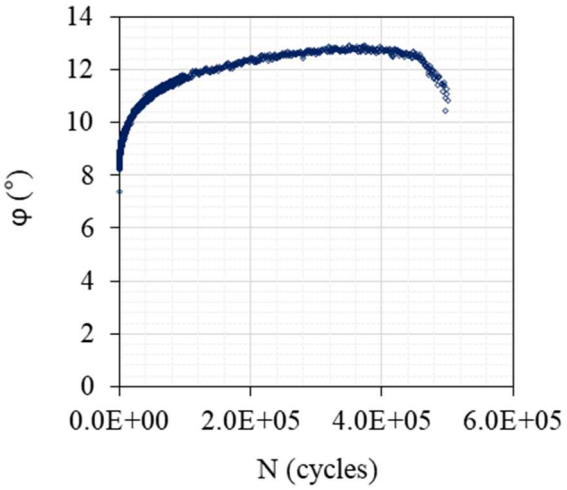

(b)

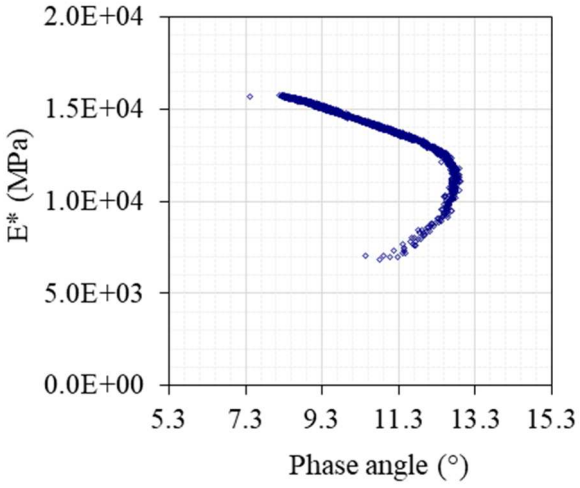

(c)

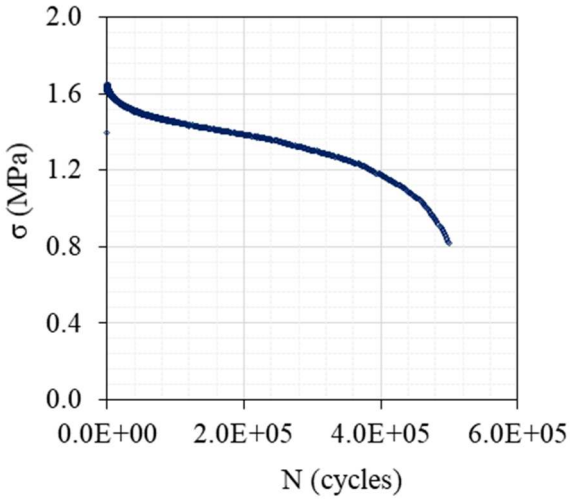

(d)

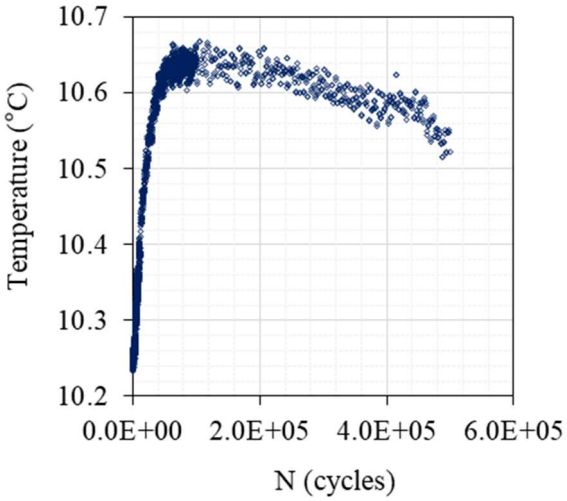

(e)

Figure C-22. Fatigue result of C4-H10 tested at 109μm/m of controlled strain amplitude

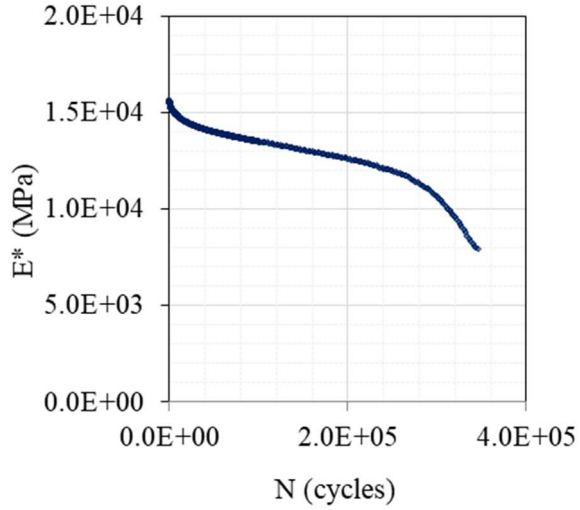

(a)

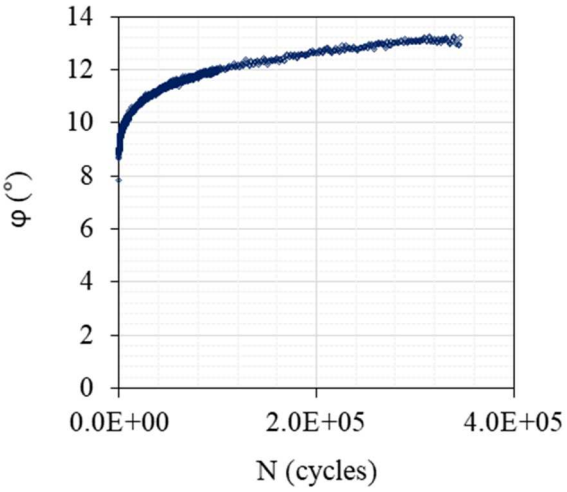

(b)

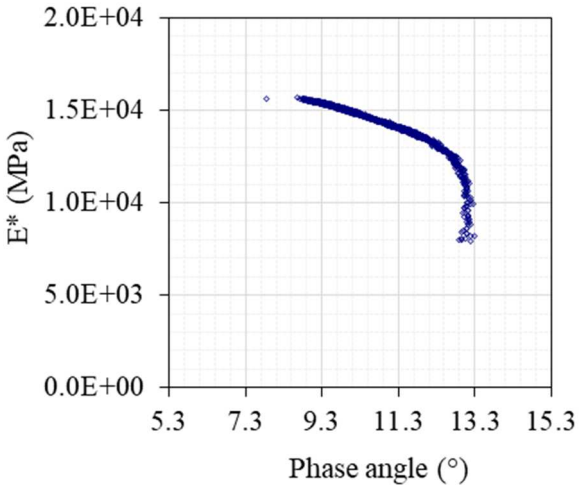

(c)

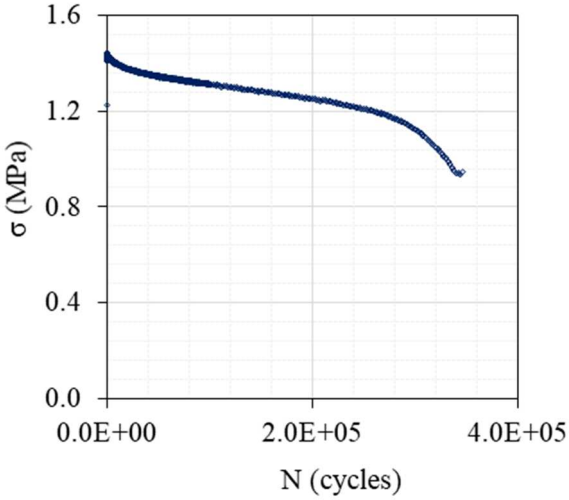

(d)

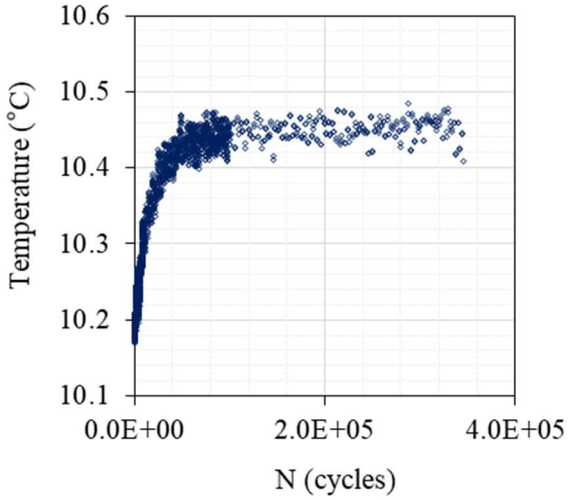

(e)

Figure C-23. Fatigue result of D3-H1 tested at 100μm/m of controlled strain amplitude

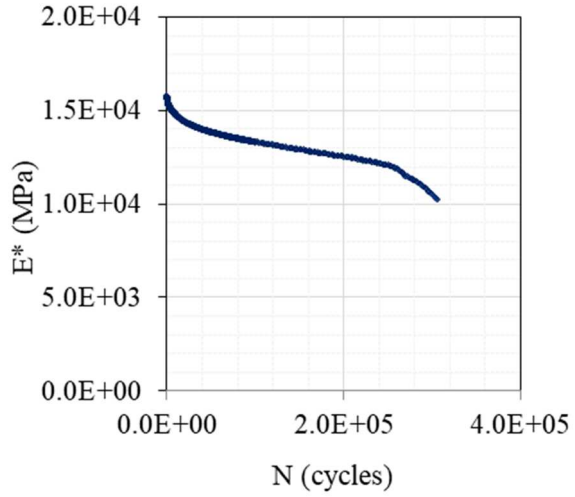

(a)

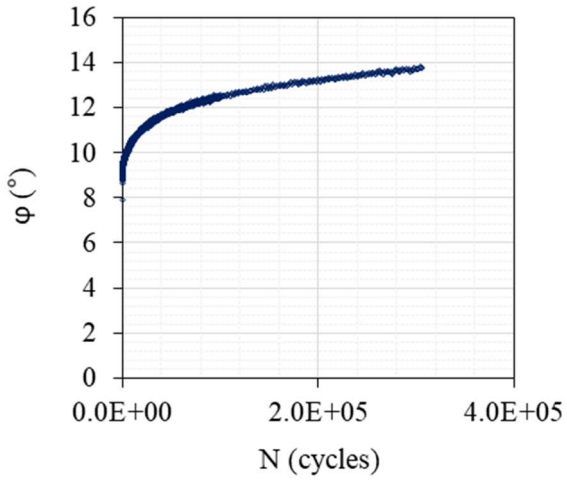

(b)

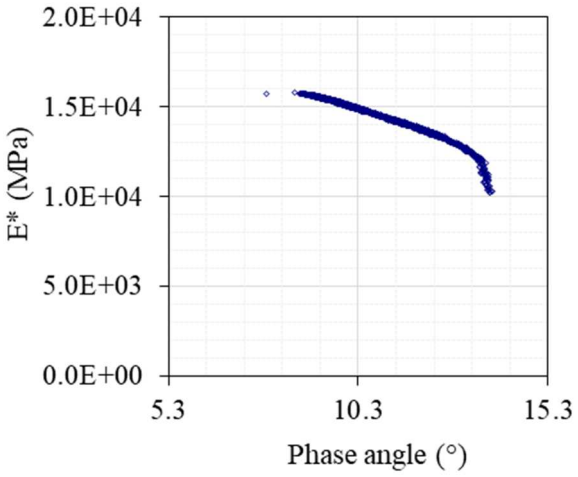

(c)

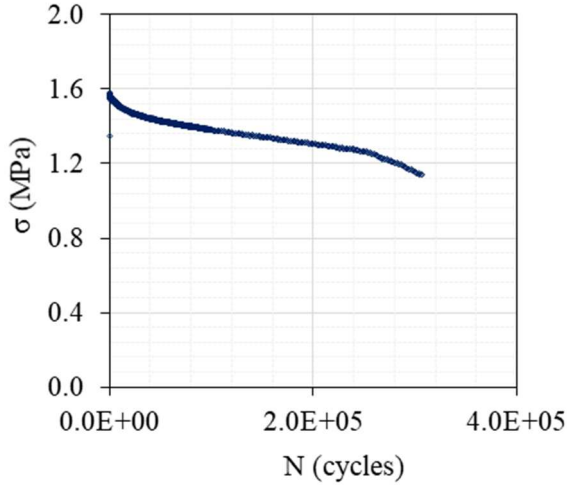

(d)

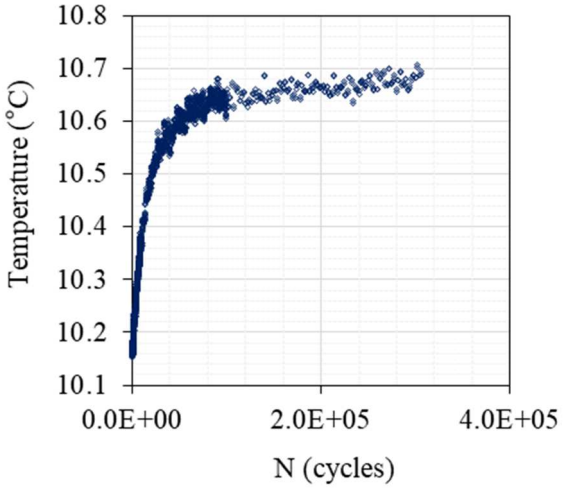

(e)

Figure C-24. Fatigue result of D3-H2 tested at 104μm/m of controlled strain amplitude

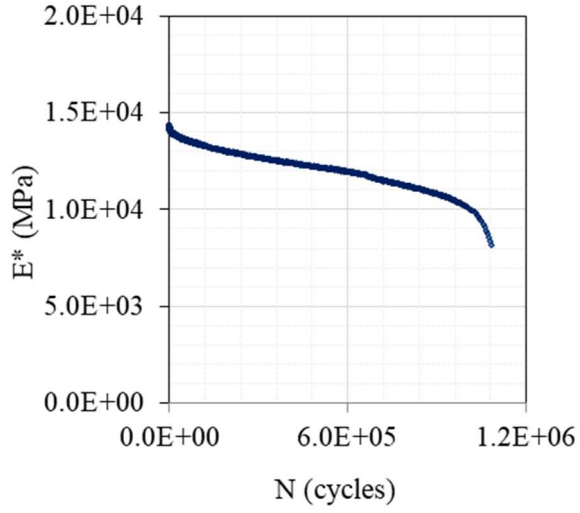

(a)

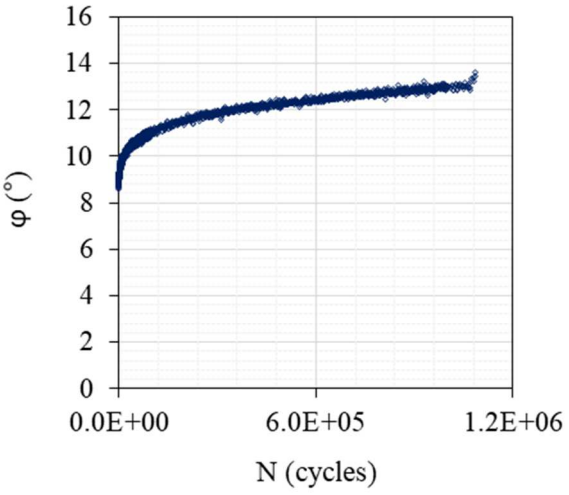

(b)

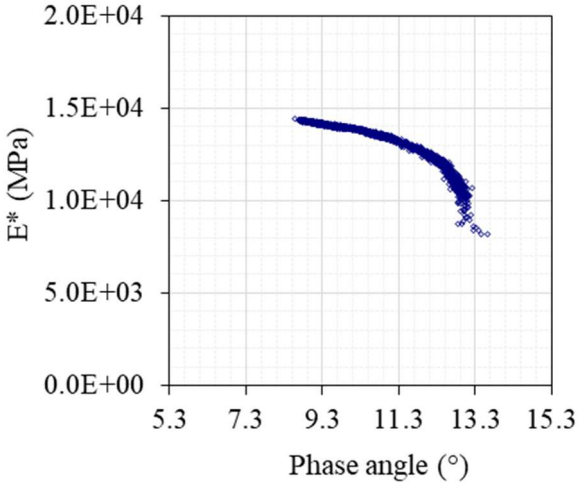

(c)

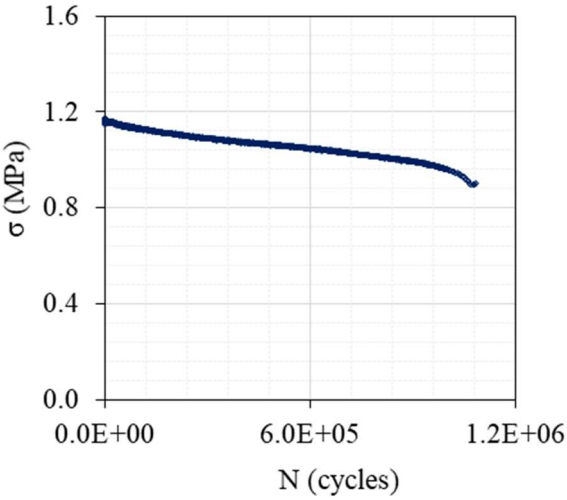

(d)

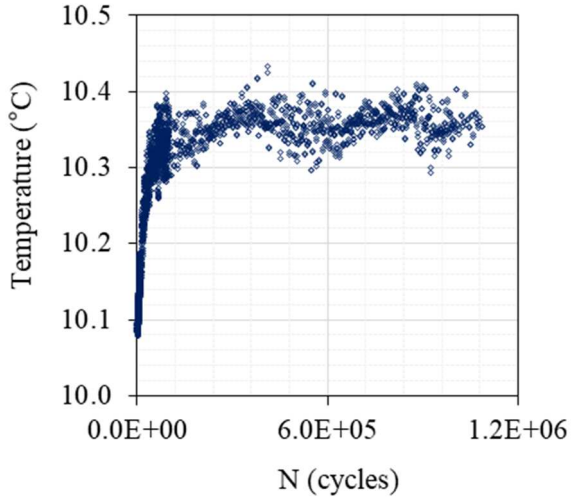

(e)

Figure C-25. Fatigue result of D3-H5 tested at 89μm/m of controlled strain amplitude

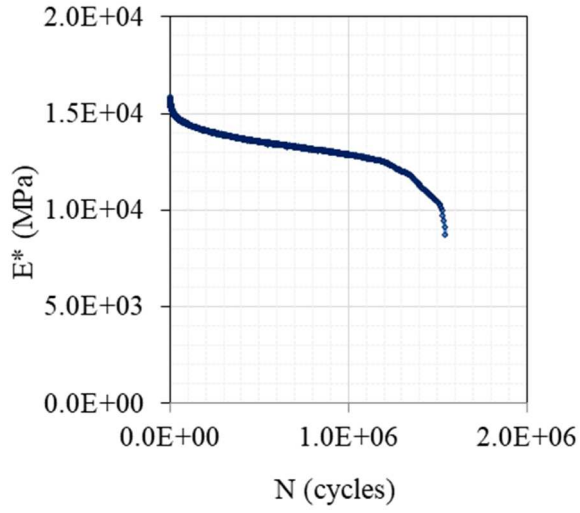

(a)

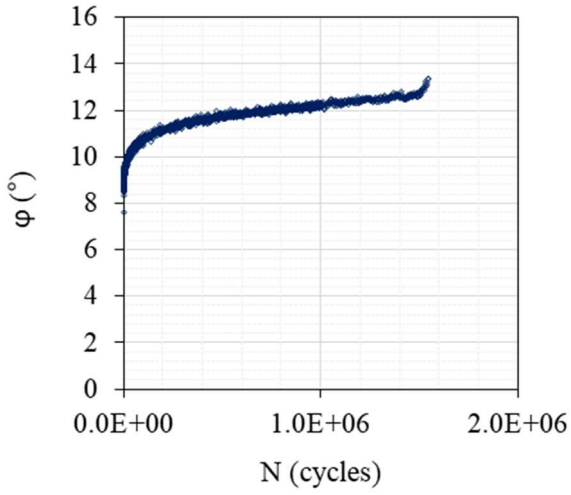

(b)

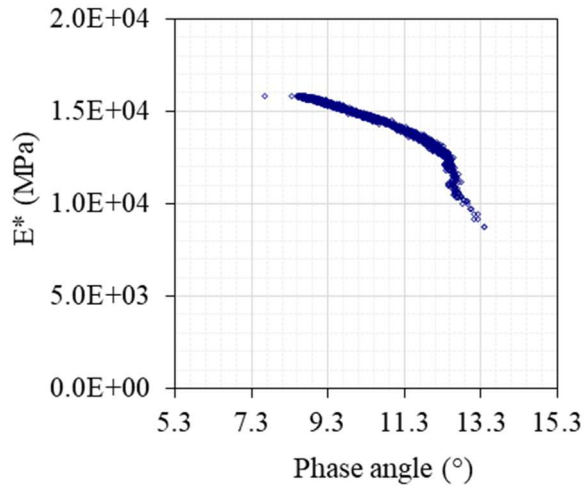

(c)

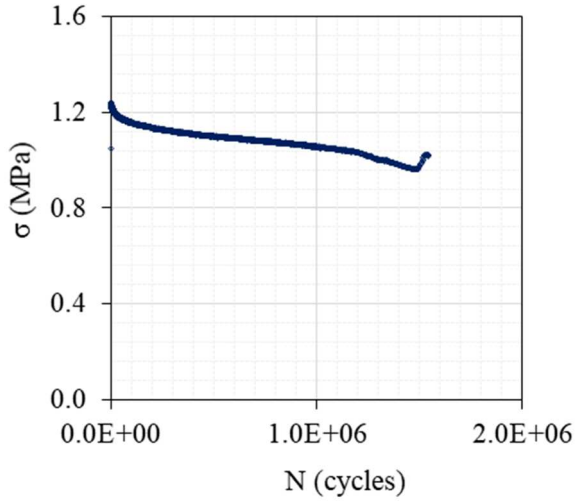

(d)

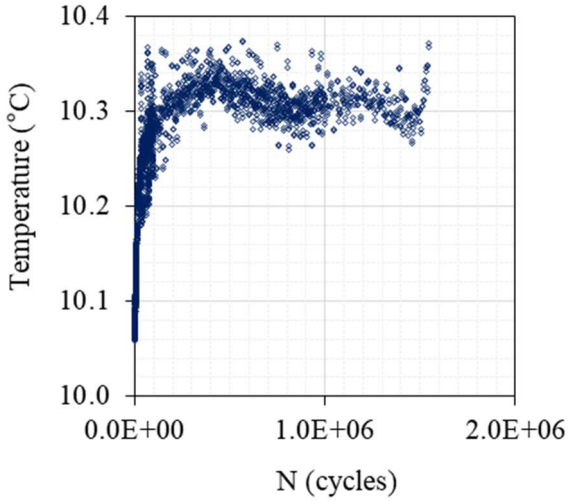

(e)

Figure C-26. Fatigue result of D3-H6 tested at 83μm/m of controlled strain amplitude

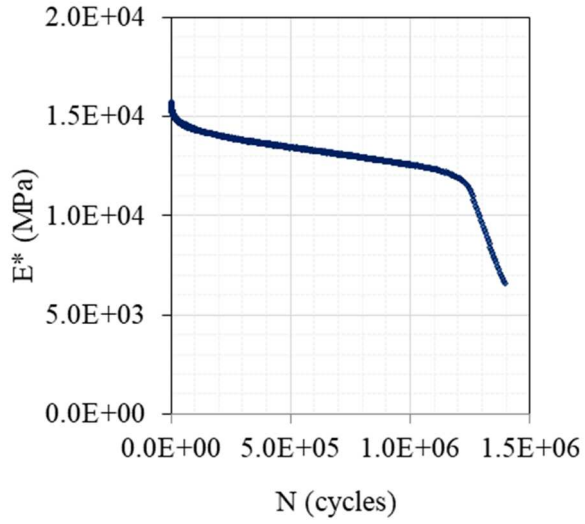

(a)

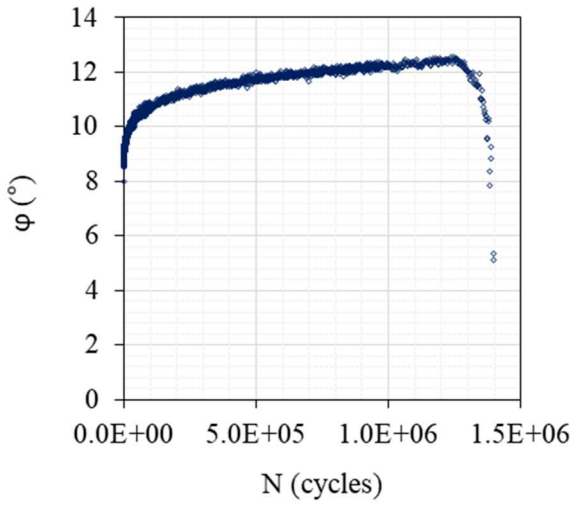

(b)

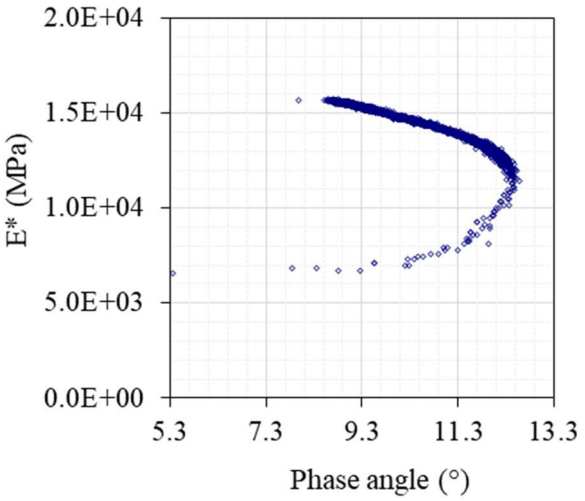

(c)

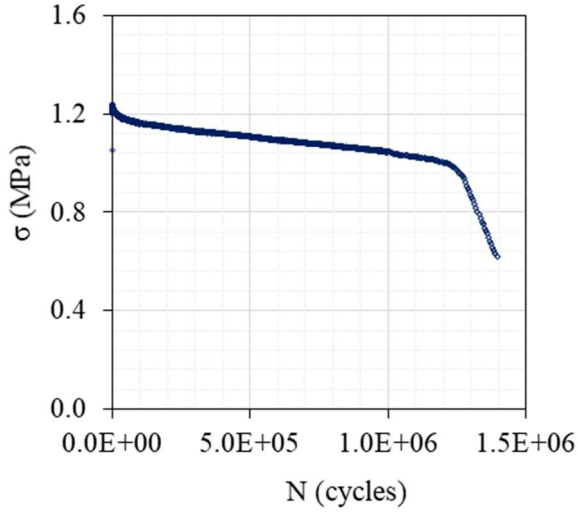

(d)

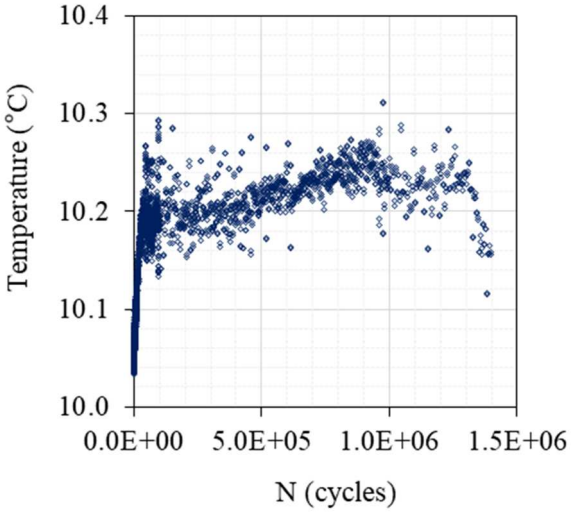

(e)

Figure C-27. Fatigue result of D3-H7 tested at 82μm/m of controlled strain amplitude

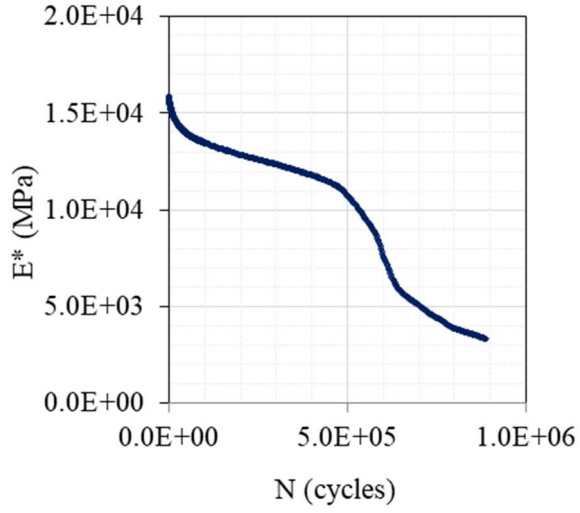

(a)

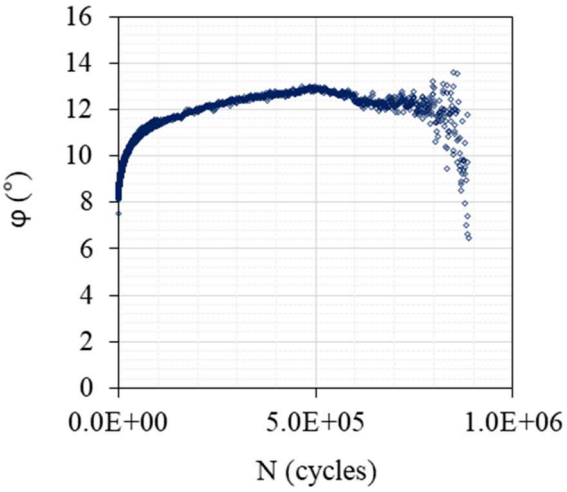

(b)

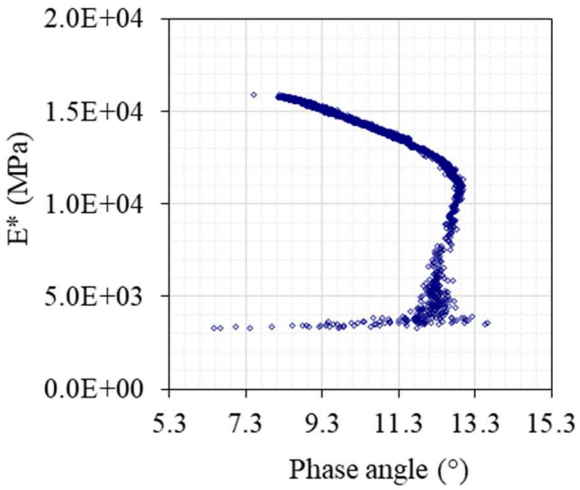

(c)

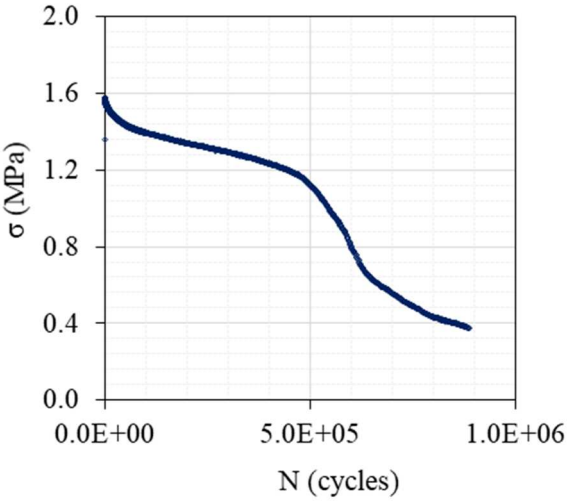

(d)

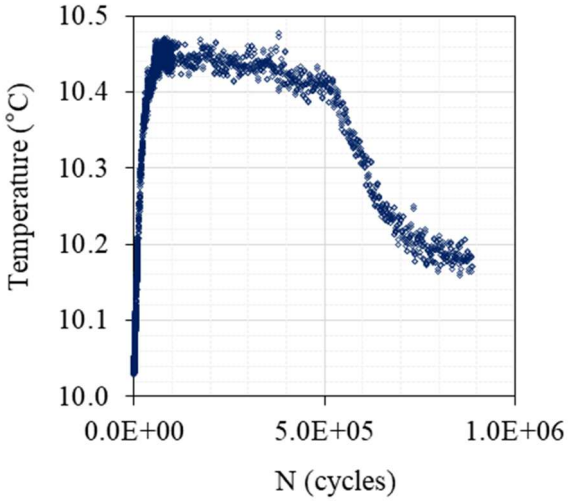

(e)

Figure C-28. Fatigue result of D3-H8 tested at 104μm/m of controlled strain amplitude

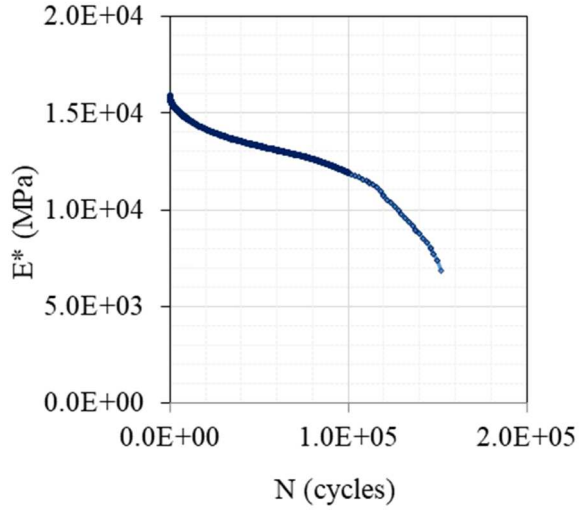

(a)

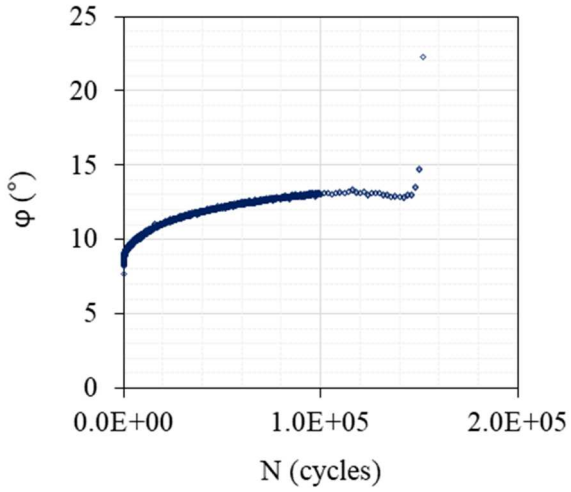

(b)

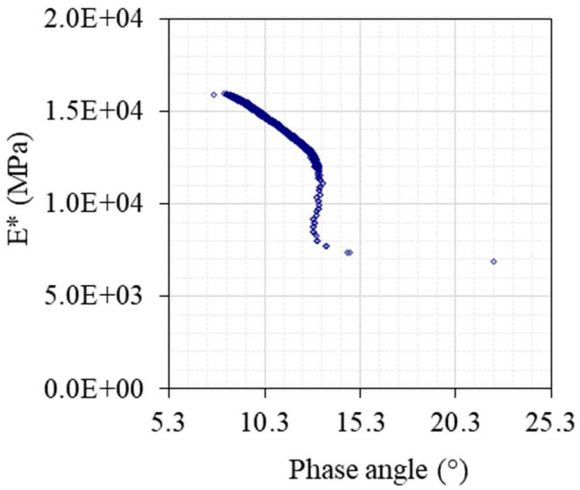

(c)

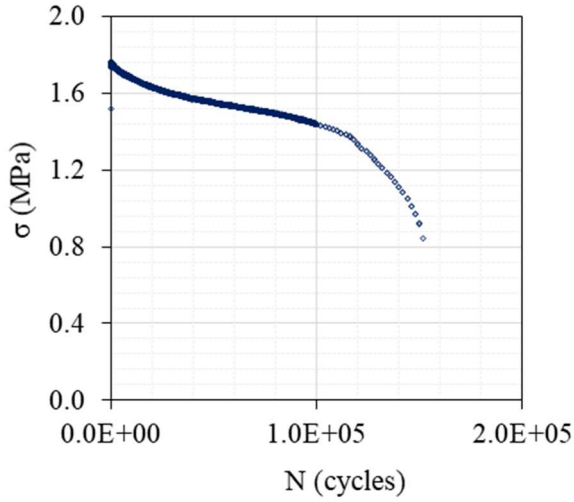

(d)

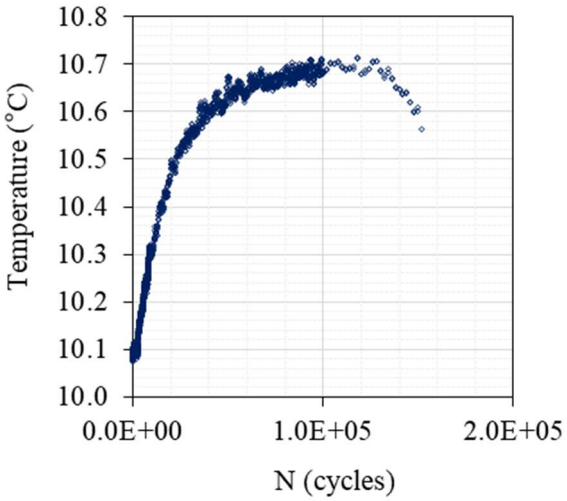

(e)

Figure C-29. Fatigue result of D3-H9 tested at 120μm/m of controlled strain amplitude

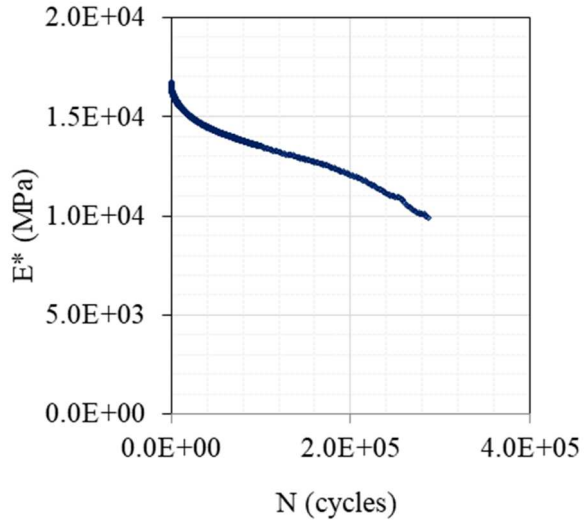

(a)

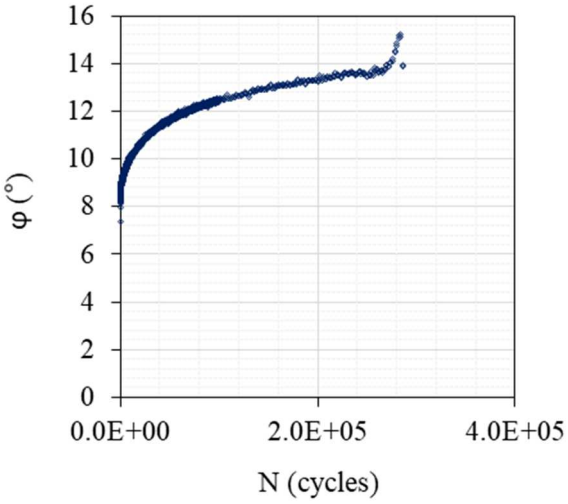

(b)

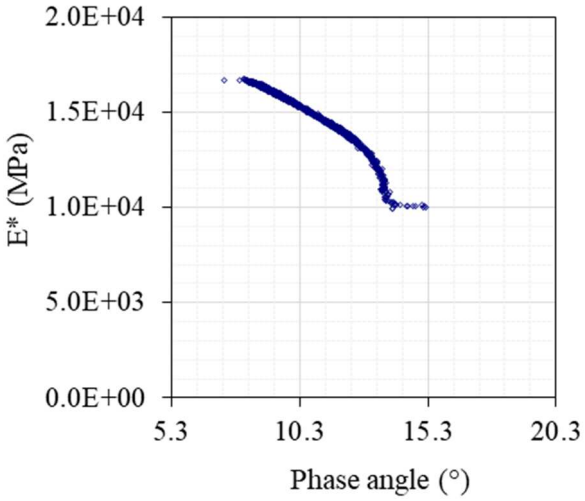

(c)

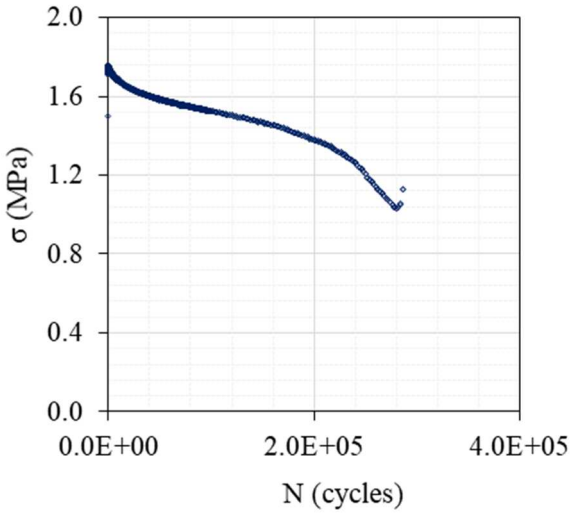

(d)

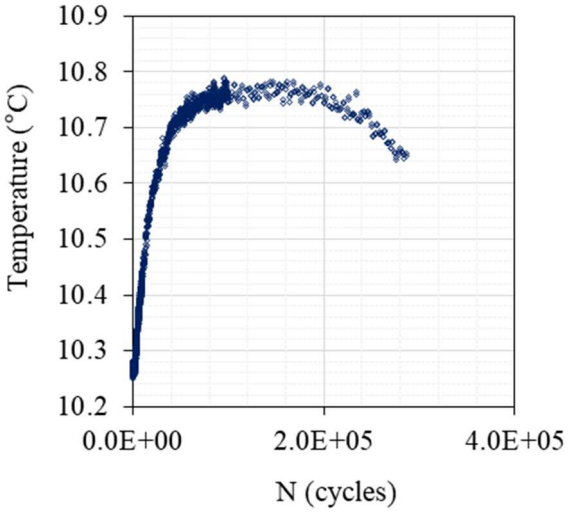

(e)

Figure C-30. Fatigue result of D3-H10 tested at 112μm/m of controlled strain amplitude

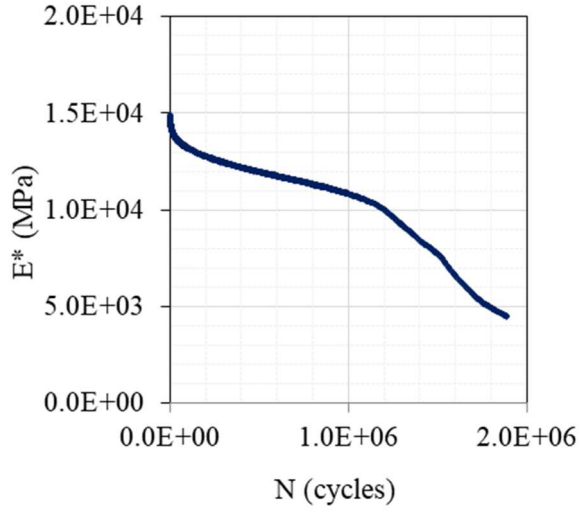

(a)

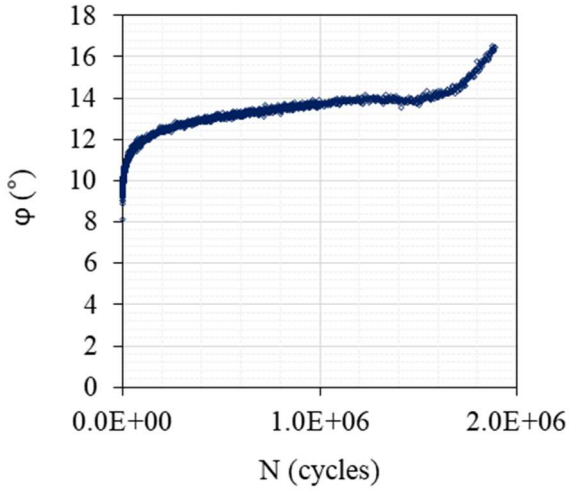

(b)

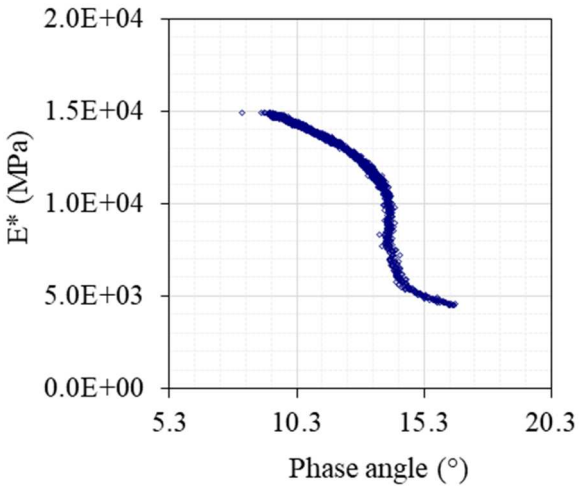

(c)

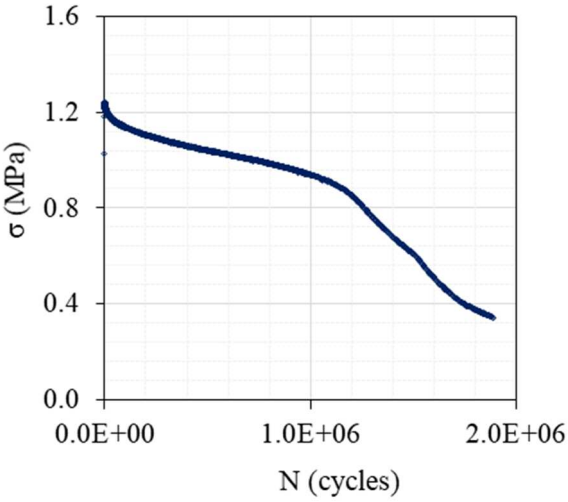

(d)

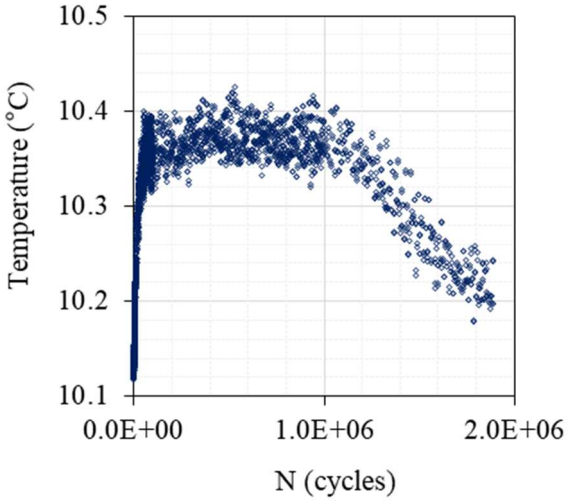

(e)

Figure C-31. Fatigue result of E3-H4 tested at 86μm/m of controlled strain amplitude

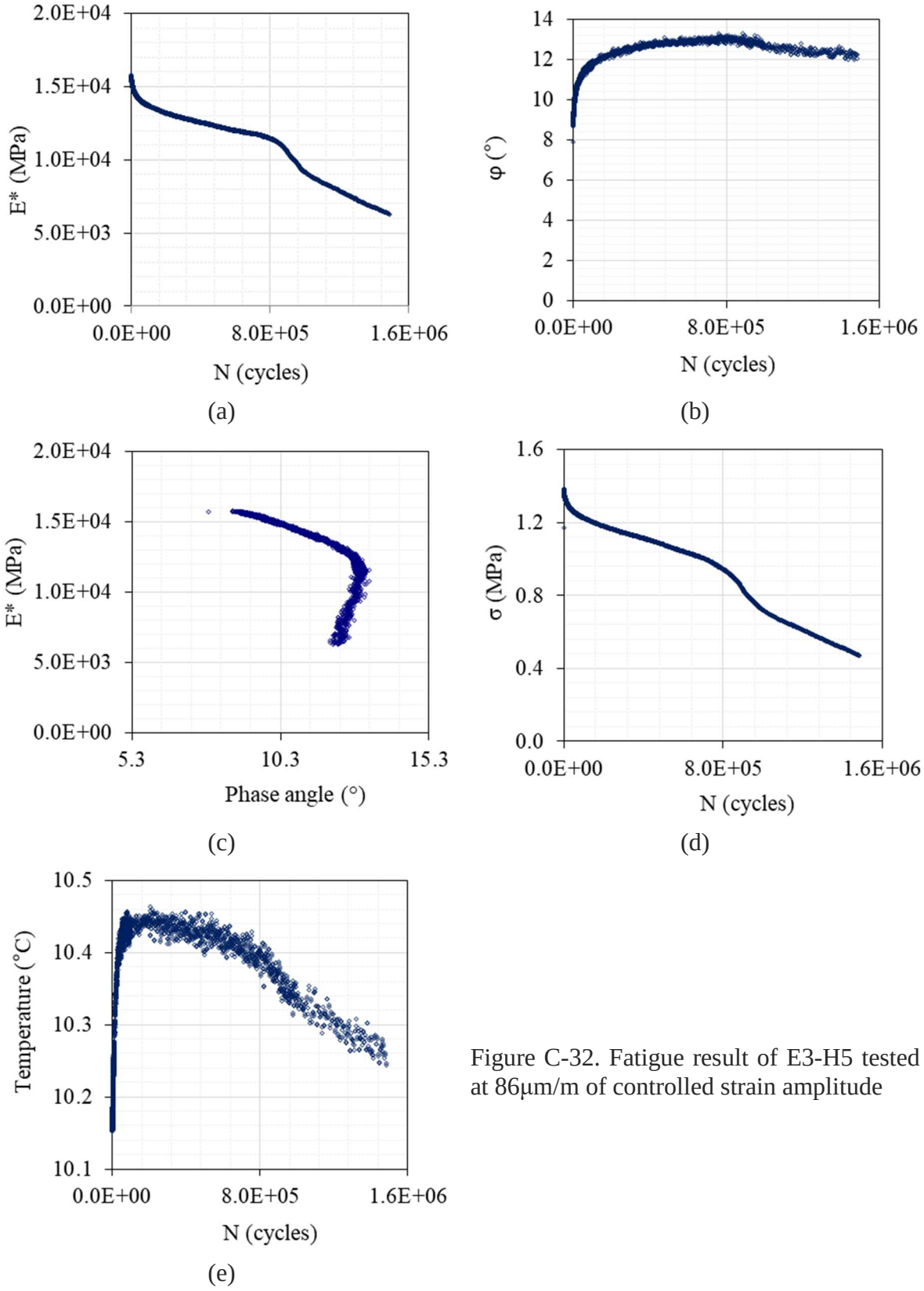

Figure C-32. Fatigue result of E3-H5 tested at 86μm/m of controlled strain amplitude

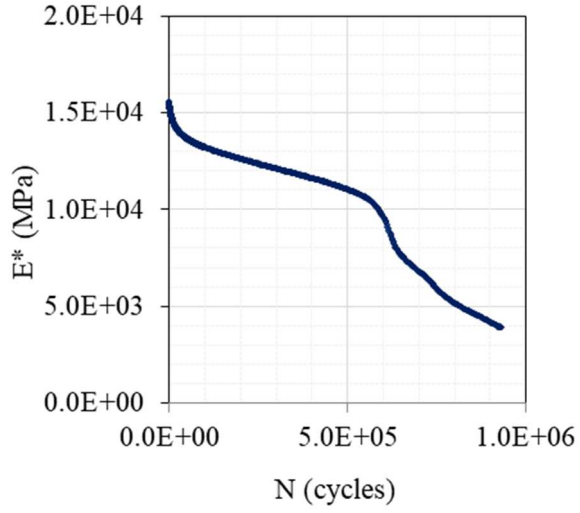

(a)

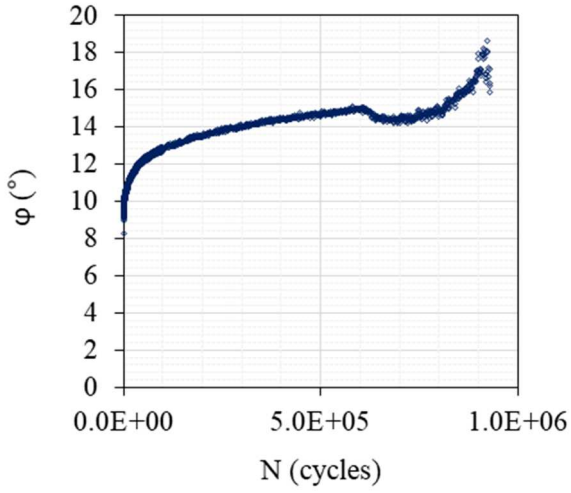

(b)

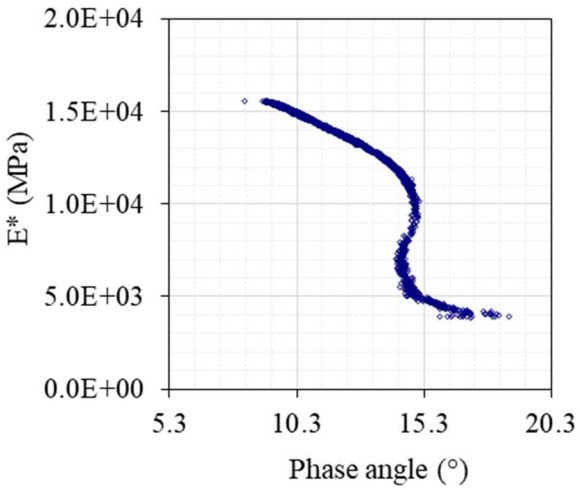

(c)

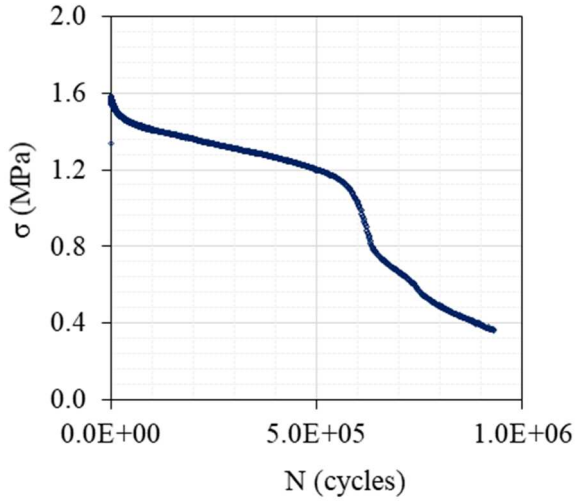

(d)

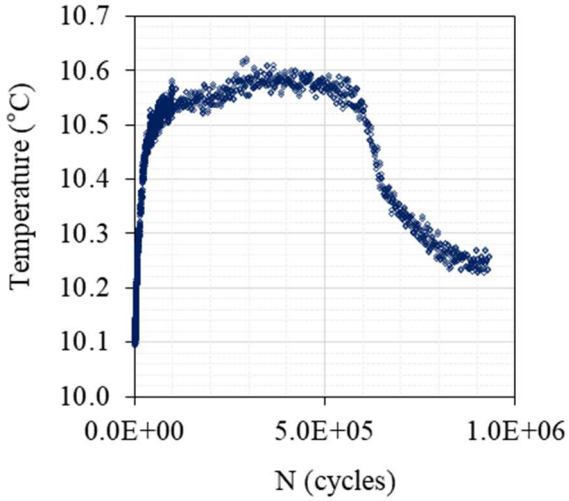

(e)

Figure C-33. Fatigue result of E3-H6 tested at 104μm/m of controlled strain amplitude

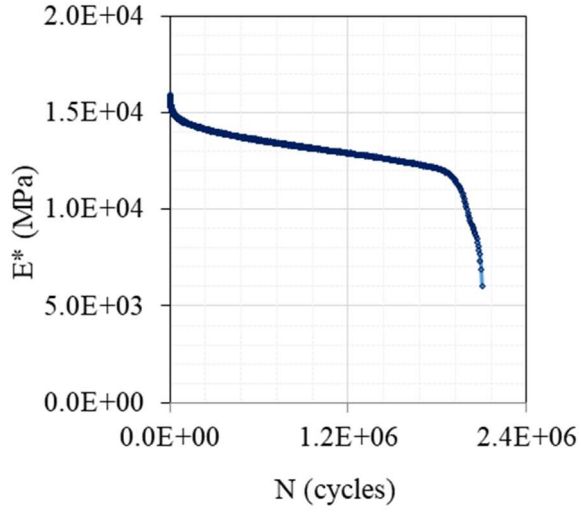

(a)

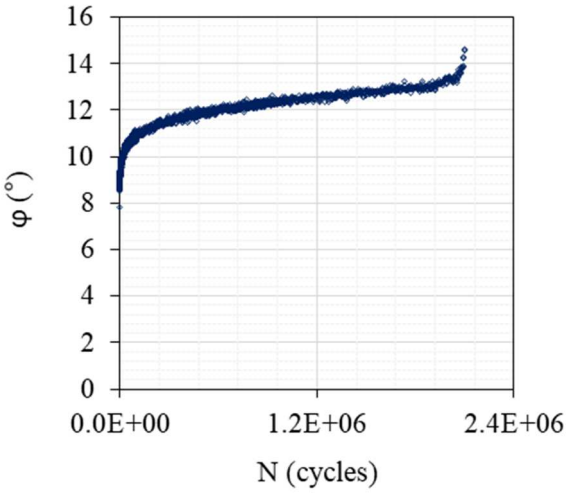

(b)

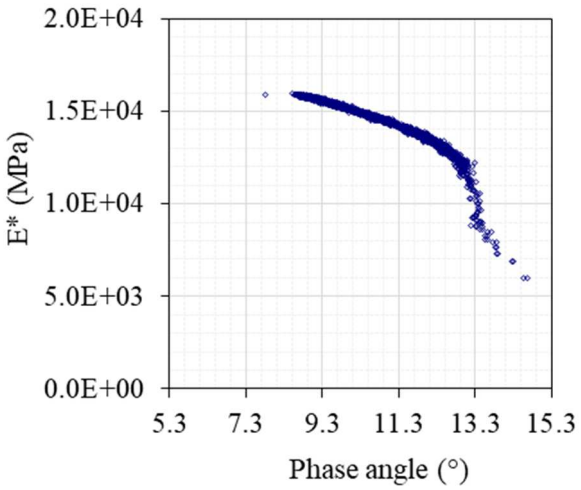

(c)

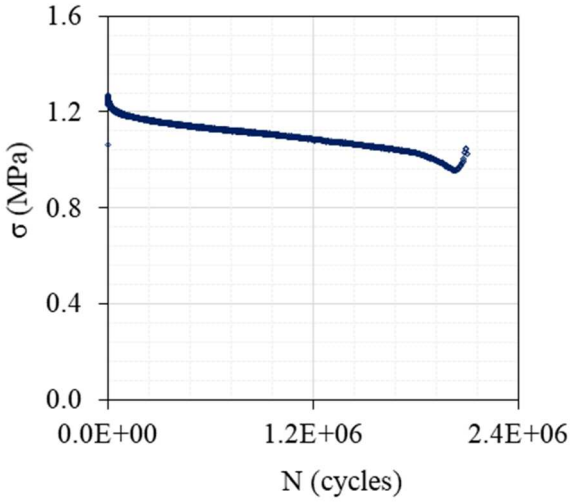

(d)

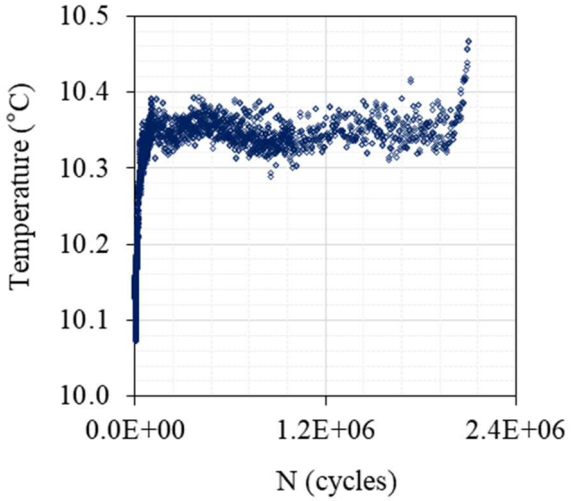

(e)

Figure C-34. Fatigue result of E3-H7 tested at 84μm/m of controlled strain amplitude

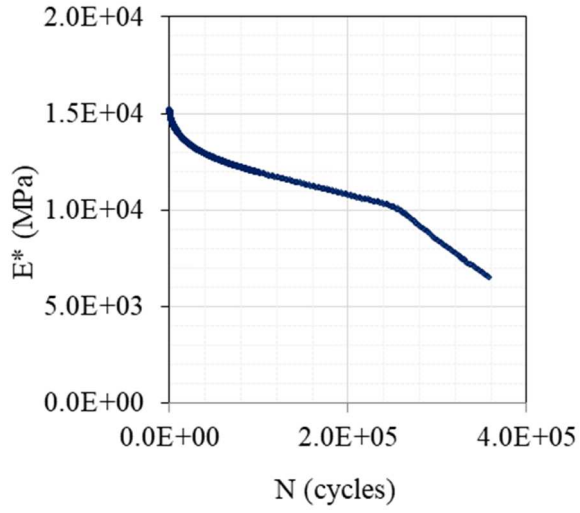

(a)

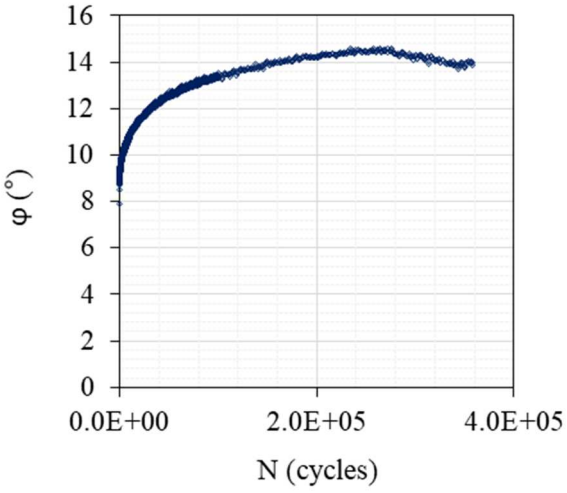

(b)

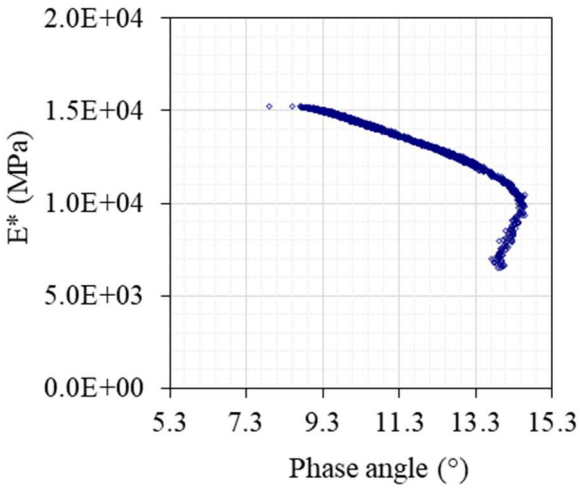

(c)

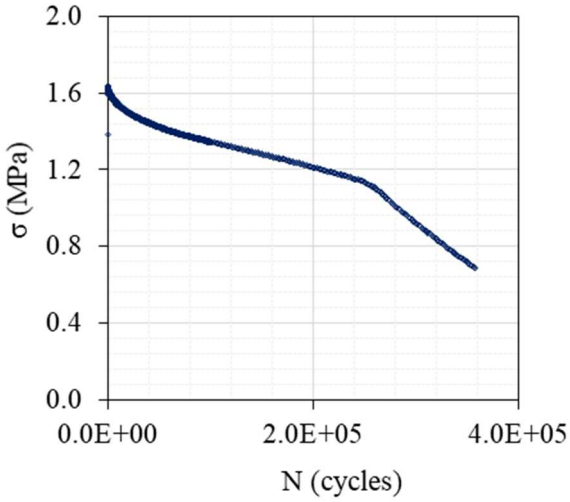

(d)

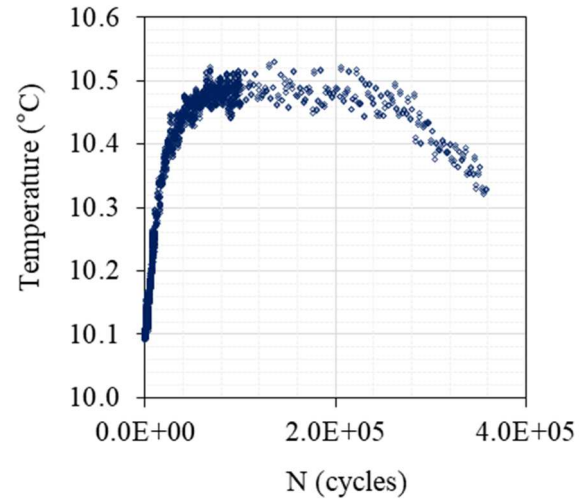

(e)

Figure C-35. Fatigue result of E3-H8 tested at 111μm/m of controlled strain amplitude

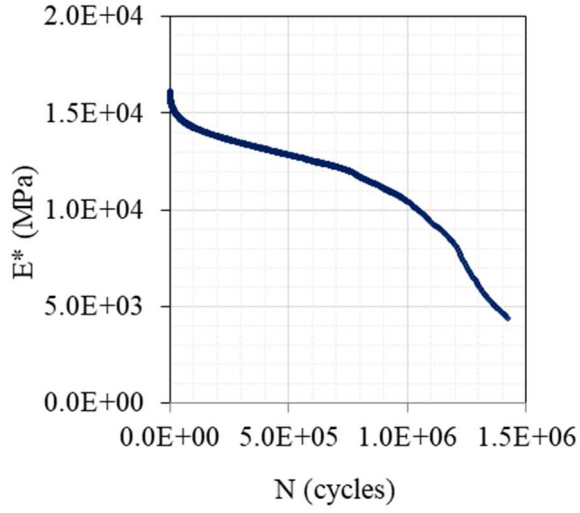

(a)

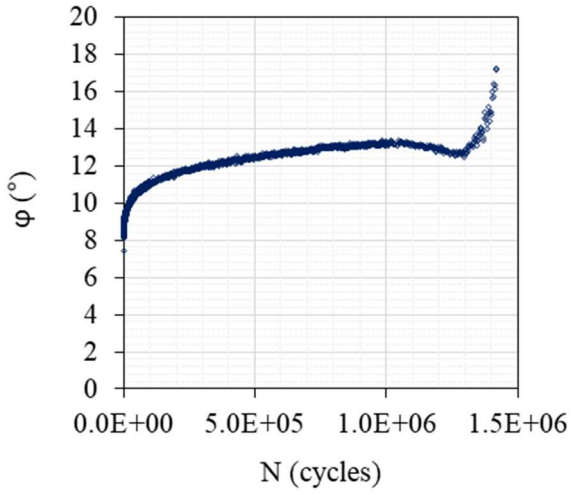

(b)

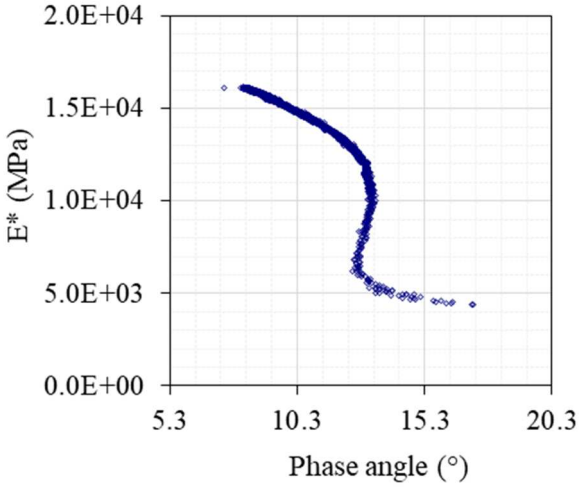

(c)

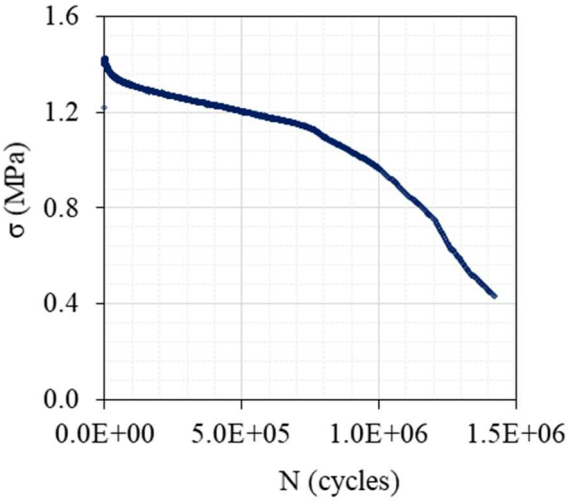

(d)

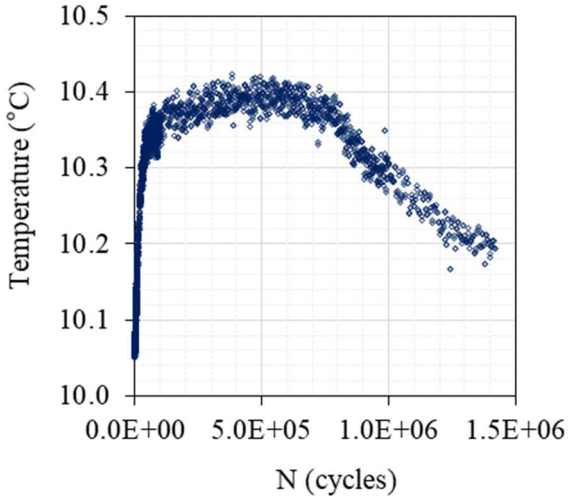

(e)

Figure C-36. Fatigue result of E3-H9 tested at 93μm/m of controlled strain amplitude

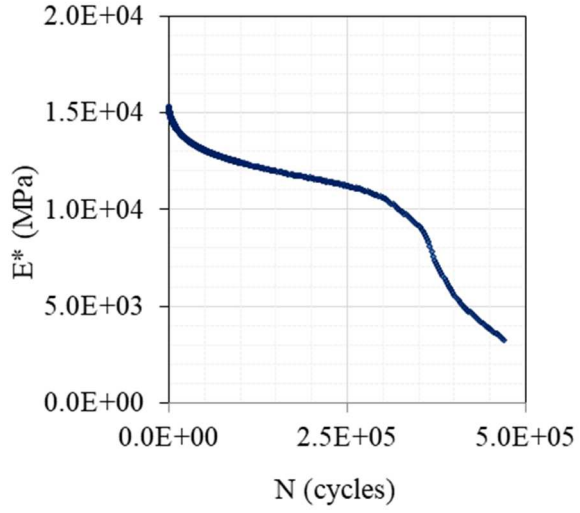

(a)

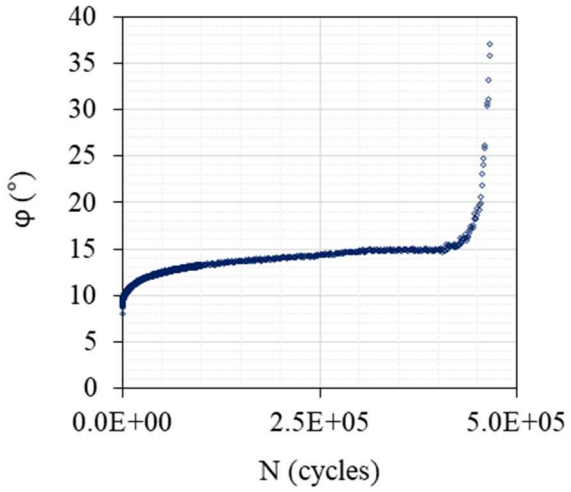

(b)

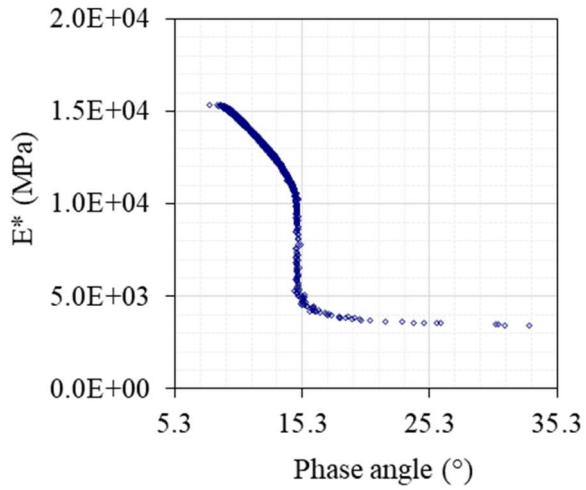

(c)

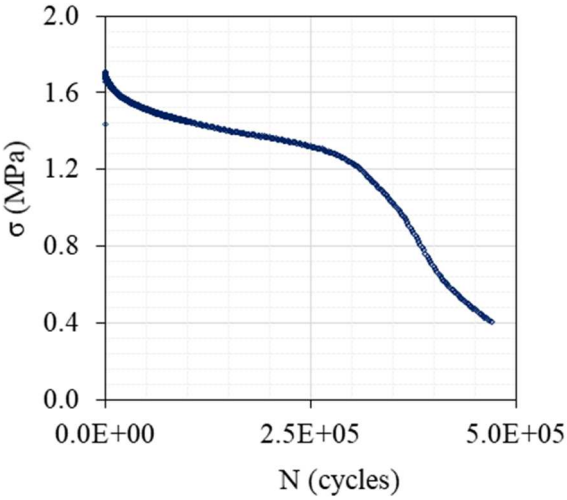

(d)

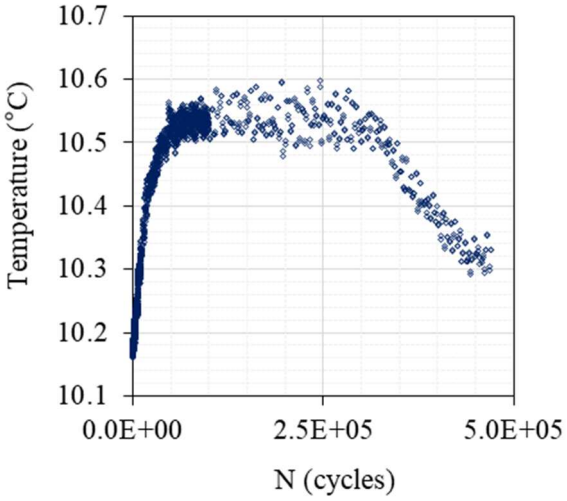

(e)

Figure C-37. Fatigue result of E3-H11 tested at 116μm/m of controlled strain amplitude

APPENDIX D1 – CRACKING PROPAGATION TEST RESULTS

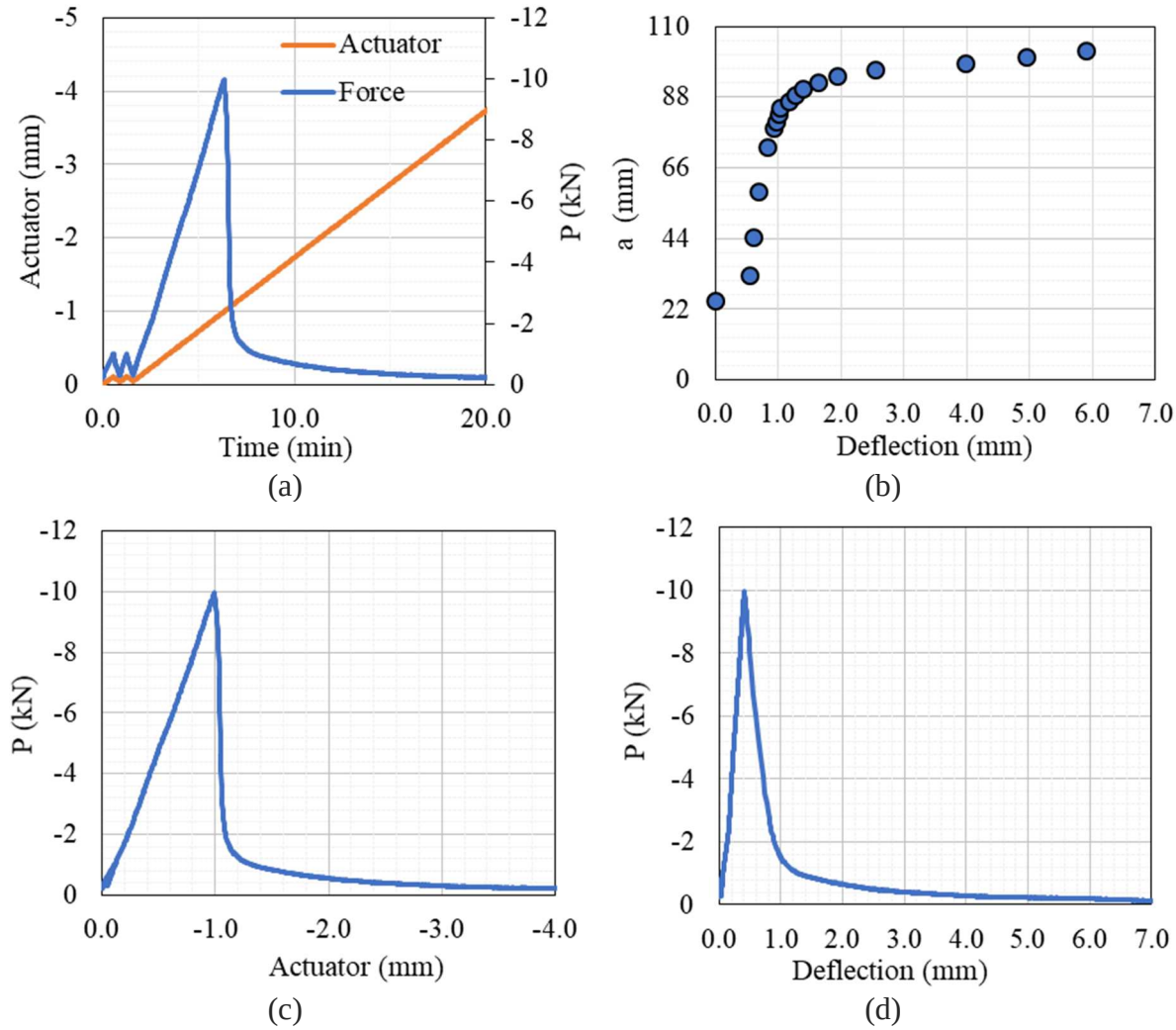

Figure D1-1. Four-point bending notched fracture test result of A2-B2

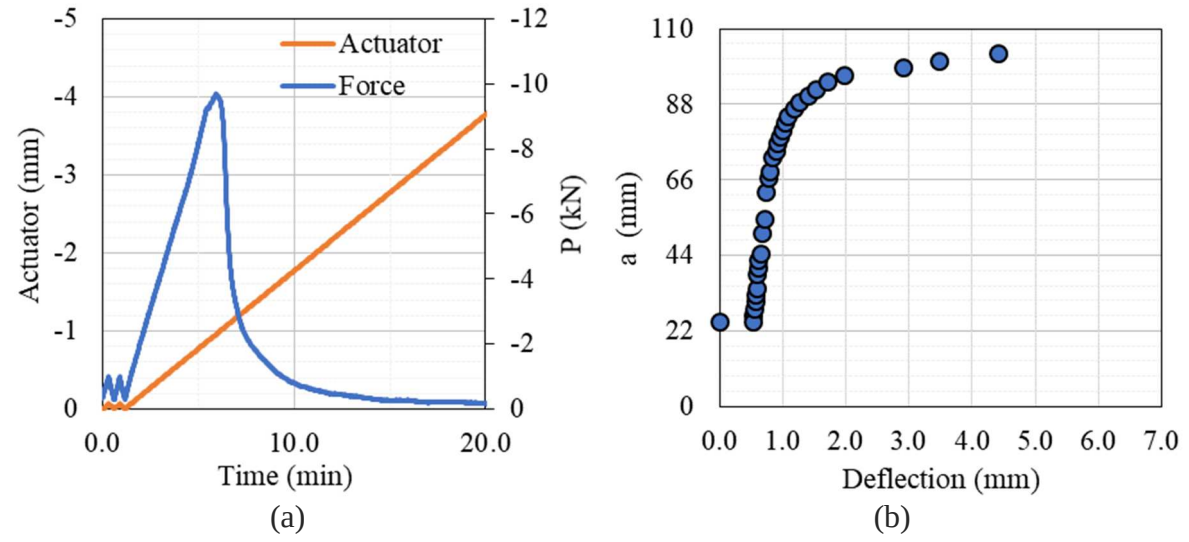

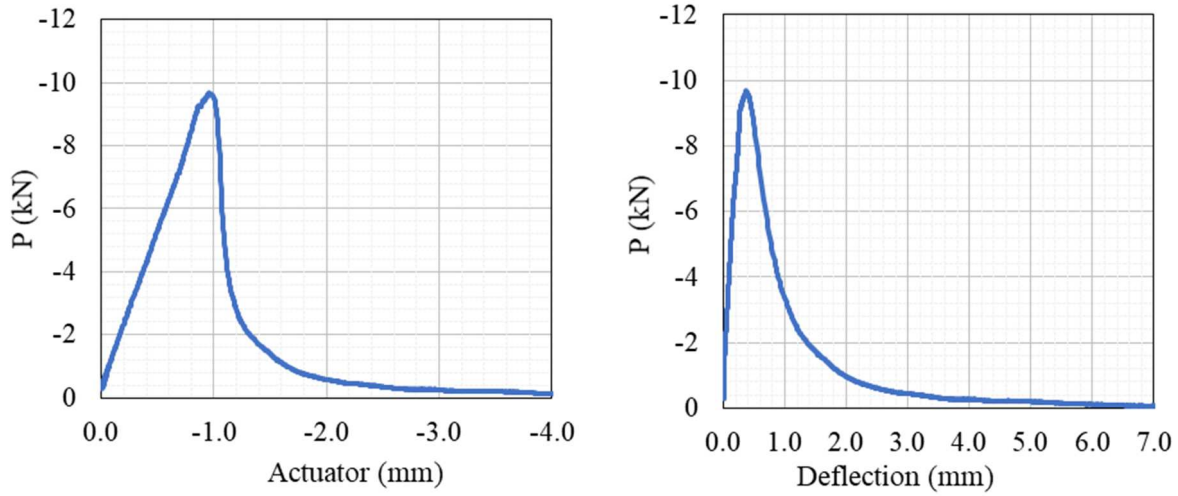

(c) (d)

Figure D1-2. Four-point bending notched fracture test result of A2-B3

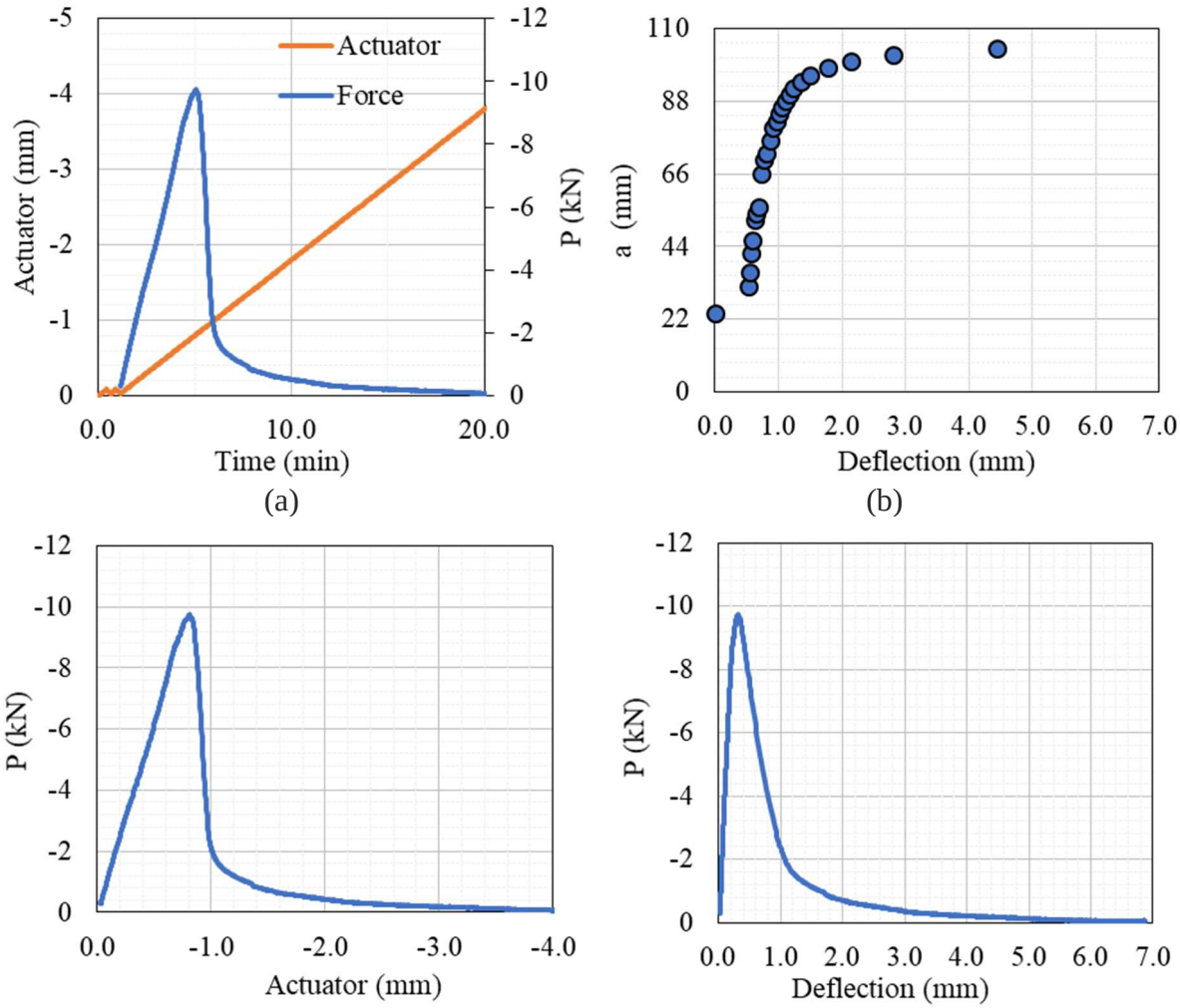

(a) (b)

(c) (d)

Figure D1-3. Four-point bending notched fracture test result of B1-B2

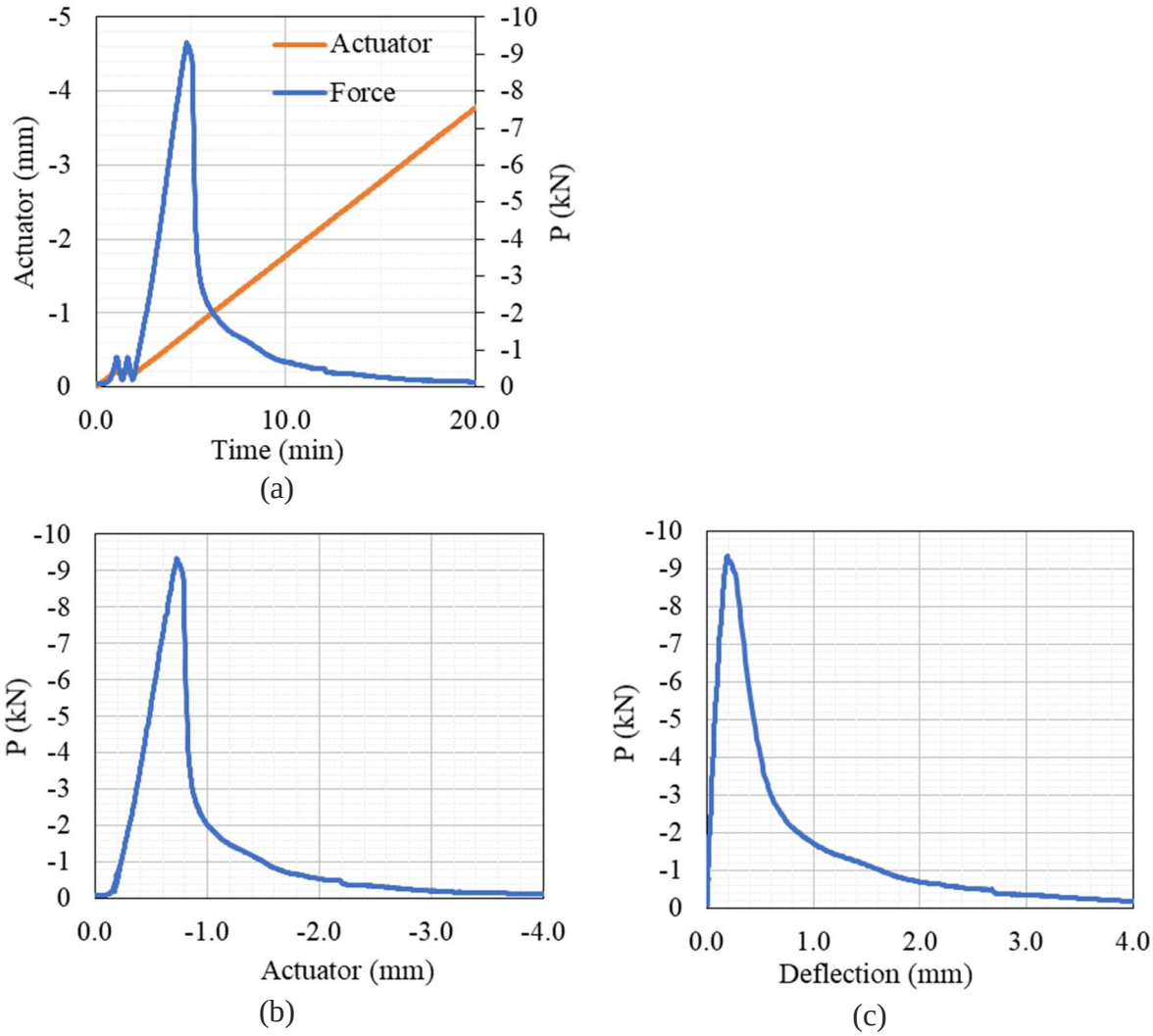

Figure D1-4. Four-point bending notched fracture test result of B1-B3

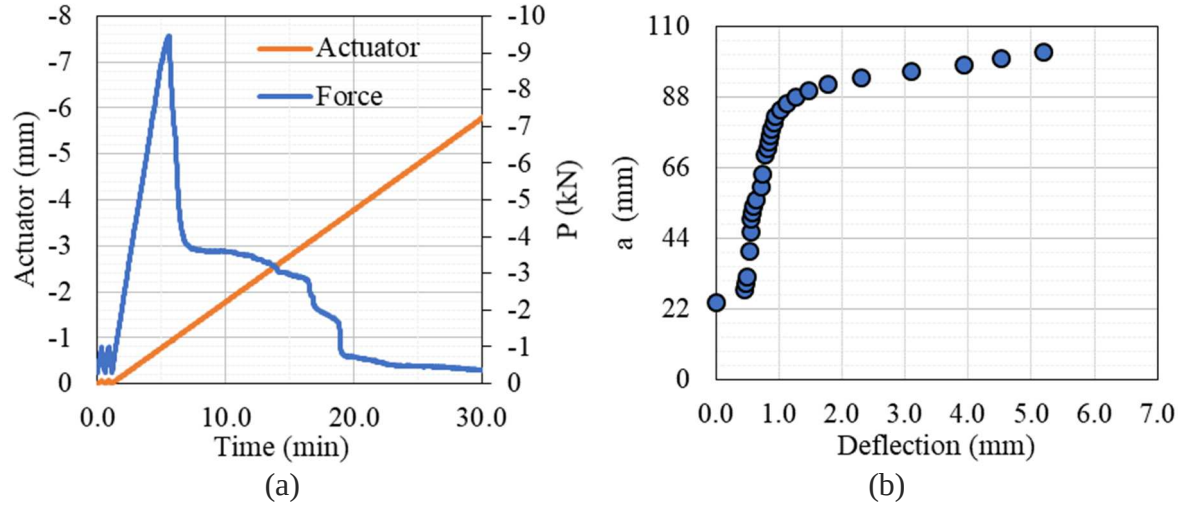

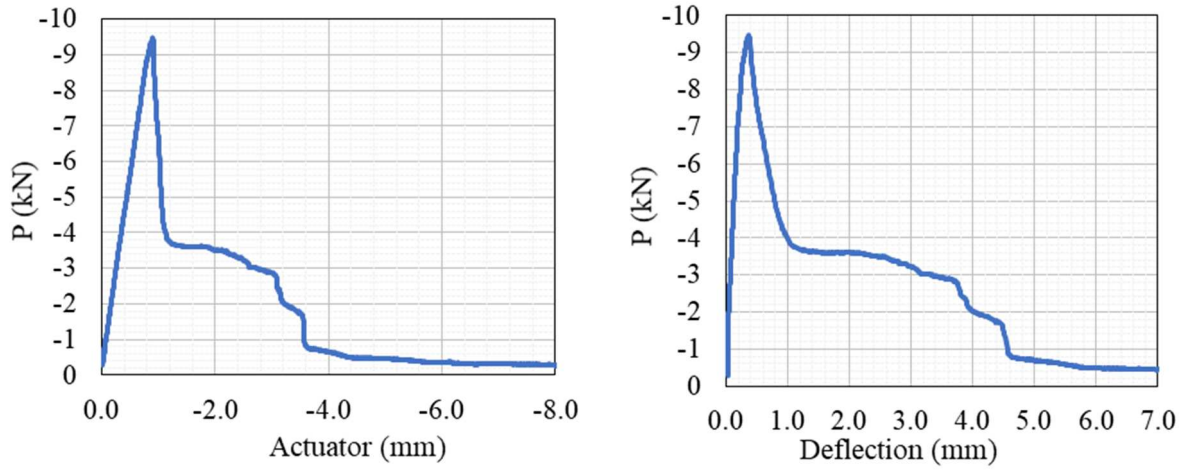

(c) (d)

Figure D1-5. Four-point bending notched fracture test result of C3-B1

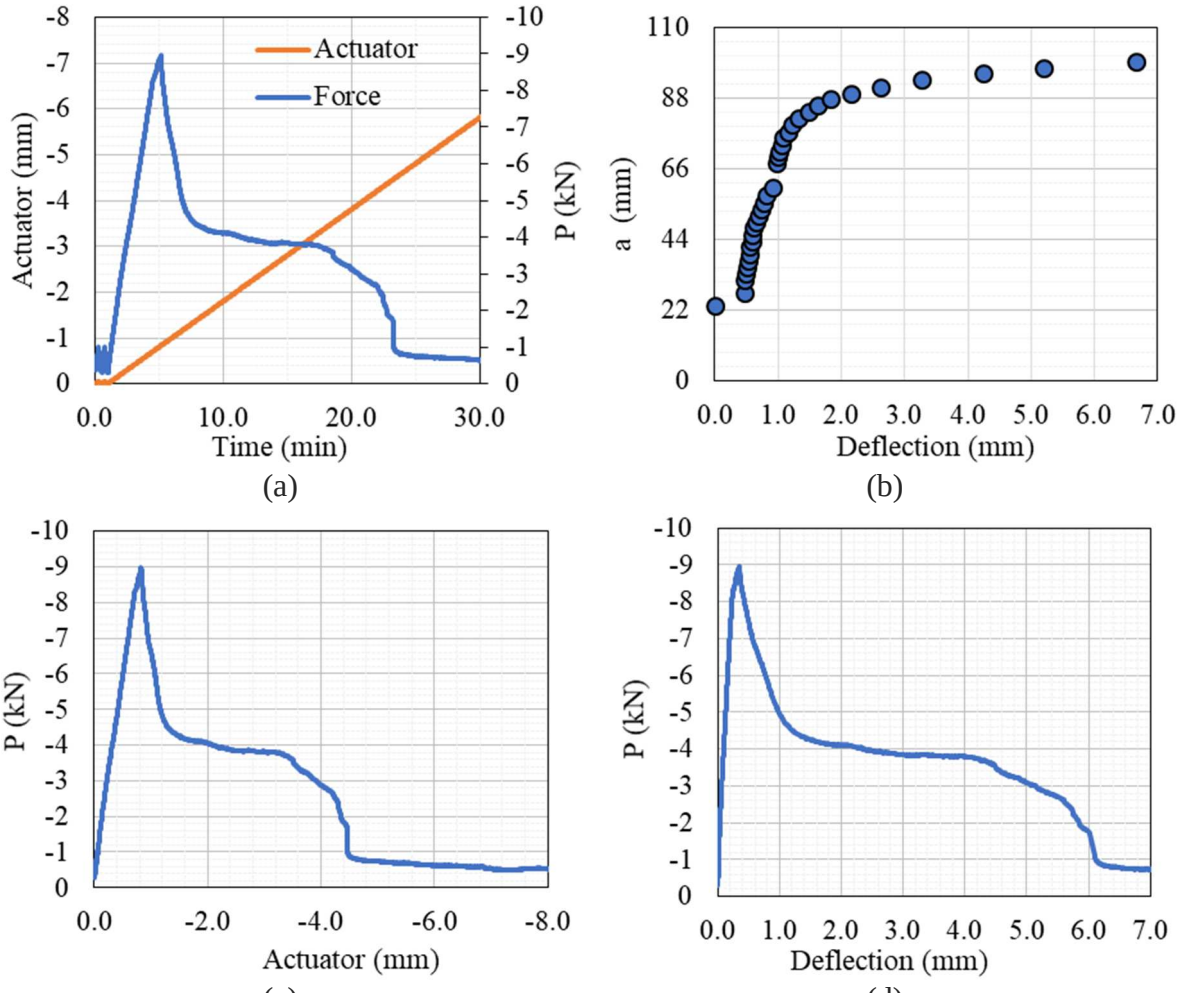

(a) (b)

(c) (d)

Figure D1-6. Four-point bending notched fracture test result of C3-B2

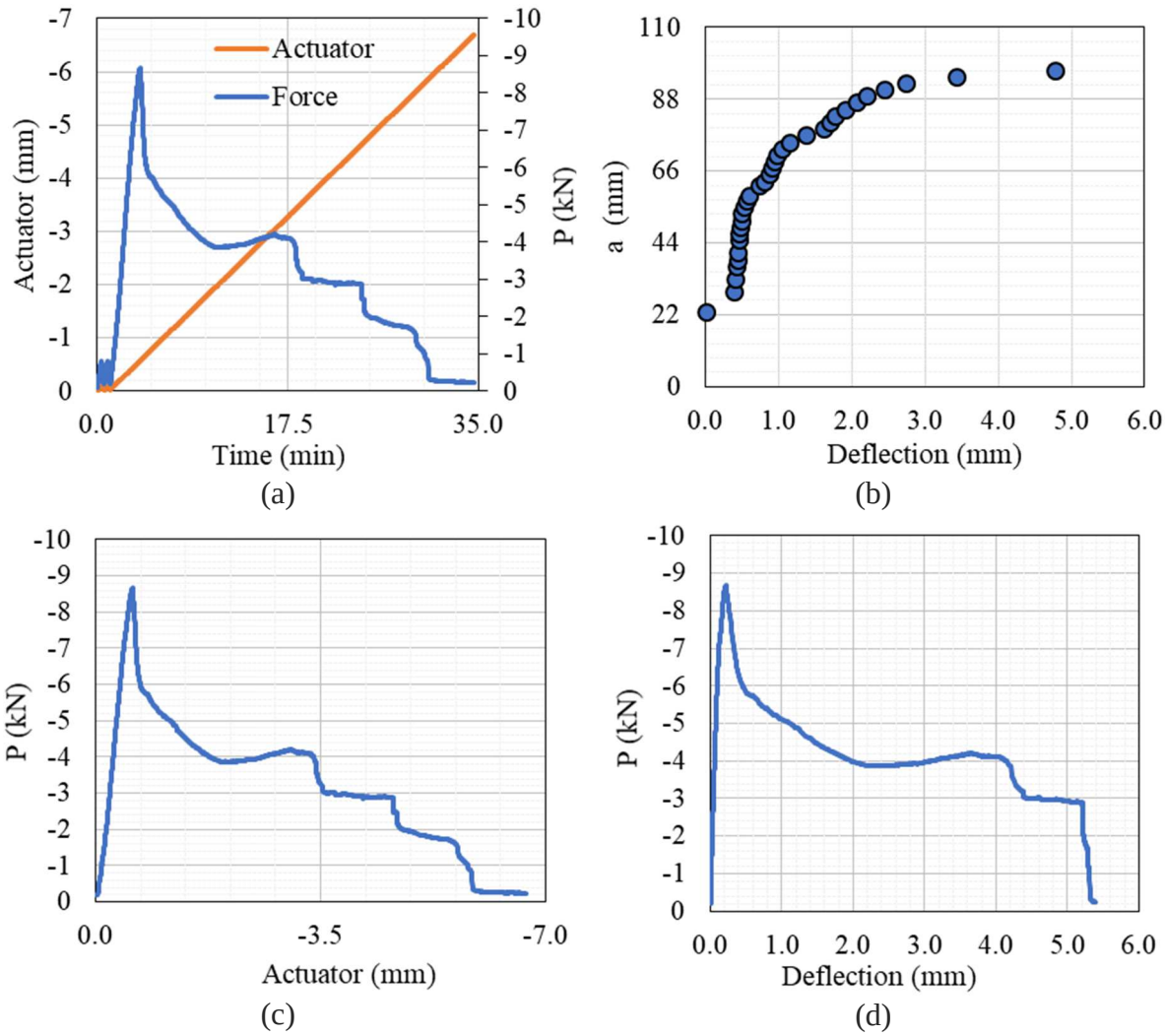

Figure D1-7. Four-point bending notched fracture test result of C3-B3

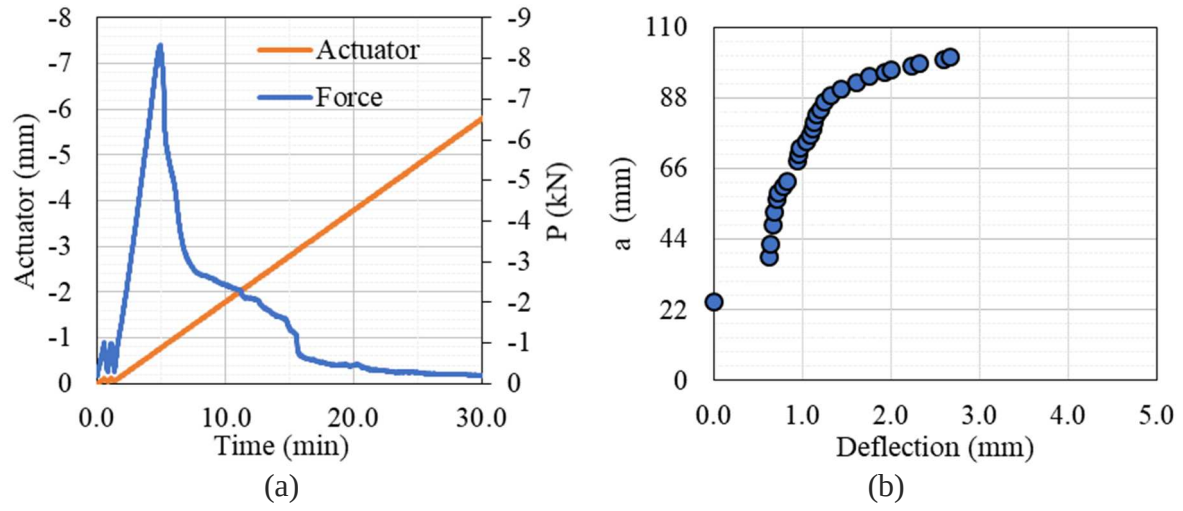

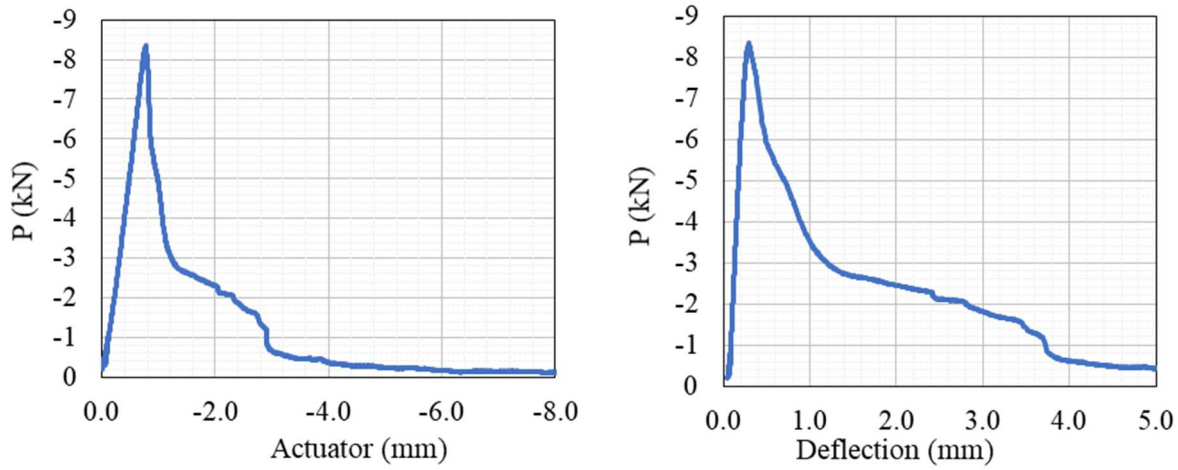

(c) (d)

Figure D1-8. Four-point bending notched fracture test result of D1-B2

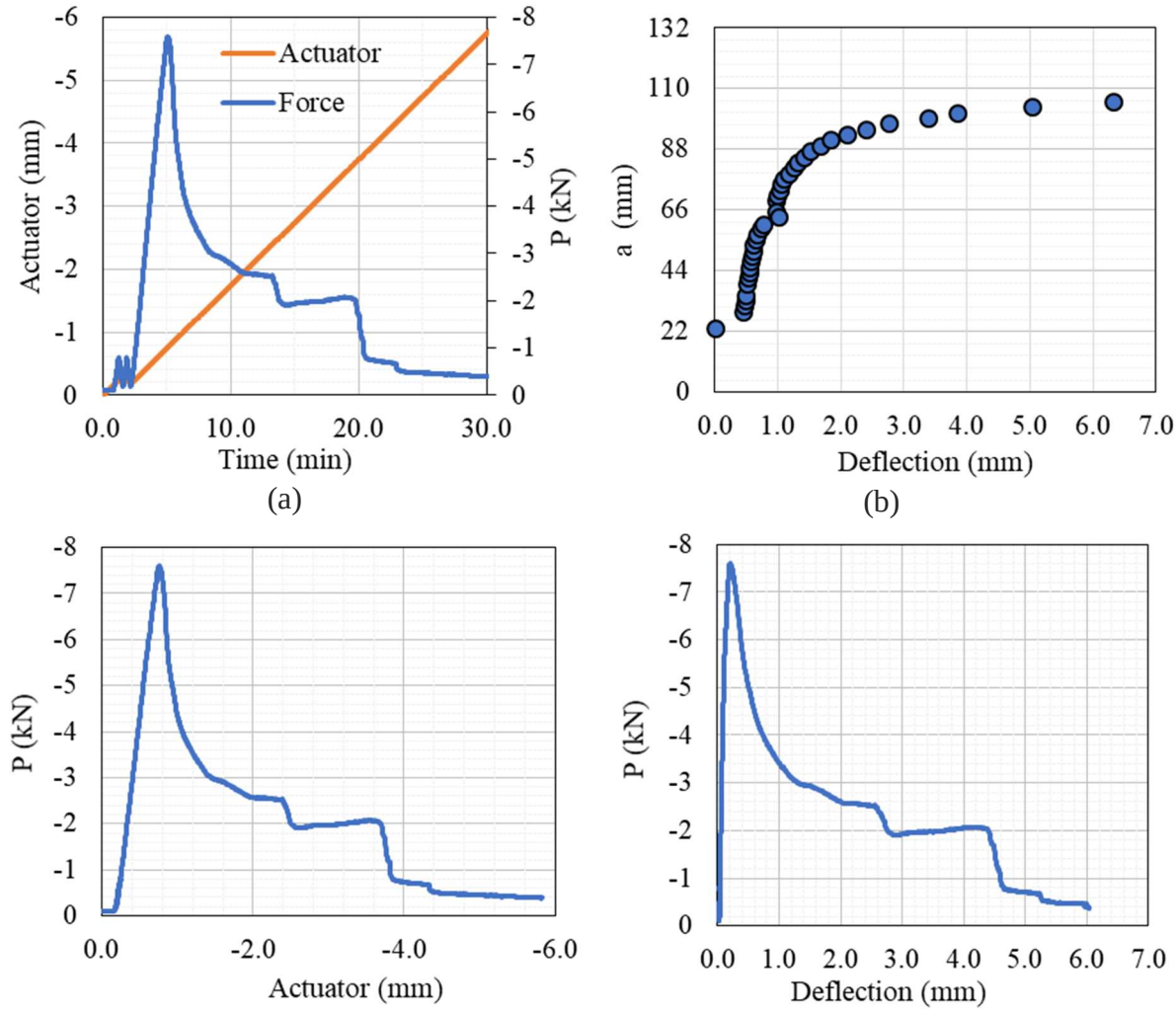

(a) (b)

(c) (d)

Figure D1-9. Four-point bending notched fracture test result of D1-B3

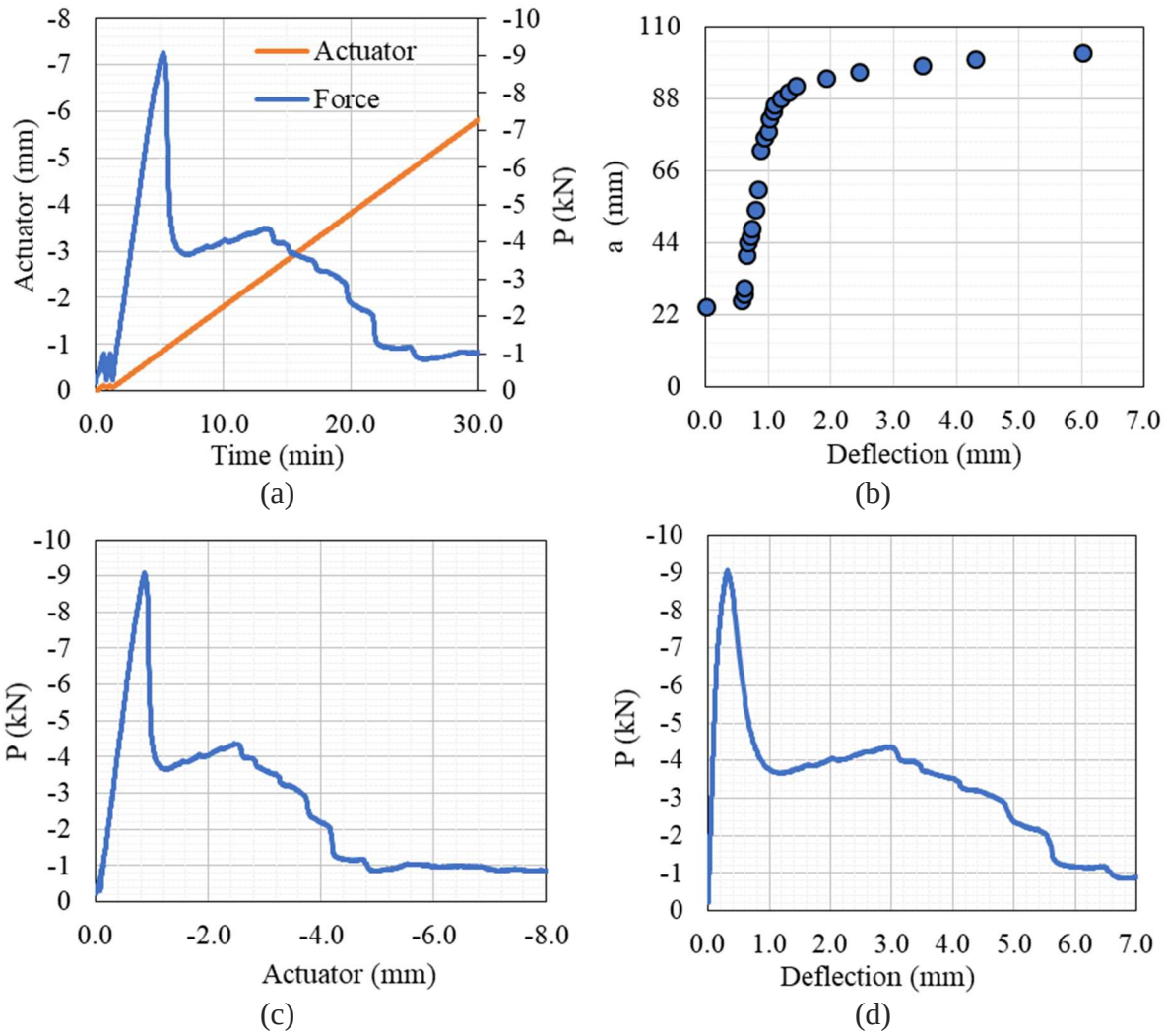

Figure D1-10. Four-point bending notched fracture test result of E1-B1

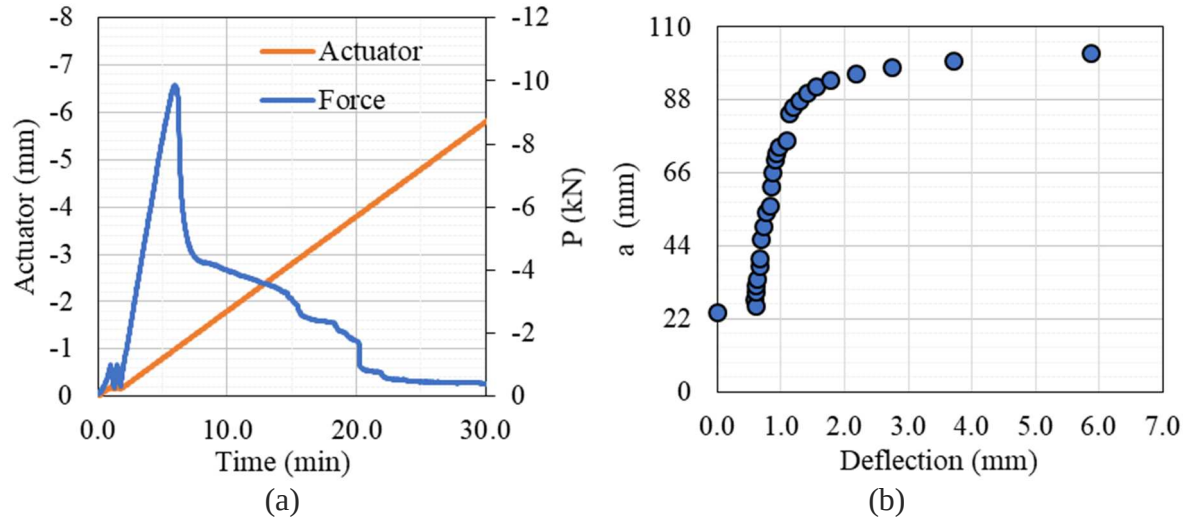

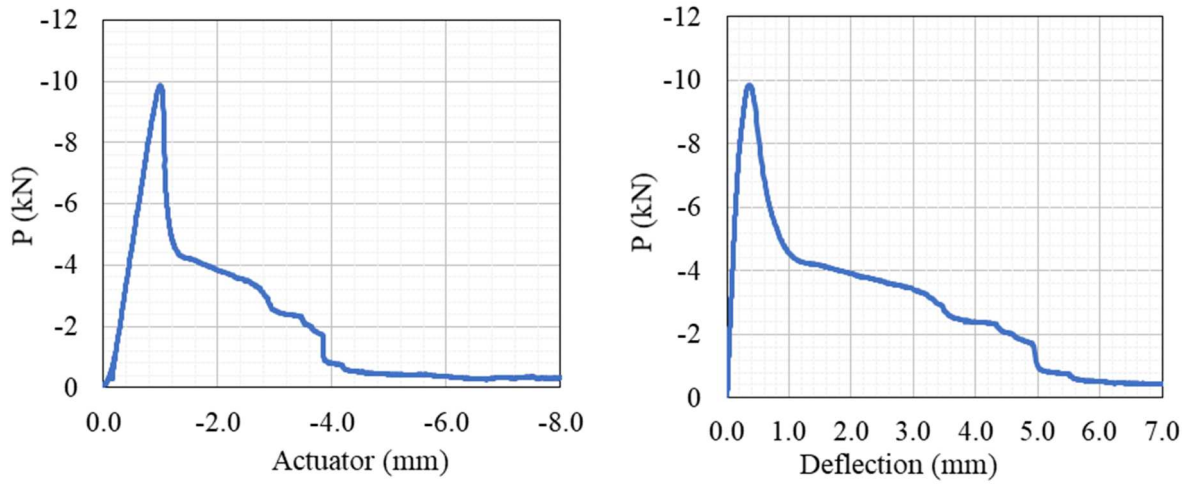

(c) (d)

Figure D1-11. Four-point bending notched fracture test result of E1-B2

APPENDIX D2 – CRACKING PROPAGATION DIC ANALYSIS

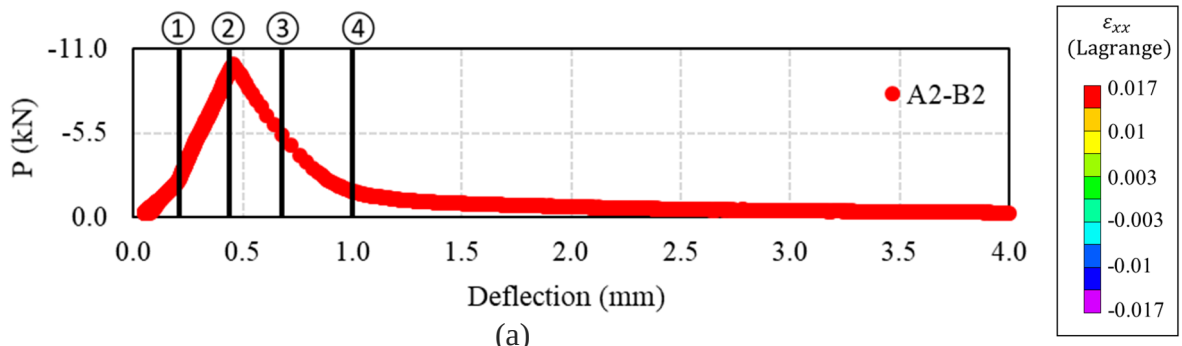
①
②
③
④
-11.0
-5.5
0.0
P (kN)
A2-B2
0.0
0.5
1.0
1.5
2.0
2.5
3.0
3.5
4.0
Deflection (mm)
ε_{xx} (Lagrange)
0.017
0.01
0.003
-0.003
-0.01
-0.017

(a)

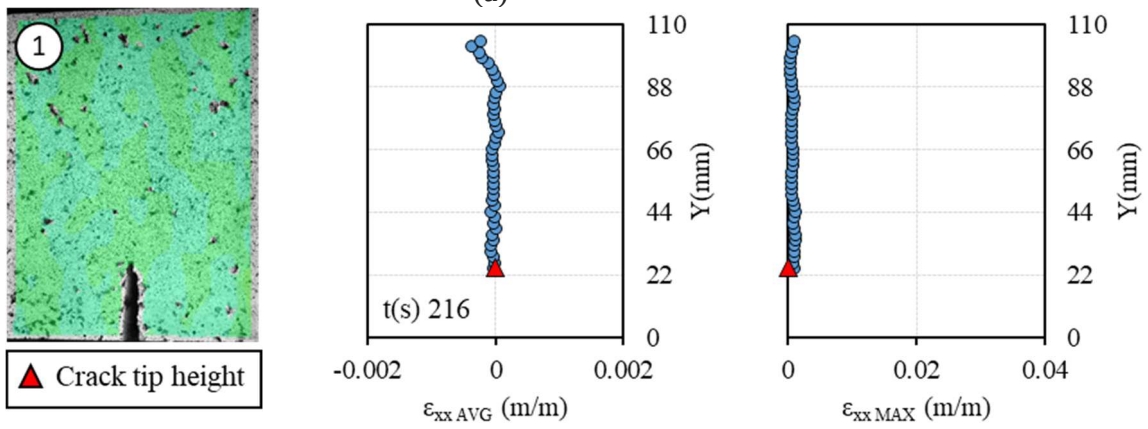
1
Crack tip height
t(s) 216
110
88
66
44
22
0
Y(mm)
-0.002
0
0.002
$\varepsilon_{xx\,AVG}$ (m/m)
0
0.02
0.04
$\varepsilon_{xx\,MAX}$ (m/m)

(b)

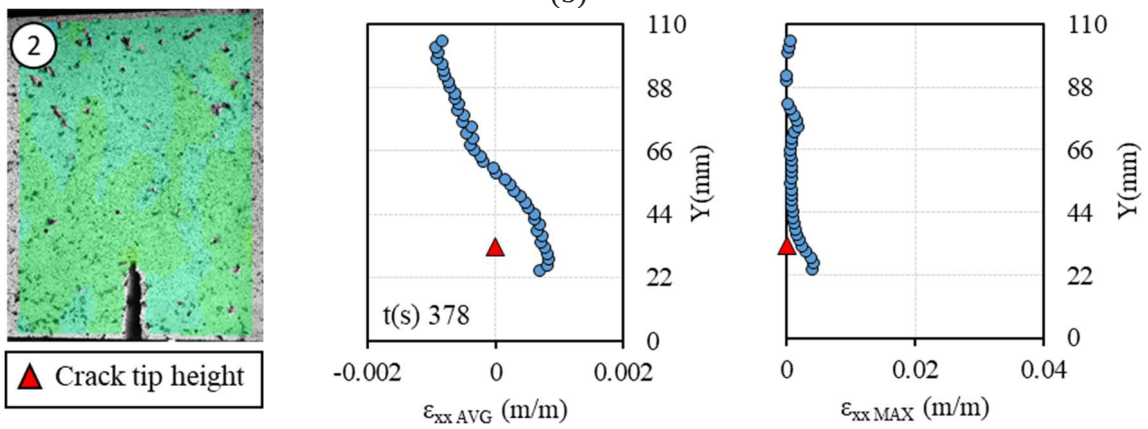
2
Crack tip height
t(s) 378
110
88
66
44
22
0
Y(mm)
-0.002
0
0.002
$\varepsilon_{xx\,AVG}$ (m/m)
0
0.02
0.04
$\varepsilon_{xx\,MAX}$ (m/m)

(c)

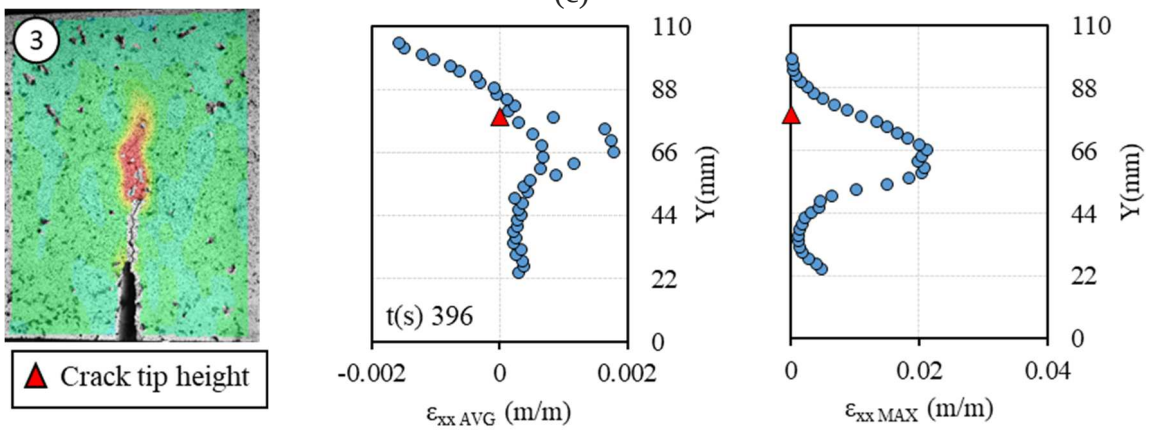
3
Crack tip height
t(s) 396
110
88
66
44
22
0
Y(mm)
-0.002
0
0.002
$\varepsilon_{xx\,AVG}$ (m/m)
0
0.02
0.04
$\varepsilon_{xx\,MAX}$ (m/m)

(d)

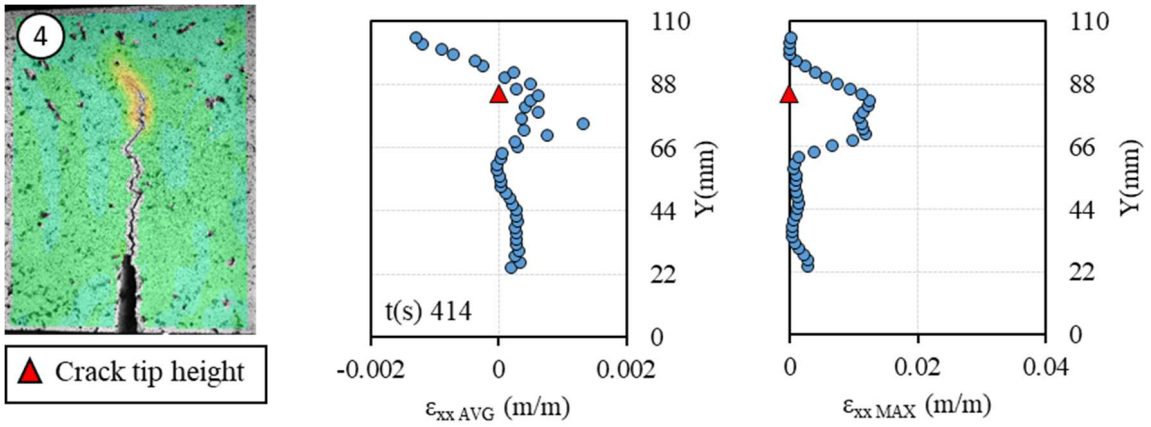

(e)

Figure D2-1. DIC Analysis of average and maximum strain versus beam height of A2-B2

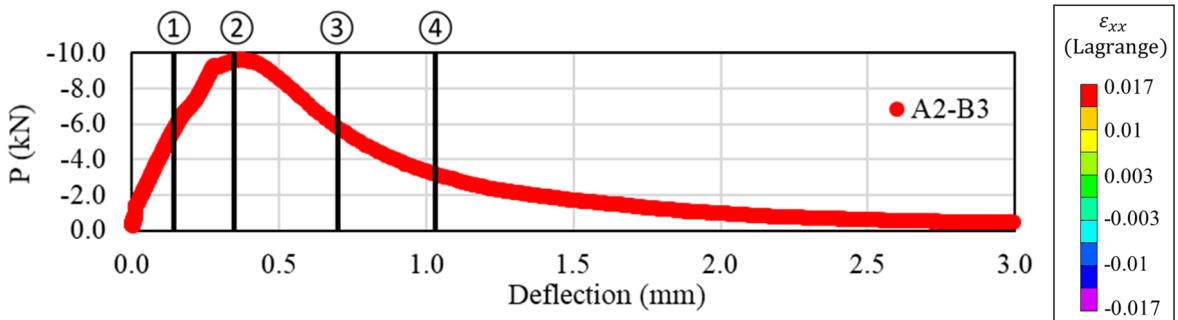

(a)

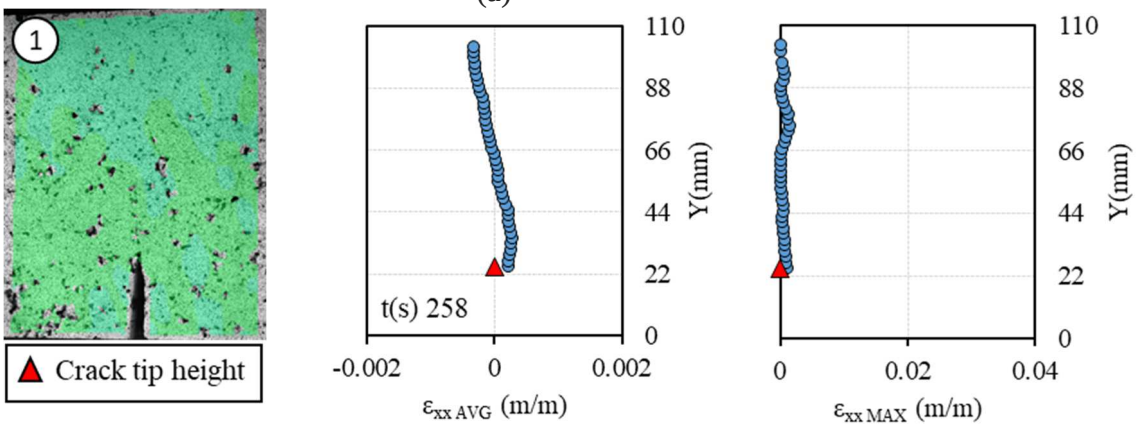

(b)

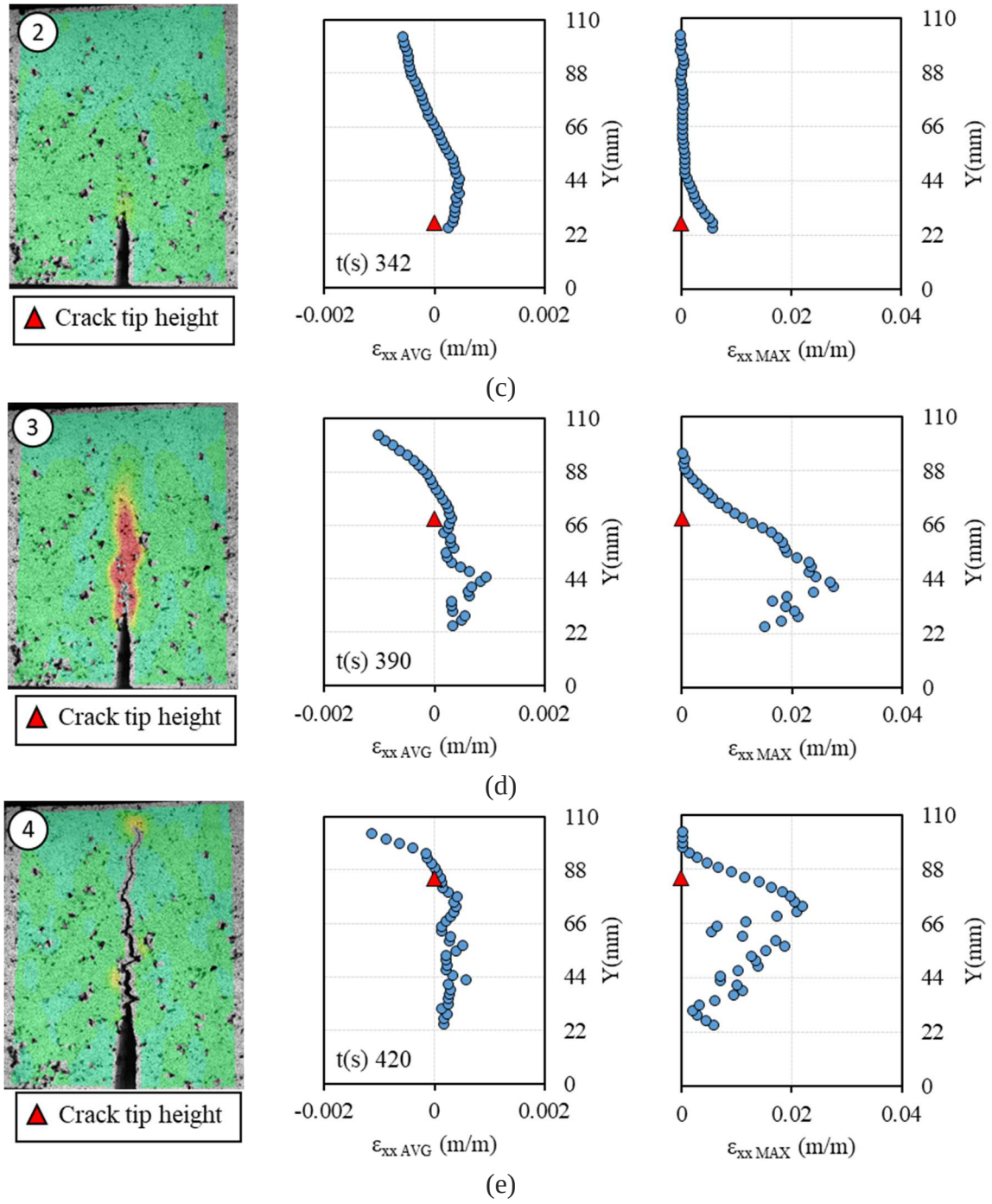

Figure D2-2. DIC Analysis of average and maximum strain versus beam height of A2-B3

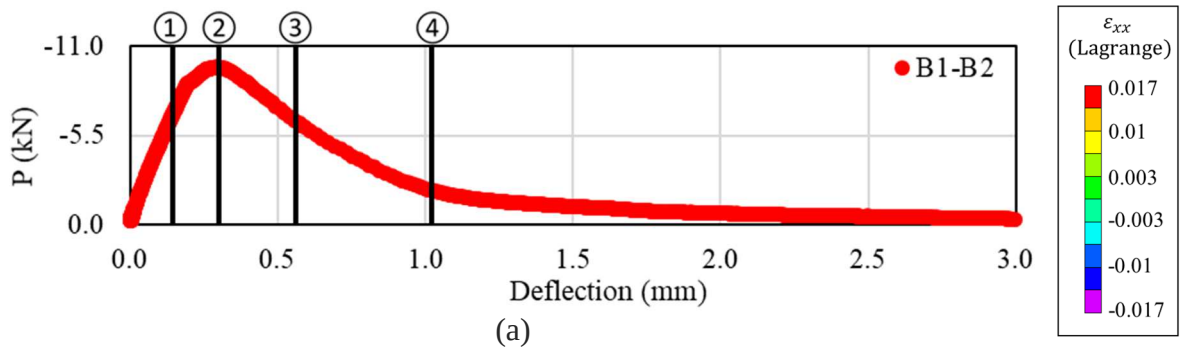
①
②
③
④
-11.0
-5.5
0.0
P (kN)
0.0
0.5
1.0
1.5
2.0
2.5
3.0
Deflection (mm)
B1-B2
ε_{xx} (Lagrange)
0.017
0.01
0.003
-0.003
-0.01
-0.017

(a)

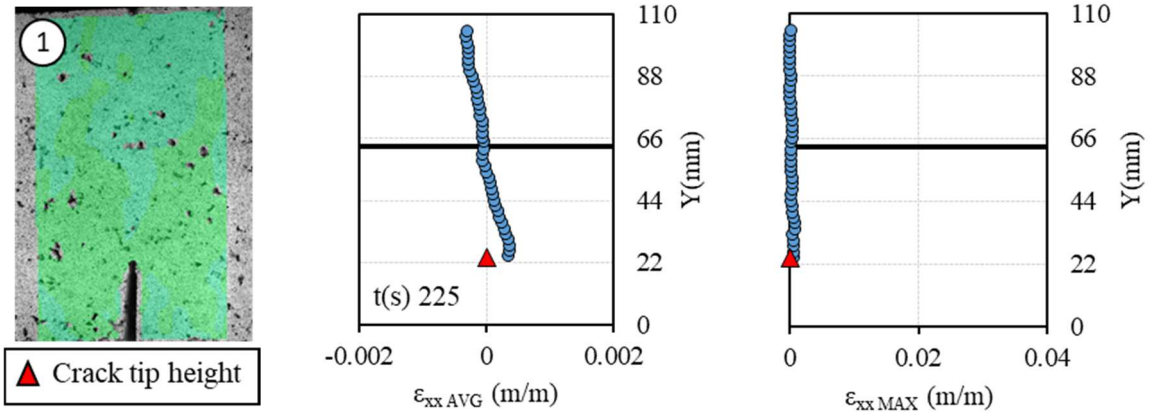
1
Crack tip height
t(s) 225
110
88
66
44
22
0
Y(mm)
-0.002
0
0.002
$\varepsilon_{xx\,AVG}$ (m/m)
0
0.02
0.04
$\varepsilon_{xx\,MAX}$ (m/m)

(b)

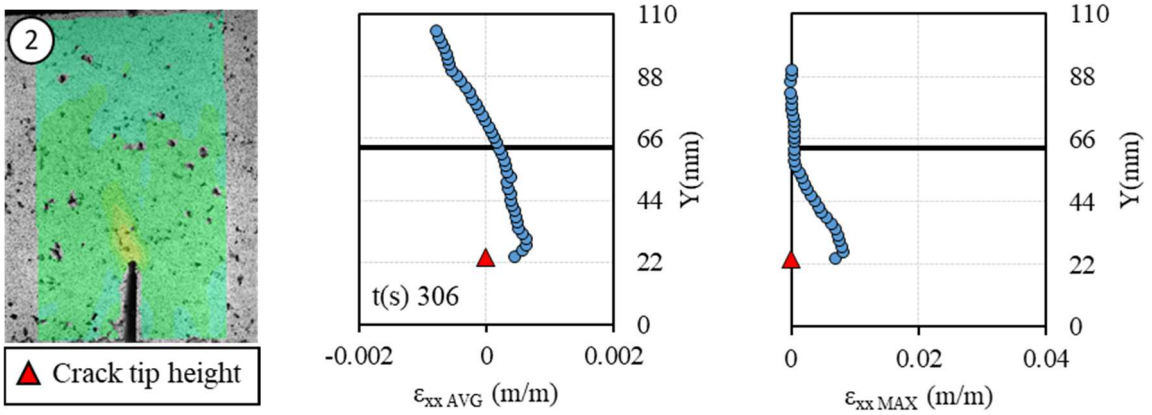
2
Crack tip height
t(s) 306
110
88
66
44
22
0
Y(mm)
-0.002
0
0.002
$\varepsilon_{xx\,AVG}$ (m/m)
0
0.02
0.04
$\varepsilon_{xx\,MAX}$ (m/m)

(c)

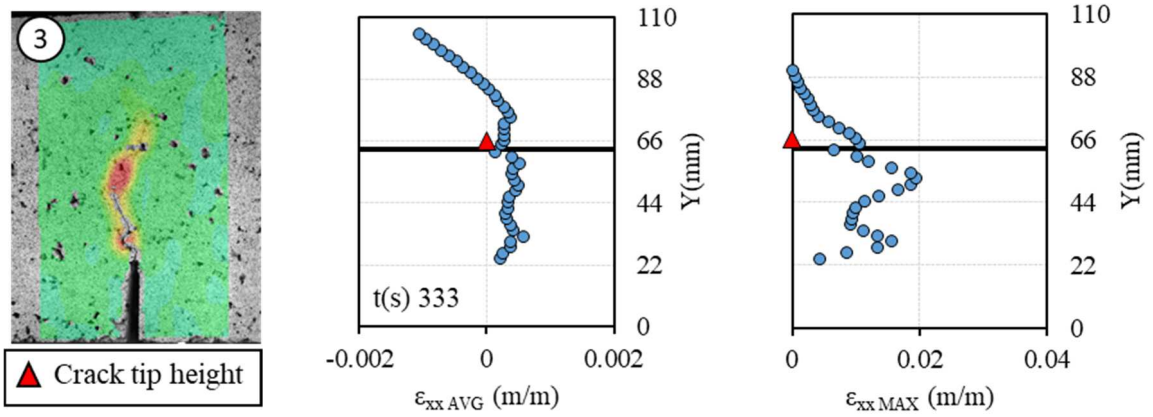
3
Crack tip height
t(s) 333
110
88
66
44
22
0
Y(mm)
-0.002
0
0.002
$\varepsilon_{xx\,AVG}$ (m/m)
0
0.02
0.04
$\varepsilon_{xx\,MAX}$ (m/m)

(d)

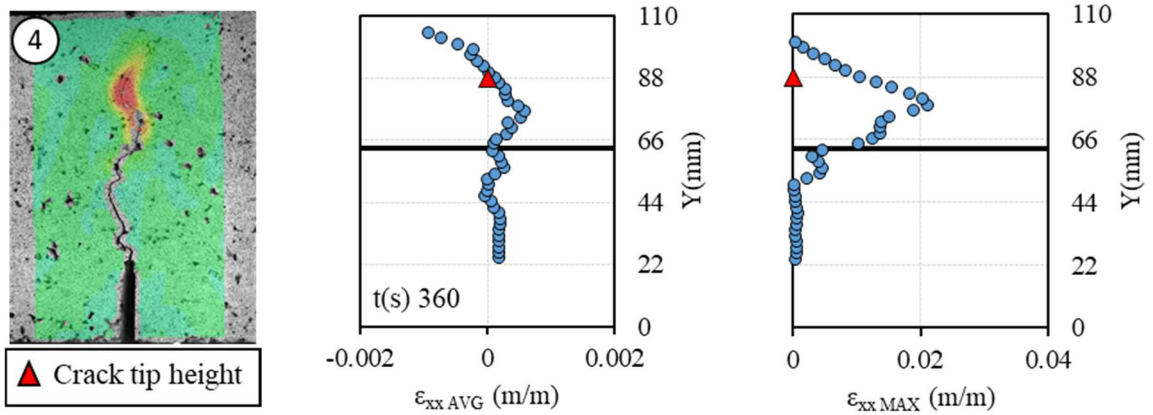

(e)

Figure D2-3. DIC Analysis of average and maximum strain versus beam height of B1-B2

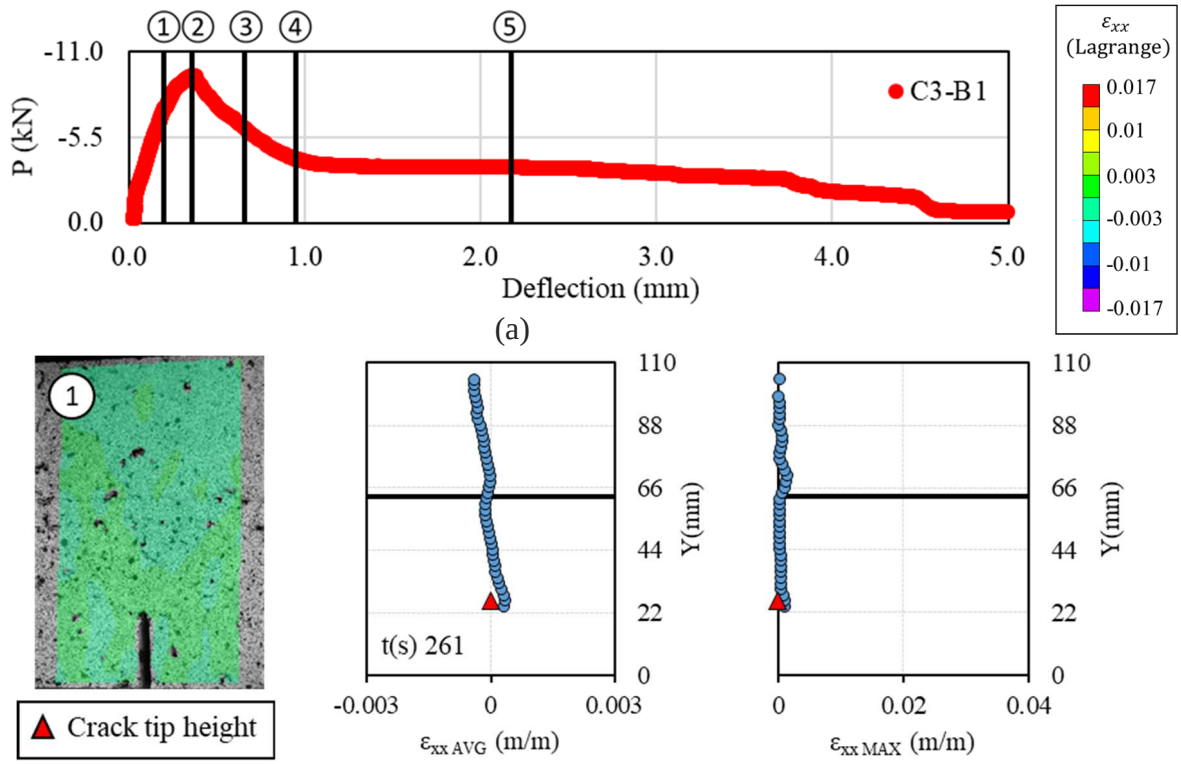

(a)

(b)

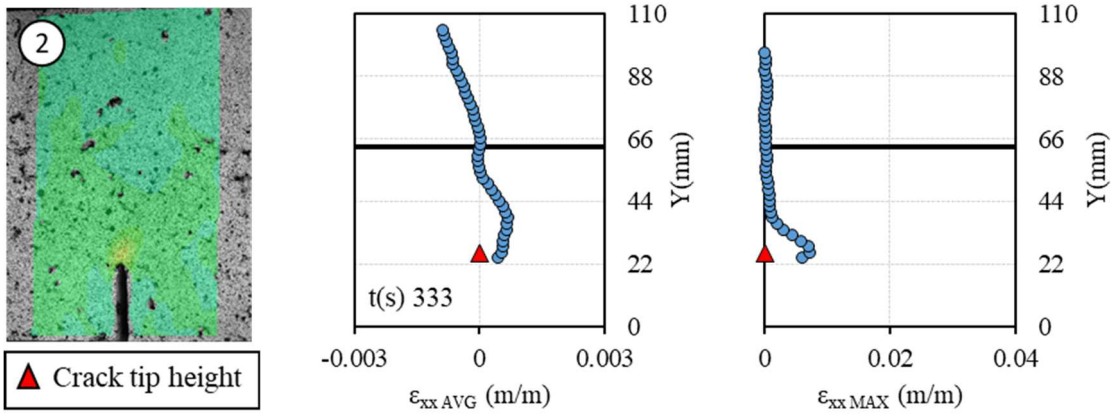
2
Crack tip height
t(s) 333
110
88
66
44
22
0
Y(mm)
-0.003
0
0.003
$\varepsilon_{xx\,AVG}$ (m/m)
0
0.02
0.04
$\varepsilon_{xx\,MAX}$ (m/m)

(c)

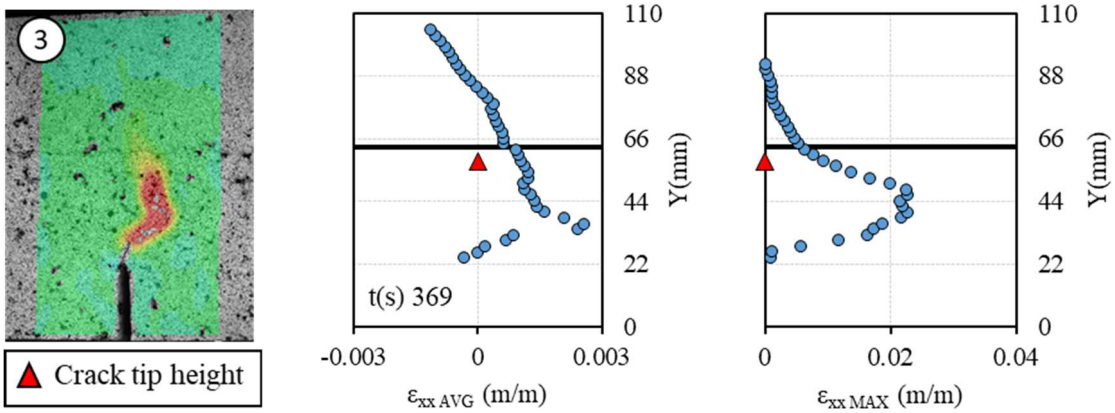
3
Crack tip height
t(s) 369
110
88
66
44
22
0
Y(mm)
-0.003
0
0.003
$\varepsilon_{xx\,AVG}$ (m/m)
0
0.02
0.04
$\varepsilon_{xx\,MAX}$ (m/m)

(d)

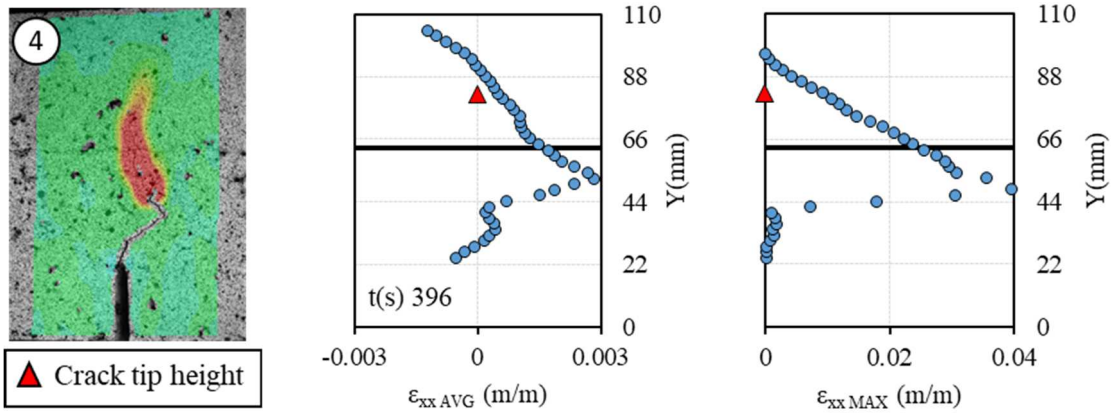
4
Crack tip height
t(s) 396
110
88
66
44
22
0
Y(mm)
-0.003
0
0.003
$\varepsilon_{xx\,AVG}$ (m/m)
0
0.02
0.04
$\varepsilon_{xx\,MAX}$ (m/m)

(e)

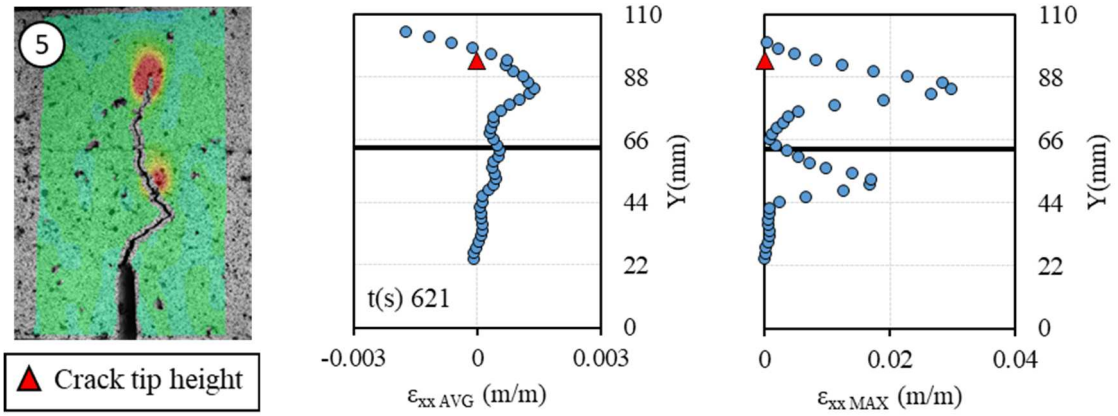

(f)

Figure D2-4. DIC Analysis of average and maximum strain versus beam height of C3-B1

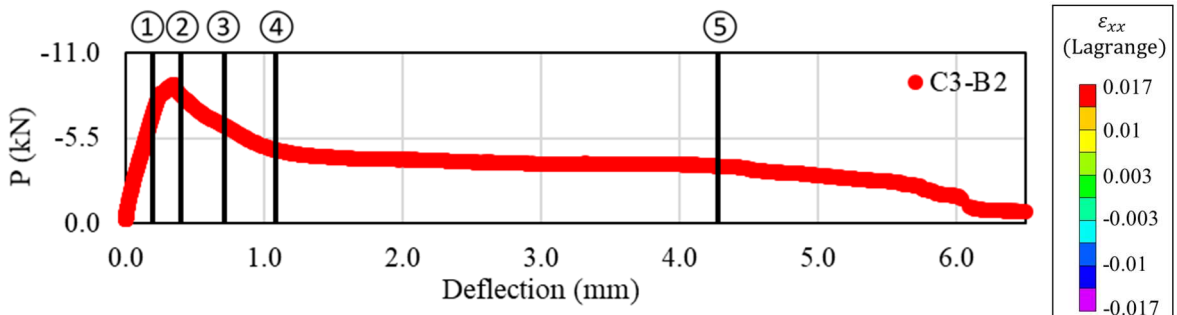

(a)

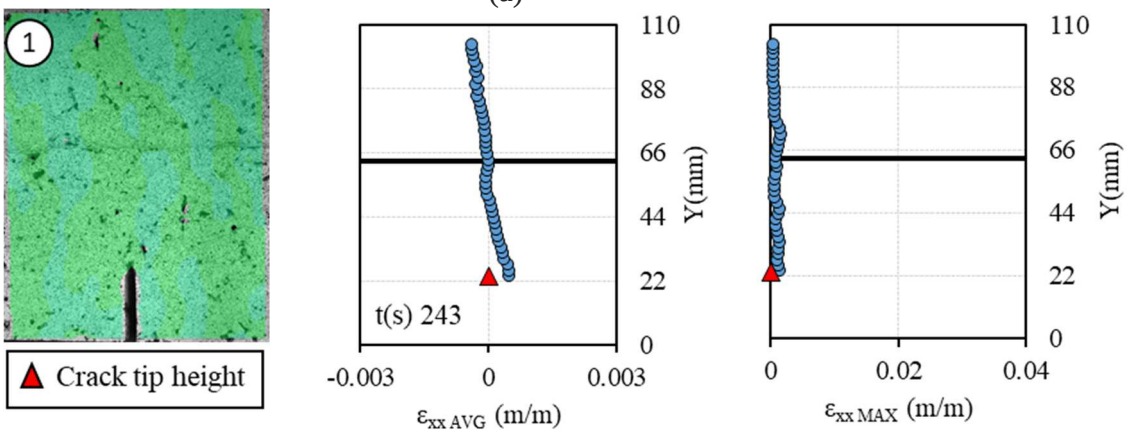

(b)

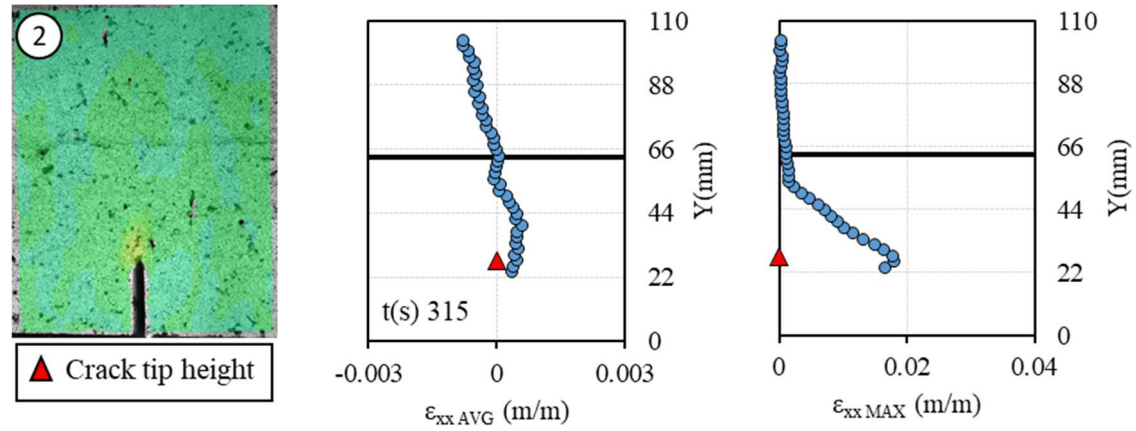
2
Crack tip height
t(s) 315
110
88
66
44
22
0
Y(mm)
-0.003
0
0.003
$\varepsilon_{xx\,AVG}$ (m/m)
0
0.02
0.04
$\varepsilon_{xx\,MAX}$ (m/m)

(c)

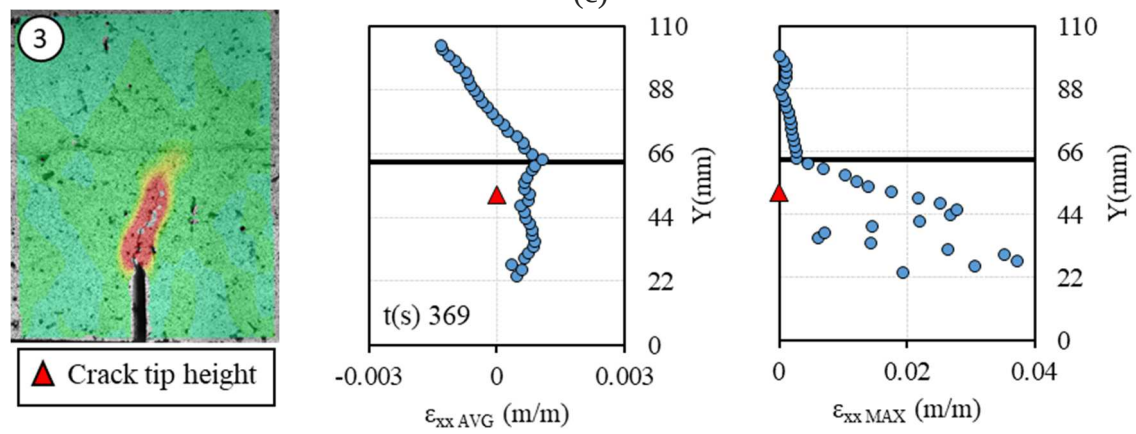
3
Crack tip height
t(s) 369
110
88
66
44
22
0
Y(mm)
-0.003
0
0.003
$\varepsilon_{xx\,AVG}$ (m/m)
0
0.02
0.04
$\varepsilon_{xx\,MAX}$ (m/m)

(d)

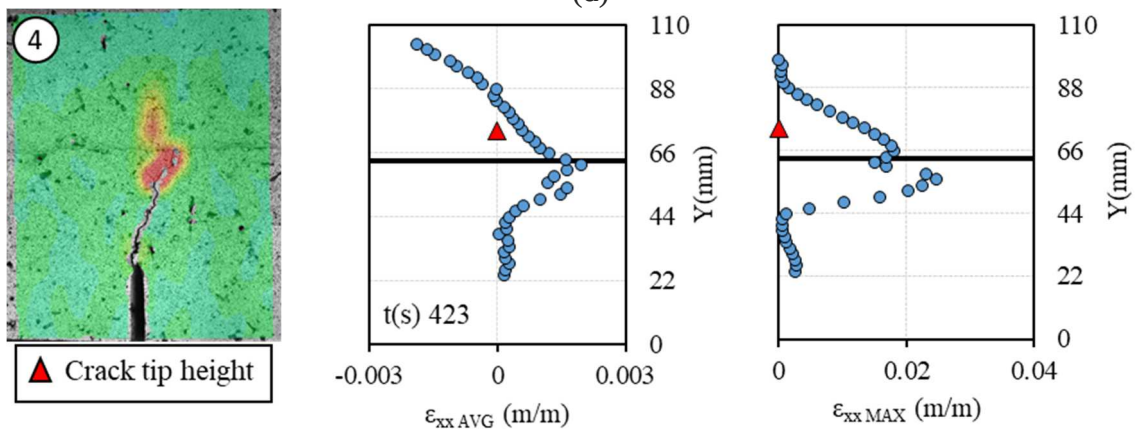
4
Crack tip height
t(s) 423
110
88
66
44
22
0
Y(mm)
-0.003
0
0.003
$\varepsilon_{xx\,AVG}$ (m/m)
0
0.02
0.04
$\varepsilon_{xx\,MAX}$ (m/m)

(e)

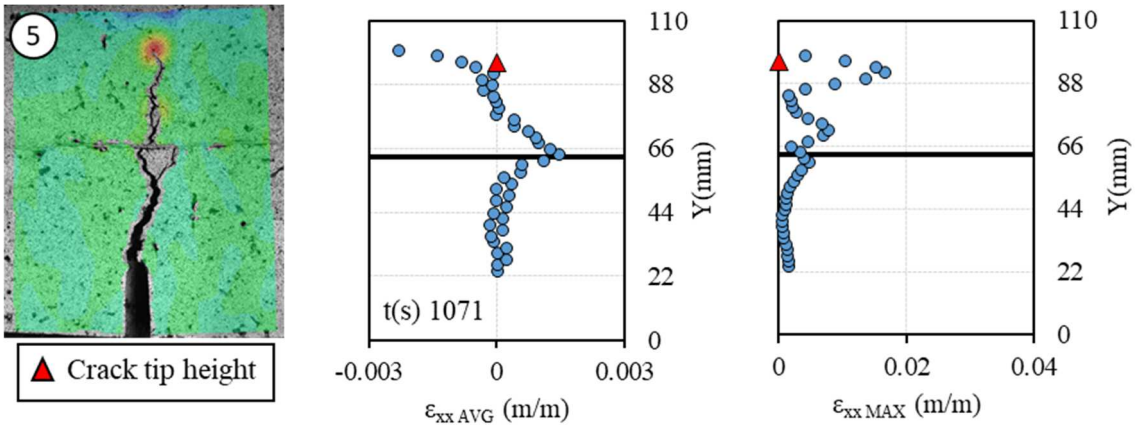

(f)

Figure D2-5. DIC Analysis of average and maximum strain versus beam height of C3-B2

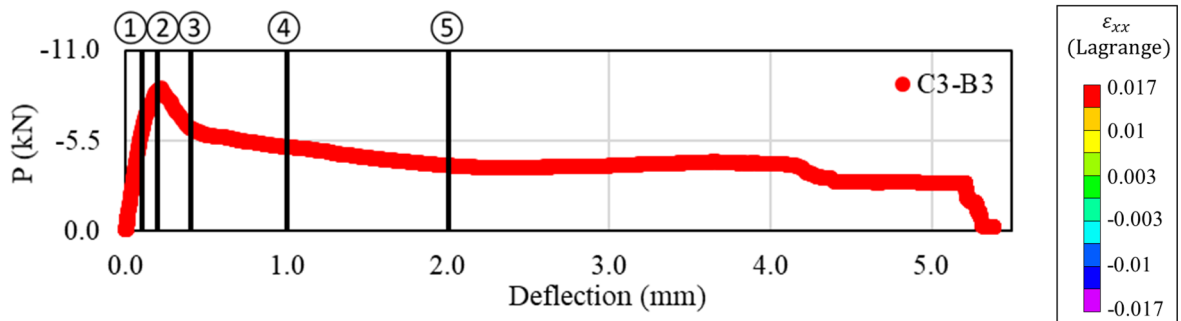

(a)

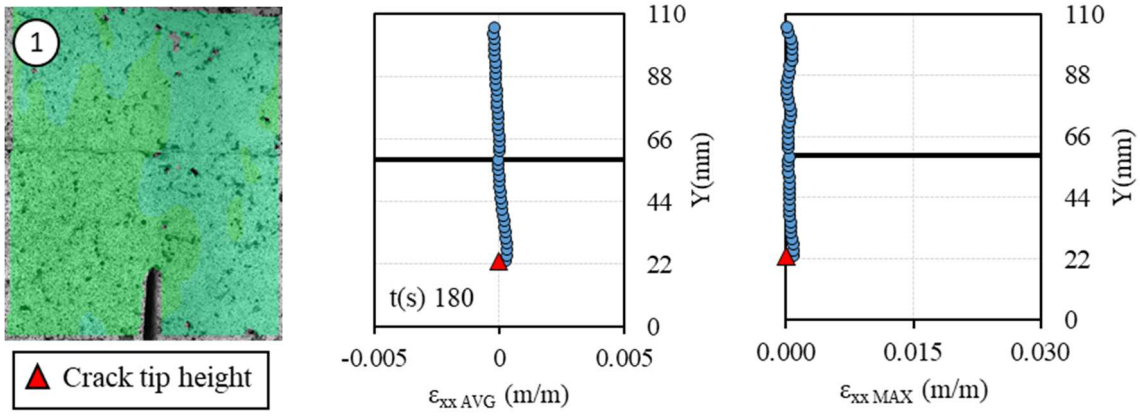

(b)

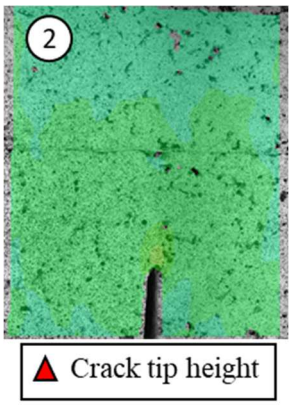
2
Crack tip height

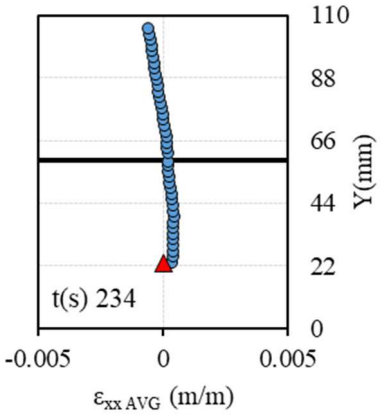
t(s) 234
110
88
66
44
22
0
Y(mm)
-0.005
0
0.005
εxx AVG (m/m)

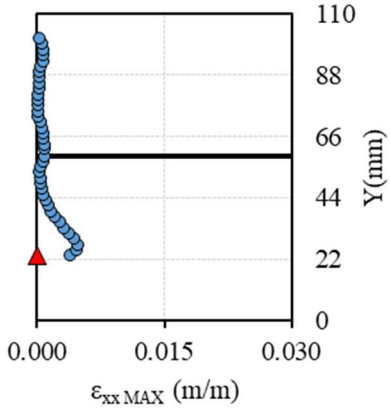
110
88
66
44
22
0
Y(mm)
0.000
0.015
0.030
εxx MAX (m/m)

(c)

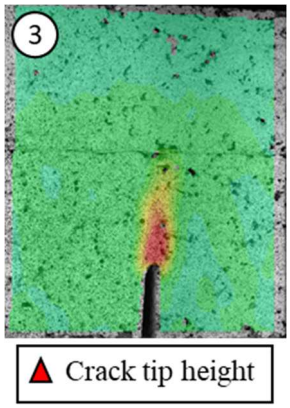
3
Crack tip height

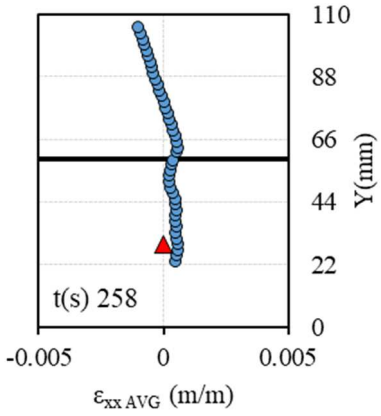
t(s) 258
110
88
66
44
22
0
Y(mm)
-0.005
0
0.005
εxx AVG (m/m)

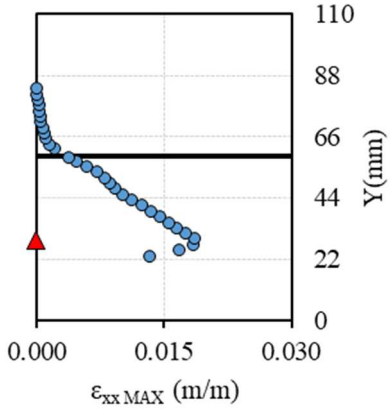
110
88
66
44
22
0
Y(mm)
0.000
0.015
0.030
εxx MAX (m/m)

(d)

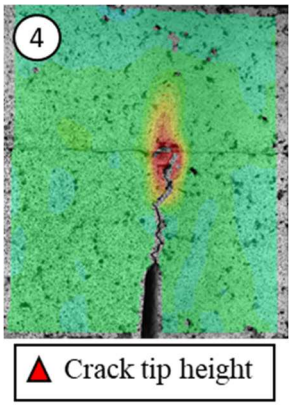
4
Crack tip height

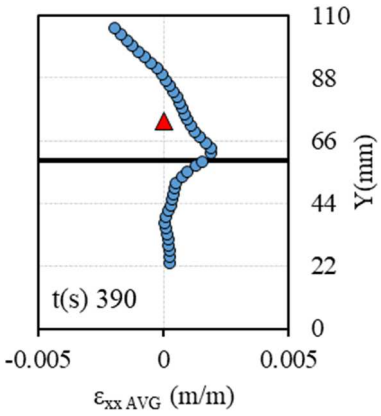
t(s) 390
110
88
66
44
22
0
Y(mm)
-0.005
0
0.005
εxx AVG (m/m)

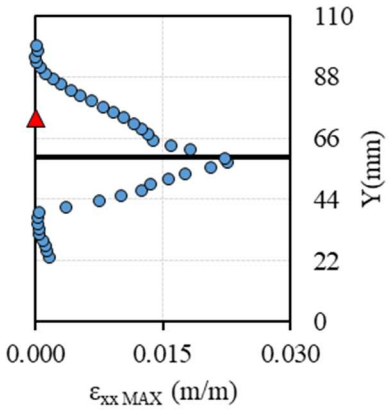
110
88
66
44
22
0
Y(mm)
0.000
0.015
0.030
εxx MAX (m/m)

(e)

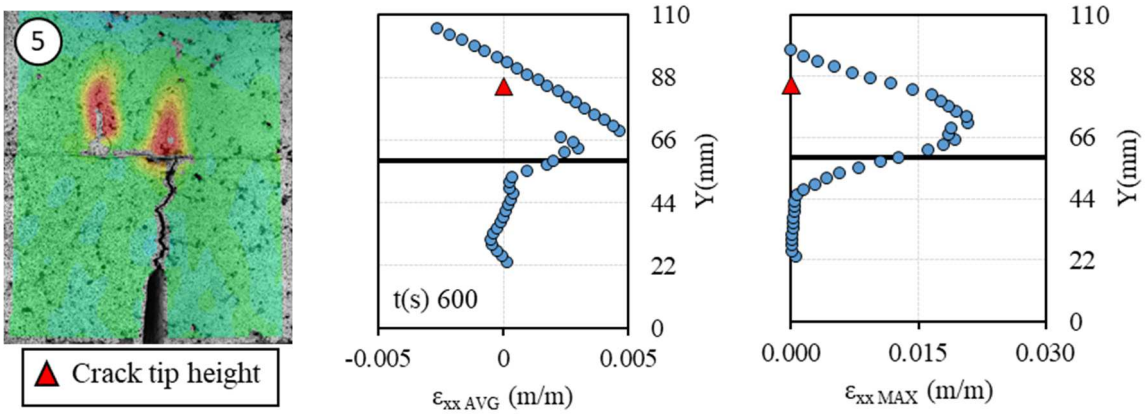

(f)

Figure D2-6. DIC Analysis of average and maximum strain versus beam height of C3-B3

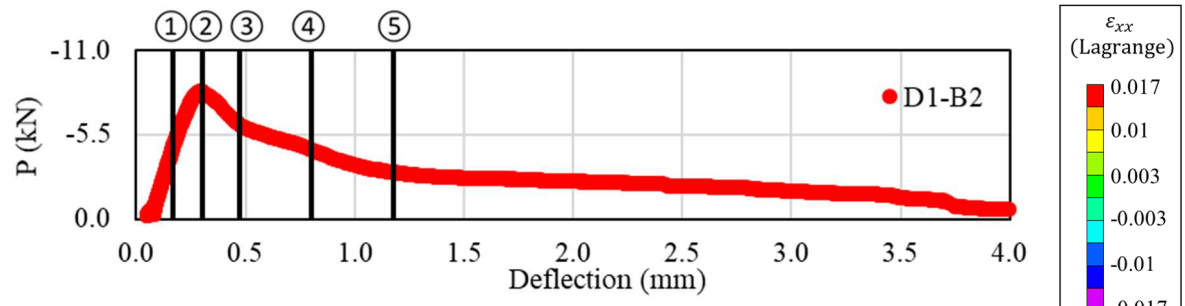

(a)

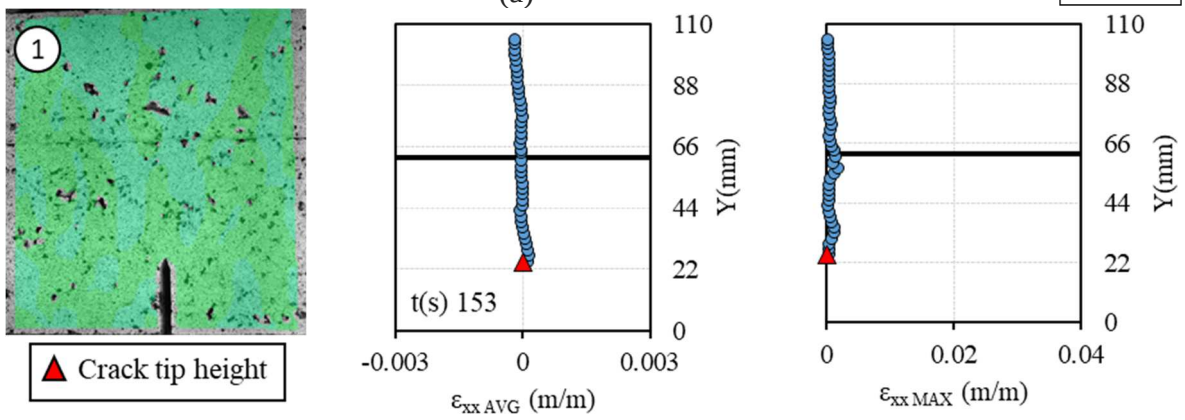

(b)

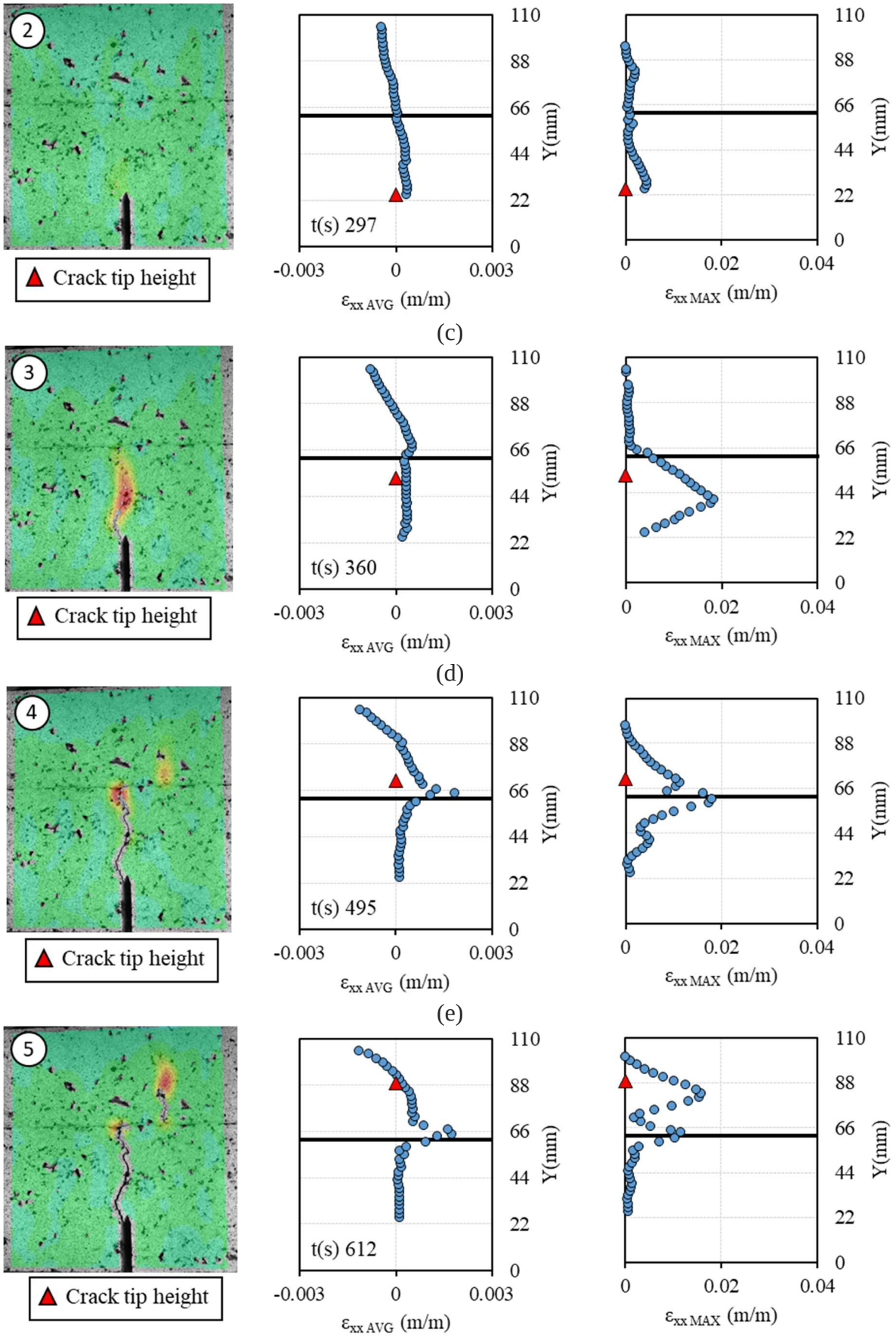

Figure D2-7. DIC Analysis of average and maximum strain versus beam height of D1-B2

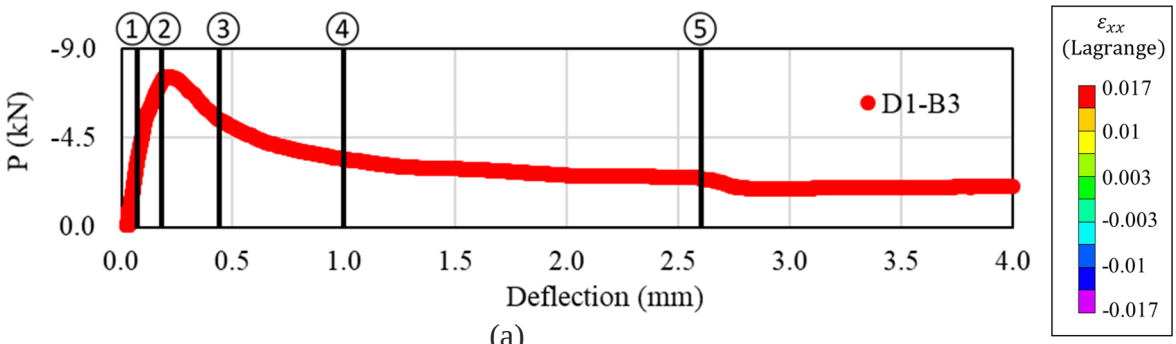
1
2
3
4
5
-9.0
-4.5
0.0
P (kN)
D1-B3
0.0
0.5
1.0
1.5
2.0
2.5
3.0
3.5
4.0
Deflection (mm)
ε_{xx} (Lagrange)
0.017
0.01
0.003
-0.003
-0.01
-0.017

(a)

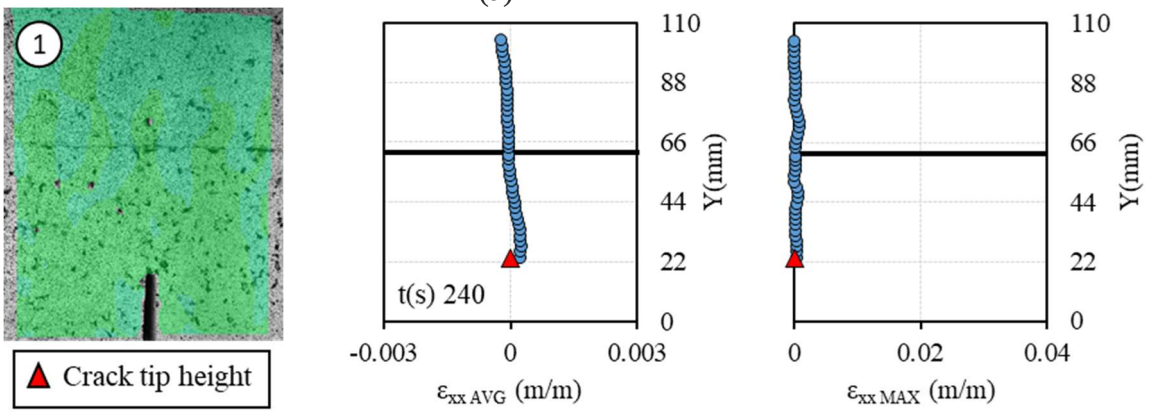
1
Crack tip height
t(s) 240
110
88
66
44
22
0
Y(mm)
-0.003
0
0.003
$\varepsilon_{xx\,AVG}$ (m/m)
0
0.02
0.04
$\varepsilon_{xx\,MAX}$ (m/m)

(b)

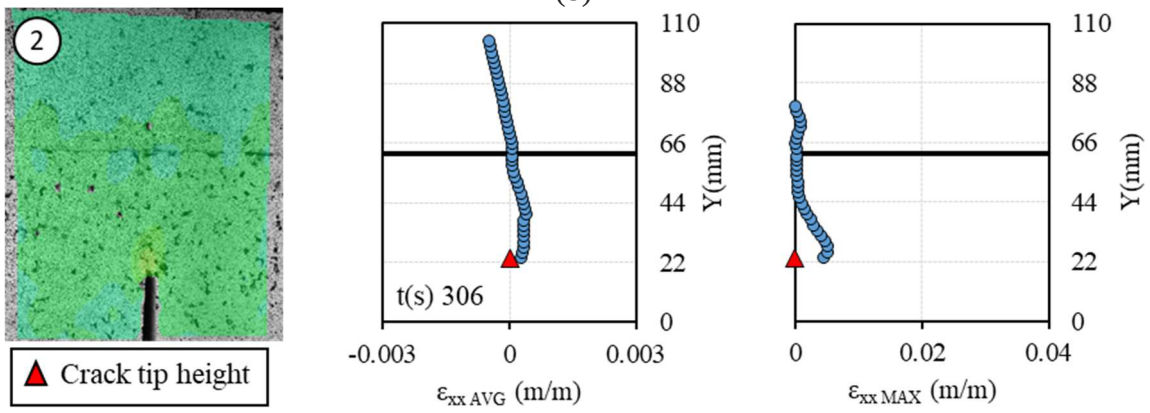
2
Crack tip height
t(s) 306
110
88
66
44
22
0
Y(mm)
-0.003
0
0.003
$\varepsilon_{xx\,AVG}$ (m/m)
0
0.02
0.04
$\varepsilon_{xx\,MAX}$ (m/m)

(c)

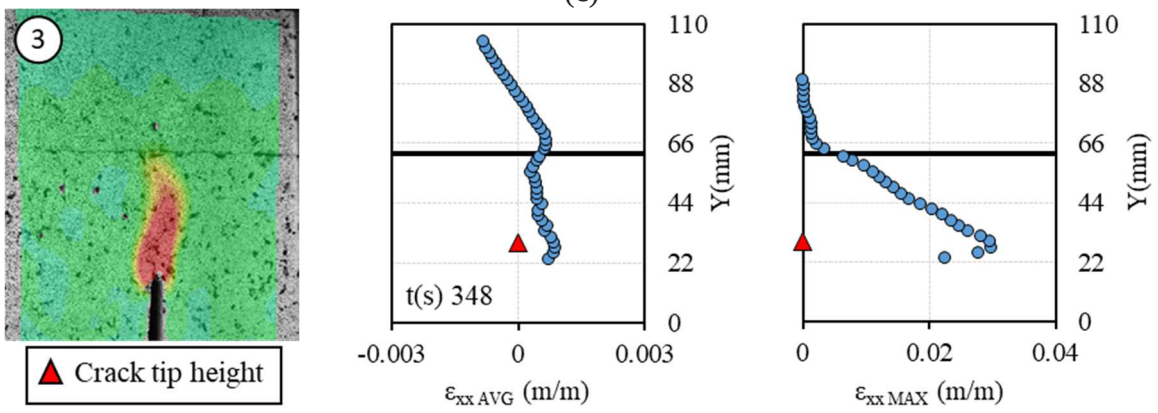
3
Crack tip height
t(s) 348
110
88
66
44
22
0
Y(mm)
-0.003
0
0.003
$\varepsilon_{xx\,AVG}$ (m/m)
0
0.02
0.04
$\varepsilon_{xx\,MAX}$ (m/m)

(d)

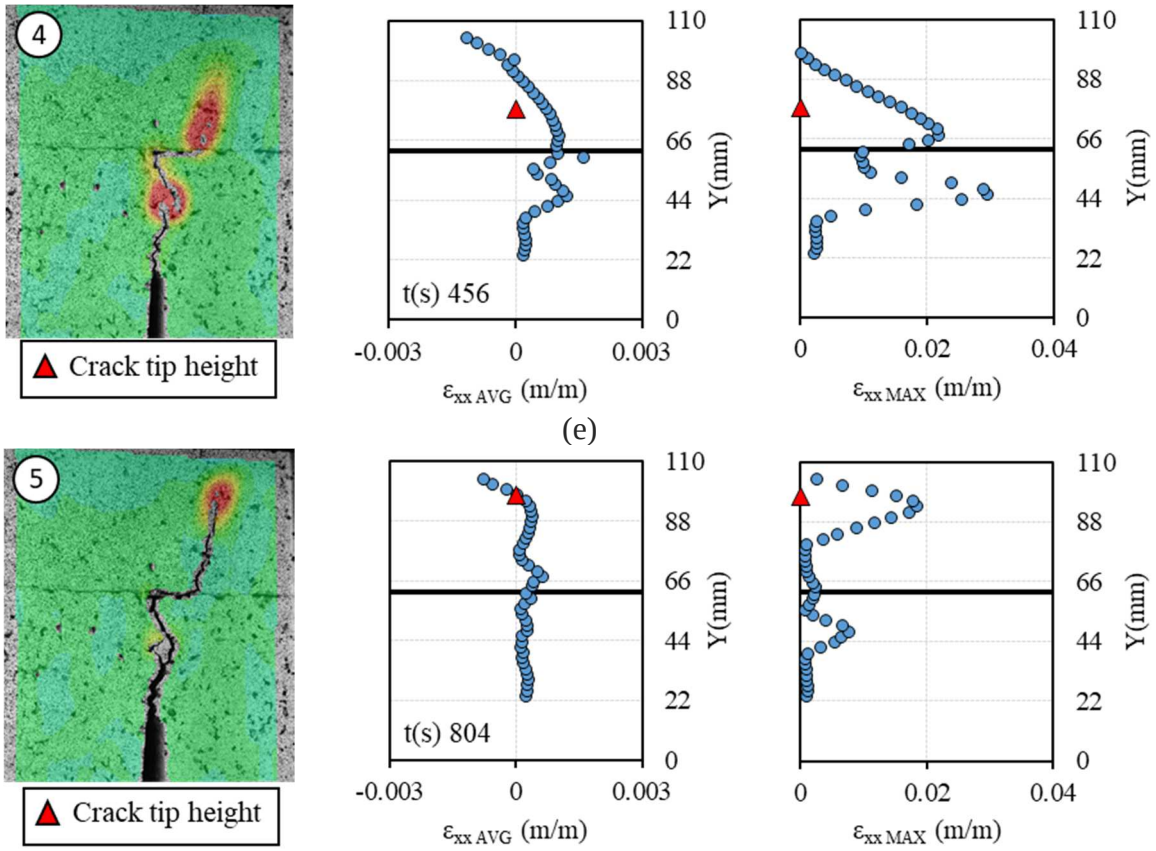

Figure D2-8. DIC Analysis of average and maximum strain versus beam height of D1-B3

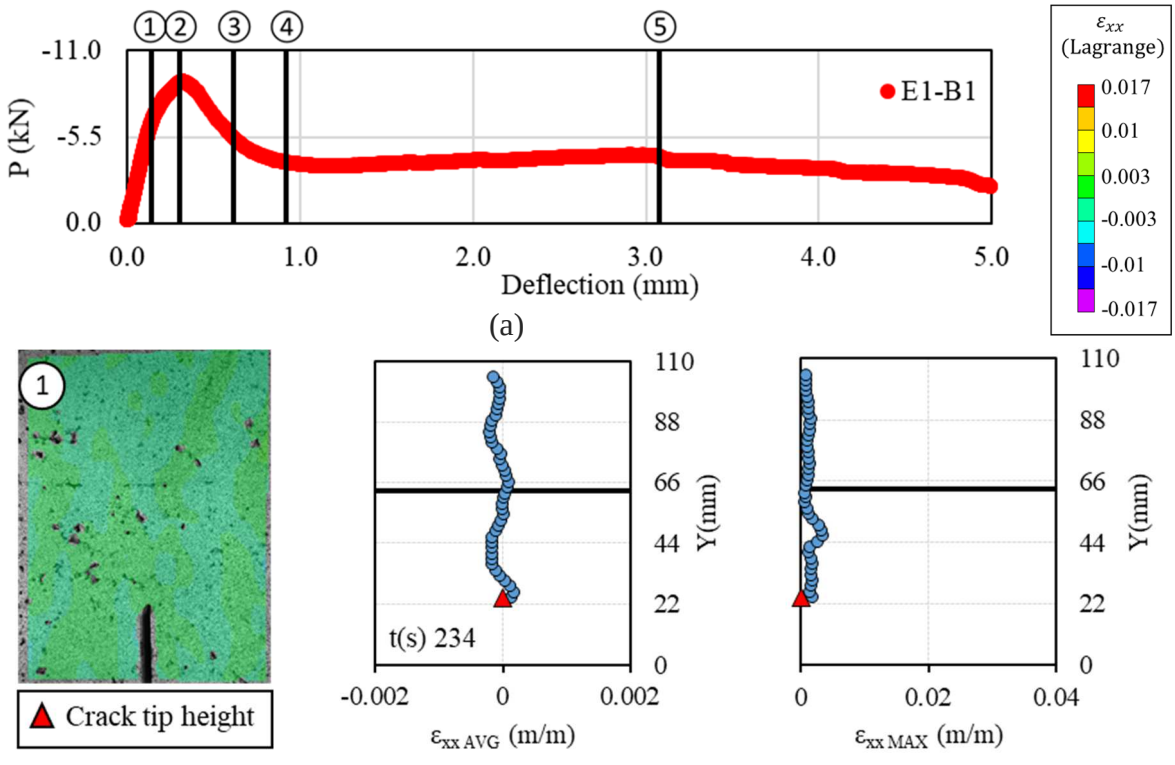

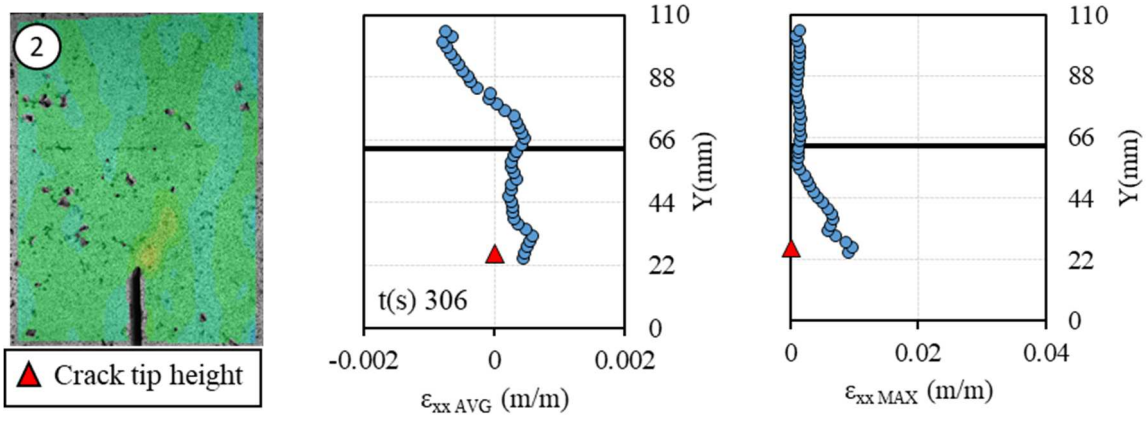
2
Crack tip height
t(s) 306
110
88
66
44
22
0
Y(mm)
-0.002
0
0.002
εxx AVG (m/m)
0
0.02
0.04
εxx MAX (m/m)

(c)

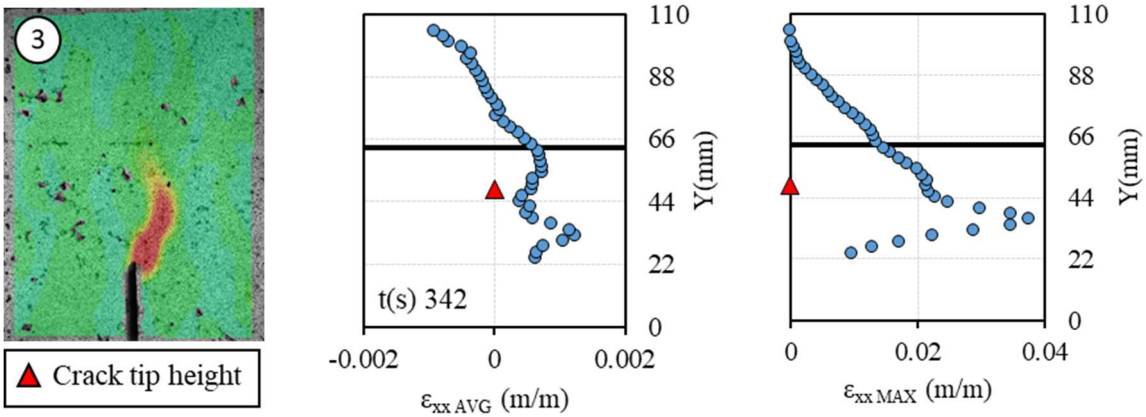
3
Crack tip height
t(s) 342
110
88
66
44
22
0
Y(mm)
-0.002
0
0.002
εxx AVG (m/m)
0
0.02
0.04
εxx MAX (m/m)

(d)

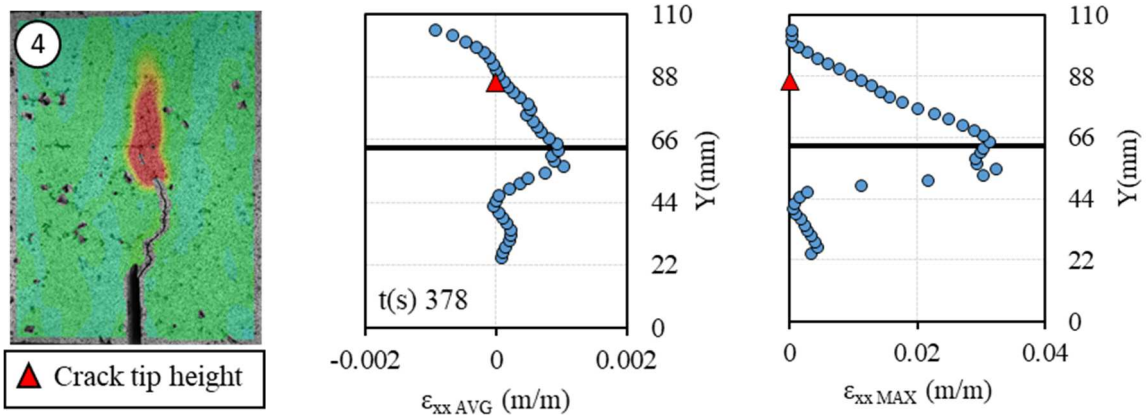
4
Crack tip height
t(s) 378
110
88
66
44
22
0
Y(mm)
-0.002
0
0.002
εxx AVG (m/m)
0
0.02
0.04
εxx MAX (m/m)

(e)

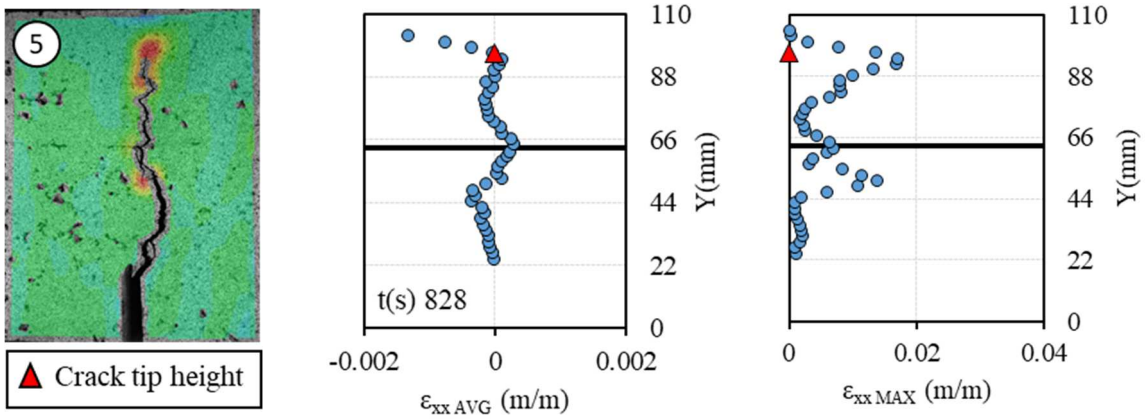

(f)

Figure D2-9. DIC Analysis of average and maximum strain versus beam height of E1-B1

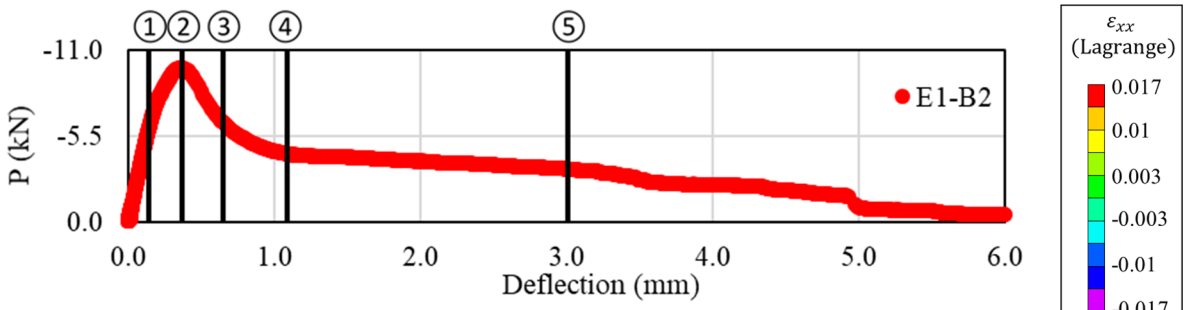

(a)

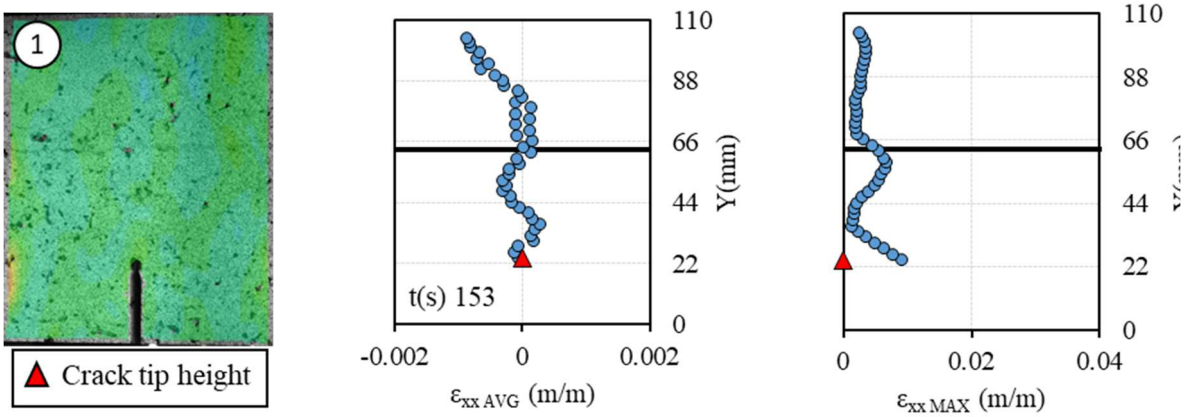

(b)

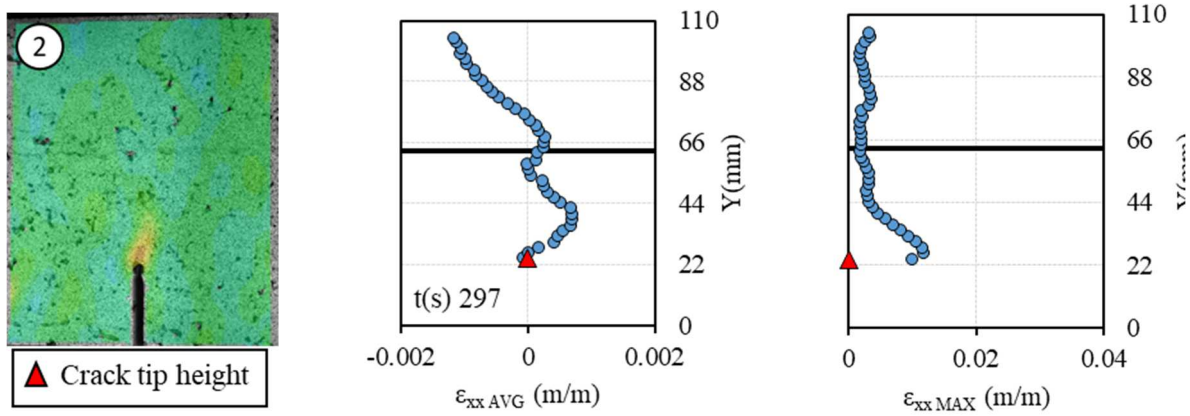
2
Crack tip height
t(s) 297
110
88
66
44
22
0
Y(mm)
-0.002
0
0.002
$\varepsilon_{xx\,AVG}$ (m/m)
0
0.02
0.04
$\varepsilon_{xx\,MAX}$ (m/m)

(c)

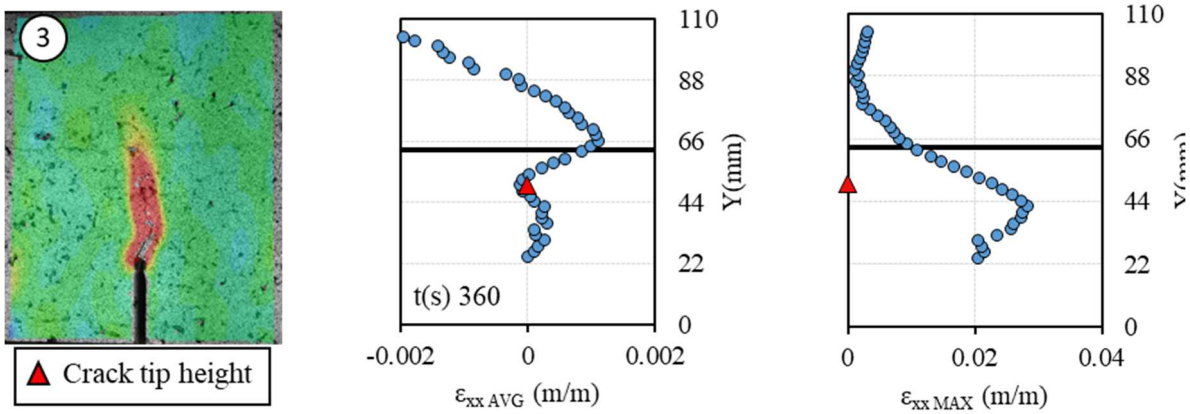
3
Crack tip height
t(s) 360
110
88
66
44
22
0
Y(mm)
-0.002
0
0.002
$\varepsilon_{xx\,AVG}$ (m/m)
0
0.02
0.04
$\varepsilon_{xx\,MAX}$ (m/m)

(d)

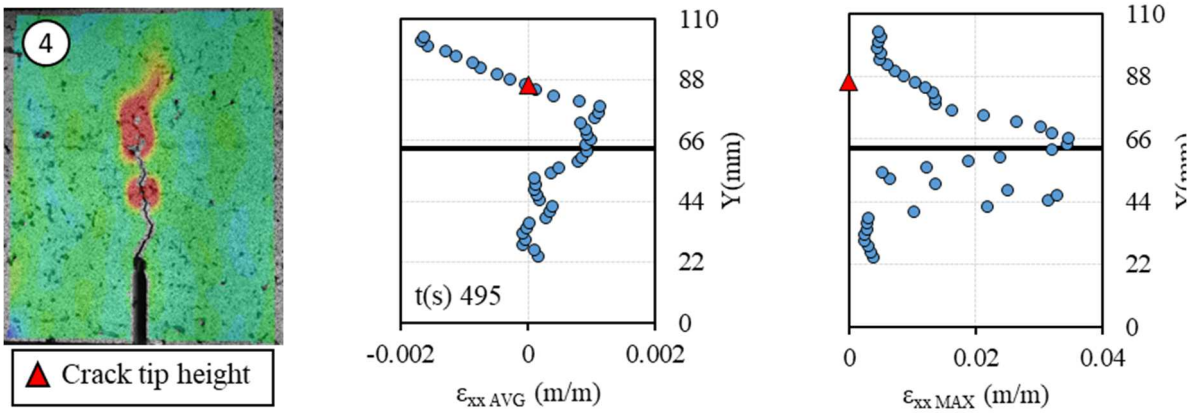
4
Crack tip height
t(s) 495
110
88
66
44
22
0
Y(mm)
-0.002
0
0.002
$\varepsilon_{xx\,AVG}$ (m/m)
0
0.02
0.04
$\varepsilon_{xx\,MAX}$ (m/m)

(e)

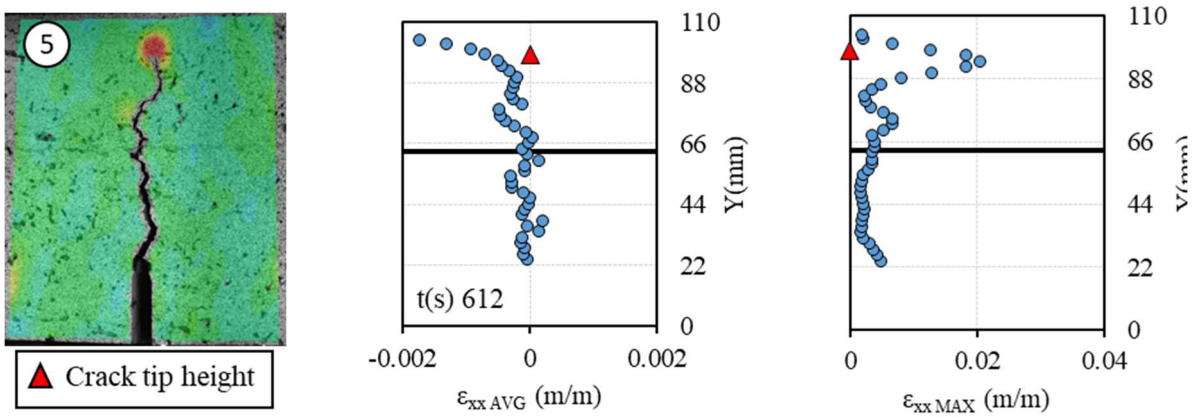

(f)

Figure D2-10. DIC Analysis of average and maximum strain versus beam height of E1-B2